Comparative studies of recombinant oncolytic viruses for the treatment of CD133-positive tumors

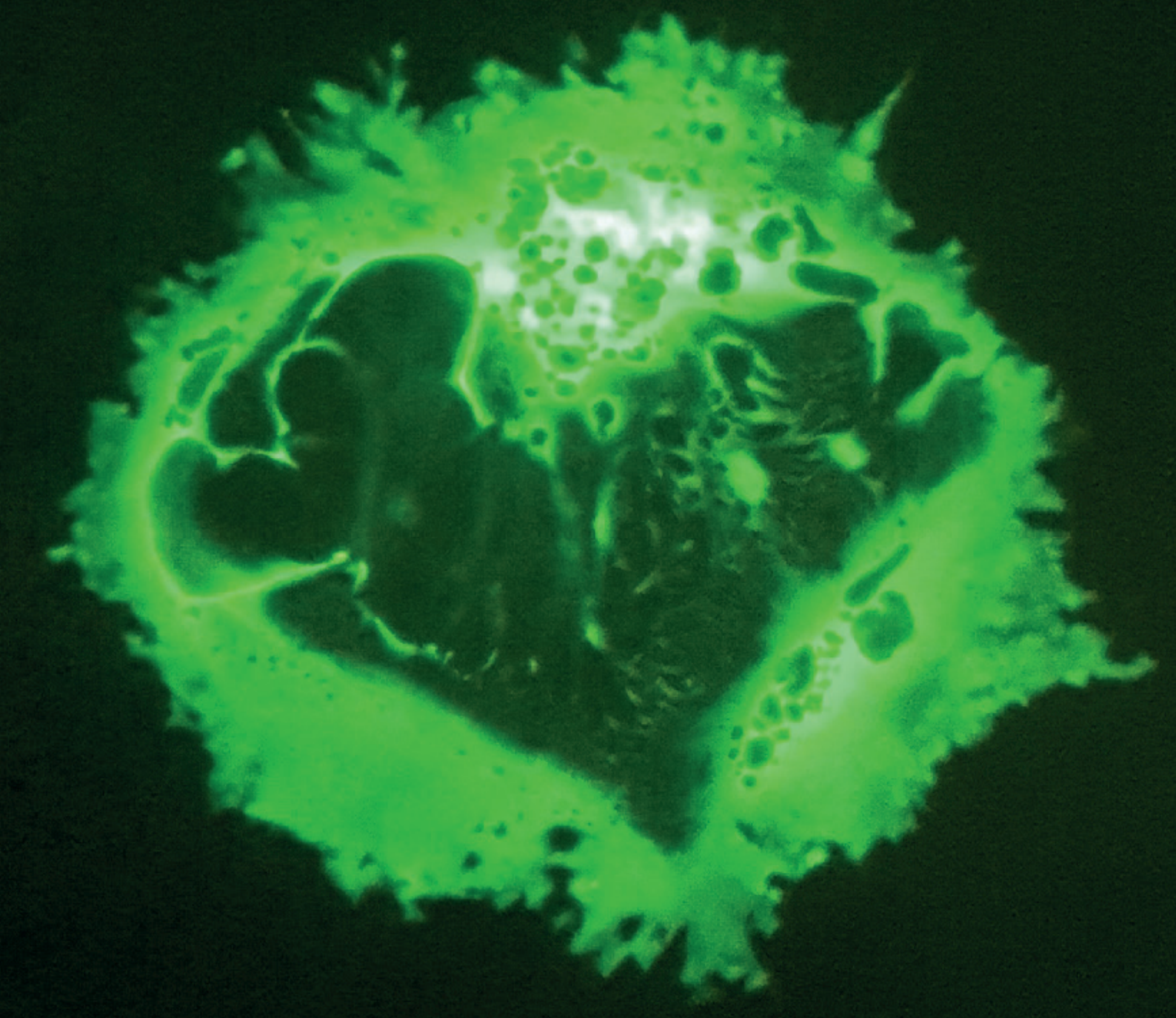

INAUGURAL-DISSERTATION

zur Erlangung des Grades eines
Dr. med. vet.
beim Fachbereich Veterinärmedizin
der Justus-Liebig-Universität Gießen

Dina Schadel geb. Kleinlützum

Bibliografische Informationen der Deutschen Bibliothek

Die Deutsche Bibliothek verzeichnet diese Publikation in der
Deutschen Nationalbibliografie;
detaillierte bibliografische Daten sind im Internet abrufbar über
http://dnb.ddb.de

Foto Umschlag
© Tatjana Weidner und Dina Schadel, Paul-Ehrlich-Institut
Fluoreszenzmikroskopische Aufnahme einer mehrkernigen Riesenzelle (Synzytium), die sich nach Infektion mit einem modifizierten Masernvirus aus mehreren Tumorzellen gebildet hat

ISBN 978-3-86345-534-7
1. Auflage 2020

Verlag:
DVG Service GmbH
Friedrichstraße 17
35392 Gießen
Tel.: 0641/24466
info@dvg.de
www.dvg.de

Aus dem Institut für Virologie

Betreuer: Prof. Heinz-Jürgen Thiel

und

Aus der Abteilung “Molekulare Biotechnologie und Gentherapie”

Paul-Ehrlich-Institut, Langen

Betreuer: Prof. Christian Buchholz

Comparative studies of recombinant oncolytic viruses for the treatment of CD133-positive tumors

INAUGURAL-DISSERTATION
zur Erlangung des Grades eines

Dr. med. vet.

beim Fachbereich Veterinärmedizin

der Justus-Liebig-Universität Gießen

Eingereicht von

Dina Schadel geb. Kleinlützum

Tierärztin aus Wolfhagen

Gießen 2019

Mit Genehmigung des Fachbereichs Veterinärmedizin
der Justus-Liebig-Universität Gießen

Dekan:	Prof. Dr. Dr. h. c. Martin Kramer
1. Gutachter:	Prof. Dr. Heinz-Jürgen Thiel
2. Gutachter:	Prof. Dr. Christian Buchholz
Prüferin:	Prof. Dr. Christiane Herden

Tag der Disputation: 04.07.2019

TABLE OF CONTENTS

1. INTRODUCTION 5

1.1. Cancer Stem Cells 5

1.2. CD133 as Marker for Cancer Stem Cells 7

1.3. Malignant Glioma 8

1.3.1. Relevance of CD133 in Glioblastoma Multiforme 10

1.4. Hepatocellular Carcinoma 11

1.4.1. Relevance of CD133 in Hepatocellular Carcinoma 13

1.5. Viruses used as Oncolytic Agents 13

1.5.1. Measles Virus 14

1.5.2. Vesicular Stomatitis Virus 21

1.6. Targeted Oncolytic Measles Virotherapy 25

1.6.1. CD133-Targeted Oncolytic Measles Virus 26

1.7. Objective 28

2. MATERIAL AND METHODS 30

2.1. Materials 30

2.1.1. Consumables 30

2.1.2. Chemicals and Reagents 31

2.1.3. Buffers and Media 33

2.1.4. Commercially available Kits 33

2.1.5. Antibodies 34

2.1.6. Cell Lines 35

2.1.7. Viruses 36

2.1.8. Medicals and Anesthetics 36

2.1.9. Instruments 37

2.1.10. Software 38

2.2. Protein Biomedical Methods 39

2.2.1. Sodium Dodecyl Sulfate-Polyacrylamide Gel Electrophoresis 39

2.2.2. Immunoblot 40

2.3. Cell Culture and Virological Methods 40

2.3.1. Cultivation of Cell Lines 41

2.3.2. Freezing and Thawing of Cells 41

2.3.3. Isolation and Cultivation of Human $CD34^+$ Cells 42

2.3.4. Flow Cytometry Analysis 42
2.3.5. Preparation of Virus Stocks 44
2.3.6. Titration of Virus Particles ($TCID_{50}$) 45
2.3.7. Infection of Cells 45
2.3.8. Colony-Forming Assays 47
2.3.9. Virus Growth Kinetics 47
2.3.10. Killing Kinetics and Dose Dependency 48
2.3.11. Bystander Assay 49

2.4. Animal Experiments 49

2.4.1. Subcutaneous HuH7 Xenograft Cell Implantation 50
2.4.2. Orthotopic Glioma Sphere Cell Implantation 51
2.4.3. Administration of Virus Particles 52
2.4.4. Transcardial Perfusion 53
2.4.5. Ex Vivo Sphere Formation Assays 53
2.4.6. Cryo Embedding and Immunofluorescence Staining of Tumor Sections 54
2.4.7. Paraffin Embedding and Immunohistochemistry of Brain Sections 54
2.4.8. Quantification of Infected Areas in Cryo Sections of Tumor Tissue 55

2.5. Statistical analysis 56

3. RESULTS 57

3.1. Characterization of Oncolytic Viruses for Protein Composition 58

3.2. Selectivity of Targeted Oncolytic Viruses 58

3.3. Replication of Targeted Oncolytic Viruses on HuH7 Hepatocellular Carcinoma Cells 60

3.4. Toxicity Testing of CD133-targeted Oncolytic Viruses towards Human $CD34^+$ Cells 62

3.4.1. Analysis of Human $CD34^+$ Cells for Susceptibility to Infection 63
3.4.2. Evaluation of Impairment of Hematopoietic Stem Cell Self-Renewal after Infection 65

3.5. Oncolytic Properties on Cultured Cells 67

3.5.1. Infection of Hepatocellular Carcinoma Cells 67
3.5.2. Potentiated Oncolysis of MV^{SCD}-CD133 through Bystander-Mediated Killing of Target-Receptor Negative Cells 70

3.6. Oncolytic Properties on Primary Tumor Cells 71

3.6.1. Cell Surface Expression Levels of CD46 and CD133 on NCH644 Cells 73
3.6.2. Time and Dose Response Killing of Primary Glioma Sphere Cells 74
3.6.3. Enhanced Killing of Primary Glioma Sphere Cells by MV^{SCD}-CD133 76

3.7. Efficacy *In Vivo* 77

3.7.1. Activity of Intratumorally Applied CD133-Targeted Viruses in a Subcutaneous Xenograft Model of Hepatocellular Carcinoma.....77
3.7.2. Characterization of Explanted Tumors Infected with MV-CD133 and VSV-CD133 79
3.7.3. Activity of Systemically Administered CD133-Targeted Viruses against a Subcutaneous Xenograft Model of Hepatocellular Carcinoma.....85
3.7.4. Activity of CD133-Targeted Viruses in an Orthotopic Glioma Model.....85
3.7.5. Direct Intracranial Application of Oncolytic Viruses into Naïve mice 91

4. DISCUSSION 93

4.1. CD133 as Target Receptor 93

4.2. Neurotoxicity..... 98

4.3. Clinical Application of Receptor-Targeted Oncolytic Viruses 102

REFERENCES 105

LIST OF PUBLICATIONS.....124

DANKSAGUNG.....127

EHRENWÖRTLICHE ERKLÄRUNG.....128

TABLE OF FIGURES

Figure 1. Models for tumor propagation 6
Figure 2. Transition of cancer stem cells (CSCs) to non-CSCs within the CSC model 7
Figure 3. Schematic drawing of the CD133 topology 7
Figure 4. The association between CD133 expression and survival of glioma patients 10
Figure 5. The association between CD133 expression and overall survival of hepatocellular carcinoma patients 13
Figure 6. Oncolytic virotherapy mechanism of action 15
Figure 7. Phylogenetic tree of Morbillivirus genus 16
Figure 8. Genome organization and virus particle structure of Measles Virus 17
Figure 9. Measles Virus replication cycle 19
Figure 10. Genome organization and structure of Vesicular Stomatitis Virus 23
Figure 11. The life cycle of Vesicular Stomatitis Virus 24
Figure 12. Therapeutic implication of cancer stem cell diversity in a tumor 28
Figure 13. Schematic overview of the genomic organization of the oncolytic viruses used in this study 57
Figure 14. Immunochemical characterization of recombinant Measles Virus and MV glycoprotein pseudotyped Vesicular Stomatitis Virus particles 59
Figure 15. Receptor tropism of targeted Measles and Vesicular Stomatitis Virus 60
Figure 16. Replication kinetics of oncolytic viruses on HuH7 cells 62
Figure 17. Cell surface expression levels of CD46 and CD133 on human $CD34^+$ cells 63
Figure 18. Infection of human $CD34^+$ cells 64
Figure 19. Hematopoietic stem cell properties are not impaired by infection 66
Figure 20. Cell surface expression levels of CD133 on infected HuH7 cells 68
Figure 21. Killing kinetics of oncolytic viruses 69
Figure 22. Dose-dependent killing of HuH7 cells 70
Figure 23. Enhanced cell killing by MV^{SCD}-CD133-mediated bystander killing 72
Figure 24. Cell surface expression levels of CD46 and CD133 on glioma sphere cells 73
Figure 25. Infection and killing of primary glioma sphere cells 74
Figure 26. Differential killing kinetics of oncolytic viruses on glioma sphere cells 75
Figure 27. Time and dose dependency of 5-FC mediated cell killing of MV^{SCD}-CD133 on primary glioma sphere cells 76
Figure 28. Oncolytic activities of intratumorally applied oncolytic viruses in a subcutaneous xenograft model of hepatocellular carcinoma 78
Figure 29. Virus distribution pattern in intratumorally infected tumors 80
Figure 30. Quantification of infected areas in explanted tumors 82

Figure 31. GFP-CD133 co-staining on subcutaneous hepatocellular carcinoma 84
Figure 32. Oncolytic activity of intravenously administered viruses in a subcutaneous xenograft model of hepatocellular carcinoma 86
Figure 33. Intracranial implantation of preinfected glioma sphere cells.....88
Figure 34. Histopathology of explanted brains of mice bearing pre-infected glioma.....90
Figure 35. Intracranial injection of oncolytic viruses into pre-established glioma 91
Figure 36. Intracranial injection of oncolytic viruses into naïve mice.....92

LIST OF TABLES

Table 1. WHO grading system for astrocytomas 9
Table 2. Staging system for hepatocellular carcinoma 12
Table 3. Formulation of SDS-polyacrylamide gel..... 39
Table 4. Time-dependent killing capabilities of oncolytic viruses 69

ABBREVIATIONS

(F) PROTEIN ..... *FUSION PROTEIN*
(H) PROTEIN..... *HEMAGGLUTININ PROTEIN*
(M) PROTEIN..... *MATRIX PROTEIN*
°C ..... *DEGREE CELSIUS*
µL, µG ..... *MICROLITER, MICROGRAM*
5-FC..... *5-FLUOROCYTOSINE*
5-FU *5-FLUOROURACIL*
ADEM..... *ACUTE DISSEMINATED ENCEPHALOMYELITIS*
APC ..... *ALLOPHYCOCYANIN*
AUC..... *AREA UNDER THE CURVE*
BALT..... *BRONCHUS-ASSOCIATED LYMPHOID TISSUE*
BBB ..... *BLOOD-BRAIN-BARRIER*
BCLC..... *BARCELONA CLINIC LIVER CANCER*
BFU-E ..... *BURST-FORMING UNIT ERYTHROID*
BITE ..... *BI-SPECIFIC T CELL ENGAGER*
BIT_{100} ..... *BOVINE INSULIN TRANSFERRIN 100*
CAR ..... *CHIMERIC ANTIGEN RECEPTOR*
CD ..... *CLUSTER OF DIFFERENTIATION*
CDV ..... *CANINE DISTEMPER VIRUS*
CEA ..... *CARCINOEMBRYONIC ANTIGEN*
CFA..... *COLONY-FORMING ASSAY*
CFU-G..... *COLONY-FORMING UNIT-GRANULOCYTE*
CFU-GM ..... *COLONY-FORMING UNIT-GRANULOCYTE, MACROPHAGE*
CFU-M..... *COLONY-FORMING UNIT-MACROPHAGE*
CHO..... *CHINESE HAMSTER OVARY*
CNS ..... *CENTRAL NERVOUS SYSTEM*
CPE..... *CYTOPATHIC EFFECT*
CSC..... *CANCER STEM CELL*
CT/SPECT ..... *COMPUTED TOMOGRAPHY/SINGLE-PHOTON EMISSION COMPUTED TOMOGRAPHY*
CY ..... *CYANINE DYE*
DAPI ..... *4', 6-DIAMIDINO-2-PHENYLINDOLE*
DC ..... *DENDRITIC CELL*
DMEM..... *DULBECCO'S MODIFIED EAGLE'S MEDIUM*
DMSO..... *DIMETHYL SULFOXIDE*
EC_{50} ..... *EFFECTIVE CONCENTRATION REQUIRED TO REDUCE CELL VIABILITY TO 50 %*
EDM ..... *EDMONSTON*
EDTA ..... *ETHYLENEDIAMINETETRAACETIC ACID*
EGF..... *EPIDERMAL GROWTH FACTOR*
EMT..... *EPIDERMAL-MESENCHYMAL TRANSITION*
ET AL..... *AND OTHERS*
EVS ..... *EXTRACELLULAR VESICLES*
F_0..... *INACTIVE PRECURSOR OF THE F PROTEIN*
F_1..... *PROCESSED, ACTIVE F PROTEIN (40 KDA)*
F_2..... *PROCESSED, ACTIVE PROTEIN (20 KDA)*

FACS ..... *Fluorescence-activated cell sorting*
FCS ..... *Fetal calf serum*
FeMV ..... *Feline morbillivirus*
FGF ..... *Fibroblast growth factor*
FIP ..... *fusion inhibiting protein*
FITC ..... Fluorescein isothiocyanate
FMDV ..... *Foot-and-Mouth Disease Virus*
g ..... *gram*
GBM ..... *Glioblastoma multiforme*
G-CSF ..... *Granulocyte colony-stimulating factor*
GFP ..... *Green fluorescence protein*
GM-CSF ..... *Granulocyte macrophage colony stimulating factor*
GSC ..... *Glioma stem cell*
HBV ..... *Hepatitis B virus*
HCC ..... *Hepatocellular carcinoma*
HCV ..... *Hepatitis C virus*
HGDN ..... *High-grade dysplastic nodule*
HSC ..... *Hematopoietic stem cell*
i.c. ..... *intracerebral*
i.p. ..... *intraperitoneal*
i.t. ..... *intratumoral*
i.v. ..... *intravenous*
IF ..... *Immunofluorescence*
IFN ..... *Interferon*
IFNAR ..... *Interferon alpha/beta receptor*
Ig ..... Immunoglobulin
IVC ..... *Individually ventilated cage*
kDa ..... *kilo Dalton*
kg ..... *kilogram*
l ..... *liter*
L protein ..... *Large protein*
LCSC ..... *Liver cancer stem cell*
LDLR ..... *Low-density lipoprotein receptor*
LV ..... *Lentiviral vector*
MCP ..... *Membrane cofactor protein*
MFI ..... *Mean fluorescence intensity*
MIBE ..... *Measles inclusion body encephalitis*
mM ..... *milli Molar*
MMP ..... *Matrix metalloprotease*
MOI ..... *Multiplicity of infection*
MV ..... *Measles virus*
N protein ..... *Nucleocapsid protein*
NDV ..... *Newcastle Disease Virus*
NHP ..... *New-world human primate*
NIS ..... *Sodium iodide symporter*
NOD/Scid ..... *Nonobese diabetic/severe combined immunodeficiency*

N.S. ..... *NOT SIGNIFICANT*
NSC ..... *NEURAL STEM CELL*
NSE ..... *NARI- AND SPEI ELIMINATED*
OV ..... *ONCOLYTIC VIRUS*
P PROTEIN ..... *PHOSPHOPROTEIN*
PBMC ..... *PERIPHERAL BLOOD MONONUCLEAR CELL*
PBS ..... *PHOSPHATE-BUFFERED SALINE*
PE ..... *PHYCOERYTHRIN*
P.I. ..... *POST INFECTION*
PPRV ..... *PESTE-DES-PETITS-RUMINANTS VIRUS*
PSMA ..... *PROSTATE-SPECIFIC MEMBRANE ANTIGEN*
PVRL4 ..... *POLIO-VIRUS RECEPTOR-RELATED-4*
RDRP ..... *RNA-DEPENDENT RNA POLYMERASE*
RNP ..... *RIBONUCLEOPROTEIN*
RPD ..... *REGIERUNGSPRÄSIDIUM DARMSTADT*
RPV ..... *RINDERPEST VIRUS*
S.C. ..... *SUBCUTANEOUS*
SCD ..... *SUICIDE GENE CYTOSINE DEAMINASE AND URACIL PHOSPHORIBOSYLTRANSFERASE*
SCFV ..... *SINGLE CHAIN ANTIBODY*
SDS-PAGE ..... *SODIUM DODECYL SULFATE POLYACRYLAMIDE GEL ELECTROPHORESIS*
SLAM ..... *SIGNAL LYMPHOCYTE-ACTIVATION MOLECULE*
SPF ..... *SPECIFIED PATHOGEN FREE*
SSPE ..... *SUBACUTE SCLEROSING PANENCEPHALITIS*
TACE ..... *TRANSARTERIAL CHEMOEMBOLIZATION*
$TCID_{50}$ ..... *50 % TISSUE CULTURE INFECTIVE DOSE*
TIC ..... *TUMOR-INITIATING CELL*
TM ..... *TRANSMEMBRANE*
TMZ ..... *TEMOZOLOMIDE*
VSV ..... *VESICULAR STOMATITIS VIRUS*
WHO ..... *WORLD HEALTH ORGANIZATION*
W/O ..... *WITHOUT*
WB ..... *WESTERN BLOT*
WT ..... *WILD-TYPE*
Δ ..... *DELTA*

SUMMARY

Despite considerable progress in cancer therapy, the available treatment options for most malignancies are still unsatisfactory. This may, amongst other reasons, be ascribed to an insufficient targeting and killing of a small subset of tumor cells endowed with stem-cell like properties such as self-renewal and extensive proliferative capacity. Such cancer stem cells (CSCs) have been found to mark the tumorigenic cell population within various malignancies including cancer of the brain and the liver. Among many putative markers, prominin-1 (also known as CD133) is frequently used to identify and isolate CSCs of the above mentioned malignancies. To date, there is no effective approach to reduce the rate of tumor recurrence ascribed to CSCs. Thus, targeting of CSCs is critical to achieve long-term success in cancer treatment. One strategy to selectively destroy CSCs is the precise targeting of this cell subset via targeted oncolytic viruses (OVs). One of the lead oncolytic agents in ongoing clinical trials is oncolytic measles virus (MV) based on the safe vaccine strain Edmonston B (Edm) that induced complete remission after one intravenous (i.v.) administration of 10^{11} infectious virus in one patient suffering from disseminated multiple myeloma (Russell et al., 2014). MV-Edm uses the ubiquitous membrane cofactor protein (MCP, also known as CD46) for cell entry, which is overexpressed on tumor cells. To restrict virus replication to tumor cells, the glycoprotein (gp) complex of MV can be engineered to redirect receptor usage to cell surface proteins of choice. Based on this approach, a CD133-retargeted MV (MV-CD133) was generated prior to this work through fusion of a CD133-specific single-chain antibody fragment (scFv) as targeting domain to the receptor attachment protein hemagglutinin (H) ablated for its natural receptors CD46, signal lymphocyte-activation molecule (SLAM) and nectin-4 (also known as Polio-virus receptor-related 4, PVRL4). MV-CD133 exhibited a stronger oncolytic activity on $CD133^+$ tumors compared to untargeted parental MVs using CD46 for cell entry (Bach and Abel et al., 2013).

As tumor regression was incomplete, this thesis pursued strategies to enhance the oncolytic activity of MV-CD133 without having to compromise on safety. For that purpose, arming with the prodrug 5-fluorocytosine (5-FC) converting suicide gene supercytosinedeaminase (SCD), or with P/V/C genes from wild-type MVs, or receptor extension through omission of blinding mutations were pursued. Additionally, a chimeric vesicular stomatitis / measles virus (VSV-MV), in which the gp VSV-G was replaced by the MV-H and MV-F gp fused to a CD133-scFv was examined. The viruses were analyzed for their oncolytic activity *in vitro* and by *in vivo* models of the hepatocellular carcinoma (HCC) cell line HuH7 and of the primary glioma sphere cells NCH644 using NOD/Scid (Nonobese diabetic/severe combined immunodefiency) mice known to be devoid of human CD46 expression. All viruses were found to be highly selective for $CD133^+$ cells as demonstrated by infection of receptor transgenic chinese hamster ovary (CHO) cells. As CD133 is also expressed on early hematopoietic progenitor cells, the prolifer-

ative and differentiation capacity of infected human hematopoietic stem cells (HSCs) was evaluated using clonal outgrowth assays. None of the CD133-retargeted viruses impaired the hematopoietic capabilities of HSCs. On HuH7 cells, VSV-MV chimeric viruses yielded substantially higher titers than their parental viruses. VSV-CD133 and MV^{SCD}-CD133 (+ 5-FC) achieved the most rapid and efficient cytotoxicity on HuH7 cells. In a subcutaneous HuH7 model, VSV-CD133 most efficiently slowed down tumor growth resulting in a prolonged survival of mice treated intratumorally (i.t.) and i.v.. VSV-CD133 infected a more than 10^4-fold larger area of the tumor than MV-CD133 did in the same period. In killing assays on NCH644 cells, all viruses killed cells dose-dependently. While MV-CD46/CD133 and MV^{SCD}-CD133 (+ 5-FC) caused a continuous decline in cell numbers over time even at low multiplicity of infection (MOI), VSV-MV chimeric viruses were only able to reduce cell viability within in the first 48 h after infection. In an orthotopic NCH644 model, MV-CD46/CD133 and MV^{SCD}-CD133 (+ 5-FC) were most effective in prolonging survival compared to mock-treated mice. *Ex vivo* sphere formation assays revealed that cells of those tumors explanted at termination showed impaired stemness properties compared to those of the other viruses. By contrast, VSV-CD133 led to severe neurotoxic symptoms such as ataxia, tremor or apathy within 10 days after infection in tumor bearing mice. The neurotoxicity was also apparent in tumor-naïve mice that were intracerebrally (i.c.) injected with VSV-CD133 as well as upon injection with nontargeted VSV-MV suggesting that deceased mice must have succumbed to another genesis than that of i.t. virus amplification or the scFv themselves. The role of the yet unknown neuronal MV receptor or a membrane fusion process that occurred independently from a contact with H need to be tested as potential causatives.

The data shown in this thesis not only demonstrate new concepts and approaches toward enhancing the oncolytic activity of CD133-targeted MVs but also heighten awareness of the importance of careful toxicity testing of novel virus types. In this context, it is also important to stress that each engineering strategy, administration schedule and combination treatment must thoroughly be assessed for each indication prior to clinical testing.

ZUSAMMENFASSUNG

Trotz erheblicher Fortschritte in der Krebstherapie sind die verfügbaren Therapiemöglichkeiten für die meisten Krebsarten nach wie vor unbefriedigend. Dies kann unter anderem auf eine unzureichende Abtötung einer kleinen Subpopulation von Tumorzellen zurückgeführt werden, die mit Stammzell-ähnlichen Eigenschaften wie Selbsterneuerung und extensiver proliferativer Kapazität ausgestattet sind. Es wurde festgestellt, dass solche Krebsstammzellen (engl. *cancer stem cells*, CSCs) die tumorigene Zellpopulation in verschiedenen Malignomen, einschließlich Tumoren des Gehirns und der Leber, kennzeichnen. Ein vermeintlicher Marker für die Identifizerung und Isolierung von CSC ist Prominin-1 (auch bekannt als CD133). Bislang gibt es keinen wirksamen Ansatz, um die Rate des Tumorrezidivs zu reduzieren, das den CSC zugeschrieben wird. Daher ist die gezielte Zerstörung von CSC entscheidend für einen langfristigen Therapieerfolg. Eine Strategie zur selektiven Zerstörung von CSC ist das präzise *targeting* dieser Zellpopulation über zielgerichtete onkolytische Viren (OVs). Eines der führenden OV in laufenden klinischen Studien ist ein onkolytisches Masernvirus (MV) auf der Grundlage des sicheren Impfstoffstammes Edmonston B (Edm), das nach einer intravenös (i.v.) verabreichten Dosis von 10^{11} infektiösen Einheiten eine vollständige Remission eines disseminierten multiplen Myeloms induzierte (Russell et al., 2014). MV-Edm nutzt das ubiquitäre CD46, das auf Tumorzellen überexprimiert wird, für den Zelleintritt. Um die Virusreplikation auf Tumorzellen zu begrenzen, kann der Glykoprotein-Komplex von MV so konstruiert werden, dass ein Zelloberflächenprotein der Wahl für den Zelleintritt verwendet wird. Basierend auf diesem Ansatz wurde zuvor durch Fusion eines CD133-spezifischen Einzelketten-Antikörperfragments (scFvs) als Targeting-Domäne an das Rezeptor-bindende Hämagglutinin (H) ein CD133-spezifisches MV (MV-CD133) erzeugt, dessen natürliche Rezeptornutzung durch vier spezifische Punktmutationen unterbunden wurde. MV-CD133 zeigte eine stärkere onkolytische Aktivität bei $CD133^+$ Tumoren im Vergleich zu ungezielten parentalen MV, die CD46 für den Zelleintritt verwenden (Bach und Abel et al., 2013).

Ziel der vorliegenden Arbeit war es, Strategien zur Verbesserung der onkolytischen Aktivität von MV-CD133 zu entwickeln, ohne Kompromisse bei der Sicherheit eingehen zu müssen. Zu diesem Zweck wurde MV-CD133 mit dem induzierbaren zytotoxischen Transgen Supercytosindeaminase (SCD) oder mit dem P/V/C-Gen des MV Wildtyps ausgestattet. Zudem wurde ein CD133-spezifisches MV mit einer breiteren Rezeptorausnutzung entwickelt (MV-CD46/CD133), indem keine *blinding mutations* eingebaut wurden. Zusätzlich wurde ein chimäres vesikuläres Stomatitis/Masernvirus (VSV-MV) untersucht, bei dem das VSV-Glykoprotein G durch die an CD133-scFv fusionierten MV-Glykoproteine ersetzt wurde. Die onkolytische Aktivität der Viren wurde auf der hepatozellulären Karzinom (HCC) Zelllinie HuH7 und den primären Gliomzellen NCH644 *in vitro* sowie *in vivo* unter Verwendung von NOD/Scid (*Nonobese diabetic/severe combined immunodefiency*) Mäusen analysiert, die keine humane

CD46-Expression aufweisen. Alle Viren infizierten selektiv CD133$^+$ Zellen, was durch die Infektion von Rezeptor-transgenen chinesischen Hamster-Eierstockzellen (CHO) gezeigt wurde. Da CD133 auch auf frühen hämatopoetischen Vorläuferzellen exprimiert wird, wurden die Stammzell-Eigenschaften infizierter humaner hämatopoetischer Stammzellen (engl. *hematopoietic stem cells*, HSCs) mittels klonalen "outgrowth assays" bestimmt. Keines der CD133-spezifischen Viren beeinträchtigte die hämatopoetischen Fähigkeiten der HSCs. Auf HuH7 Zellen ließen sich mit den VSV-MV Hybridviren wesentlich höhere Titer als mit den jeweiligen parentalen Viren erzeugen, wobei VSV-CD133 und MV^{SCD}-CD133 (+ 5-FC) die schnellste und effizienteste Zytolyse induzierten. In einem subkutanen HuH7-Modell verlangsamte VSV-CD133 das Tumorwachstum am effizientesten und führte zu einem verlängerten Überleben der Mäuse, die intratumoral (i.t.) bzw. i.v. therapiert wurden. VSV-CD133 infizierte eine 10^4-fach größere Fläche des Tumors als MV-CD133 in dem selben Zeitraum. Auf NCH644-Zellen töteten alle Viren die Zellen dosisabhängig ab. Während MV-CD46/CD133 und MV^{SCD}-CD133 (+ 5-FC) selbst bei geringer *multiplicity of infection* (MOI) einen kontinuierlichen Rückgang der Zellzahlen im Laufe der Zeit verursachten, konnten VSV-MV Hybridviren die Zellvitalität nur innerhalb der ersten 48 Stunden nach der Infektion reduzieren. In einem orthotopen NCH644 Modell führte die Infektion der Tumore mit jeweils MV-CD46/CD133 und MV^{SCD}-CD133 (+ 5-FC) zu den längsten Überlebenszeiten im Vergleich zu Kontroll-Mäusen (*mock*). *Ex vivo "sphere formation assays"* zeigten, dass explantierte Tumorzellen, die mit den o.g. Viren infiziert wurden, im Vergleich zu den Tumorzellen der restlichen Therapiegruppen ihre Stammzell-Eigenschaften verringert oder sogar verloren hatten. Im Gegensatz dazu führte VSV-CD133 innerhalb von 10 Tagen nach der Infektion bei tumortragenden Mäusen zu schweren neurotoxischen Symptomen wie Ataxie, Tremor oder Apathie. Die Neurotoxizität zeigte sich auch bei mit VSV-CD133 intracerebral (i.c.) injizierten nicht-Tumor tragenden Mäusen sowie bei der Injektion mit nicht zielgerichtetem VSV-MV, was darauf hindeutet, dass diese Mäuse aus anderen Gründen als eine i.t. Virusamplifikation oder eine scFv-vermittelte Toxizität eine gesteigerte Letalität aufwiesen. Die Rolle des noch unbekannten neuronalen MV-Rezeptors oder eines Membranfusionsprozesses, der unabhängig von einem Kontakt mit H auftritt, müssen als mögliche Ursachen getestet werden.

Die in dieser Arbeit gezeigten Daten präsentieren nicht nur neue Konzepte und Ansätze zur Verbesserung der onkolytischen Aktivivität von CD133-spezifischen OV, sondern betonen auch die Wichtigkeit einer sorgfältigen Toxizitätsprüfung neuartiger Virustypen. In diesem Zusammenhang ist es auch wichtig zu betonen, dass vor einer klinischen Prüfung jede Modifikation, jedes Applikationsregime und jede Kombinationstherapie für jede Indikation gründlich bewertet werden müssen.

1. INTRODUCTION

1.1. Cancer Stem Cells

Therapy resistance and tumor relapses have been repeatedly linked to a small refractory and highly tumorigenic subpopulation of neoplastic cells with stem-cell like properties (Batlle and Clevers, 2017). The so-called cancer stem cells (CSC) are able to generate tumors through their stem-cell like properties such as self-renewal and extensive proliferation. The first conclusive evidence for the existence of CSCs came from acute myeloid leukemia, in which a subset of the total tumor population was capable of initiating leukemia in immunocompromised mice (Bonnet and Dick, 1997). Following this report, CSCs have been found in many solid neoplasia including cancers of breast, brain, liver and intestine (Al-Hajj et al., 2003; Singh et al., 2003; Kemper et al., 2010a). Since then, research on CSCs intensified leading to the creation of multiple tumor propagation models accounting for heterogeneity, cancer cell plasticity and differences in the ability for oncogenesis. All models suggest that continuous mutagenesis and environmental differences contribute to cancer cell heterogeneity. The phenotypic and functional differences between cells are either ascribed to a small subset of cells with tumorigenic potential (referred to as the “CSC model”, Figure 1B, upper panel) or to all undifferentiated cells within the tumor (referred to as the “clonal evolution model”, Figure 1A). Until now, it is not clear, which model applies. However, it has gradually become clear that many tumors host CSCs in dedicated niches (Matsuda et al., 2014; Calabrese et al., 2007), and yet their behavior within stem cell hierarchies seems to be more plastic and complex than initially anticipated (Kreso and Dick, 2014; Kuhlmann et al., 2016). Interaction with the tumor environment and / or (epi)genetic modification additionally contribute to tumor cell heterogeneity (referred to as “cancer plasticity model”, Figure 1B. bottom panel and Figure 2).

The CSC signature of a tumor can be determined by CSC markers. However, identifying CSCs and their niches were impeded by evidence for bi-directional transitions between tumorigenic and non-tumorigenic states and a differentially regulating tumor niche (Gupta et al., 2011; Plaks et al., 2015; Kuhlmann et al., 2016). This tumor plasticity has been approached by transition models (Figure 2). CSC marker expression between cancer subtypes or even tumors of the same subtype is not necessarily uniform in the phenotype and frequency between cancer subtypes or even tumors of the same subtype (Kreso and Dick, 2014).

Given that CSCs are the tumor-propagating cells and exhibit a high degree of resistance towards conventional therapy strategies, like radio- and chemotherapy (Magee et al., 2012; Krause et al., 2017), resulting in repopulating the tumor, they are indeed a prime target in cancer research (Pattabiraman and Weinberg, 2014).

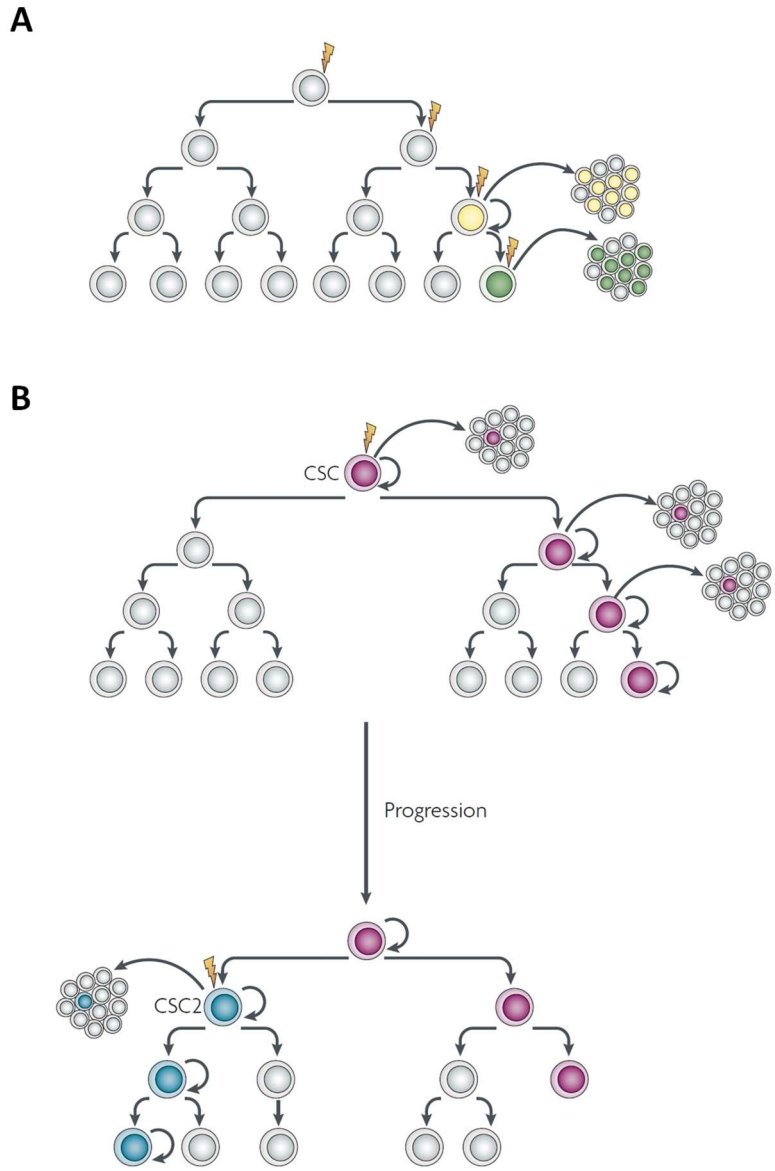

Figure 1. Models for tumor propagation
Cancer stem cells (CSCs) relate to a subset of cancer cells that has the ability to self-renew and proliferate extensively to generate the diverse cells that comprise the tumor. There are mainly two models accounting for functional heterogeneity in cancers. **(A)** In the "clonal evolution model", all undifferentiated cells have equal tumorigenic capacity creating a hierarchical organization. **(B)** In the "CSC model", the tumorigenic capacity is restricted to a distinct CSC (upper panel). To explain the intratumoral and inter-patient variability as well as kinetics of tumors, the "cancer plasticity model" was defined. It postulates that another distinct CSC (termed CSC2) may arise from tumor progression as a result from an additional mutation or epigenetic alteration. This CSC2 may drive tumor formation due to positive selection of its progenies. The tumor may become functionally different (e.g. metastasis initiating properties). The different colors indicate different cell clones with phenotypic and functional differences. The flash signs indicate mutagenic or epigenetic events. The rounded arrows indicate self-renewal capacity. Adapted from (Visvader and Lindeman, 2008).

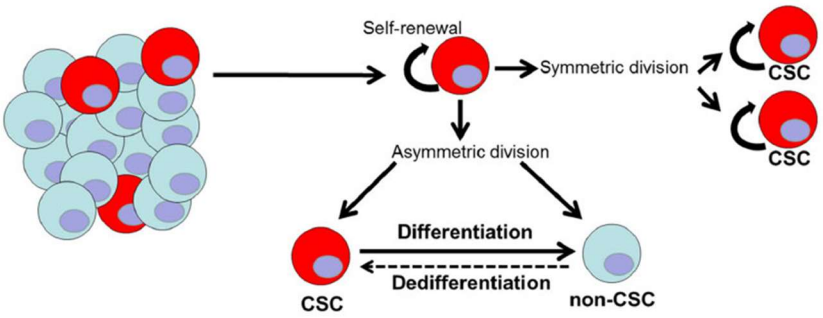

Figure 2. Transition of cancer stem cells (CSCs) to non-CSCs within the CSC model
In response to micro-environmental stimuli (e.g. inflammation, cancer therapy) tumor cells can bi-directionally transit between cancer stem cells (CSCs) and non-CSC cellular states resulting in a plasticity of the CSC pool of a tumor. The rounded arrows indicate self-renewal capacity. The light-blue cells indicate the non-CSCs of which the bulk of the tumor population (left) is composed and that can dedifferentiate to CSCs (bottom). The red cells indicate the CSCs that differentiate to form the bulk tumor (light blue cells, left and bottom). Adapted from (Kuhlmann et al., 2016).

1.2. CD133 as Marker for Cancer Stem Cells

One of many putative CSC markers used by researchers to identify and isolate CSCs is CD133, also known as prominin-1 (Figure 3) (Grosse-Gehling et al., 2013; Schmohl and Vallera, 2016). The 120 kilo Dalton (kDa) pentaspan transmembrane glycoprotein was among the first CSC marker to be discovered in solid cancers such as of the brain and of the liver to induce clinically equivalent xenografts upon transplantation (Singh et al., 2003; Singh et al., 2004; Yin et al., 2007; Brescia et al., 2012; Sun et al., 2016). Following, $CD133^{+}$ tumors were assumed to contain CSC, and thus CD133 was referred to as a CSC marker. Since its discovery, CD133 became one of the most studied and promising markers for identification and isolation of CSCs in solid cancers (Schmohl and Vallera, 2016).

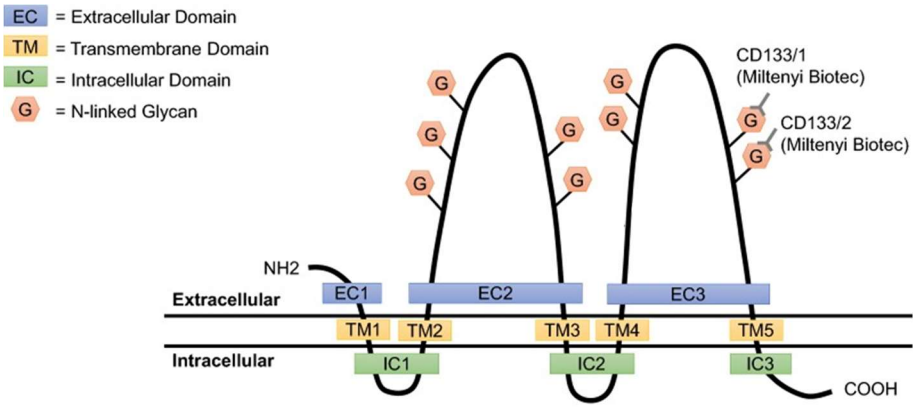

Figure 3. Schematic drawing of the CD133 topology
The CD133 glycoprotein comprises five transmembrane domains that are constituted by two large extracellular loops (EC2 and EC3). Together, they comprise nine N-linked glycan residues (depicted as G). The commonly used CD133/1 and CD133/2 epitopes for CD133 detection are located on the EC3 region of CD133. Adapted from (Glumac and LeBeau, 2018).

In the healthy organism, CD133 is mainly expressed on hematopoietic stem cells (HSCs) and endothelial progenitors, as well as on embryonic neural stem cells (NSCs), ependymal NSC in the early postnatal stage and in the adult brain, where it is localized in membrane protrusions. While the protein expression gets lost in healthy progenitor cells upon differentiation, it is expressed on cancer cells of solid tumors in varying proportions between <2 % (e.g. hepatocellular carcinoma (HCC), gastric cancer, melanoma, prostate cancer) up to 18 % (e.g. head and neck squamous cancer, ovarian cancer, pancreatic cancer). Although there is evidence for a role of CD133 in cell differentiation and epidermal-mesenchymal transition (EMT), its precise physiological function is yet unknown (Li, 2013; Schmohl and Vallera, 2016).

Detection of CD133 is done with the antibody clones AC133 or W6B3C1 (directed against epitope 1, CD133/1), or AC141 or 293C3 (directed against epitope 2, CD133/2) (Figure 3) (Bidlingmaier et al., 2008). However, genetic and epigenetic changes influence CD133 expression and therewith modify the detection with the above mentioned antibodies (Jeon et al., 2010; Kemper et al., 2010b). To date, 12 different splice variants in rodents and primates are known (Fargeas et al., 2007). Despite the limited knowledge of its function, the unique expression pattern in malignant cancers and its correlation to disease progression make CD133 is a promising marker for CSC targeted therapeutics.

1.3. Malignant Glioma

Gliomas are the most prevalent primary intracranial neoplasm in adults accounting for 30 % of all tumors and more than 80 % of all primary malignant brain tumors (Ostrom et al., 2014). As they arise from glial (progenitor) cells or stem cells that develop glial characteristics, they are classified histologically on the basis of their resemblance to different glial cell lineages. Accordingly, the major types include astrocytomas (astrocyte-derived), oligodendrogliomas (oligodendrocyte-derived) and ependymomas (ependymocyte-derived) (Aldape et al., 2015; Perry and Wesseling, 2016; Wesseling and Capper, 2018). Gliomas considerably vary in histological differentiation that correlates well with clinical course and outcome. Hence, disease grading by histology is crucial to design accurate treatment. Grading is done in accordance with the biological behavior taking into account (1) histological malignancy criteria, (2) tendency to recurrence, and (3) therapeutic response and disease progression (Wesseling and Capper, 2018). These factors have implied the definition of four World Health Organization (WHO) grades (Table 1). The histological criteria for determining the WHO grade of a tumor include, inter alia, the degree of anaplasia that is most pronounced in glioblastoma multiforme (GBM) specimens, defining it as a WHO IV grade glioma (Table 1, bottom row). On the basis of gene expression analyses, GBM can be divided into four subtypes (classical, proneural, neural and mesenchymal) (Bhat et al., 2013; Reifenberger et al., 2017). The mesenchymal expression signature has

been associated with the poorest response to radiation and most unfavorable outcome. However, plasticity between the different GBM subtypes, in particular a transition from proneural to mesenchymal transcriptome, has been described (Bhat et al., 2013).

Table 1. WHO grading system for astrocytomas

WHO grade	Histological maligancy criteria	Median survival / Recurrency
Grade I (pilocytic astrocytoma)	Slow-proliferating, well-circumscribed cystic mass	10 years / unlikely
Grade II (diffuse astrocytoma)	Moderately-proliferating, increased hypercellularity, diffuse infiltration +/- nuclear atypia	5.6 years / likely
Grade III (anaplastic astrocytoma)	Rapidly proliferating and highly invasive high rate of hypercellularity + nuclear atypia + brisk mitotic activity in oligodendroglial origin: +/- florid microvascular proliferation +/- necrosis	1.6 years / high
Grade IV (glioblastoma multiforme)	Rapidly proliferating and higly invasive extreme hypercellularity, vascular proliferation and necrosis, highly infiltrative + nuclear atypia + mitotic activity + necrosis and/or florid microvascular proliferation	12-15 months / inevitable

GBM is not only one of the most aggressive cancer types, but it is also epidemiologically significant: it is the most common malignant histology (incidence rate of 3.20 in 100,000 population per year), and one of the most devastating malignant progression having one of the worst 5-year survival rates of all human cancers (5.5 %) (Ostrom et al., 2017). Despite accurate standard of care, which implies the surgical resection followed by radiation and chemotherapy with the alkylating agent temozolomide (TMZ), most patients die within 1-2 years after diagnosis. The classical therapeutic triad has improved patients' survival significantly, with median survival of 14.6 months for those receiving the above-mentioned multimodal therapy versus 12.1 months for those receiving radiotherapy alone (Stupp et al., 2014). Nevertheless, virtually all patients eventually die of a relapse, despite of salvage treatment with the angiogenesis inhibitor bevacizumab (Quail and Joyce, 2017). In contrast, patients with low-grade astrocytoma may survive for over 10 years, however, will generally slowly progress to a higher WHO grade (Johnson et al., 2012; Louis et al., 2016).

So far, the therapeutic benefit of most of the new therapeutic directions for GBM has been very modest and often tends to fail eventually in late phase clinical trials (Buerki et al., 2018). Even the promising immunotherapeutic approach of checkpoint blockade (e.g. the checkmate-143-trial) failed to reproduce comparable striking efficacy as in melanoma (Reardon et al., 2017). Nevertheless, there are high hopes in therapeutics that encounter the challenges of the brain as relatively immune privileged organ (Buerki et al., 2018). Thus, the control of high-grade glioma continues to challenge for developing effective therapeutic strategies.

1.3.1. Relevance of CD133 in Glioblastoma Multiforme

The dismal prognosis of GBM is mainly due to near-universal tumor recurrence attributed to its highly infiltrative and proliferative growth pattern driven by glioma stem cells (GSCs) (Lathia et al., 2015). These high recurrence rates are mainly ascribed to an insufficient targeting and killing of GSCs that are resistant to conventional therapies and re-initiate neoplastic growth primarily along the resection margin (Xie et al., 2014). GSCs share many markers normally expressed by NSC such as CD133, and are able to generate renewable neuro-spheres in culture (Singh et al., 2004; Pallini et al., 2008; Zeppernick et al., 2008). Tumors containing

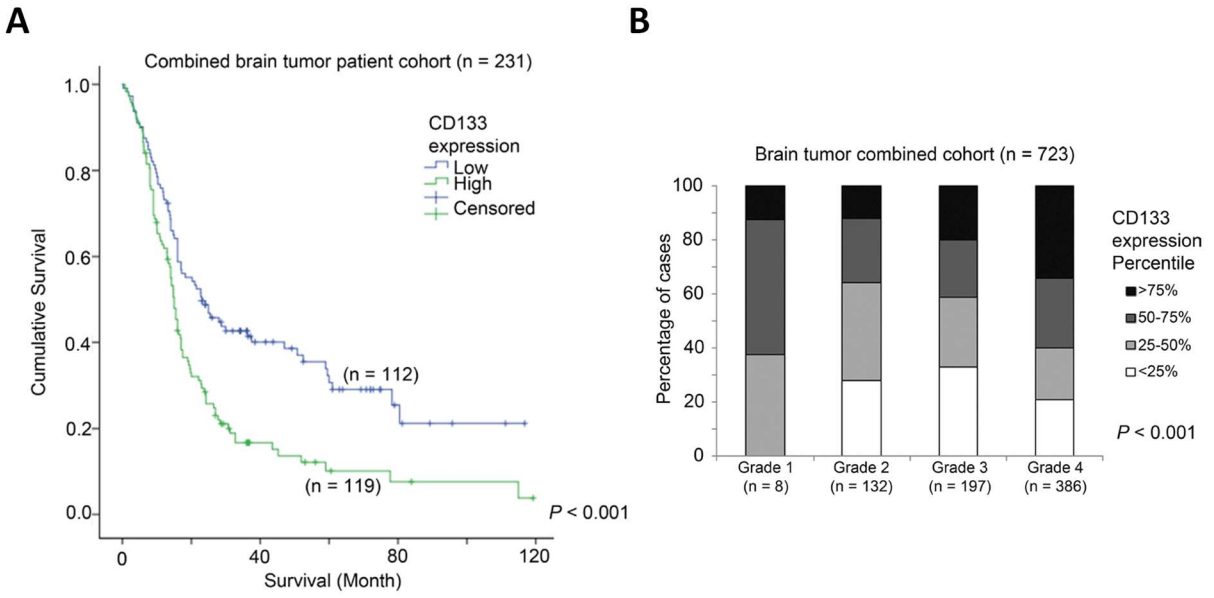

Figure 4. The association between CD133 expression and survival of glioma patients
Patients suffering from glioma were treated with the standard of care (surgical resection followed by radiotherapy combined with temozolomide). The combined brain tumor patient cohort (comprising WHO grade I to IV) was analyzed for the CD133 expression level. **(A)** Kaplan-Meier survival curves of patients' cumulative survival time suffering from glioma WHO grade I to IV expressing high or low CD133 expression levels, respectively. Patients whose tumors expressed a high level of CD133 exhibited a mean survival time of 25.7 months compared to 45.7 months for patients whose tumors expressed lower levels of CD133; $p < 0.001$. **(B)** Chi-square analysis of the association between CD133 mRNA expression and the particular tumor grade displayed as a histogram. The correlation between CD133 expression is most pronounced for WHO grade IV glioma; $p < 0.001$. Adapted from (Li et al., 2017).

≥ 2 % $CD133^+$ cells behave more aggressive, and the CD133 expression rate is related to the tumor grade (Figure 4). There is evidence by systematic meta-analysis for a strong correlation between CD133 expression in GBM and the high recurrence rates and short survival of GBM patients that is independent of tumor grade, extent of resection, or patient age (Pallini et al., 2008; Zeppernick et al., 2008; Wu et al., 2015). However, GSCs are not entirely restricted to the $CD133^+$ population, as some gliomas contain $CD133^-$ cells that otherwise fulfill the criteria for CSCs (Beier et al., 2007; Irollo and Pirozzi, 2013). In particular, $CD133^-$ cells were able to re-acquire CD133 expression *in vivo* (Chen et al., 2010; Lottaz et al., 2010). Both subtypes were comparably tumorigenic both in mice and man, but differed in proliferation index (determined by Ki-67 expression level), being higher for $CD133^+$ cells (Campos and Herold-Mende, 2011; Glumac and LeBeau, 2018). These findings raised the possibility that CD133 alone might not be a reliable universal marker for GSCs.

1.4. Hepatocellular Carcinoma

HCC is the sixth most common malignancy worldwide and the third leading cause of cancer deaths, representing approximately 5.4 % of all tumors and nearly 90 % of all primary liver tumors (Lafaro et al., 2015). Its incidence varies widely in different parts of the world, ranging from 5 cases / 100,000 inhabitants (Europe) to 15 cases / 100,000 inhabitants (Asia and Africa) (Carr, 2018). The heterogeneous global distribution is closely related to the different prevalence of the risk factors that are, amongst others, Hepatitis B virus (HBV), Hepatitis C virus (HCV), aflatoxin exposure (developing countries), smoking and cirrhosis. The latter is the most significant risk factor, accounting for almost 85 % of cases. In Western populations, HCC rarely manifests before the age of 60, however, mortality is increasing due to the high prevalence of the above-mentioned disease-associated factors (Bruix et al., 2016). Vaccination against hepatitis B virus can effectively reduce HCC incidence (Llovet et al., 2015).

Patients with HCC usually present with symptoms of cancer and liver failure unless the cancer is detected at an early stage, which usually is rather by chance (Bruix et al., 2016). Usually, every HCC in cirrhosis is preceded by multiple events of hepatocarcinogenesis to form precancerous dysplastic cirrhotic nodules as a result of chronic inflammation. The so-called high-grade dysplastic nodules (HGDN's) can eventually transform into early-stage HCC (Llovet et al., 2015). To date, the diagnosis is solely based on findings from imaging and biopsy, but still difficult to rely on due to the high intra- and internodular heterogeneity (Zucman-Rossi et al., 2015). As the severity of HCC depends not only on the tumor burden but also on the extent of co-associated liver disease and patients' performance status, multiple staging systems have been developed in the past years considering those determinants to better predict prognosis. One of them, the Barcelona Clinic Liver Cancer (BCLC) algorithm (Table 2) is the only one that

links staging with treatment, and thus is increasingly applied by clinicians (Marrero et al., 2005; Bruix et al., 2016). According to BCLC, patients can be given the treatment for a more advanced-stage tumor if they are not candidates for first-line therapy as per stage. However, although therapeutic interventions can lead to cure of early-stage disease (Table 2), the majority of HCC cases is detected in late-stage HCC for which curative options are limited (Table 2) (Bruix et al., 2016). The high mortality rate of HCC is mainly due to its high rate of recurrence, which can yet be as high as 70 % following conventional treatments, such as resection, chemotherapy, transarterial chemoembolization (TACE) and ablation (Sun et al., 2016).

There is an active search for agents that are more effective than sorafenib, a multikinase inhibitor (Bruix et al., 2016). However, till now, all tested agents failed in late-phase clinical trials to be superior to sorafenib, both in first-line and second-line settings (Wörns and Galle, 2014). Improvement can be expected from the programmed cell death protein 1 (PD1)-specific immune checkpoint inhibitor nivolumab that was approved in 2017 for the treatment of advanced-staged HCC that has relapsed after first-line regimens (Finkelmeier et al., 2018).

Table 2. Staging system for hepatocellular carcinoma

BCLC stage	Tumor burden and severity of liver disease	Therapeutical interventions	Survival
BCLC 0 or BCLC A (very early and early-stage HCC)	Solitary lesion or up to 3 nodules ≤3 cm w/o vascular invasion or extrahepatic spread with preserved liver function	Resection Transplantation Ablation#	5-year: 60 % to 80 %
BCLC B (intermediate – stage HCC)	Large, multifocal tumors w/o vascular invasion or extrahepatic spread with or without preserved liver function	TACE*	Median survival time: 28.7 months with TACE vs. 17.9 months for control after diagnosis
BCLC C (advanced-stage HCC)	Large, multifocal tumors with vascular invasion and/or extrahepatic spread mild-cancer related symptoms	Sorafenib	Median survival: 10.7 months with Sorafenib vs. 7.9 months after diagnosis
BCLC D (end-stage HCC)	Large, multifocal tumors with vascular invasion and/or extrahepatic spread poor liver function and marked cancer-related symptoms	Supportice care	Poor prognosis: 3 to 6 months after diagnosis

*if liver function is preserved; # ablation includes radiofrequency, microwaves or instillation of chemicals (e.g. ethanol)
BCLC = Barcelona Clinic Liver Cancer; TACE = transarterial chemoembolization via doxorubicin or cisplatin. Adapted from (Bruix et al., 2016)

1.4.1. Relevance of CD133 in Hepatocellular Carcinoma

The high recurrence rate of HCC is probably due to presence of undetectable micrometastasis at initial stage (Correnti and Raggi, 2017) caused by liver cancer stem cells (LCSCs) that present a subset of cancer cells with stem cell like properties (Sun et al., 2016). Poor response to sorafenib for advanced-stage tumors (Table 2) was shown to be inversely correlated with CD133 expression (Xiang et al., 2016). Therefore, CD133 was assumed to serve as marker to identify the chemoresistant LCSC population, either alone or in combination with other markers (Sun et al., 2016). $CD133^+$ cells in HCC have been reported to feature higher cell migration activity, tumorigenic capacity and more pronounced invasivity (Qiu et al., 2018). These data are in line with meta-analysis of the CD133 expression in HCC tissue specimens which revealed shorter overall survival (OS) and higher recurrence rates in patients with increased CD133 compared to patients with low CD133 expression (Song et al., 2008; Zhong et al., 2015). These studies highlighted the predictive relevance of CD133 (Figure 5). Furthermore, CD133 expression seemed to be increased in low differentiated tumors that also exhibit a loss of mature hepatocyte markers (Sun et al., 2016). Preventing the tumor-initiating potential of CSCs like the CD133 expressing subpopulation would provide novel, more efficient strategies for the treatment of HCC.

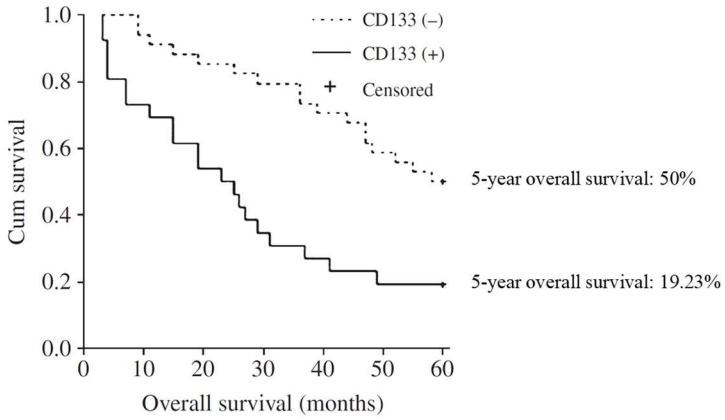

Figure 5. The association between CD133 expression and overall survival of hepatocellular carcinoma patients

Kaplan-Meier curves of the overall survival (OS) of patients suffering from hepatocellular carcinoma (HCC). Patients with increased CD133 expression had a significantly shorter OS than those with low expression. Adapted from (Song et al., 2008).

1.5. Viruses used as Oncolytic Agents

The first concept of oncolytic virotherapy emerged more than a century ago from occasional reports of cancer regressions occurring spontaneously in patients following naturally acquired viral infection or vaccination (Kelly and Russell, 2007). Based on this observation, treatment attempts were undertaken with different virus types or virus-containing body fluids. However,

success was moderate and virotherapy was associated with severe side effects. Accordingly, a lot of effort was put in to understand the mechanisms behind and achieving better and safer results. Despite this, for many years, experimentation in cancer patients did not reach good clinical outcomes and much less long-term results, which was mainly due to the fact that associated side effects prevailed oncolytic effects because technologies needed to tailor safe and effective oncolytic viruses (OVs) were lacking. Further efforts in that field sidelined in favor of conventional cancer therapeutics such as chemo- and radiotherapy, until the advent of recombinant DNA techniques and the gain of a particular understanding of molecular virology and tumorigenesis. This knowledge allowed the generation of OVs engineered on the basis of attenuated vaccine strains to increase tumor specificity and efficacy without compromising safety. Ever since, a variety of oncolytic DNA and RNA viruses have been tested in preclinical studies, with some of them being able to transition into clinical testing (Bell and McFadden, 2014). More recently, Imylgic, formerly called T-vec (talimogene laherparepvec), an oncolytic agent based on herpes virus developed by Amgen, has obtained marketing approval for the treatment of malignant melanoma (Pol et al., 2016).

Nowadays, OVs are considered as realistic alternative to conventional cancer treatments because of their inherent tumor-selective nature that is independent of various acquired resistance mechanisms and cell cycle status. As such, they specifically infect and replicate in tumor cells, eventually resulting in tumor cell lysis (Figure 6). The preference for cancer cells is due to defects in innate immune defenses, which tumor cells acquire during carcinogenesis, and importantly, is absolutely independent of the cell cycle as well as type and number of mutations. The inherent tumor selectivity can be further restricted and thus be controlled on the basis of receptor usage by genetically modified OVs that preferentially infect and destroy tumor cells of choice. The tumor cell lysis eventually results in the release of tumor antigens that can trigger an effective antitumoral immune response. As such, oncolytic virotherapies are increasingly recognized as immune therapeutics (Breitbach et al., 2016).

1.5.1. Measles Virus

Measles virus (MV) belongs to the genus *Morbillivirus* within the family of *Paramyxoviridae* of the order *Mononegavirales*. It causes systemic disease, called measles, in previously unexposed humans and old- and new-world human primates (NHPs), and is efficiently transmitted by the respiratory way. Measles is one of the most contagious infectious diseases reaching up to 90 % infection of non-immunized humans exposed to an infected individual (Naim, 2014; Laksono et al., 2016). Closely related members of the genus *Morbillivirus* include, amongst others (Figure 7), the canine distemper virus (CDV) that infects a broad range of domestic and wild carnivores (canines, mustelids like ferrets and big cats like the lion), the Rinderpest virus

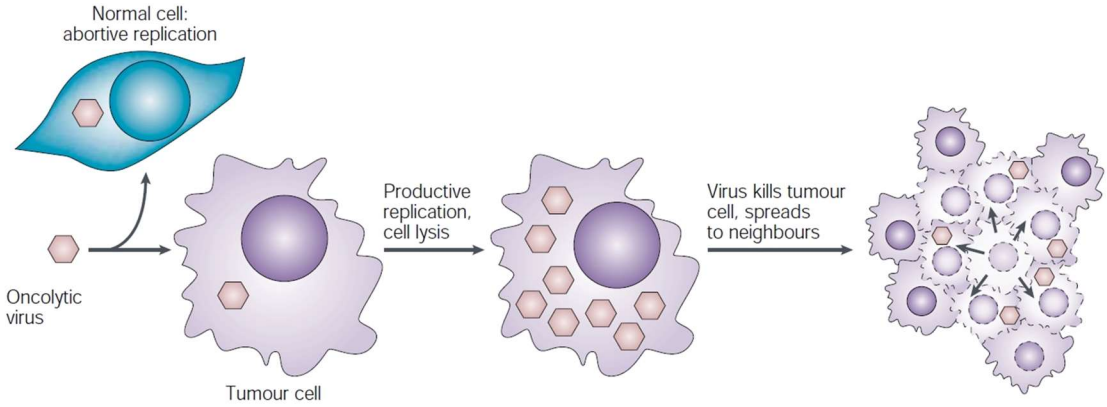

Figure 6. Oncolytic virotherapy mechanism of action
Oncolytic viruses selectively infect tumor cells leading to productive replication and eventually cell lysis (oncolysis). Viral progeny are released from lysed cells and spread to neighboring tumor cells thereby sparing normal cells. Adapted from (McCormick, 2001).

(RPV) that causes the Rinderpest in cattle (also referred to as the “cattle plague”) and the Peste-des-petits-ruminants virus (PPRV) that causes a Rinderpest-like disease in various ruminants and pigs (Vries et al., 2015). Most recently, the first feline morbillivirus (FeMV) was found in domestic cats in China. Unlike the distemper-associated viruses, FeMV seems to have tissue tropism for the urinary tract rather than for the central nervous system. Accordingly, it has been associated with feline renal disease (Amarasinghe et al., 2017).

Measles occurs worldwide and remains a leading cause of mortality, particularly among young children ≤5 years of age in developing countries, where still 115,000 to 160,000 patients die from measles every year (Holzmann et al., 2016). During the last decades, live-attenuated measles vaccine strains have been proven to be among the safest and most efficient vaccines available, and thus the availability of measles vaccination significantly decreased disease incidence and mortality rates. The present MV vaccine strain Edmonston-B (MV-Edm) that was originally isolated from an 11-year old patient with measles named David Edmonston is a laboratory passaged nonpathogenic derivative that has been safely used as vaccine conferring lifelong immunity against measles. While wild-type (wt) MV strains enter cells predominantly via the signal lymphocyte-activation molecule (SLAM or CD150) primarily expressed on activated B- and T-lymphocytes, memory lymphocytes, dendritic cells (DCs) and immature thymocytes (Tatsuo et al., 2000), MV-Edm vaccine strains can use the membrane cofactor protein (MCP, CD46) as an additional cellular receptor. CD46 is ubiquitously expressed on all nucleated cells including erythrocytes of primates and functions as inhibitor of the complement-mediated cell lysis (Fishelson et al., 2003). The entry via CD46 was acquired by multiple *in vitro* passages on CD46 expressing cells (Galanis, 2010). Both viruses, wt and MV-Edm vaccine strains utilize a third MV receptor, nectin-4 (also known as Polio-virus receptor-related 4, PVRL4), which is expressed basolaterally in the respiratory epithelium (Mühlebach et al., 2011; Noyce and Richardson, 2012).

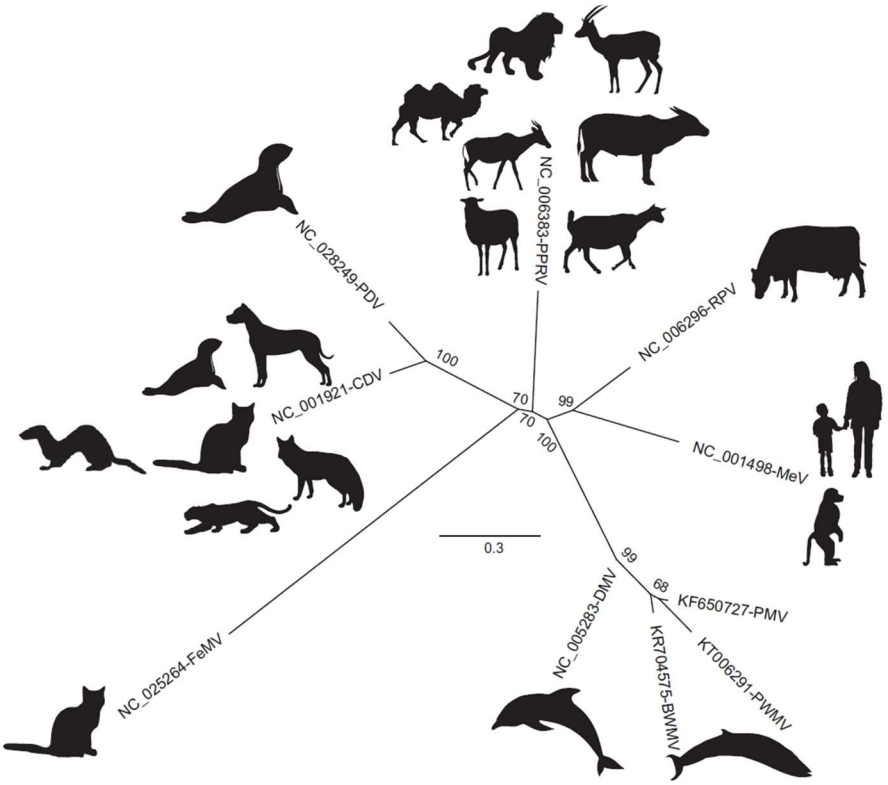

Figure 7. Phylogenetic tree of Morbillivirus genus
Maximum likelihood phylogenies of the virus species within the genus *Morbillivirus* based on representative phosphoprotein gene sequences using the Molecular Evolutionary Genetics Analysis 6 (MEGA6). The virus names and GenBank accession numbers are depicted at the branches. The numbers at the nodes represent bootstrap values (1,000 replicates). The scale bar indicates amino acid substitutions per site. CDV, *Canine distemper virus*; DMV, *Dolphin morbillivirus*; BWMV, *Beaked whale morbillivirus*; FeMV, *Feline morbillivirus*; MeV, *Measles virus*; PDV, *Phocine distemper virus*; PMV, *Porpoise morbillivirus*; PPRV, *Peste-des-petits-ruminants virus*; PWMV, *Pilot whale morbillivirus*; RPV, *Rinderpest virus*. Adapted from (Pfeffermann et al., 2018).

1.5.1.1. MV Structure and Viral Proteins

The MV particle is a pleomorphic enveloped particle with a diameter of 120 to 300 nm comprising a non-segmented, single-stranded RNA genome of approximately 16 kb in antisense orientation. There are six genes coding for eight viral proteins arranged as illustrated in Figure 8, upper panel, each flanked by gene-end and gene-start sequences. The V and C proteins are accessory proteins and encoded by the P gene. The V protein is a result of RNA editing, while the C protein is coded by an alternative reading frame. The genome arrangement is helical bearing essential similarity to that of most other members of the family *Paramyxoviridae*. The genome is tightly encapsidated by a helically arranged nucleocapsid (N protein), which is encoded by the N gene and forms the ribonucleoprotein (RNP) complex together with the RNA-dependent RNA polymerase (the large protein, L protein) and the polymerase cofactor (phosphoprotein, P protein) to ensure proper replication and transcription. The RNP complex is condensed by the hydrophobic matrix (M) protein that lines the inner side of the viral envelope. The M protein accomplishes connection between the cytoplasmic tails of the

surface glycoproteins and the RNP complex to play a supportive role in cell fusion as well as in viral particle assembly (Bhattacharjee and Yadava, 2018). By contrast, it has also an inhibitory effect on viral polymerase. The V and C proteins are non-structural proteins and as such have functional implications in the host cell: they act as virulence factors to suppress the host innate immune response by interfering with interferon (IFN) signaling pathways. The envelope surrounding the RNP complex contains two glycoproteins, the tetrameric hemagglutinin (H) protein and the trimeric fusion (F) protein, which protrude about 10-15 nm from the envelope surface, and mediate attachment and subsequent fusion with the host cell membrane. Both glycoproteins are N-glycosylated, and the type II transmembrane protein MV-H has a molecular weight of 69.1 kDa, while that of the type I transmembrane protein MV-F is 59.5 kDa (UniProtKB database, online available at www.uniprot.de). In the endoplasmic reticulum, the inactive precursor protein (F_0, 60 kDa) is synthesized and glycosylated at three sites. Biologically active F consists of two disulfide linked subunits (F_1, 40 kDa and F_2, 20 kDa), which are proteolytically cleaved from F_0 by the host ubiquitous endoprotease Furin in the *trans* Golgi network. The large F_1 protein is anchored to the membrane by a transmembrane domain, while the membrane-distal F_2 protein contains a new N-terminus, referred to as the fusion peptide (Bhattacharjee and Yadava, 2018). The particle structure of measles virus is schematically depicted in Figure 8, lower panel.

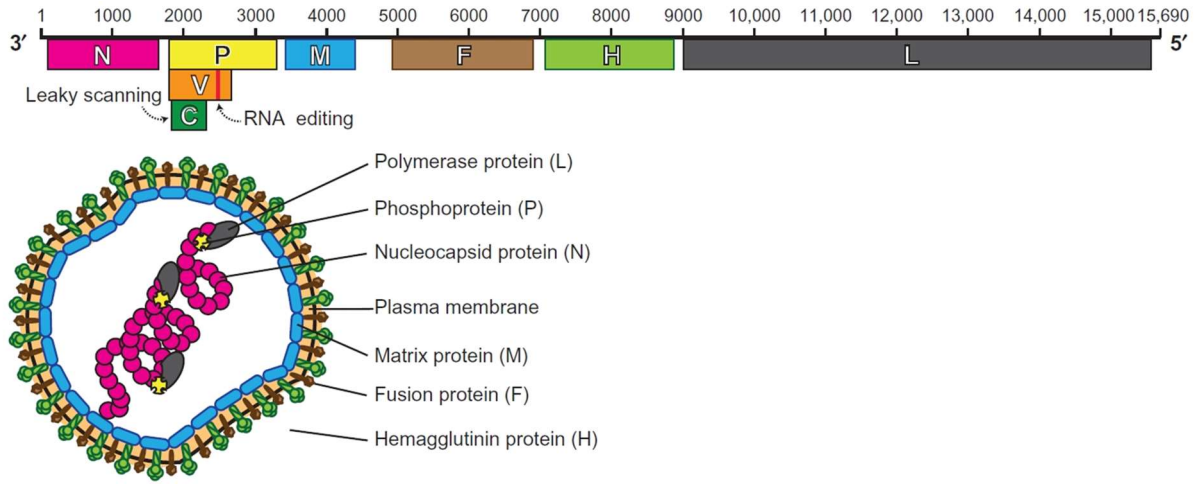

Figure 8. Genome organization and virus particle structure of Measles Virus
The single-stranded negative-sense RNA genome of measles virus (MV) (and other members of the family *Paramyxoviridae*) comprises approximately 16,000 nucleotides that are organized in six structural (N, P, M, F, H and L) and two non-structural genes (V and C). The latter genes encode the accessory V and C proteins that are transcribed from the (phosphoprotein) P gene yielding the ribonucleoprotein (RNP) complex with the (nucleocapsid) N protein encapsidated viral RNA. The MV genome is enclosed by a pleomorphic envelope that is composed of the hemagglutinin (H), the fusion protein (F), the matrix protein (M) and lipids from the host cell membrane. Adapted from (Pfeffermann et al., 2018).

1.5.1.2. Measles Virus Life Cycle

Upon attachment of the viral particle via the H protein to a receptor positive host cell, the trimeric F protein undergoes conformational changes that initiate the fusion with the host cell membrane (Bhattacharjee and Yadava, 2018). Therewith, the fusion peptide plays a major role by actively bringing the membranes of both, the viral particle and the host cell, into close proximity that eventually leads to membrane fusion (Plemper, 2011). Along with the process of fusion, the RNP complex is released into the cytoplasm. The RNP complex serves as a template for the viral polymerase that starts at a non-coding leader, from the 3´-end to continue transcription of six expression cassettes for eight viral proteins to the 5´-end that is terminated by a non-coding trailer. As the expression cassettes start with an initiation and end with a poly-A termination sequence, respectively, mRNAs are sequentially transcribed from each cassette. Thus, the resulting protein amount is governed by a transcriptional gradient from N protein to L protein. The transcribed mRNA is translated into proteins by using the host translation machinery, while the viral polymerase also synthesizes complementary positive strand from negative-sense genome for replication of more genome copies. Following the process of transcription and replication, for each newly generated viral particle a complete single-stranded genome in anti-sense orientation associates with newly synthesized N, P and L proteins to form the RNP complex. This in turn is connected by the M protein to the cytoplasmic tails of H and F proteins. All components are assembled for generation of progeny viral particles and released from the infected cell by budding from the cell membrane (Jiang et al., 2016; Bhattacharjee and Yadava, 2018). The MV replication cycle is schematically depicted in Figure 9.

Although the released viral particles are fully infectious and can infect neighboring cells, MV can also spread efficiently from cell-to-cell, provided that adjacent cells express one of the MV receptors to induce fusion. This Paramyxovirus-specific mechanism is due to fully functional glycoproteins on the cell membrane and can lead to the formation of multinucleated giant cells, termed syncytia (Griffin et al., 2012). Other previously discovered attachment receptors are the C-type lectins DC-specific intercellular adhesion molecule-3-grabbing on-integrin (DC-SIGN) and Langerin, expressed on DCs and Langerhans cells, respectively. DC-SIGNs are thought to “capture” MV particles and facilitate SLAM-mediated virus-to-cell fusion of DCs or lymphocytes (Laksono et al., 2016).

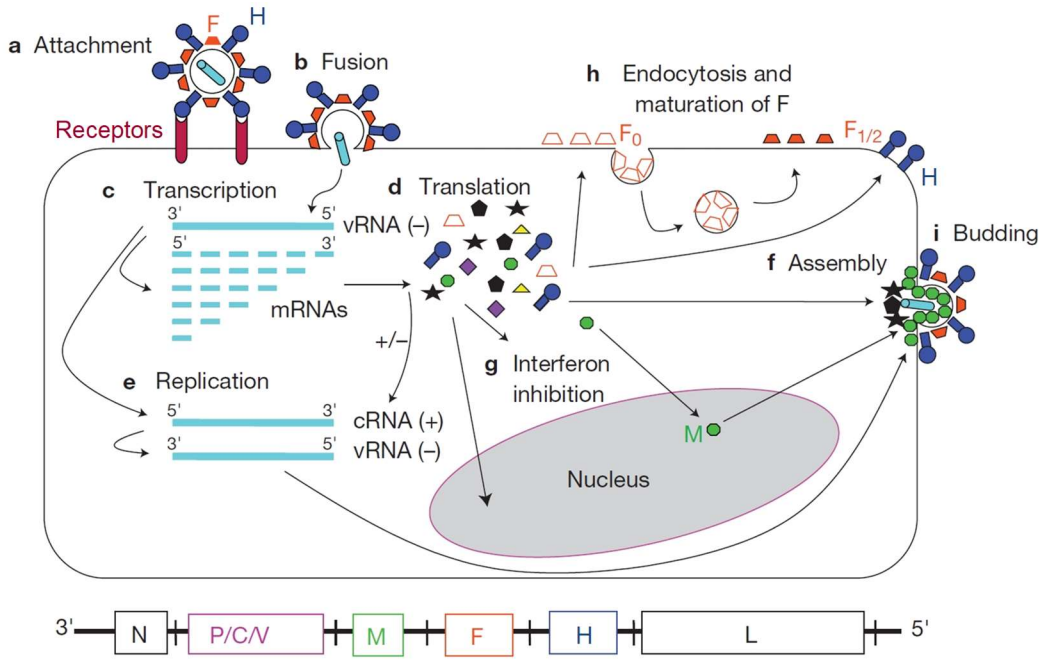

Figure 9. Measles Virus replication cycle
After attachment of the viral particle by the hemagglutin (H) protein to a measles virus (MV) receptor **(a)** and subsequent entry that is mediated by the fusion (F) protein **(b)**, the MV's ribonucleoprotein (RNP) complex, which is formed by the nucleoprotein (N), the phosphoprotein (P) and the large (L) protein, is liberated into the cytoplasm. The viral polymerase initiates the transcription of the negative RNA genome [vRNA (-)] into viral mRNAs following a 3´ to 5´ attenuation gradient from N to L **(c)**. While the transcribed viral mRNAs are translated into proteins **(d)**, the vRNA (-) also functions as a template for cRNA (+). This in turn is a template for vRNA (-) genomes during replication **(e)**. New vRNA (-) genomes are incorporated into new virions during viral assembly **(f)**. Various viral proteins that are newly translated **(d)** operate in interferon (IFN) signaling pathways **(g)**. The precursor F protein (F_0) is endocytosed and matured ($F_{1/2}$) **(h)**. The assembly of the RNP complex and the glycoproteins H and F are orchestrated primarily by the M (matrix) protein **(f)**, and result in the budding and release of fully infectious virions **(i)**. Adapted from (Aguilar and Lee, 2011).

1.5.1.3. Measles Virus Pathogenesis

MV is transmitted via the respiratory route by aerosols or respiratory droplets. Due to it lymphotropic nature MV spreads from the respiratory tract to local lymphoid tissue including peribronchial lymphoid tissue and local draining lymph nodes. In these tissues the virus initially infects cells SLAM$^+$ lymphocytes, DCs and macrophages, followed by massive replication in these cells and subsequent transport to secondary lymphoid tissue, e.g. bronchus-associated lymphoid tissue (BALT) and trachea-bronchial lymph nodes. This phase takes approximately 10-14 days and is clinically inapparent. Subsequently the virus is systemically spread via the blood and lymphatics to more distant lymphoid tissues, e.g. the thymus, spleen, gastrointestinal tract and peripheral lymph nodes. This event coincides with a fever spike of more than 40 °C that, together with cough, coryza and conjunctivitis, and belongs to the onset of the prodrome. Virus amplification in lymphoid tissues results in a drastic leukopenia, which is aggravated by peripheral blood mononuclear cell (PBMC) sequestration in these tissues and inhibition of lymphocyte proliferation along with virus-induced cell death (Pfeffermann et al.,

2018). Shortly afterwards the three “C”, the measles hallmark Koplik spots on the buccal mucosa and maculopapular skin rash appear to start behind the ears and spread to the face, trunk and extremities. In healthy patients, this phase comes along with MV-specific immune responses that result into clearance of infectious virus, although RNA remains detectable for months after infection. While dissemination occurs via the infection of SLAM$^+$ cells, viral shedding occurs by apical release of viral particles by nectin-4$^+$ cells that are infected from the basolateral side by SLAM$^+$ cells or directly by SLAM$^+$ lymphocytes through damaged epithelium. The latter one can induce cough thereby enhancing the discharge of aerosols containing MV particles. Besides the receptor-mediated mechanisms, receptor-independent entry-mechanisms are assumed to take place, although these are less efficient (Laksono et al., 2016).

In most cases, these robust immune responses lead to a complete resolve without complications, accompanied by life-long immunity to measles (Laksono et al., 2016). In contrast, the concomitant immune suppression usually persists several months after infection, incapacitating the immune system to respond adequately to other immune stimuli increasing the risk for opportunistic or secondary infections (Pfeffermann et al., 2018). In rare occasions, mainly in immune-compromised patients, the virus can remain persistent and infect the central nervous system (CNS) (Griffin, 2014). The most incident CNS complication is acute disseminated encephalomyelitis (ADEM), which accounts for 1:1000 patients. ADEM is accompanied by demyelination, which can cause ataxia, motor and sensory loss and mental status changes and death. Measles inclusion body encephalitis (MIBE) is another feared CNS complication after wt MV infection or live-virus vaccination occurring in patients with congenital or acquired immunodeficiency. It is characterized by mental status change and focal seizures and progresses rapidly to coma and death in the majority of patients. The rarest neurological complication of measles is subacute sclerosing panencephalitis (SSPE), and its onset is at higher risk when MV infection occurs at a very young age (about 1 in 2,500 children who develop measles before the age of five). However, it develops several years after an infection with wt MV, and clinically appears with behavioral changes, myoclonic seizures, ataxia and death within one to three years. While there is evidence for endothelial-mediated CNS infection and non-productive trans-neuronal spread via interconnected processes *in vitro* and *in vivo*, the conclusive explanation of the underlying mechanisms of persistence and CNS infection remain to be elucidated (Ludlow et al., 2015; Laksono et al., 2016; Griffin et al., 2018).

1.5.1.4. Oncolytic Measles Virus

First reports documenting tumor regressions in the setting of natural MV infection date back to the seventies, and provided evidence of MV activity in Burkitt's lymphoma, Hodgkin lymphoma and leukemia (Bluming and Ziegler, 1971; Mota, 1973). Since this finding, the increasing understanding of the context of MV and cancer facilitated the rationale for the design of modified MV for the treatment of cancer leading to multiple clinical studies (Robinson and Galanis, 2017). Since then, oncolytic MV strains derived from attenuated vaccine lineage strains were used in numerous clinical trials to assess their safety and oncolytic activity against different cancer entities. The first clinical trial using the unmodified attenuated MV-Edmonston Zagreb (MV-EZ) strain for the treatment of cutaneous lymphoma demonstrated clinical evidence of treatment in five of six treated patients after multiple intratumoral injections (Heinzerling et al., 2005; Msaouel et al., 2018). In recent trials, oncolytic MVs are based on the molecular clone MV-NSe (NSe = NarI- and SpeI-eliminated), which is derived from the MV-Edmonston B vaccine strain (Radecke et al., 1995), and genetically modified to express thyroidal sodium iodide symporter (MV-NIS) or carcinoembryonic antigen (MV-CEA) to non-invasively monitor MV activity. CEA is expressed in the embryonic development, but can be upregulated in certain tumor types, and thus functions as a tumor marker. As MV-CEA infected cells secrete CEA into the serum, it can be used as a reporter for viral gene expression. This can also be achieved using the NIS transgene by administration of Tc99m or ^{124}I and subsequent computed tomography/single-photon emission computed tomography (CT/SPECT) or γ-camera imaging. The antitumoral activity of NIS expressing MVs can further be augmented by utilizing an ionizing radiation treatment with the β emitter ^{131}I (Penheiter et al., 2012). To date, the clinically most successful outcome was achieved for two patients suffering from multiple myeloma after a systemic injection of a high MV-NIS dose that led to a complete and durable response in one of the patients (Russell et al., 2014). Promising therapeutic responses were also demonstrated for solid tumors such as ovarian cancer (Galanis et al., 2015) and GBM (ClinicalTrials.gov Identifier: NCT00390299).

The extraordinary tumor tropism of MV-Edm based OVs can be explained by the additional usage of CD46 as entry receptor and its high expression levels on tumor cells of various tumor entities. Besides, oncoselection is determined by defects in the innate antiviral immune responses on the level of the virus' post entry steps in malignant cells (Guillerme et al., 2013).

1.5.2. Vesicular Stomatitis Virus

Vesicular stomatitis virus (VSV) is an enveloped non-segmented negative-stranded RNA virus of the genus *Vesiculovirus* of the family *Rhabdoviridae* within the order *Mononegavirales*. A closely related member of the same virus family is the Rabies Lyssavirus belonging to the

genus *Lyssavirus* that causes invariably fatal encephalitis (rabies) (Walker et al., 2018). Wt VSV is transmitted by insect vectors (arthropod-borne virus) to livestock (cattle, pigs, horses) in which it causes non-lethal febrile illness with blister-like lesions of the oral cavity, feet and teats. Among nine confirmed strains of VSV, two strains, the New Jersey (VSV-NJ) and the Indiana (VSV-I) strain cause sporadic disease in cattle in the United States. Due to its clinical similarity to the vesicular stomatitides (World Organization for Animals Health (OIE), 2013, VS General Disease Information Sheet. Retrieved from http://www.oie.int/animal-health-in-the-world/technical-disease-cards/), it is considered a differential diagnosis in disease diagnostic work-up of regulatory agencies with Foot-and-Mouth Disease Virus (FMDV) being the most important (Kleinlützum et al., 2013). Serological evidence suggests that VSV is capable of infecting wild mammals, birds and reptiles in endemic regions (Kumar et al., 2018). Unlike livestock, infections are asymptomatic to mild febrile associated with mild blister-like lesions in the head region in humans and limited to agriculture and laboratory workers. To date, only one case of VSV-mediated non-lethal encephalitis is known (Felt and Grdzelishvili, 2017) and thus is only considered a minor zoonosis (OIE 2013). The pantropism of VSV can be explained by the widespread expression of low-density lipoprotein receptor (LDLR), which was recently identified as entry receptor for VSV in human and mouse cells (Finkelshtein et al., 2013).

1.5.2.1. Vesicular Stomatitis Virus Structure and Viral Proteins

VSV particles display the bullet morphology characteristic for members of the family *Rhabdoviridae* (Bishnoi et al., 2018). Assembled virions are approximately 70 nm wide and 200 nm long (Ge et al., 2010) and contain the small RNA genome of VSV comprising of 11,616 nt encoding five proteins in the order of 3'-leader - Nucleocapsid protein (N) - Phosphoprotein (P) - Matrix protein (M) - Glycoprotein (G) - Large polymerase protein (L) – trailer-5' (Bishnoi et al., 2018). While the mRNAs for N, M, G and L are each translated into a single protein, the mRNA for P is translated into three proteins with the major translation product of this mRNA being the P. The negative-sense virus genome is completely coated by the N protein, which constitutes the RNP complex in conjunction with the L and the P protein, and is responsible for both viral transcription and replication. The RNP complex is covered by a lipid envelope that is derived from the host cell plasma membrane and is densely decorated with approximately 1200 identical copies of the G protein. The receptor recognition and fusion activities are governed by the G protein while the M protein is essential for virus assembly, budding, cellular apoptosis and disruption of the host-cell innate-immune response (Lichty et al., 2004). The latter role of the M protein is genetically separated from its role in viral assembly and budding and essential for replication in infected cells (Jayakar et al., 2000). The VSV particle structure is schematically depicted in Figure 10.

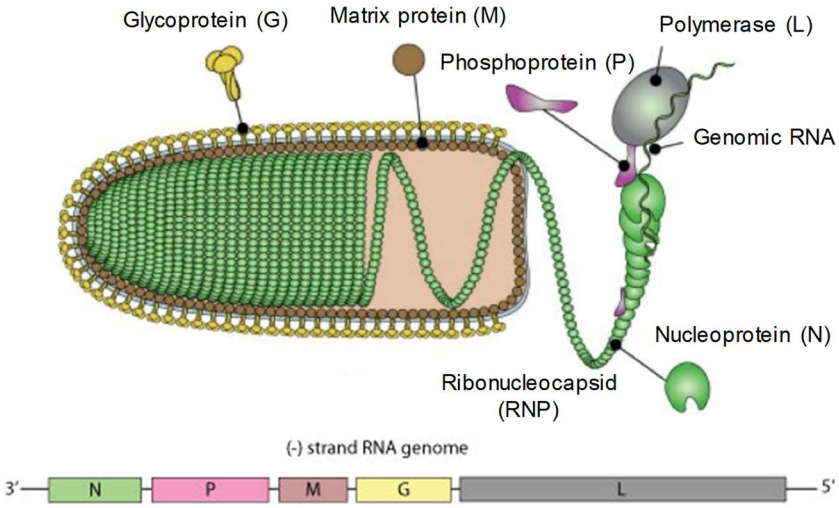

Figure 10. Genome organization and structure of Vesicular Stomatitis Virus
Vesicular Stomatitis Virus (VSV) virions exhibit a bullet-shaped form and comprise a single ss(-)RNA genome, the five viral proteins N (nucleoprotein), P (phosphoprotein), M (matrix protein), G (glycoprotein), L (polymerase), and a lipid envelope. Adapted from the Swiss Institute of Bioinformatics.

1.5.2.2. VSV Viral Life Cycle

The attachment and fusion to host cells via the ubiquitously expressed LDLR is mediated by the G protein, followed by a receptor-mediated endocytosis and internalization into endosomes (Melzer et al., 2017). Following endocytic entry, acidification (pH <6.2) triggers conformational change in the G protein to induce fusion of the viral envelope with the endosomal membrane, followed by release of the viral RNP into the cytosol (World Scientific (Firm), 2015). The latter infection status can be detected already 20-30 min after binding of the virus. Primary transcription of viral mRNA from the input template is initiated by the viral RNA-dependent RNA polymerase (RdRp) complex, followed by translation by the host translational machinery mRNAs to generate the viral proteins including N, P and L proteins. While the latter proteins compose the replicase complex carrying out replication of the input viral genome for multiplication of progeny genomes, newly generated M protein interferes with cellular antiviral immunity facilitating unimpeded viral replication. The newly synthesized ss(-)RNA genome then undergoes secondary transcription for replication rounds. Finally, viral proteins and genomic RNA assemble in the cytosol prior to transportation to the plasma membrane for M protein assisted virus budding and release (World Scientific (Firm), 2015). The VSV replication cycle is schematically depicted in Figure 11.

Unlike Paramyxoviruses, the mRNA synthesis occurs throughout the host cell cytosol in inclusion bodies. In common with MV, replication in the VSV life cycle underlies a sequential transcriptional gradient from N protein to L protein with the N protein being the most abundant (Stojdl et al., 2003; Melzer et al., 2017).

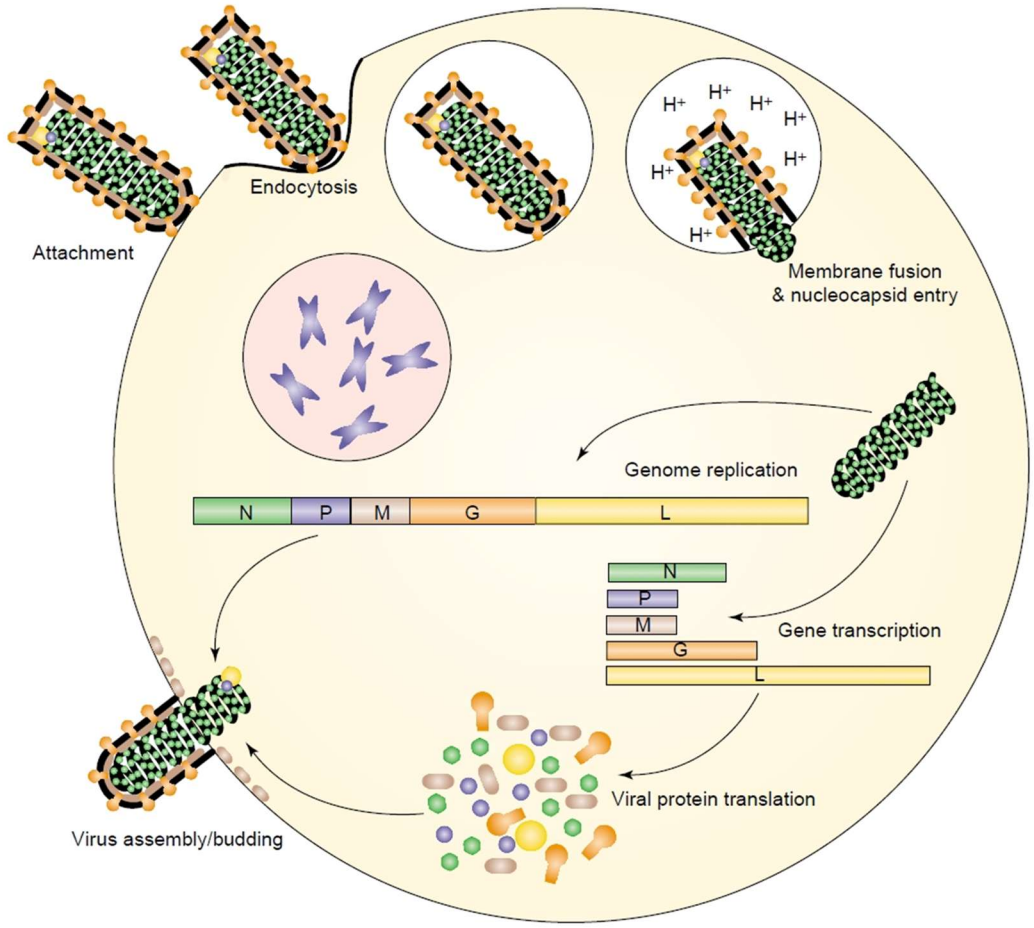

Figure 11. The life cycle of Vesicular Stomatitis Virus
Vesicular stomatitis viral (VSV) particles attach host cell surface by the glycoprotein (G) of VSV, followed by endocytosis and cellular endosomal trafficking that eventually leads to the release of the VSV nucleocapsid (N) into the cytosol. The N protein initiates transcription of mRNAs for each gene, which are translated by the host translational machinery. Following replication of viral proteins and VSV genomic copies through positive strand intermediates, these components assemble into virions that bud at the cell plasma membrane. Adapted from (Lichty et al., 2004).

1.5.2.3. Oncolytic Vesicular Stomatitis Virus

VSV is among the most rapidly cytopathic viruses in mammalian cells. Its cytotopathic effects (CPE) are characterized by cell rounding and eventual cell lysis that are both associated with apoptosis. The induction of apoptosis by VSV is based on both the death receptor and the mitochondrial apoptotic pathways. The latter one is activated by the shut-off of host cell gene expression by the viral M protein (Redondo et al., 2015). There are several factors that make VSV a promising oncolytic agent that include, amongst others, (1) the lack of pre-existing immunity against VSV, (2) an easy to manipulate genome, (3) a high sensitivity to IFN, (4) strong lytic properties and (5) a short replication cycle (1 to 2 h in tumor cells) that leads to high titres (VSV-wt can yield up to 10^9 pfu/ml) in a broad range of cell lines allowing large-scale production of virus. One of the distinctive features of VSV is its pantropism, whilst being tremendously

oncoselective. This is a result of the differential IFN-associated antiviral immune responses of normal and malignant cells that render the latter ones susceptible to oncolysis by VSV. As such, the majority of normal cells are able to inhibit viral replication prior to potential initiation of cell damage (Felt and Grdzelishvili, 2017). However, in some IFN competent tissues, such as non-malignant tissues and some malignant tissues (e.g. head and neck cancer) unmodified VSV is able to antagonize IFN signaling pathways through the actions of the M protein (Bishnoi et al., 2018). As a result, VSV can cause neurotoxicity that can be clinically apparent as viral encephalitis upon experimental infection of rodents (Hastie et al., 2013; Felt and Grdzelishvili, 2017). As the off-target toxicities in non-malignant tissue, particularly the neurovirulence of VSV, are primarily mediated by G and partly by the M protein, they can be addressed by making alterations of the encoding genes using molecular techniques such as reverse genetics tools (Bishnoi et al., 2018). These alterations enable the generation of safer and more efficacious recombinant VSVs that are, amongst others (Felt and Grdzelishvili, 2017),

(i) attenuation of VSV through disruption of normal gene order (van den Pol and Davis, 2013);
(ii) using semi-replicative VSV (Muik et al., 2012).
(iii) mutating or ablating the VSV G protein (VSVΔG) to limit / direct VSV tropism (Ayala-Breton et al., 2012; Ammayappan et al., 2013);
(iv) encoding mutant M protein unable to inhibit antiviral response in normal IFN competent cells while retaining oncolytic capacity in IFN-deregulated tumor tissue (Fang et al., 2012);
(v) pseudotyping VSV with MV envelope glycoproteins (VSV-FH) to inhibit VSV neurotropism (Ayala-Breton et al., 2013; Ayala-Breton et al., 2014); and
(vi) using VSV encoding IFNβ to attenuate viral replication in normal IFN competent cells and stimulate antitumor immunity (Patel et al., 2015; Zhang et al., 2016).

Many of these recombinant oncolytic VSV virotherapeutics have shown promising results in preclinical studies (Felt and Grdzelishvili, 2017). Among these, VSV-IFNβ is the first OV to be tested in a phase I clinical trials for the treatment of sorafenib-refractory HCC (ClinicalTrials.gov Identifier: NCT01628640). Due to its excellent safety, it was additionally armed with the NIS to harness for non-invasive virus tracking and enhanced oncolysis through the use of radioisotopes (ClinicalTrials.gov Identifier: NCT02923466).

1.6. Targeted Oncolytic Measles Virotherapy

Besides exploiting the inherent oncoselectivity of MV, target cell selection can further be restricted or redirected to tumor cells by rational engineering at the level of receptor recognition and cell entry. Due to the functional separation of target cell attachment and fusion, the glycoprotein complex of paramyxoviruses is very amenable for engineering receptor usage (Aref et al., 2016). On the level of fusion, this can be done by replacing the cleavable site of the F

protein by any sequences of choice (e.g. matrix metalloprotease, MMP) to achieve replication in tumor tissues that abundantly secrete the particular protease (Springfeld et al., 2006; Bhattacharjee and Yadava, 2018). On the level of attachment, targeting can be modified by engineering the H protein to restrict infection to cell types defined by a cell surface marker of choice. In particular, tumor-specific targeting ligands are displayed on H along with the introduction of mutations ablating entry through the natural receptors CD46 and SLAM. This strategy resulted in oncolytic MVs that exclusively infect cells that express the cognate antigen on their cell surface. The first breakthrough of fully retargeted oncolytic MV was achieved in 2005 by fusing a single chain antibody (scFv) specific for CD38 or epidermal growth factor receptor (EGFR) to the ectodomain of the H-protein to obtain fully CD38 or EGFR retargeted MVs. To overcome associated detrimental effects on virus rescue, a 6-histidine tag was incorporated at the N terminus of the retargeted H for easy rescue on Vero cells stably expressing a scFv against 6-His (Nakamura et al., 2005). Since then, the methodology was used to prove targeted MV glycoproteins specific for different cell surface markers in the context of lentiviral vectors (LV), which can be generated and tested for functionality much faster than recombinant MVs (Buchholz et al., 2015; Frank and Buchholz, 2019).

The MV envelope retargeting system can be exploited to generate OVs that specifically eliminate CSCs, e.g. $CD133^+$ tumor cells (Bach et al., 2013) capable of initiating new tumor growth and tumor recurrence after conventional therapy (Tong and Qian, 2014). Furthermore, MVs can be genetically modified to further augment the inherent oncolytic effects. Modifications include the delivery of (i) suicide genes that encode enzymes able to convert a non-toxic prodrug into a cytotoxic compound, (ii) immunomodulatory genes, which stimulate an antitumoral immune response, or render an immunosuppressive microenvironment responsive to therapies, and (iii) tumor-suppressor genes, which induce apoptosis in cancer cells (Kane et al., 2015).

1.6.1. CD133-Targeted Oncolytic Measles Virus

On the basis of the MV envelope retargeting approach oncolytic MVs have been generated that specifically recognize and infect $CD133^+$ cells that are considered CSCs. As such, CD133-retargeted MVs are meant to eradicate the small and highly refractory tumorigenic subpopulation that is responsible to repopulate a tumor following cytoreductive treatment (Figure 12).

To achieve selectivity to CD133, MV-H was blinded for its native receptors by introducing four mutations at the residues interacting with the MV receptors (*detargeting*). The targeting domain CD133-specific scFv (H-CD133scFv) was genetically fused to the mutant MV-H (*retargeting*). More precisely, the scFv-reading frame was cloned from the hybridoma cell line HB-12346 that produces antibodies against CD133/2, clone AC141.7) (Figure 3) (Funke et al., 2008; Anliker

et al., 2010). *In vitro*, MV-CD133$^{141.7}$ (hereinafter referred to as MV-CD133) turned out to exclusively infect cells that express CD133 on their cell surface and to mediate cell lysis through MV-specific cytopathic effects (CPEs). Compared to non-targeted MV, MV-CD133 was shown to be more effective in killing CD133$^+$ HCC after subcutaneous and intraperitoneal engraftment in nonobese diabetic/severe combined immunodeficient (NOD/Scid) mice, respectively. MV-CD133 also exerted stronger antitumoral activity in orthotopic GBM and primary colon cancer. In each of the tested tumor models, survival of mice treated with MV-CD133 was prolonged as compared to non-targeted MVs. In contrast, MV-CD133 and MV-NSe infected only a few CD133$^+$ HSCs but these cells did not give rise to productive infection (Bach et al., 2013).

The oncolytic activity of MV is at least in part based on cell killing by syncytia formation that requires close proximity between target receptor positive cells. However, in the patient, CD133$^+$ tumor cells might be scarce in tumor tissue and thus may present a major challenge for the cell-associated killing mechanisms of MV-CD133. Another pitfall poses the non-neoplastic tumor stroma that acts as physical barrier to the dissemination of OVs (Wojton and Kaur, 2010). To tackle these potential challenges, CD133-retargeted viruses can further be modified to enhance the antitumoral activity. This can be achieved by enhancing receptor engagement through the use of non-mutated H protein to expand tropism to CD46$^+$ tumor cells (Anderson et al., 2004). Another strategy are arming technologies that are based on the expression of a protein by the OV that elicit enhanced cytotoxicity, e.g. the MV-NIS (chapter 1.5.1.4). Another strategy is the expression of the suicide gene cytosine deaminase and uracil phosphoribosyltransferase (SCD) derived from yeast, which catalyze the conversion of the anti-mycotic drug 5-Fluorocytosine (5-FC) into the highly cytotoxic agent 5-Fluorouracil (5-FU). Importantly, cytotoxic effects are not restricted to infected cells but can also evolve in neighboring cells as 5-FU and its metabolites are able to diffuse across membranes without relying on gap junctional transport ("bystander effect") (Kane et al., 2015). Untargeted MV armed with the SCD (MV^{SCD}) proved superior to unarmed MV in xenograft models of HCC, cholangiocarcinoma and ovarian carcinoma, (Lampe et al., 2013; Lange et al., 2013; Hartkopf et al., 2013) and proved excellent safety in mice and rhesus macaques (Völker et al., 2013). The oncolytic activity of MV can also be enhanced by exchanging the P gene with that from wt MV (MV$_{Pwt}$-GFP-). MV encoding the P gene products (P/V/C proteins) have been shown to circumvent the IFN-mediated antiviral immune responses in some tumors translating in an improved efficacy in a myeloma xenograft model (Haralambieva et al., 2007).

To unify the advantages of both viruses, MV and VSV, the MV-H scFV display technology was used to retarget VSVΔG to cancer cells expressing EGFR, folate receptor or prostate-specific membrane antigen (PSMA) (Ayala-Breton et al., 2012). Compared to targeted MV, these hybrid viruses exhibit faster replication kinetics, stronger CPE and can be produced at higher titres (Ayala-Breton et al., 2012; Ayala-Breton et al., 2013).

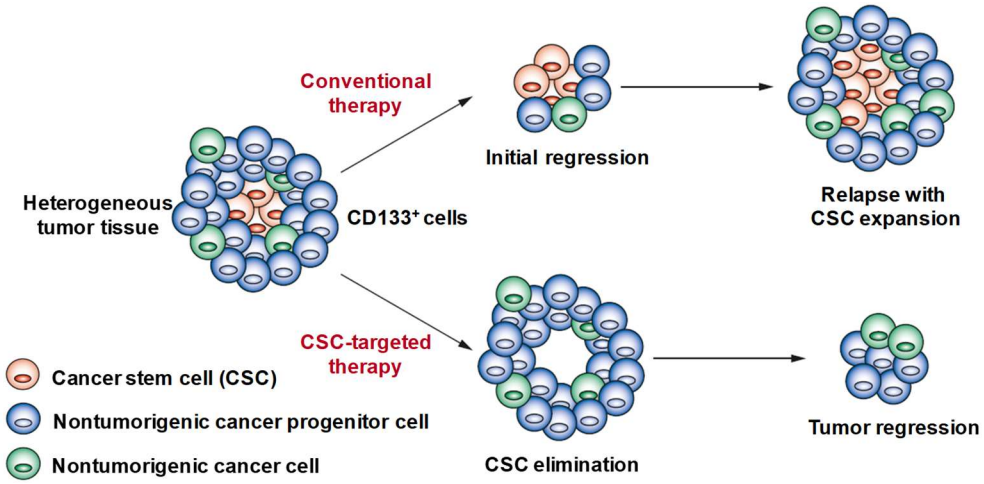

Figure 12. Therapeutic implication of cancer stem cell diversity in a tumor
Conventional cancer therapy (e.g. radiotherapy, chemotherapy) may shrink the tumor initially by destructing the tumor bulk, alleging full tumor regression. Putative cancer stem cells (CSCs) may survive after therapy and re-constitute the tumor if they are less sensitive to these therapies (upper panel). By contrast, CSC-targeted therapies might be more effective against the tumor by specifically eliminating the fraction of CSCs. These therapies render the tumor unable to self-renew and proliferate and may eventually lead to full tumor regression (lower panel).

1.7. Objective

Based on the observations demonstrated by Bach et al., (Bach et al., 2013) the objectives of this thesis were to further enhance the oncolytic activity of CD133-targeted OVs without having to compromise on safety. To address these objectives, the following genetic modifications were pursued:

(i) arming SCD to obtain destruction of $CD133^-$ tumor tissue, and augment direct virus-mediated cytotoxicity on $CD133^+$ tumor cells (MV^{SCD}-CD133).
(ii) exchanging the P gene with that from wt MV (MV^{Pwt}-CD133), which are known to exhibit reduced IFN sensitivity and diminished capacity to induce IFN (Haralambieva et al., 2007).
(iii) extending receptor usage to CD46 by omitting implementation of ablation mutations for the natural receptors of MV (MV-CD46/CD133) to combine the inherent tropism of MV-NSe for the natural MV receptors, and the CD133-selective infection of MV-CD133.
(iv) pseudotyping of VSVΔG with the MV H-CD133scFv protein (VSV-CD133) to exploit VSV kinetics.

These OVs were comparatively analyzed for their oncolytic activity on two neoplastic $CD133^+$ cell lines, the immortalized HCC cell line HuH7 and primary cells derived from a patient who had suffered from GBM. Additionally, the OVs were examined for their safety on non-malignant human HSCs with respect to off-target toxicity that may result in myelosuppression in treated patients.

In the first part, the OVs were characterized *in vitro* with regard to specificity for target cells, replication kinetics and toxicity towards non-malignant target receptor positive HSCs, as well

as time and dose dependent killing capabilities. To directly quantify the bystander effect of MV^{SCD}-CD133 + 5-FC on $CD133^-$ cancer cells, virus-mediated and bystander-mediated cytotoxicity on a mixed culture were measured by discriminating exposed cells according to their cell surface receptor expression.

In the second part, the OVs were tested in a mouse subcutaneous HuH7 xenograft model for their oncolytic activity after multiple intratumoral and intravenous dosing regimens, respectively. The tumors had to be explanted and analyzed for their intratumoral virus spread.

In the third part, the OVs were studied for their oncolytic activity in a mouse orthotopic glioma xenograft model. This was performed by stereotactically implanting cells that were infected as single cell suspensions *in vitro* prior to implantation in order to exclude possible detrimental effects of Vero-αHis lysate on cell viability. Besides monitoring animal survival, the therapeutic effect was evaluated by determining the residual self-renewal and proliferative capacity of explanted cells in the residual post-treated tumor masses. Additionally, this was qualitatively assessed by pathohistology on a random basis. To validate the oncolytic activity of the OVs in a clinically more relevant orthotopic glioma xenograft, in a next step, tumors were intratumorally treated after intracranial stereotact-assisted tumor development.

A particular focus in the intracranial models was given to the development of potential neurotoxicity that was further evaluated by intracranial stereotact-assisted injection of the respective OVs in naïve mice (that do not bear a tumor).

Ultimately, the novel recombinant CD133-targeted OVs were tested for their oncolytic activity in two different preclinical models to allow an assessment of the therapeutic potential and clinically relevant limitations.

2. MATERIAL AND METHODS

2.1. Materials

2.1.1. Consumables

Name	Supplier
4-0 thread suture material (VICRYL rapide)	Ethicon, Johnson & Johnson Medical GmbH
Black-opaque-walled tissue culture plates (96-well) with clear bottoms and lid (Cellstar)	Greiner Bio-One
Bottle top filters 500 ml, SFCA/CN; 0.45 µm, 0.2 µm	Nalgene, Thermo-Fisher Scientific
Cell culture dishes (5 cm, 10 cm, 15 cm)	Greiner Bio-One
Cell scraper, fixed	Techno Plastic Products AG
Cell strainer; 70 µm, 100 µm	BD Biosciences
Cryo freezing container (with isopropyl alcohol)	Nalgene
Cryo tubes, sterile (2 ml)	Greiner Bio-One
Disposable scalpel blade	Bruno Bayha GmbH
Disposable scalpels	Aesculap AG, Braun Medical
DURAN® laboratory glassware	SCHOTT
FACS tubes	BD Biosciences
Falcon tubes, sterile (15 ml, 50 ml)	Greiner Bio One
Gas Permeable adhesive plate seal, sterile	VWR
GentleMACS C Tubes	Miltenyi Biotec
Hybond ECL, nitrocellulose membrane	Amersham, GE-Healthcare
Hybond-P, PVDF membrane	Amersham, GE-Healthcare
HyperfilmTM ECL films	Amersham, GE-Healthcare
Insulin syringes, 29G (0.5 and 1.0 ml)	Becton Dickinson
Micro centrifuge tubes (1.5 ml, 2 ml)	Eppendorf
Micronic tubes	Micronic
Microplates 96-well, round-bottom	Nunc, Thermo Fisher Scientific
Needle (27 gauge) Sterican®	Braun Medical
Disposable counting chamber, KOVA Glasstick™ Slide 10 with grids	KOVA
Pasteur pipettes, glas	VWR
Pipette tips (filter tips) (10 µl, 100 µl, 200 µl, 1000 µl)	Nerbe Plus GmbH
Reagent reservors	Nalgene
Serological pipettes (2 ml, 5 ml, 10 ml, 25 ml)	Greiner Bio-One
Slides, SuperFrostTM Ultra Plus	Menzel

Name	Supplier
Syringe (1 ml, 2 ml, 5 ml, 10 ml, 20 ml)	Braun Medical
Syringe filters, Minisart PRFE (0.45 µm, 0.2 µm)	Sartorius
Tissue Culture flask (T25)	Sarstedt
Tissue Culture flask (T25, T75, T125)	Greiner Bio-One
Tissue Culture Plates (6-, 12-, 24-, 48-, 96-well)	Thermo Fisher Scientific
Tissue, Cell-Tork	Tork
Whatman paper	Whatman

2.1.2. Chemicals and Reagents

Name	Supplier
Acrylamide bisacrylamide solution	Carl Roth GmbH
Ammonium persulfate (APS)	Carl Roth GmbH
BD Safety-Lock™ blood collection and infusion set, 23 G butterfly	BD Medical
Bit_{100} Supplement	Provitro
Destilled water	Paul Ehrlich Institute
Dimethylsulfoxide (DMSO)	Sigma-Aldrich
Dithiothreithol (DTT)	Sigma-Aldrich
DMEM/Ham´s F12 (1:1)	Gibco, Life Technologies
Donkey serum	Gibco
Dulbecco's Modified Eagle Medium (DMEM) High Glucose	Sigma-Aldrich
Entellan® Rapid Embedding Agent	Electron Microscopy Sciences
Eosin	Carl Roth GmbH
Ethanol	Paul Ehrlich Institute
Ethylenediaminetetraacetic acid (EDTA)	Paul Ehrlich Institute
Ethylenediaminetetraacetic acid (EDTA)	Paul Ehrlich Institute
Fetal calf serum (FCS)	Biochrom
Fluoroshield with DAPI® mounting medium	Sigma-Aldrich
Formaldehyde solution 37 %	Carl Roth GmbH
Formalin	Carl Roth GmbH
G418 Geneticin	Invitrogen
Glycine	Carl Roth GmbH
H2O (tissue culture grade)	Sigma-Aldrich
Hanks' Balanced Salt Solution (HBSS) w/o MG2+/Ca2+	Sigma-Aldrich
Hanks' Balanced Salt Solution (HBSS) with MG2+/Ca2+	Sigma-Aldrich
Hematoxylin	Carl Roth GmbH
Human epidermal growth factor (EGF) 0,1 mg/ml	PeproTech

Name	Supplier
Human fibroblast growth factor (FGF)-basic 0,1 mg/ml	PeproTech
Human Thrombopoeitin (TPO)	PeproTech
hydrochloric acid	Carl Roth GmbH
Hydrogen Peroxide (H_2O_2)	Carl Roth GmbH
Isopropyl Alcohol	Paul Ehrlich Institute
L-glutamine	Sigma-Aldrich
Liquid Nitrogen	Paul Ehrlich Institute
Methanol	Carl Roth GmbH
MethoCult GF H4434 medium	Stem cell technologies
N,N,N´,N´-Tetramethyl-ethylendiamin (TEMED)	Carl Roth GmbH
OCT-Medium (Tissue-Tek)	Sakura Finetek
OptiMEM	Gibco, Life Technologies
Paraffin	Vogel GmbH
PBS (w/o MG^{2+}/Ca^{2+})	Lonza
Penicillin-Streptomycin-Fungizone	PromoCell
Prestained Plus Protein Ladder	Fermentas
Roti-Histofix, 4 % and 10 %	Carl Roth GmbH
Skim milk pulver	Carl Roth GmbH
Sodium Azide 10 mM	Sigma-Aldrich
Sodium Chloride (NaCl)	Sigma-Aldrich
Sodium lauryl sulfate (SDS), 10 % solution	Paul Ehrlich Institute
StemSpan™ CC100	Stem cell technologies
StemSpan™ Serum-Free Expansion Medium (SFEM)	Stem cell technologies
Target Retrieval solution 10x	Dako
Thrombopoietin (TPO)	Peprotech
Tris(hydroxymethyl)aminomethan (Tris), pH 6.8	Carl Roth GmbH
Tris(hydroxymethyl)aminomethan (Tris), pH 8.8	Carl Roth GmbH
Triton™ X-100	Sigma-Aldrich
Trypsin	Paul Ehrlich Institute
Tween®-20	Sigma-Aldrich
Urea, p.a.	Sigma-Aldrich
VP-SFM	Thermo Fisher Scientific
Xylene	Carl Roth GmbH

2.1.3. Buffers and Media

Name	Composition
1x Blotting buffer	48 mM Tris-HCl, 39 mM Glycine, 20 % Methanol
2x Urea sample buffer	200 mM Tris-HCl, 8 M Urea, 5 % SDS, 100 mM EDTA, 0.03 % Bromphenol blue, 1.5 % Dithiothreithol, pH 8.0
FACS Dissociation-Buffer	0.25 % Sodium Azide and 4 mM EDTA in PBS w/o MG2+/Ca2+
FACS-Fix	1 % Formaldehyde in PBS w/o MG2+/Ca2+
FACS-Wash	2 % FCS in PBS w/o MG2+/Ca2+
Freezing medium	10 % dimethylsulfoxide (DMSO) in FBS
MethoCult GF H4434 medium	Supplemented with 2 mM L-glutamine and 0.5 % Penicillin-Streptomycin-Fungizone
Plaque Agarose	DMEM and Agarose (1:1)
SDS running buffer	25 mM Tris, 192 mM Glycine, 1 % SDS in H20
StemSpanTM Serum-Free Expansion Medium (SFEM)	Supplemented with 2 mM L-glutamine and 0.5 % Penicillin-Streptomycin-Fungizone
Succrose 30 %	20 % Sucrose in PBS w/o MG2+/Ca2+
Suspension buffer	2 mM EDTA and 2 % FCS in in PBS w/o MG2+/Ca2+
TBS	50 mM Tris, 150 mM NaCl in H20
TBS-T	0.05 % Triton in TBS
TBS-T	0.1 % Tween®-20 in TBS (pH 7.4)
Transfer buffer	48 mM Tris, 39 mM Glycine, 20 % Methanol in H20 (pH 7.4)
Trypsin working solution	2 mM EDTA, 0.25 % Trypsin-Melnick in PBS w/o MG2+/Ca2+

2.1.4. Commercially available Kits

Name	Version	Supplier
Adobe Photoshop	cs6	Adobe ®
Axio Vision	4.8	Carl Zeiss
BD FACSDiva	6.0	BD Biosciences
CellProfiler	2	Broad Inst. Imaging Platform
Ctavi	3.4	Swiss Academic Software
FCS-Express	V4	De Novo Software
GraphPad Prism	5.4	Graph Pad Software
Microsoft Office	2010, 2016	Microsoft®

2.1.5. Antibodies

Name	Application	Dilution	Supplier
Donkey α-mouse-Cy5	IF	1:200	Jackson ImmunoResearch
Donkey α-rabbit-Cy2	IF	1:200	Jackson ImmunoResearch
FcR blocking reagent (human, mouse)	FC	1:10	Miltenyi Biotec
Goat α-rabbit HRP	WB	1:2000	Dako
Mouse α-human CD133/1 APC / PE (AC133)	FC	1:10	Miltenyi Biotec
Mouse α-human CD133/1 pure (W6B3C1)	IF	1:20 (5 µg/ml)	Miltenyi Biotec
Mouse α-human CD133/2 APC / PE (AC141)	FC		Miltenyi Biotec
Mouse α-human CD46 FITC (REA312)	FC	1:10	Miltenyi Biotec
Mouse IgG1 isotype PE / APC	FC (isotype control for mouse α-hCD133/1 and hCD133/2 antibodies)	1:10	Miltenyi Biotec
Mouse IgG1 pure	IF (isotype control for mouse α-hCD133/1 pure)	1:200	Miltenyi Biotec
Rabbit α-GFP	IF	1:200	Invitrogen
Rabbit α-MV-F	WB	1:4000	Abcam
Rabbit α-MV-H-Cyt	WB	1:1000	Abcam
Rabbit α-MV-N	WB	1:1000	Novus Biologicals
Rabbit α-VSV serum	WB	1:1000	Hoffmann et al., J Gen Virol 2010
REA control (S) FITC (recombinant human IgG1)	FC (isotype control for mouse α-hCD46 FITC ab)	1:10	Miltenyi Biotec

α = anti-; APC = allophycocyanin; Cy = cyanine dye; FcR = Fc receptor; FITC = fluorescein thiocyanate; GFP = green fluorescent protein; h = human; IF = immunofluorescence; IgG = immunglobulin G; MV = Measles Virus; PE = phycoerythrin; VSV = Vesicular Stomatitis Virus; WB = western blot.

2.1.6. Cell Lines

Cell line	Characteristics	Medium	Split ratio	Source
CHO-CD133	CHO-K1 cells stably expressing CD133	DMEM, 10 % FCS, 2 mM L-glutamine, 10 µg/ml puromycin	2x 1:12	Kleinlützum et al., 2017
CHO-CD46	CHO-K1 cells stably expressing CD46	DMEM, 10 % FCS, 2 mM L-glutamine, 10 µg/ml puromycin	2x 1:12	Manchester et al., 1994
CHO-K1	Ovarian epithelial cells from Cricetulus griseus	DMEM, 10 % FCS, 2 mM L-glutamine	2x 1:12	ATCC CCL-61
CHO-SLAM	CHO-K1 cells stably expressing SLAM	DMEM, 10 % FCS, 2 mM L-glutamine, 10 µg/ml puromycin	2x 1:12	Tatsuo et al., Nature 2000
HT1080	Human fibrosarcoma cells	DMEM, 10 % FCS, 2 mM L-glutamine	2x 1:12	ATCC CCL-61
HT1080-CD133	Human fibrosarcoma cells	DMEM, 10 % FCS, 2 mM L-glutamine, 0.5 mg/ml G418	2x 1:12	Abel, 2013, Doctoral thesis
HuH7	Human hepatocellular carcinoma cells	DMEM, 10 % FCS, 2 mM L-glutamine	2x 1:8	JCRB JTC-39
hHSCs	Human hematopoietic stem cells	SFEM (thawing medium), SFEM supplemented with 1 % CC100 and 2µl/ml TPO (activation medium); MethoCult GF H4434 medium, 2 mM L-glutamine, 0.5 % Penicillin-Streptomycin-Fungizone (CFA)	1 – 2x 1:2	Blood donation center in Frankfurt
KM-H2	Human Hodgkin lymphoma cells	Cryosections 8 µm for IF establishment	n.a.	Hanauer, 2018, Doctoral thesis
NCH644	Human primary glioma cells	DMEM/Ham´s F12 (1:1), 2 % L-glutamine, 20 % BIT_{100} Supplement, 20 ng/ml hEGF, 20 ng/ml hFGF-basic	1 – 2x 1:2	Prof. Christel Herold-Mende, University Heidelberg
Vero-αHis cells	Kidney epithelial cells from Cercopithecus aethiops expressing αHis6-tag scFv displayed on the PDGFR TM domain	DMEM, 10 % FCS, 2 mM L-glutamine	2x 1:12	ATCC®CCL-81TM

α = anti-; CD(digit) = cluster of differentiation; CFA = colony-forming assay; CHO = Chinese hamster ovary; h = human; PDGFR = platelet-derived growth factor receptor; scFv = single chain variable fragment; SLAM = signaling lymphocyte activation molecule; TM = transmembrane

2.1.7. Viruses

Name	Nomenclature	Description	Source
MV-CD133	MV-NSe-scFvCD133$^{141.7}$-GFP	MV-NSe retargeted to epitope 141.7 of CD133 using anti-CD133-scFv fused to a mutant H protein. Encodes a GFP gene in the ATU(N).	Bach et al., 2013
MV-CD46/CD133	MV-HNSe-scFVCD133$^{141.7}$-GFP	MV-NSe retargeted to epitope 141.7 of CD133 using anti-CD133-scFv fused to a non-mutant H protein. Encodes a GFP gene in the ATU(N).	Kleinlützum et al., 2017
MV-NSe	MV-NSe-GFP (N)	MV laboratory strain derived from the Edmonston B vaccine strain. Encodes a GFP gene in the ATU(N).	Martin et al., J Virol 2006
MV^{Pwt}-CD133	MV-NSe-Pwt-scFvCD133$^{141.7}$-GFP	The P gene of MV-CD133 is exchanged against the P gene from a wt MV strain. Encodes a GFP gene in the ATU(N).	Kleinlützum et al., 2017
MV^{SCD}-CD133	MV-NSe-scFvCD133$^{141.7}$-SCD	MV-CD133 encodes a SCD gene in the ATU(N) instead of a GFP gene in the ATU(N).	Völker, 2013, Doctoral thesis
VSV-CD133	VSV-FH-scFvCD133$^{141.7}$	VSV-MV retargeted to epitope 141.7 of CD133 using anti-CD133-scFv fused to a mutant H protein. Encodes a GFP gene at position 7.	Kleinlützum et al., 2017
VSV-MV	VSV-FH (VSV-MV)	Chimeric VSV that encodes MV-F and MV-H at position 4 and 5 instead of the VSV-G glycoprotein at position 4. Encodes a GFP gene at position 6.	Kleinlützum et al., 2017

2.1.8. Medicals and Anesthetics

Name	Composition / Dose	Supplier
5-Fluorocytosine (Ancotil®)	200 mg/kg body weight (i.p.) twice per week	Meda Pharma
Carprofen (Rimadyl®)	5 mg/kg body weight	Zoetis GmbH
Isoflurane	Induction with 3-4 %, maintenance with 2 %	CP-Pharma
Ketamine (Ketavet®)/Xylazine (Rompun®)	Ketamine (100 mg/kg body weight), Xylazine (4 mg/kg body weight)	Warner-Lambert AG, Bayer AG
Lubricating eye Gel (Corneregel®)	Cornea gel applied peri-operative	Bausch + Lomb
PVP Iodine (Braunol®)	According to surgical site	B. Braun Melsungen

2.1.9. Instruments

Name	Model	Manufacturer
Cell incubator	BRD6220	Heraeus Thermo Scientific
Centrifuge	Multifuge X3, Multifuge 3	Heraeus Thermo Scientific
Cryostat	CM1850	Leica
Digital caliper	PRECISE PS 7215	Burg Wächter
Flow cytometer	MACSQuant Analyzer 10	Miltenyi Biotec
Fluorescence microscope	Axiovert 200	Carl Zeiss
Fluorescence microscope with optical sectioning unit	Axio Observer X1 (motorized) with ApoTome	Carl Zeiss
Freezer -20 °C	Comfort	Liebherr
Freezer -80 °C	Hera freeze	Heraeus Thermo Scientific
Fridge 4 °C	Comfort	Liebherr
Gel electrophoresis system	n/a	Bio-Rad
Gel electrophoresis system	Model B3	Owl Separation Systems
GentleMACS™ Dissociators	n.a.	Miltenyi
Hamilton syringe 25 µl	1702 RN Neuros Syringe	Miltenyi
Ice machine	n.a.	Ziegra
Infiltrator	STP-120	Mikrom
Laminar Flow Cabinet Class II	SterilGARD® III Advance	The Baker Company
Light microscope	Axiovert 25	Carl Zeiss
Luminescence detection system	Fusion FX7	Vilber Lourmat
Magnetic stirrer	n.a.	Leica
Micropipettes	Research plus®	Eppendorf
Microplate luminometer	Microlumat Plus LB 96V	Berthold Technologies
Microtiter plate (ELISA) reader	n.a.	Multiskan
Mini-Protean Tetra Handcast System	Tetra Cell	Bio-Rad
Multichannel pipettes	Finnpipette F2	Thermo Scientific
Pipetboy	Accu-jet®	Brand
Precision scale	Scout Pro	Ohaus
Roller mixer	SRT6	Stuart
Rotation microtome	RM 2255	Leica
Semi-dry blotter	Transfer Cell SD	Bio-Rad
Shaker	n.a.	Biometra
Shaver	VET Isis GT420	Aesculap
Small animal anesthetic device	Indulab-vet	HME-Highland Medical Equipment
Stereotact injector	UMP3	Stoelting Co.
microsyringe pump controller	Micro 4™	WPI GmbH

Name	Model	Manufacturer
Surgical Instruments	Bone scissors, forceps (Straight, curved, angled, serrated), needle holder by Mathieu, scissors (Sharp-Blunt, Sharp)	Fine Science Tools GmbH
Thermomixer	Comfort	Eppendorf
Vortexer	Vortex Genie 2	Scientific Industries Inc.
Water bath	n.a.	GFL

2.1.10. Software

Name	Version	Supplier
Adobe Photoshop	cs6	Adobe ®
Axio Vision	version 4.8	Carl Zeiss
BD FACSDiva	6.0	BD Biosciences
CellProfiler	2	Broad Inst. Imaging Platform
Ctavi	6	Swiss Academic Software
FCS-Express	V4 and V6	De Novo Software
GraphPad Prism	5.4	Graph Pad Software
Microsoft Office	2010, 2016	Microsoft®

2.2. Protein Biomedical Methods

2.2.1. Sodium Dodecyl Sulfate-Polyacrylamide Gel Electrophoresis

Sodium dodecyl sulfate polyacrylamide gel electrophoresis (SDS-PAGE) is a commonly used method to separate proteins according to their molecular mass by electrophoresis. The amphiphilic detergent SDS denatures proteins and coats amino acids conferring a negative charge to the linearized protein. The denatured linearized protein migrates to the anode when applied to an electrical field. This way, the protein spectrum of a sample can be separated by the gel matrix of a polyacrylamide gel according to their molecular mass. For this purpose, the gels were prepared according to Table 3 and casted as follows. 3 ml of the 8 % or 10 % separation gel was poured between the glass plates. The cast was overlaid with isopropyl alcohol until complete polymerization of the separation gel to ensure an even and a smooth surface. After removal of isopropyl alcohol, the 5 % stacking gel was casted onto the separation gel. To obtain sample pockets a 1.5 mm spacer with 10 lanes was placed between the glass plates. After polymerization the gels were used directly or stored at 4 °C for up to one week.

Table 3. Formulation of SDS-polyacrylamide gel

Reagent			Separating gel		Stacking gel
			8 %	10 %	
30 %	**acrylamide solution**		4.8 ml	6.0 ml	1.5 ml
	H_2O		6.2 ml	5.0 ml	5.7 ml
1 M	**Tris, pH 8.8**	[375 mM]	6.8 ml		----
1 M	**Tris pH 6.8**	[190 mM]	----		1.7 ml
10 %	**SDS**	[0.1 %]	180 µl		90 µl
	Color	(red)	----		20 µl
20 %	**APS**	[0.1 %]	90 µl		45 µl
	TEMED	[0.04 %]	7 µl		4 µl

Virus stocks (5.0×10^5 $TCID_{50}$: MV-NSe, MV-CD133, MV^{Pwt}-CD133, MV^{SCD}-CD133, MV-CD46/CD133; $2.5 \times 10^5 TCID_{50}$: VSV-MV and VSV-CD133) were mixed with urea sample buffer 2x in equivalent amounts. Samples were incubated 10 min at 95 °C and cooled down on ice. The gels containing 10 % acrylamide was used for the detection of the MV-H and MV-F glycoproteins and the N protein, while the gel containing 8 % acrylamide was used for the detection with α-VSV serum. The 8 % acrylamide gel allowed a more distinct separation of the heterogeneous protein composite to be detected with the α-VSV serum. 3 µl Prestained Plus Protein Ladder and 40 µl of samples were loaded on polyacrylamide gels in an assembled gel-electrophoresis chamber filled with SDS running buffer (chapter 2.1.3). Initially, the gel was run at

80V until the samples entered the separating gel and then set on 120 V for approximately 90 min until the bromophenol blue front left the stacking gel.

2.2.2. Immunoblot

For detection of specific proteins in the samples separated by SDS-PAGE, the gels were applied to a semi-dry blot apparatus. Whatman paper layers and a nitrocellulose membrane were soaked with 1x blotting buffer. The nitrocellulose membrane was placed on three layers of Whatman paper and covered with the polyacrylamide gel which was carefully flattened to avoid air bubbles. The gel was covered with three other layers of Whatman paper. The gel was blotted for 90 min at max. 24 V and 0.18 A. Successful transfer of proteins to the membrane was recognized by the colored protein marker. The membrane was washed once with TBS-T and then transferred to TBS-T with 5 % skim milk pulver and incubated for 1 hour at room temperature (or overnight at 4 °C) to block unspecific binding sites. Afterwards the membrane was transferred to TBS-T containing 5 % skim milk pulver and the respective dilution of the primary antibody (chapter 2.1.4) and incubated overnight at 4 °C. Next, the membrane was washed three times with TBS-T and then transferred to TBS-T containing 5 % skim milk pulver and the respective dilution of the secondary antibody (chapter 2.1.4). After 1h of incubation (or overnight at 4 °C), the membrane was washed three times with TBS-T. For signal detection the Pierce ECL Plus Western Blotting Substrate was prepared according to manufacturer's protocol and given onto the membrane. A luminescent image was acquired using exposure times ranging from 3 seconds to 10 min on Hyperfilm™ ECL films.

2.3. Cell Culture and Virological Methods

Cells were monitored regularly by microscopy for any abnormality regarding their morphology and growth characteristics as an indication for bacterial or fungal contamination and to verify cell line characteristic phenotype. Cells were regularly checked for mycoplasma contamination by PCR. Viruses and cells were handled using sterile standard techniques and were only opened below laminar flow class two cabinets. All viruses were handled under biosafety level 2 conditions as authorized by the Regierungspräsidium Darmstadt, Germany.

2.3.1. Cultivation of Cell Lines

Adherent cell lines

Cells were cultivated in the appropriate medium (chapter 2.1.6) in a humidified cell culture incubator at 37 °C, 5 % CO_2 and 90 % humidity. Culture vessel size was chosen according to the demand. Volumes of medium were 5 ml for T25-, 10-12 ml for T75- and 20 ml for T175-tissue culture flask. Cells were splitted two to three times per week (before reaching full confluence). Adherent cells were washed with PBS and detached using trypsin working solution (chapter 2.1.3). Cells were resuspended in fresh pre-warmed medium and the appropriate fraction of cell suspension was transferred into a new cell culture vessel containing fresh pre-warmed cell culture medium.

Primary glioma sphere cells

The primary glioma sphere cells NCH644 were cultured in 5-7 ml of the appropriate medium (chapter 2.1.6) in uncoated T25 tissue culture flasks for suspension cells. Culture flask were positioned upright to avoid attachment. Medium was replenished 2 times per week by carefully removing 3-4 ml of supernatant medium and adding the same amount of fresh, pre-warmed medium.

If the mean diameter of spheres reached approximately 200 µm and above, cells were splitted (1-2 times per week). The complete content of the cell culture vessel was transferred into a 15 ml Falcon tube and centrifuged (300 x g, 5 min, 10 °C). After removing the supernatant, the cell pellet was resuspended with 1 ml of fresh pre-warmed medium until achieving a single cell suspension. A 1:2 fraction of the cell suspension was transferred to a new cell culture flask and fresh pre-warmed medium was added to a volume of 5 ml.

2.3.2. Freezing and Thawing of Cells

Adherent cell lines

Cells were treated as described in chapter 2.3.1 up to and including the resuspension step. Cells were centrifuged (800 rpm, 4 min, 4 °C) and the cell pellet was resuspended in pre-cooled freezing medium and aliquoted in cryo tubes. Aliquots were frozen at -80 °C using a 5100 Cryo Freezing container. The following day, cryo tubes were transferred to the gas phase of liquid nitrogen at approximately -160 °C for long-term storage.

Frozen cells were thawed rapidly at 37 °C in a water bath and immediately resuspended in 3 ml pre-warmed cell culture medium. The cell suspension was transferred into a fresh cell culture vessel containing 5 ml of the appropriate pre-warmed cell culture medium. Cells were

incubated as described in chapter 2.3.1. Between 8 and 16 hours later, medium was fully exchanged without washing the cells. Thereafter, cells were continued to be cultivated.

Primary glioma sphere cells

Cells were treated as described in chapter 2.3.1 up to and including the resuspension step, but with resuspending in 2 ml PBS instead of medium. Cells were strained through an equilibrated 70 µm Cell strainer into a new 50 ml Falcon tube and the filter was washed with 8 ml PBS. Cells were counted and centrifuged (300 x g, 5 min, 4 °C). The cell pellet was resuspended in the appropriate amount of pre-cooled freezing medium to obtain 1.0 – 2.0 x 10^6/ml per cryo tube. Cells were further handled as described above for adherent cells.

Frozen cells were thawed rapidly at 37 °C in a water bath and transferred immediately to a 15 ml Falcon tube containing 5 ml fresh pre-warmed medium. Cells were centrifuged (300 x g, 5 min, 10 °C) and the supernatant was completely removed. Cells were resuspended in fresh 5 ml pre-warmed medium and centrifuged for further two times to completely remove FCS. The cell pellet was resuspended in 1 ml fresh pre-warmed medium and transferred to a new T25-tissue culture flask. Cells were cultivated as described in chapter 2.3.1.

2.3.3. Isolation and Cultivation of Human CD34$^+$ Cells

Primary human CD34$^+$ cells derived from granulocyte colony-stimulating factor (G-CSF) mobilized peripheral blood were obtained from anonymous stem cell donors from the blood donation center in Frankfurt. The donors gave written consent and the donation was in accordance with the ethical standards of the responsible committee on human experimentation (IRB permit 329/19). Cells were centrifuged (1200 rpm, 5 min, 20 °C) and the cell pellet resuspended in SFEM stem cell culture medium (chapter 2.1.6). Cells were cultivated in a humidified cell culture incubator at 37 °C, 5 % CO_2 and 90 % humidity. After 4 hours of cultivation, StemSpan CC100 cytokine cocktail (1 %) and TPO (2 µl/ml) were added to the medium to stimulate cells. Cells were subjected to experiments (e.g. flow cytometry and colony-forming assays) not before 24-hour duration of cultivation in medium supplemented with CC100 cytokine cocktail and TPO.

2.3.4. Flow Cytometry Analysis

Adherent cell lines

Adherent cells were once washed with FACS-Wash (1200 rpm, 4 min, 4 °C) before they were incubated with FACS Dissociation-Buffer for 15 min at 37 °C. Cells were detached by pipetting them carefully up and down several times. Cell suspension was transferred to 1.4 ml Micronic

tubes containing 500 µl FACS-Wash. Cells were centrifuged (1200 rpm, 4 min, 4 °C) to obtain pellet. For staining of cell surface expression of CD133 and CD46, cells were resuspended with 50 µl antibody solution diluted in FACS-Wash to the appropriate dilution as described in chapter 2.1.4. After 20 min incubation at 4° in the dark, cells were washed twice with 1 ml FACS Wash. Cell pellet was resuspended by vortexing prior to resuspension in FACS-Fix. Cells were analyzed by the MACSQuant Analyzer 10 and data analyzed using the FCS Express software.

Primary glioma sphere cells

Cells were once washed with FACS-Wash (300 x g, 5 min, 10 °C) and strained through an equilibrated 70 µm Cell strainer into a new 50 ml Falcon tube. The filter was washed with 5 ml PBS and cells were counted. 2.0 × 10^5 cells/micronic were stained with antibody solution diluted in FACS-Wash to the appropriate dilution as described in chapter 2.1.4 and incubated 20 min incubation at 4° in the dark. Afterwards, cells were washed twice with PBS and incubated with LIVE/DEAD® Fixable Dead Cell Stain according to manufacturer's protocol for 30 min at 4 °C in the dark. Cells were washed twice with PBS and the cell pellet was resuspended by vortexing before resuspension in FACS-Fix. For analysis, the following gating strategy was applied, unless stated differently. Cells were excluded from debris, dead and sublethal cells. The resulting gate defining viable cells was further gated for singlets. Finally, these single viable cells were gated for CD133, CD46 and green fluorescence protein (GFP) expression, respectively. To set gates for live-dead discrimination, heat-killed cells (1min at 70 °C) were mixed with viable cells. Cells were analyzed by the MACSQuant Analyzer 10 and data analyzed using the FCS Express software.

Hematopoietic stem cells

5.0 × 10^5 cells per micronic were washed once with FACS-Wash and incubated with 10 µl human FcR blocking reagent according to manufacturer's protocol. After 10 min incubation at 4 °C in the dark, 40 µl antibody solution diluted in FACS-Wash to the appropriate dilution as described in chapter 2.1.4 was added and incubated 20 min incubation at 4° in the dark. Afterwards, cells were washed twice with PBS and incubated with LIVE/DEAD® Fixable Dead Cell Stain according to manufacturer's protocol for 30 min at 4 °C in the dark. Cells were washed twice with PBS and cell pellet was resuspended by vortexing before resuspension in FACS-Fix. For analysis, the following gating strategy was applied, unless stated differently. Cells were excluded from debris, dead and sublethal cells. The resulting gate defining viable cells was further gated for singlets. Finally, these single viable cells were gated for CD133, CD46 and GFP expression, respectively. To set gates for live-dead discrimination, heat-killed cells (1min at 70 °C) were mixed with viable cells. Cells were analyzed by the MACSQuant Analyzer 10 and data analyzed using the FCS Express software.

2.3.5. Preparation of Virus Stocks

For production of cell-associated MVs and VSV-MV hybrid viruses, Vero-αHis cells were seeded at a density of 4.0×10^6 in 10 ml medium per 15 cm cell culture dish. After full confluence, supernatant of cells was removed from the dishes and cells were infected at an MOI of 0.03 (recombinant MVs) or at an MOI of 0.01 (VSV-MV hybrid viruses) by dribbling 5 ml virus suspension diffusely onto the cell monolayer. After 4-5 hours of cultivation as described in chapter 2.3.1, further 5 ml were added to cells and cells were cultivated in a humidified cell culture incubator at 32 °C, 5 % CO_2 and 90 % humidity. Cells were regularly adspected for the degree of syncytia formation by light microscopy. Once 90-100 % of cells were syncytial (approximately 48-72 hours after infection), cells were harvested (5 dishes one by one). For that purpose, medium were removed without disturbing cell layer and scaped in 300 µl OptiMEM. Scraped cells in OptiMEM were completely transferred to the next dish and used as scraping media and so on. The pool of 5 dishes was transferred into a cooled 15 ml Falcon tube and immediately transferred to liquid nitrogen to crack cells and release virus in the supernatant of the cell lysate. If another 5 dishes needed to be processed that way, a new 15 ml Falcon tube was used for pooling. After complete freezing, the pool was thawed at 37 °C in a water bath and centrifuged (3500 rpm, 5min, 4 °C). Virus-containing supernatant was aliquoted and stored at -80C°. Virus titer was determined using the method of Spearman and Kärber (chapter 2.3.6) and propagated on Vero-αHis cells.

From culture medium supernatant of infected Vero-αHis cells, only VSV-MV hybrid viruses could yield sustaining titers. For production of VSV-MV hybrid virus, Vero-αHis were infected as described above for the production of cell-associated VSV-MV hybrid viruses up to and including the infection of cells. Once 100 % of cells were syncytial and almost detaching (approximately 16-24 hours after infection), cell culture supernatant was carefully removed. Cell culture supernatant was pooled from all dishes and centrifuged (1200 rpm, 5min, 4 °C) to remove debris. Supernatant was transferred to Amicon filter tubes and centrifuged (3000 x g, 4 °C) until concentrated approximately thirtyfold (50 ml supernatant yield approximately 1500 µl virus supernatant).

Each production yield was termed “passage” (P) x + 1. All virus stocks used in this thesis were only used up to 5 production passages. If no passage <P5 was available, virus production was started from a single virus syncytium to obtain a homogenous virus suspension. For this purpose, Vero-αHis cells were seeded at a cell density of 1.0×10^6 in 2 ml per well in a 6-well plate. A dilution series of virus suspension from 10^{-1} to 10^{-6} was used to infect full confluent Vero-αHis cells with an MOI of 0.03. The following day, the supernatant was removed and cells were overlaid with Plaque Agarose to prevent confluence between xenogenous syncytia. 6 to 24 hours later, each single well-defined syncytia was picked using a sterile pipette tip and

transferred each to a different well of confluent Vero-αHis cells seeded at a density of 4.0 × 10^5 in 0.5 ml per well in a 12-well plate. This purification step was once again repeated and the virus clone was transferred to Vero-αHis cells in a 6-well plate. The 6-well plates were cultivated until they were 90-100 % syncytial, scraped in OptiMEM as described above and scaled up to 15 cm cell culture dishes. Upon full confluence, virus was harvested with 500 µl OptiMEM and further processed as described above and titrated (chapter 2.3.6), This virus production passage was termed “P1” and used for a scaled-up production of P2 virus stocks.

2.3.6. Titration of Virus Particles ($TCID_{50}$)

Titers of MV and VSV-MV were determined using the 50 % tissue culture infective dose ($TCID_{50}$) method as described by Spearman and Kärber (Ramakrishnan, 2016). 1.0 × 10^4 Vero-αHis cells in 100 µl medium per well were seeded in a flat-bottom 96-well plate. A dilution series of the virus suspension to be titrated ranging from 10^{-1} to 10^{-12} was prepared in duplicates in a round-bottom 96-well plate in 270 µl DMEM without FCS. 30 µl of each dilution was transferred to the fully confluent Vero-αHis cells. After four days of incubation at 37 °C, 5 % CO_2 and 90 % humidity, the titration was analyzed by identification and enumeration of infected cells relative to uninfected wells. Infection was detected by CPEs (syncytia formation) and/or expression of the marker protein GFP and a well defined as “infected” upon one single cytopathic effect within this well. The titer was calculated using the following equation according to Spearman and Kärber:

$$\frac{TCID_{50}}{ml} = \frac{10^{V_{ci}} \times F_V}{V_1 * 10^{\left[lg(V_1)\times\sum i\left(\frac{n_i}{R}\right)\right]} \times \sqrt{10}}$$

Equation 1: Equation fo the calculation of the tissue culture infective dose 50 / ml ($TCID_{50}$ / ml) according to Spearman and Kärber.
$\boldsymbol{V_{ci}}$ = *-lg(dilution)*: the last dilution in which all replicates were infected, when the dilutions are expressed as 10^{-1} to 10^{-12};
$\boldsymbol{F_V}$ = *33,3*: a factor to calculate the titer per 1000 µl based on the input volume of 30 µl;
$\boldsymbol{V_1}$ = *0.1:* the first dilution, which was used to infect Vero-αHis cells (10^{-1} = 0.1);
$\boldsymbol{n_i}$ = the number of wells infected in dilution ***i***, where not all wells of this dilution were infected anymore;
R = the amount of replicates
Detection limit: 1 × 10^2 $TCID_{50}$/ml

2.3.7. Infection of Cells

Hematopoietic stem cells

After overnight stimulation with medium supplemented with CC100 cytokine cocktail and TPO as described in chapter 2.1.6 and chapter 2.3.3, CD46 and CD133 cell surface expression was analyzed by flow cytometry (chapter 2.3.4). Cells were counted and 5.0 × 10^4 cells per 200 µl

medium were seeded into a 48-well tissue culture plate. Cells were infected with virus at an MOI of 1 in a volume of 50 µl/well. Lysate of uninfected Vero-αHis cells was added to equilibrate all samples to identical amounts of cell lysate. For the control wells, lysate of uninfected Vero-αHis was added to equal amounts as in virus-infected wells (referred as to “Cell lysate”). For the mock control, medium was used instead of virus. Infected cells and control cells were plated in triplicates, respectively. 21 hours after infection, 5-FC was added to the cells to a final concentration of 0.1 mM. The following day, cells were washed twice with medium without cytokines by two centrifugation steps (1200 rpm, 5 min, 20 °C) and the cell pellet was resuspended in 200 µl medium supplemented with cytokines. Cells were cultivated as described above. 3, 6 and 10 days after infection, GFP expression was analyzed by fluorescence microscopy and flow cytometry. The cell number was determined by flow cytometry to determine the input volume for the colony-forming assay (CFA) (chapter 2.3.8).

Adherent cell lines

Cells were seeded in an appropriate medium described in chapter 2.1.6 at an density adapted to the area of the respective culture vessel and ensuring approximately 60 to 75 % confluence to allow cells to grow as monolayer and to enable cell-to-cell spread of virus. Cell density was also dependent on the length of the respective experiment. Approximately 4 to 16 hours after seeding, cells were microscopically controlled for adherence and infected at the envisaged MOI by exchanging the complete medium with fresh pre-warmed virus-containing medium. Uninfected cells served as mock control. The following conditions were used, unless stated differently. For the receptor tropism experiments, Chinese hamster ovary (CHO)-K1 and transgenic CHO cells transgenic for the natural entry receptors CD46 and SLAM, or the target receptor CD133, respectively, were seeded in 24-well plates at a density of 1.4×10^5 cells in 1000 µl per well. Cells were infected at an MOI of 0.3 and infection was checked 72 hours after infection by fluorescence microscopy. HuH7 cells were infected at a density of 1.6×10^4 cells in 100 µl per well and infected at an MOI of 0.1 and 1. Cells were checked for GFP expression regularly by fluorescence microscopy. For quantitative kinetic analysis via flow cytometry, at 4, 8, 24 and 32 hours after infection, cells were subjected to staining with APC-labeled anti-CD133 antibodies as described in chapter 2.1.4. and chapter 2.3.4. For quantitative kinetic analysis of cell viability via the WST-1 assay, cells were treated as described in chapter 2.3.10.

Primary glioma sphere cells

If not stated differently, cells were treated as described in chapter 2.3.1, and were additionally strained through an equilibrated 100 µm Cell strainer to obtain a single cell suspension prior to infection. Single cells were seeded at a density of 7.0×10^3 in 40 µl per well of 96-well plates and immediately infected with virus (in a volume of 10 µl) at various MOIs (0.001, 0.005, 0.01, 0.05, 0.1, 1, 5, 10) to determine dose dependency. 21 hours after infection, different doses of

5-FC (0 mM to 10 mM in steps of power of 10) in a volume of 20 µl per well were added to the culture medium of cells infected with MV^{SCD}-CD133 to determine the optimal dose response of the SCD/5-FC regime. As negative control for the SCD/5-FC system, 5-FC was omitted in cells infected with MV^{SCD}-CD133. Uninfected cells served as mock control. For qualitative analysis of cell infection, cells were monitored by fluorescence microscopy and GFP expression was recorded twice a day. For quantitative analysis of cell infection, cell viability was determined using the RealTime-Glo MT Cell Viability assay as described in chapter 2.3.10.

2.3.8. Colony-Forming Assays

Human HSCs were cultured in methylcellulose-based semi-solid matrix supplemented with appropriate cytokines to allow hematopoietic progenitor cells to proliferate and differentiate to form discrete cell clusters comprised of microscopically recognizable progeny. Therewith, the CFA provides information about the frequency and the types of progenitor cells present in the input cell population that was infected with virus. For this purpose, 1.5×10^3 viable cells (determined by the gating strategy using flow cytometry, 2.3.4) were resuspended in a total volume of 300 µl fresh pre-warmed StemSpan medium and transferred to 3 ml MethoCult GF H4434 medium 72 hours after infection. Cells were handled according to manufacturer's protocol and plated in triplicates. After 10 days of incubation in a humidified cell culture incubator at 37 °C, 5 % CO_2 and 95 % humidity, clonal clusters (colonies) of maturing cells of the myeloid and erythroid lineage were counted and morphologically classified by light microscopy in a blinded manner.

2.3.9. Virus Growth Kinetics

HuH7 cells (3.0×10^4/1 ml medium/well) were seeded in duplicates in 12-well plates as described in chapter 2.1.6. The following day, cells were infected at an MOI of 0.03 by exchanging medium with fresh pre-warmed medium with the appropriate volume of virus. Samples of MV-infected cells were harvested at 24, 36, 48, 72, 96, 100 and 124 hours after infection, and samples of VSV-infected cells were harvested at 6, 12, 20, 24, 36, 55, 72 and 82 hours after infection. Virus in the cell culture medium (referred to as "supernatant virus") and cell-associated virus (referred to as "lysate virus") was analyzed. For this purpose, the cell culture medium was collected and centrifuged (3000 rpm, 5 min, 4 °C). The supernatant was aliquoted and immediately stored at -80 °C. For harvesting cell-associated virus, adherent cells were scraped into 1 ml OptiMEM and lysed by one cycle of freezing/thawing in liquid nitrogen (chapter 2.3.5). Cell debris was removed by centrifugation (3000 rpm, 5 min, 4 °C). The resulting medium containing cell-associated virus was aliquoted and immediately stored at -80 °C. Titers were determined as $TCID_{50}$/ml on Vero-αHis cells as described in chapter 2.3.6 in duplicates.

2.3.10. Killing Kinetics and Dose Dependency

For analyzing the cell viability of virus-infected HuH7 cells over time, 1.0×10^4 cells in 100 µl per well were seeded in a 96-well plate. After full confluence, cells were infected with virus at an MOI of 0.1 and 1 in a volume of 10 µl. Uninfected cells served as mock control and for normalization of data. To determine the killing kinetics of added viruses, cell viability was analyzed at specific time points using the premixed WST-1 Cell Proliferation Reagent according the manufacturer's protocol. The WST-1 Cell Proliferation Assay is a colorimetric end-point assay that is based on the cleavage of a tetrazolium salt, MTS, by mitochondrial dehydrogenases to form formazan in viable cells. The amount of formazan produced is in direct proportion to the number of viable cells in the medium. Unlike the MTT assay, there is no need to wash or harvest the cells for analysis. To determine the dose-dependent killing, cells were infected with different MOIs (0 mM to 10 mM in steps of power of 10) upon full confluence. After the cells were infected with MV^{SCD}-CD133, different concentrations of 5-FC were added to culture medium 21 hours after infection. Uninfected cells served as mock control and for normalization of data. 72 hours after infection, cell viability was analyzed using the premixed WST-1 Cell Proliferation Reagent according the manufacturer's protocol. Absorbance was measured 4 hours after addition of WST substrate at 450 nm versus a 650 nm reference by using a Microtiter plate (ELISA) reader. Data was analyzed using Excel 2010 and 2016. By generating sigmoid curves using GraphPad Prism, the EC_{50}, which defines the MOI required to kill 50 % of the cells was determined for each virus.

To analyze cell viability in glioma sphere cultures, cells were cultured and infected as described in chapter 2.3.7. Cell viability of infected cells was determined over time for up to 72 hours after infection using the RealTime-Glo MT Cell Viability assay according to the manufacturer's protocol. The RealTime-Glo MT Cell Viability assay is a multiplexing nonlytic bioluminescent method to detect cell viability in real time which principle relies on the continuous reduction of the MT cell viability substrate exclusively by viable cells. The signal correlates with the number of viable cells. Luminescence detection was started 1 hour after addition of the MT Cell Viability Substrate and NanoLuc Enzyme using the Microplate luminometer. After the cell were infected with MV^{SCD}-CD133, different concentrations of 5-FC were added to culture medium 21 hours after infection and luminescence detection was continued 1 hour later. As negative control for the SCD/5-FC system, 5-FC was omitted in cells infected with MV^{SCD}-CD133. Uninfected cells served as mock control and for normalization. Luminescence was continuously measured up to 72 hours after infection. Data was analyzed using Excel.

2.3.11. Bystander Assay

To directly quantify the bystander effect of MV^{SCD}-CD133 (+ 5-FC) on non-infected cells, the following FACS assay was established. Mixed cultures of HT1080 and HT1080-CD133 in a 1:1 ratio were seeded in a 24-well plate to a final cell density of 3.0×10^4 and cultured as described in chapter 2.1.6. After 4 hours, cells were infected in quadruplicates with MV-CD133 and MV^{SCD}-CD133 at an MOI of 1 (related to the total cell concentration), respectively. Uninfected cells (referred to as “mock”) served as negative control and were also equilibrated to equal amounts of cell lysate as in virus-infected cells. 16 hours after infection, the medium of all wells was removed and exchanged with fresh pre-warmed medium supplemented with various 5-FC doses ranging from 0.001, 0.01, 0.1, 1 and 10 mM, respectively. After 72 hours, cells were washed once with PBS and detached by 200 µl Trypsin working solution. After detachment, cells were resuspended in 800 µl Suspension buffer and transferred into 1.4 ml Micronic tubes and centrifuged (1000 rpm, 4 °C, 4 min). Cells were washed once with PBS and the cell pellet was resuspended with 1 µl LIVE/DEAD® Fixable Dead Cell Stain and incubated at 4 °C in the dark. After 10 min of incubation, antibody solution APC-labeled anti-CD133/1 diluted in FACS-Wash) was added and the cell suspension was further incubated for 20 min incubation at 4° in the dark. Afterwards, cells were washed twice with 1 ml PBS and the cell pellet was resuspended by vortexing before resuspension in 250 µl FACS-Fix. It was crucial to yield identical volumes at this final step in order to obtain accurate absolute cell counts. The experiment was done in three independent assays each done at quadruplicates.

For analysis by the MACSQuant Analyzer 10, identical volumes of all individual samples were acquired by flow cytometry. The following gating strategy was applied. Cells were excluded from debris and further discriminated of lethal and sublethal cells by their uptake behavior of the amine reactive dye LIVE/DEAD® Fixable Dead Cell Stain. The resulting gate of viable cells was further gated for singlets. Finally, these single viable cells were gated for CD133 expression. To set gates for live-dead discrimination, heat-killed cells (1 min at 70 °C) were mixed with viable cells. The GFP reporter gene of MV-CD133 was used for unambiguous detection of virus infected cells. Data was analyzed using the FCS Express V4 and V6 software and Excel 2010 and 2016. For each sample in a defined volume, the absolute cell count was determined. Based thereon, the absolute number of viable red cells (amine non-reactive $CD133^+$ cells) and the viable proportions of $CD133^-$ cells relative to $CD133^+$ cells were calculated.

2.4. Animal Experiments

To analyze the antitumoral effect of OVs, different tumor models were applied. Subcutaneous xenograft models were peformed for easy monitoring of tumor growth by digital caliper

emasurement. An orthotopic glioma model was applied to mimick the disease more accurately by transplanting the tumor in its anatomical site of origin (chapter 2.4.2).

All animal experiments were conducted according to current guidelines for animal welfare and were submitted for review by the institutional ethical committee and local agency review board for approval. All experiments were accredited by the local authority (RP Darmstadt) under the file numbers F107/1002 (subcutaneous HuH7 model) and F107/105 (orthotopic glioma model). The animals were scored on a daily basis by the animal care-takers, and sacrificed painlessly in case of body weight loss exceeding 20 % or increase in any signs of suffering and pain. NOD/Scid mice were purchased from Charles River and housed under a specified pathogen free (SPF) environment in individually ventilated cages (IVCs) and handled under a laminar flow hood. Mice were transferred to freshly bedded cages on a weekly basis.

2.4.1. Subcutaneous HuH7 Xenograft Cell Implantation

HuH7 cells were cultured under standard cell culture conditions (chapter 2.1.6 and chapter 2.3.1) and were treated as described in chapter 2.3.1, but washed once with PBS and counted. After cells were washed once again in PBS, the pellet was resuspended in the appropriate amount of PBS to adjust to 5.0×10^7 HuH7 cells per ml. Cells were kept on ice until procedure. NOD/Scid mice were anesthetized with 3-4 % isoflurane for anesthetic induction and afterwards with 2 % isoflurane for maintenance. Mice were positioned on the ventral recumbancy on a heat pad. When mice did not react to toe pinches, the cell suspension was resuspended and 5.0×10^6 cells in 100 µl cell suspension were injected subcutaneously using a 23 G needle. Solid tumor mass was palpable between 10 and 14 days after implantation and from then on tumor growth was measured twice a week using a digital caliper. Body weight was determined in parallel. Tumor size was calculated according to the formula $W^2xL/2$ (L = length and W = perpendicular width of the tumor, L>W. At a mean tumor volume of approximately 100 mm^3 (range 60 – 140 mm^3), mice were randomized into respective treatment groups according to tumor size (approximately 14 - 21 days after tumor implantation). The treatment was initiated on the day of group allocation. For the intratumoral treatment regime, tumor cells were implanted into both flanks. For the intravenous treatment regime, cells were injected into the right lateral flank only. Animals were sacrificed when either tumor volumes were >1200 mm^3 or mice need to be sacrificed due to other ethical reasons (e.g. ulceration of tumor, lack of motility, general signs of pain). For that purpose, animals were anesthetized using ketamine / xylazine (KX) (until mice entered surgical tolerance) and sacrificed by transcardial perfusion (chapter 2.4.4) and a necropsy was performed. Tumor samples were collected at terminus and cut into half and processed for cryo embedding (chapter 2.4.5).

2.4.2. Orthotopic Glioma Sphere Cell Implantation

Preparation of cell inoculum

NCH644 tumor sphere cells were cultured under standard cell culture conditions (chapter 2.1.6 and chapter 2.3.1) for at least 10 days to ensure CD133 expression that was monitored by flow cytometry (chapter 2.3.4). Cells were centrifuged (300 x g, 5 min, 10 °C) and the pellet was resuspended in 1 ml PBS using a micropipette and in further 5 ml using a serological pipette. Cell suspension was strained through an equilibrated 70 µm Cell strainer to obtain a single cell suspension. Cells were infected at an MOI of 0.5. After 16 hours of incubation, cells were microscopically checked for the presence of GFP expression. Cells were centrifuged (300 x g, 2 min, 10 °C) and the supernatant was accurately removed using a micropipette. Cell pellet was resuspended with 1 ml PBS and counted. After centrifugation (300 x g, 2 min, 10 °C), the cell pellet was resuspended in an appropriate volume of PBS to obtain 1.0×10^5 NCH644 tumor sphere cells per ml. Cells were cooled on ice until transplantation.

Intracranial stereotact-assisted implantation

Intracranial injection of tumor cells mimics clinical response to tumor growth in the organ of origin. NOD/Scid mice received pre-operative analgesics (Carprofen, 5 mg/kg body weight). Approximately 30 min after analgesia, the mouse was anesthetized with an intraperitoneal injection of 0.1 ml anesthetics per 10 g body weight containing ketamine (100 mg/kg body weight) and xylazine (4 mg/kg body weight). Upon weakened reflexes the mouse was placed onto a heat pad and eye gel were applied to the eyes. The surgical site was shaved and wiped with gaze soaked with PVD-Iodine. After the mouse was unresponsive to toe pinches, it was positioned straightly onto the stereotact holder using the ear bars of the device. A median incision through the skin and the periosteum along the sagital suture was made. To expose the bregma, which is used for orientation, the periosteum was removed by a gaze soaked with hydrogen peroxide. A burr hole was made at the coordinates 1.7 mm lateral, 0.5 mm rostral at 3 mm depth (in relation to the bregma that is set to zero) using a 27 G needle.

Using a Hamilton syringe, 1.0×10^5 NCH644 tumor sphere cells in 5 µl PBS either uninfected (referred to as “mock”) or infected at an MOI of 0.5 were stereotactically implanted into the corpus striatum of the right hemisphere at the coordinates prepared by a burr hole as described above. Cell injection flow was 1 µl per 1 min. After pausing for 5 min to allow the diffusion of the carrier fluid into the brain parenchyma, the injection needle was slowly removed. The Hamilton needle was washed three times with 70 % ethanol and subsequently with PBS before the first injection, between each treatment group and after finishing injections. During the whole procedure, which took approximately 15 min per mouse, breathing and the anesthetic stage was continuously checked. If necessary, anesthetics were re-injected. The skin was sutured

with 4-0 vicryl thread. Mice were settled into a fresh cage with tissue-bedding and gloves filled with body-warm water to avoid post-operative hypothermia. After full recovery from anesthesia, the separately kept mice were placed together with their group mates into a new cage. Survival and general condition of mice were monitored daily. Body weight was determined twice a week. The experimental end point was reached at the onset of neurological symptoms and/or weight loss of more than 20 % or other ethical reasons (e.g. lack of motility, general signs of pain). Mice were anesthetized using Ketamin Xylazine (until mice entered surgical tolerance) and sacrificed by transcardial perfusion (chapter 2.4.4). Brains were explanted and either processed for tumor cell dissociation (chapter 2.4.5) or paraffin embedding (chapter 2.4.7).

2.4.3. Administration of Virus Particles

For intratumoral administration, mice were anesthetized using isoflurane. After the mice were unresponsive to toe pinches, 1.0×10^6 $TCID_{50}$ of virus suspension in 50 µl Vero-αHis lysate was injected intratumorally. To achieve a homogenous virus delivery in tumor tissue, injection was performed in a fan-shaped manner using an Insulin syringe (29 G). Mice received the virus applications on four consecutive days, resulting in a total dose of 4.0×10^6 $TCID_{50}$ of each virus.

For intravenous administration, mice were placed underneath a heating lamp for 5 min to dilate the tail-veins. Mice were transferred to a restrainer without applying anesthesia. Three injections with 1.0×10^6 $TCID_{50}$ of each virus in 50 µl Vero-αHis lysate were injected *via* the lateral tail vein every second day. Mice were released and placed back into their cage.

In both treatment schedules, virus-free Vero-αHis lysate was used to equilibrate each dose of all treatment groups to equal amounts. Control mice received virus-free Vero-αHis lysate in medium (referred to as “mock”). Treatment and monitoring were performed in a blinded manner over the whole course of the study until mice were sacrificed. To avoid the fluctuation of the tumor volume growth curves, the last data score obtained before sacrifice was carried forward until termination of the study (LOCF, last observation carried forward).The area under the curve (AUC) was determined for each animal and was normalized against the value obtained from the mouse that survived the longest among the mock group. For the intratumoral administration schedule that were 40 days after transplantation, and for the systemic administration schedule that were 38 days after transplantation.

Intracranial injection of virus was performed stereotactically in 5 µl PBS into the same coordinates as described in chapter 2.4.2. The intracranial injection of virus into pre-established glioma was performed 5 days after intracranial glioma sphere cell implantation. As control, PBS was injected instead of virus, if not stated differently.

2.4.4. Transcardial Perfusion

The transcardial perfusion was performed to deplete erythrocytes from tissue. This method was preferred to red blood cell lysis for practical reasons. On one hand, red blood cell lysis is known to diminish the tumor cell yield of a subsequent cell dissociation. On the other hand, the wash-out can minimize unspecific reactions of immunohistochemistry. For that purpose, animals were anesthetized using KX (until mice entered surgical tolerance) (chapter 2.4.2) and sacrificed by transcardial perfusion. After intraperitoneal administration of KX, the mouse was separately kept in a cage until loss of positional reflexes. After transition to surgical tolerance the mouse was secured in a supine position by taping the forepaws and hindpaws to a pinnable Styrofoam work surface below a laminar flow class two cabinets. The skin was incised with surgical scissors along the Linea alba from the umbilicus cranially to just beneath the xiphoid. After separation of the diaphragm from the chest wall on both sides, the ribcage was opened by two paramedian incisions from the xiphoid cranially towards the base of the ventral ribcage using a bone scissor. The ribcage was folded cranially and pinned laterally. The apex of the heart was grasped with blunt forceps and a 23 G butterfly catheter attached to a 20 ml syringe filled with pre-warmed PBS was inserted into the left ventricle. To allow perfusion through the entire systemic circulation, the right atrium (at the site of the right auriculum) was cut. Using constant pressure, the systemic circulation was perfused with 20 ml prewarmed PBS at an approximate flow rate of 5ml / min until the exuding liquid was completely clear and the liver appeared pale due to washout of blood. The destined organs were transplanted and further processed according to chapter 2.4.5, chapter 2.4.6 and 2.4.7).

2.4.5. Ex Vivo Sphere Formation Assays

To analyse whether treated tumors were able to produce tumor spheres *ex vivo* as a measure indicating residual stemness properties of CSCs, an *ex vivo* sphere formation assay was established. For that purpose, the brain was excised and the cerebellum and the Bulbus olfactorius were removed to decrease in the input weight for further processing. The specimen was dissociated using the Miltenyi Brain tumor dissociation Kit (P) according to the manufacturers' instructions of automated dissociation using the gentleMACS™ Dissociators. 2.0×10^5 single cells were transferred to a T25 tissue culture flasks. Cells were cultured under standard cell culture conditions and medium was replenished as described in 2.3.1. Cells were cultivated until spheres had formed, and an absolute cell density of 1.0×10^6 cells per T25 flask was reached. The growth potential was evaluated as the time required for dissociated tumor specimens to generate 1.0×10^6 and this time was plotted against the survival of the respective tumor bearing mouse using GraphPadPrism.

2.4.6. Cryo Embedding and Immunofluorescence Staining of Tumor Sections

HuH7-derived tumors were explanted, cut into half and fixed in 4 % formaldehyde solution for 24 hours. When the specimen was greater than 1 cm in diameter, the halves were sliced to approximately 0.5 cm thick slices. Tissues were dehydrated in 30 % sucrose in PBS until sunk to the bottom (approximately 24-48 hours) and then embedded in optical cutting temperature (OCT) medium and frozen on dry ice. Specimens were stored at -80 °C. Tissue was cut into 8 µm thick slices and at -19 °C chamber temperature and -9 °C object temperature using a Leica cryostat CM1850 and directly mounted on SuperFrost™ Ultra Plus Slides. The slides were air-dried 3 hours to overnight and then either directly processed for immunofluorescence staining or stored at -80 °C for up to 12 months. Sections were shortly rehydrated in PBS and then transferred to distilled water. Slides were transferred to Target Retrieval Solution prepared according to manufacturer's instructions and incubated at 92 °C for 10 min. Slides were rinsed with distilled water and afterwards washed three times in PBS. Then, sections were permeabilized by incubation in 0.2 % Triton™ X-100 in PBS for 10 min at room temperature. Slides were washed three times in PBS and unspecific binding was blocked by incubation with 5 % donkey serum in PBS for 30 min at room temperature. Then, slides were incubated with the primary antibody mix diluted in 2.5 % donkey serum in PBS overnight at 4 °C, followed by incubation with the secondary, fluorescently labeled antibodies for 4 hours at room temperature and protected from light (chapter 2.1.4). Sections were washed 4 times with PBS, rinsed with distilled water and mounted with Fluoroshield with (4`, 6-diamidino-2-phenylindole) DAPI® mounting medium. Sections were stained separately and co-stained against GFP and CD133 (chapter 2.1.4).

Controls included an unstained section after the same fixation as the experimental samples, an isotype control for the CD133 staining or secondary antibody only for the GFP staining. As negative control for CD133 staining, cryo sections from KM-H2 tumor tissue was used that do not test positive for CD133. As negative control for GFP staining, uninfected tumors were used (referred to as "mock"). Images were captured by a fully motorized Axio-Observer Z1 microscope, equipped with an ApoTome optical sectioning unit. Sections were analyzed by triple fluorescence, at 20 x magnification detecting nuclei in the blue channel (Dapi, 460 nm), Cy2-labeled antibodies against GFP in the green channel (Cy2, 490 nm, 508 nm) and Cy5-labeled antibodies against CD133 in the far red channel (Cy5, 649 nm, 673 nm).

2.4.7. Paraffin Embedding and Immunohistochemistry of Brain Sections

Brains were routinely fixed in 10 % formaldehyde solution for 72 hours. After fixation, tissue was rinsed with PBS and dehydrated using an automated tissue processor that applies under gentle agitation an ascending sequence of ethanol infiltration followed by a xylene infiltration

sequence to remove the ethanol from tissue. Afterwards tissues were embedded in Paraffin. After hardening of paraffin blocks on a cooled plate, 4 µm thick slices were sectioned using a rotation microtome. Sections were straightened on the surface of a water bath at 37 °C and floated onto SuperFrost™ Ultra Plus Slides. Slides were air-dried for 30 min and then transferred into a heating cabinet at 45 °C overnight to melt excess paraffin and bond the tissue to the glass surface. 30 min prior to further processing, the slides were transferred into a heating cabinet at 60 °C. Sections were deparaffinized in Xylene followed by a descending ethanol infiltration sequence for hydration and finally one sequence of each Kardasewitsch solution, soapy water and distilled water. To allow assessment of microscopic structures sections were subjected to hematoxylin and eosin stain (hematoxylin, hydrochloric acid/ethanol, distilled water, eosin, 96 % ethanol, propanol, xylene) and finally embedded with Entellan® Rapid Embedding Agent. Sections were viewed and interpreted using a light microscope in a blinded manner. Pathomorphological features were graded, negative, mild, moderate and severe.

2.4.8. Quantification of Infected Areas in Cryo Sections of Tumor Tissue

Sections were analyzed as described in chapter 2.4.6. For quantification, up to 600 adjacent tiles per section were acquired using the MosaiX module (Carl Zeiss). For quantification of the GFP-fluorescent areas, computational analysis was conducted using the Cell Profiler software (Kamentsky et al., 2011, Bioinformatics). The following input module pipeline was used if not stated differently. Tumor areas were identified by the “ImageMath” module and the “IdentifyPrimaryObjects” according to the pixel intensities and diameters of the input image. The threshold was set on 0.915. Using the exclusion method “MaskImage”, objects parts outside the identified objects were masked out. The resulting object parts, defined as “tumor tissue” were further processed with smoothing filter for exclusion of autofluorescent tumor areas. Sub-regions within these masks were identified by the “IdentifyPrimaryObjects” analysis module using a pipeline panel based on the Otsu two-class thresholding method with weighed variance. The threshold correction factor was set to 0.8 with lower and upper bounds by 0.13 and 1.0. The area occupied (defined as “tumor tissue infected”) of infected tumors was calculated by pixel intensities of the identified infected objects relative to object pixel intensities in mock control tumors. The determined threshold levels were used to calculate the total identified GFP^+ area for each tumor of mice treated with MV-CD133 and VSV-CD133. As VSV infection resulted in a higher GFP fluorescence, the “RescaleIntensity” module was different for both virus types. For VSV-infected tumors, the upper limit rescale pixels were set on “Mask pixels” while for MV- and mock-infected tumors, it was set on “set to one”. Data was analyzed using Excel 2010 and 2016.

2.5. Statistical analysis

Statistical significance was determined as indicated in figure legends. In general, statistical significance between two groups was determined using unpaired student's t, Mann-Whitney test and 1-way ANOVA followed by multiple comparison test (Sidak's or Dunnett's depending on the sets of mean to be compared). P values are given in the figure legends. Graph Pad Prism 7 software was used for statistical analysis. Survival data were depicted as Kaplan-Meier survival curves. Group comparisons were conducted by a log-rank test with Bonferroni adjustment for multiple comparisons.

3. RESULTS

This thesis describes a comprehensive characterization of MVs targeted to CD133$^+$ tumor cells (MV-CD133). Based upon the highly CD133 selective retargeting strategy initially applied to the vaccine strain MV-NSe (Bach et al., 2013) genetic modifications were performed to achieve more efficacious tumor eradication without detrimental effects on overall safety. These strategies involved (1) the extension of receptor usage to CD46 (MV-CD46/CD133) by omitting mutations of the MV-H for ablation of recognition of the natural MV receptors CD46 and SLAM, (2) arming with the suicide gene SCD (MV^{SCD}-CD133) or (3) with genes from wt MV strains (MV^{Pwt}-CD133) or (4) VSV-MV hybrid viruses (VSV-CD133), respectively (Figure 13). While specificity of all viruses was maintained upon respective modifications, VSV-CD133 revealed the most potent oncolytic activity in a subcutaneous tumor model of HCC. Moreover, VSV-CD133 infected a more than 10^4-fold larger area of the tumor than its MV counterpart MV-CD133 did. In an orthotopic glioma model, MV-CD46/CD133 and MV^{SCD}-CD133 were superior to other MV variants whereas VSV-CD133 led to fatal neurotoxic symptoms.

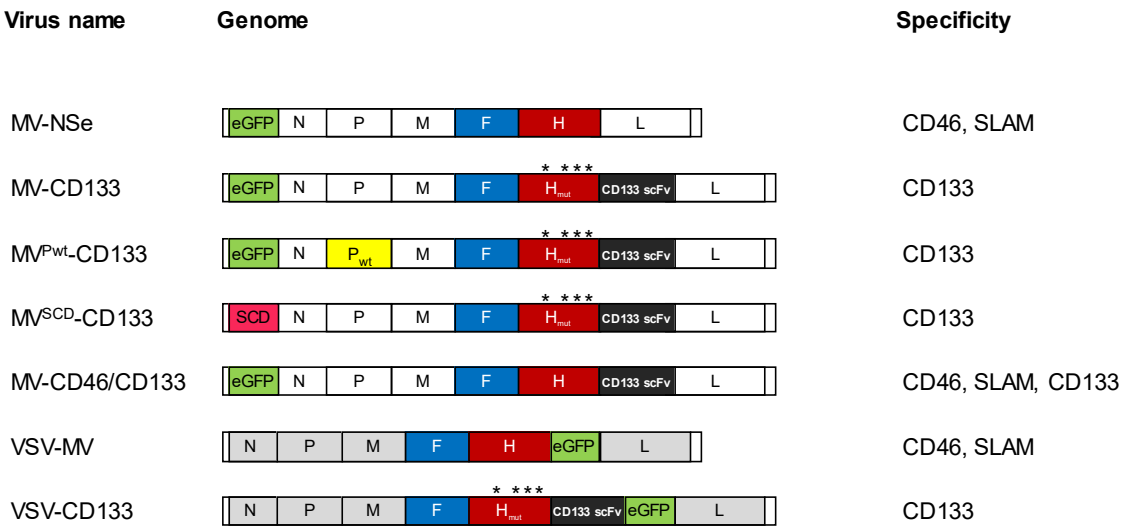

Figure 13. Schematic overview of the genomic organization of the oncolytic viruses used in this study

The oncolytic viruses (OVs) used in this study were generated on the basis of the measles virus (MV) vaccine strain MV-NSe. The green fluorescence protein (GFP) cassette was inserted upstream of the N gene for easy detection of infected cells. For CD133 targeting, the hemagglutinin (H) of MV-NSe was mutated in its residues (H_{mut}) interacting with the natural receptors and a single-chain antibody (scFv) specific for the target receptor CD133 (CD133 scFv) was genetically fused to the H protein. Exchange of the P gene against the P gene of a wild-type (wt) MV strain resulted in MV^{Pwt}-CD133. To generate MV^{SCD}-CD133, the GFP reporter gene was replaced by the suicide gene super cytosine deaminase (SCD). For receptor tropism of both CD46$^+$ and CD133$^+$ cells, the CD133-specific scFv was genetically fused to an unmodified H protein resulting in MV-CD46/CD133. The exchange of the VSV glycoprotein gene against the fusion (F) and the H protein of MV resulted in either the hybrid virus VSV-MV (unmodified H protein) or the hybrid virus VSV-CD133 (CD133-targeted MV-H). Point mutations in H proteins introduced to ablate natural receptor usage are indicated by asterisks. Adapted from (Kleinlützum et al., 2017).

3.1. Characterization of Oncolytic Viruses for Protein Composition

To acquire fully functional targeted measles virotherapeutics, the successful incorporation and display of the envelope glycoproteins on viral particles had to be ensured prior to further applications.

To assess the protein composition of each virus type, western blot analyses of virus stocks harvested from cell lysates of virus-infected Vero-αHis cells were conducted. MV-NSe, VSV-MV and VSV served each as negative control for their respective CD133-targeted counterparts. Both MV glycoproteins, H and F1, were detected in all MV (Figure 14A) and VSV-MV hybrid virus (Figure 14B) samples. Moreover, the viruses with CD133-specific scFv (H-scFv-CD133) protein display showed an increase of the molecular weight of approximately 30 kDa as compared to the unmodified MV-NSe (Figure 14A) or the VSV-MV chimeric virus (Figure 14B), as expected. For MV, signal strength of MV-N, H and F1 was strongest in the lane loaded with MV-NSe, albeit, no differences in the amounts of these proteins were detected between the CD133-targeted MVs. Of note, whereas the glycoprotein G was detected in the lane loaded with VSV, the signal was absent in the lanes loaded with the hybrid viruses VSV-MV and VSV-CD133. The amounts of the VSV-N, P and M proteins were comparably strong between VSV-MV and VSV-CD133.

The immunoblots showed the successful incorporation of the MV glycoproteins H and F into the envelope of recombinant oncolytic MVs and MV glycoprotein-pseudotyped VSV. All CD133-targeted viruses showed the expected shift in the electrophoretic mobility of the H-scFv fusion proteins compared to unmodified H present in MV-NSe or VSV-MV, respectively. Notably, the glycoprotein G, which is associated with neurotoxicity of the wt VSV, was successfully deleted in the VSV-MV chimeras.

Having proved the required protein composition of the recombinant viruses, the next experiments had to investigate their cellular tropism.

3.2. Selectivity of Targeted Oncolytic Viruses

Another requirement of a safe oncolytic agent is its selectivity for cells expressing the target receptor. To confirm that the modified viruses use CD133 as entry receptors, CHO cells either transgenic for the natural entry receptors CD46 or SLAM of the measles vaccine strain MV-NSe or the target receptor CD133 were infected with MV-NSe, MV-CD133, MV^{Pwt}-CD133, MV-CD46/CD133 or VSV-CD133 at a multiplicity of infection of 0.03. The parental CHO-K1 served as negative control. GFP fluorescence was visualized by fluorescence microscopy 72 hours after infection. MV^{SCD}-CD133 was not included in analysis as it lacks the GFP reporter gene

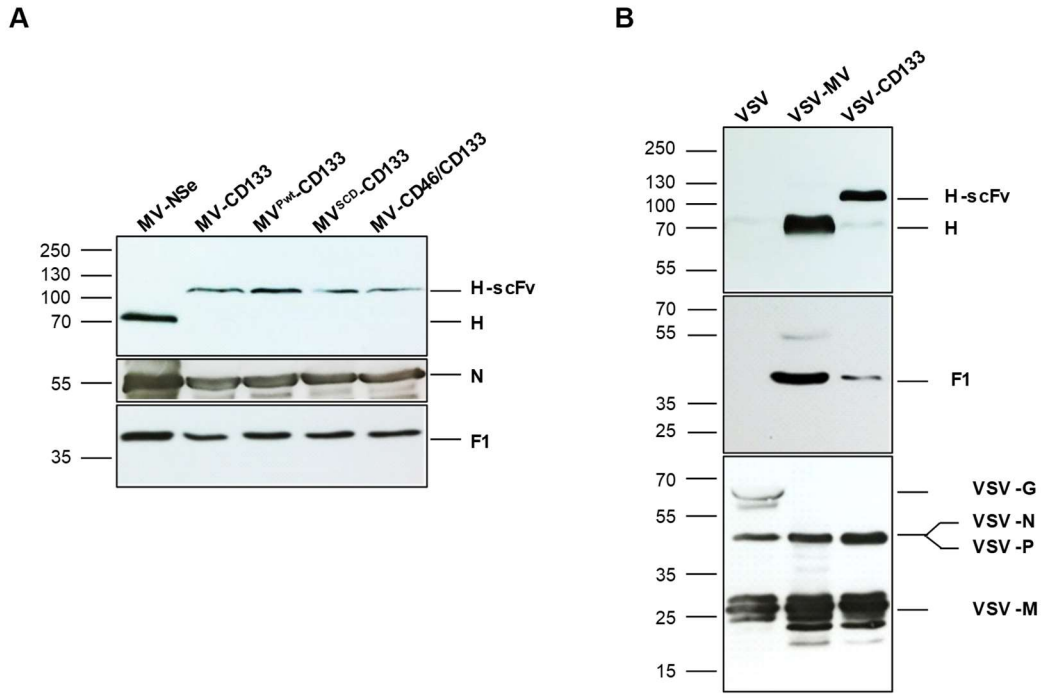

Figure 14. Immunochemical characterization of recombinant Measles Virus and MV glycoprotein pseudotyped Vesicular Stomatitis Virus particles

Supernatants of Vero-αHis cells infected with the indicated viruses were denatured followed by fractionation by sodium dodecyl sulfate-polyacrylamide gel electrophoresis (SDS-PAGE). Viral glycoproteins were detected with polyclonal antibodies directed against the indicated proteins. Nucleocapsid (N) blots served as loading controls in both cases. The numbers on the left of each immunoblot refer to the molecular weight in kDa. **(A)** Immunoblot showing the incorporation of measles virus (MV) glycoproteins into recombinant MV particles. The parental MV-NSe served as unmodified control. **(B)** Immunoblot showing the incorporation of MV glycoproteins into recombinant vesicular stomatitis virus (VSV) particles. VSV and VSV-MV served as unmodified controls. Adapted from (Kleinlützum et al., 2017).

(Figure 13). However, cell tropism and extent of lysis of target cells infected with MV^{SCD}-CD133 without 5-FC addition were expected to be identical to MV-CD133.

Fluorescence microscopic images in Figure 15 indicate absolute cell tropism for target receptor positive cells: While the vaccine strain MV-NSe only infected cell lines expressing the natural receptors CD46 and SLAM, MV-CD46/CD133 additionally infected $CD133^+$ target cells besides $CD46^+$ and $SLAM^+$ cells. Infection by CD133-targeted MV and VSV was restricted to $CD133^+$ target cells. Syncytia formation was comparably strong among all MVs. Of note, lysis was most pronounced in cells that were infected with VSV-CD133. The parental cell line CHO-K1 showed no green fluorescence, as expected.

The results show that cell tropism of the OVs was successfully redirected to cell lines expressing the respective target receptors. Therewith the viruses fulfill a mandatory prerequisite for CSC directed tumor therapy.

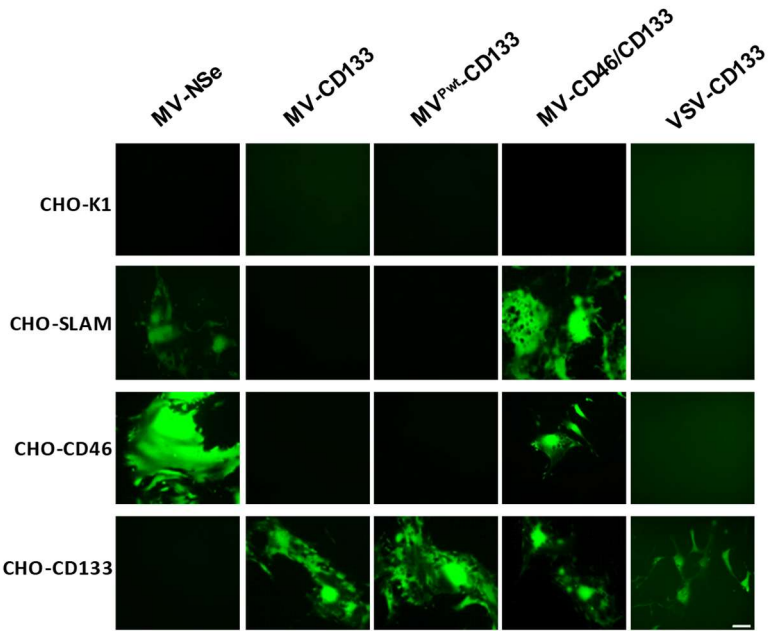

Figure 15. Receptor tropism of targeted Measles and Vesicular Stomatitis Virus
A panel of receptor-transgenic Chinese hamster ovarian (CHO)-cells (as indicated) were infected with MV-NSe, MV-CD133, MV^{Pwt}-CD133, MV-CD46/CD133 and VSV-CD133 with a multiplicity of infection (MOI) of 0.03. CHO-K1 served as negative cell line. Green fluorescence protein (GFP) fluorescent images were taken 72 hours post infection. Scale bar, 200 µm. Adapted from (Kleinlützum et al., 2017).

3.3. Replication of Targeted Oncolytic Viruses on HuH7 Hepatocellular Carcinoma Cells

After confirming that the recombinant targeted viruses are highly specific for their target cells the kinetics of replication on target cells were analyzed. It was hypothesized that utilization of unmodified H protein (MV-CD46/CD133) or P/V/C proteins of wt MV (MV^{Pwt}-CD133), but in particular chimerism with VSV (VSV-CD133), would result in faster replication kinetics. To test these assumptions virus production was analyzed over a period of time following infection of target cells. This was performed on the HCC cell line HuH7 because this cell line was used in further *in vitro* and *in vivo* efficacy studies.

HuH7 cells were infected with MV-NSe, MV-CD133, MV^{SCD}-CD133, MV^{Pwt}-CD133, MV-CD46/CD133 and VSV-CD133 at an MOI of 0.03. Viral titers of cell-associated virus (lysate) and of viral particles released into the medium (supernatant) were obtained for a time period from 4 to 82 hours post infection (VSV) or 20 to 124 hours post infection (MV) in order to receive a virus growth curve. Within these time frames, samples were harvested in a 24-hourly manner or less. At each time point, samples of medium supernatant and cell lysates obtained from scraping in OptiMEM were subjected to one freeze-thaw cycle and centrifuged to clear from cells. Viral titers were determined by $TCID_{50}$ titration on the producer cell line Vero-αHis according to Spearman-Kärber (Ramakrishnan, 2016).

As shown in Figure 16A, MV-CD133 reached a maximal cell-associated titer of 2 x 10^4 $TCID_{50}$/ml on average within 100 hours after infection, which dropped down to mean values of 4.6 x 10^3 $TCID_{50}$/ml at 124 hours after infection. Mean cell-associated titer of MV-NSe, MV^{Pwt}-CD133 and MV^{SCD}-CD133 increased uniformly to 5.2 x 10^3 $TCID_{50}$/ml at 72 hours after infection, before each of them developed differently: while viral titers of MV^{Pwt}-CD133 steadily increased reaching maximum mean values of 7.9 x 10^3 $TCID_{50}$/ml within 124 hours post infection, viral titers of MV-NSe decreased rapidly to 1.7 x 10^2 $TCID_{50}$/ml within 124 hours after infection. However, MV^{SCD}-CD133 decreased slowly to 1.3 x 10^3 $TCID_{50}$/ml within 124 hours after infection. Maximum cell-associated titers of MV-CD46/CD133 (2.9 x 10^3 $TCID_{50}$/ml) were reached at 100 hours after infection, which decreased to same titers as MV^{SCD}-CD133 within 124 hours after infection.

MV titers of supernatants were not detectable before 72 hours post infection except MV^{SCD}-CD133 that reached maximum titers of 1.4 x 10^3 $TCID_{50}$/ml on average at 48 hours after infection. At 72 hours after infection, MV-CD46/CD133 and MV^{Pwt}-CD133 reached comparable high titers as MV^{SCD}-CD133. While titers of MV-CD46/CD133 dropped down beyond detectable, titers of MV^{Pwt}-CD133 steadily increased to maximum titers of 2.6 x 10^2 $TCID_{50}$/ml within 124 hours after infection. The highest titers of supernatant virus were reached with cells infected with MV-CD133 100 hours after infection ranging up to 3.9 x 10^2 $TCID_{50}$/ml on average.

As shown in Figure 16B, VSV-MV reached maximum titers of cell-associated virus of 1.25 x 10^6 $TCID_{50}$/ml at 24 hours after infection, and afterwards steadily decreased down to mean titers of 5.2 x 10^5 $TCID_{50}$/ml within 82 hours. Titers of VSV-CD133 showed a comparable replication curve as VSV-MV, but mean titers were 1.5 log levels lower in general.

Viral titers of VSV-related viruses from the supernatant were much higher than those from lysate: Maximum titers of VSV-MV with 5.9 x 10^7 $TCID_{50}$/ml were 1.5 log levels higher than those obtained from supernatant and were reached at 36 hours after infection. However, VSV-CD133 reached the maximum titers 1.4 x 10^6 within 55 hours after infection, being 1 log level higher than supernatant-related titers. While titers of VSV-MV remained steady until the last detection time point of 82 hours post infection, titers of VSV-CD133 slowly declined to 9.2 x 10^4 $TCID_{50}$/ml.

The results show that all viruses are able to replicate in HuH7 cells. Notably, the CD133-scFv did not affect replication kinetics of all viruses. In fact, with the exception of MV-CD46/CD133, all CD133-targeted MVs revealed higher and more sustainable titers than MV-NSe. While the highest titers were obtained from MV-CD133 lysates, the most stable titers were achieved from MV^{Pwt}-CD133 lysates. Compared to MV-related viruses, VSV-related viruses yielded higher titers not only in cell-associated but also in supernatant-associated samples. Among VSV, the fastest replication kinetics were obtained from cells infected with VSV-MV. Importantly, VSV-

related viruses generated almost up to 10^2 times more infectious particles in supernatant than in lysate and more than 10^3 times more infectious particles compared to their MV-based counterparts (if highest values of MV- and VSV-related viruses are compared).

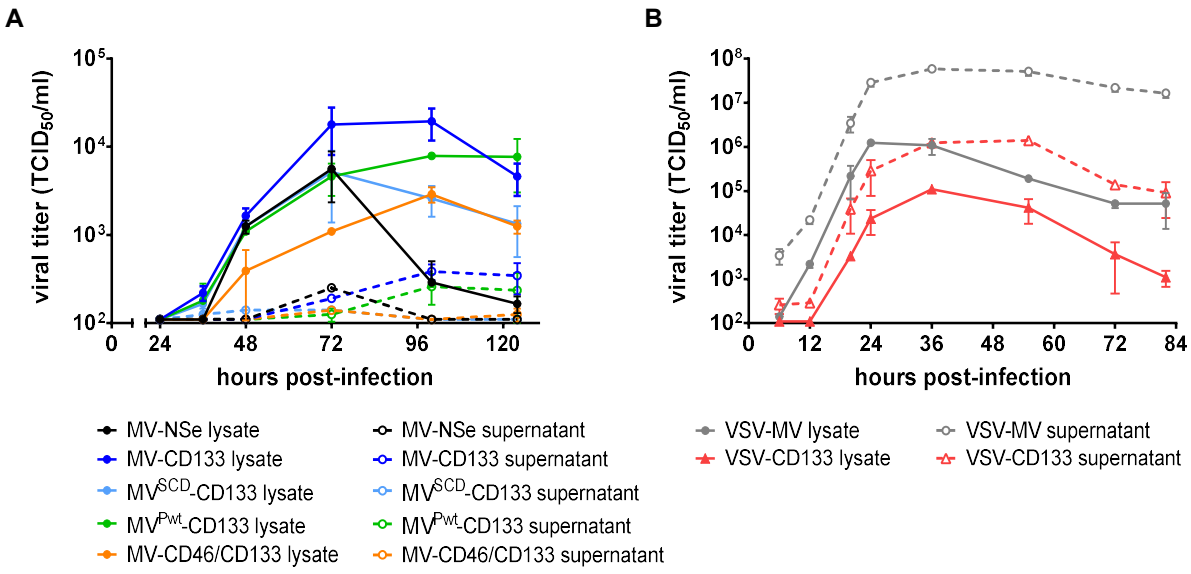

Figure 16. Replication kinetics of oncolytic viruses on HuH7 cells
Multi-step replication curves of CD133-targeted measles virus (MV) and vesicular stomatitis virus (VSV) and the respective untargeted viruses on HuH7 cells. Cell-associated (lysate) virus and virus from cell culture medium (supernatant) were obtained at indicated time points after infection with a multiplicity of infection (MOI) of 0.03. Titers were determined as 50 % tissue culture infective dose ($TCID_{50}$/ml) by titration on Vero-αHis cells according to Spearman-Kärber. **(A)** Replication kinetics of CD133-targeted MVs and the untargeted parental virus MV-NSe. **(B)** Replication kinetic of VSV-CD133 and the untargeted virus VSV-MV. The continuous lines represent titers obtained from lysate. The dotted lines represent titers obtained from supernatant. Mean values ±SD of three technical replicates.

3.4. Toxicity Testing of CD133-targeted Oncolytic Viruses towards Human CD34$^+$ Cells

OVs must not only be effective, above all, they must be safe. In particular, this means that healthy cells endowed with the target receptor should to be spared by the targeted OV while retaining its activity to lyse neoplastic cells. CD133 is not only a marker for tumor-initiating cells in a variety of tumor entities but also for early progenitors of the hematopoietic system (Yin et al., 1997). It has already been shown that HSCs can be infected with MV-CD133, albeit infection rates were low-to-negligible and non-productive (Bach et al., 2013). Here, we intended to elucidate potential adverse effects of the newly established MV recombinants. This referred in particular to the additional receptor usage, arming with the P gene of the MV wt, employment of the SCD/5-FC system and VSV-MV chimeras.

3.4.1. Analysis of Human CD34⁺ Cells for Susceptibility to Infection

In order to analyze if human HSCs are permissive to infection by the newly generated MV recombinants, the cell surface expression levels of CD133 and CD46 were determined prior to infection. Therefore, human G-CSF-mobilized CD34⁺ peripheral blood progenitor cells were stimulated overnight with cytokines prior to flow cytometry using Fluorescein Isothiocyanate (FITC)-labeled antibodies directed against human CD46 and Allophycocyanin (APC)-labeled antibodies directed against human CD133/1 (AC133 epitope). To avoid false positive antibody binding due to Fc receptor-mediated antibody labeling, FcR Blocking Reagent was used. Cells stained with mouse IgG1 isotype control antibodies served as negative controls.

As shown in Figure 17, the cell surface expression levels of human CD46 (99.10 %) and human CD133 (94.16 %) were comparably high. The CD46 and CD133 expression of this high degree can go along with a high risk of infection with viruses that use these receptors for cell entry. Testing of the sensitivity of human HSCs to infection therefore was the next reasonable step towards safety evaluation of targeted OVs.

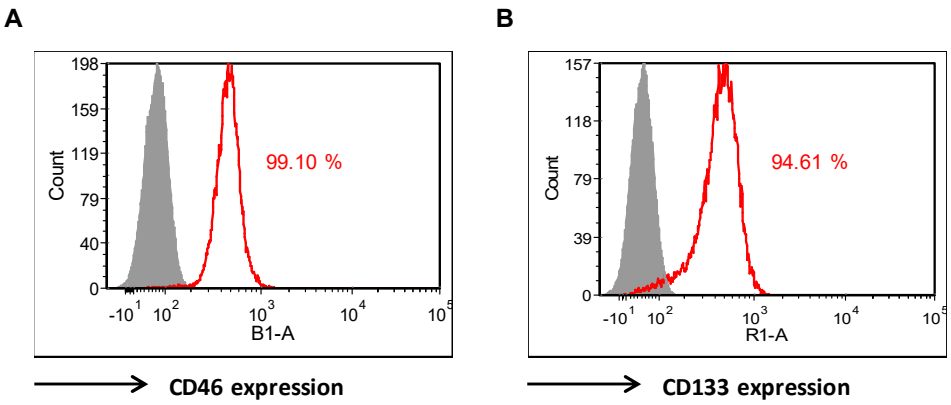

Figure 17. Cell surface expression levels of CD46 and CD133 on human CD34⁺ cells
CD34⁺ cells were obtained after purification from granulocyte colony-stimulating factor (G-CSF) mobilized peripheral blood using CD34 MACS beads and stimulation with Flt-3 ligand, stem cell factor, IL-3, IL-6 and TPO. After 24 hours, cell surface expression of CD133 (the epitope AC133) and CD46 were analyzed by flow cytometry using APC- or FITC-labeled antibodies, respectively. FcR Blocking Reagent was used to avoid Fc receptor-mediated antibody labeling. Percent of receptor positive cells for **(A)** CD46⁺ and **(B)** CD133⁺ cells are shown as red lined histograms in relation to cells stained with mouse IgG1 isotype control antibodies, which are depicted as gray-filled histograms. Adapted from (Kleinlützum et al., 2017).

Following the confirmation of high cell surface expression levels of both, CD46 and CD133, the cells were infected at an MOI of 1 with the OVs and cultivated for 10 days. During that time, GFP expression was evaluated at day 3, 6 and 10 post infection using fluorescence microscopy and flow cytometry. Flow cytometry was used as a complementary tool to fluorescence microscopy to render the read-out comparable and quantifiable. To avoid false-positive events in flow cytometry analyses, viable cells were assessed for their GFP expression after being discriminated from dead cells and debris by applying the LIVE/DEAD Fixable Violet Dead Cell

Staining Kit. Due to the absence of the reporter gene GFP in MV^{SCD}-CD133, infection by this virus could neither be assessed by fluorescence microscopy nor by flow cytometry. Since all OVs were set at the same MOI, however, MV-CD133 was used for the evaluation of MV^{SCD}-CD133. Thus, MV^{SCD}-CD133 was only subjected to functional assays (chapter 3.4.2).

As shown in Figure 18A, the quantity of GFP$^+$ cells infected with MV-NSe increased over time, from 10.28 % GFP$^+$ cells by day 3 post infection to 87.72 % by day 6 post infection and afterwards remained steady until day 10 post infection. While the number of GFP$^+$ cells incubated with CD133-targeted MVs remained constant over the whole observation period, it steadily increased over time in cells incubated with MV-CD46/CD133: At day 3 post infection, GFP expression of cells incubated with MV-CD46/CD133 was about 5-fold less compared to GFP expression of cells incubated with MV-NSe at that time point. GFP expression steadily

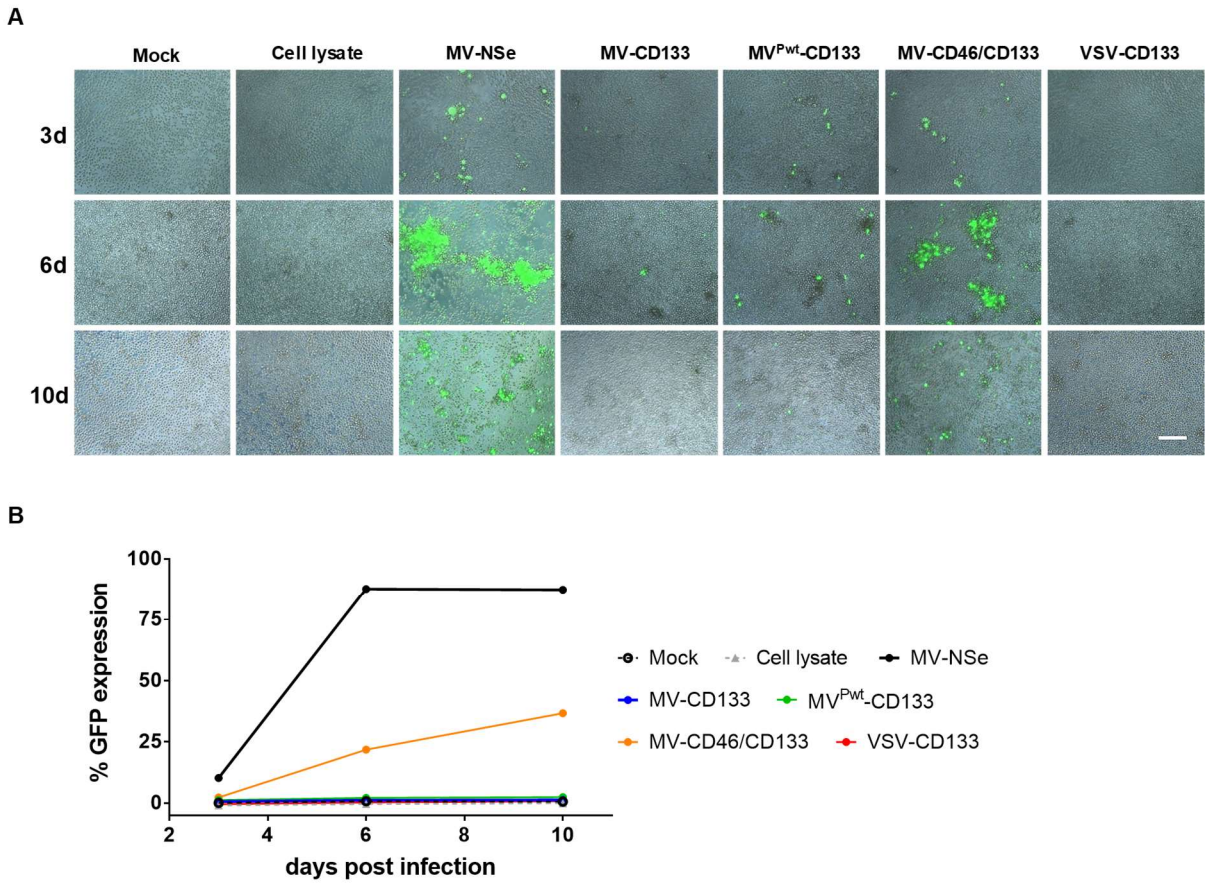

Figure 18. Infection of human CD34$^+$ cells
CD34$^+$ cells were infected with the indicated viruses at a multiplicity of infection (MOI) of 1. Cells were cultured in a 96-well plate and provided with fresh medium supplied with nutritives and cytokines. Infection was followed up for 10 days after infection and analyzed at the indicated time points by **(A)** visualization of GFP$^+$ cells using fluorescence microscopy. GFP and bright field images are merged to illustrate the number of GFP$^+$ cells relative to the number of cells present in a representative area of the well corresponding to an area of 500 µm (depicted by the white scale bar). **(B)** Quantification of GFP$^+$ cells using flow cytometry.

rised, to 21.84 % GFP$^+$ cells at day 6 post infection and up to 36.71 % GFP$^+$ cells at day 10 post infection. Among all groups, the numbers of green fluorescent cells detected by flow cytometry were not fully consistent with the numbers of GFP$^+$ cells detected by fluorescence microscopy (Figure 18B). Here, at day 10 post infection, the number of GFP$^+$ cells in samples incubated with MV-CD46/CD133 appeared less than determined by flow cytometry. Besides, the number of GFP$^+$ cells was slightly greater in cells incubated with MV^{Pwt}-CD133 than in cells incubated with MV-CD133 although there was no difference detectable by means of flow cytometry. By contrast, no single GFP$^+$ cell was detected by fluorescence microscopy or by flow cytometry in cells incubated with VSV-CD133. Notably, at day 6 post infection, GFP$^+$ cells in HSCs incubated with MV-NSe appeared to be clustered together while at day 10 post infection, GFP$^+$ cells rather appeared diffusely distributed.

As we cannot distinguish between transfer of GFP as protein from the producer cells to HSCs by this assay, functional tests will be particularly important and revealing – in particular for the safety assessment of MVs with an extended receptor usage and in conjunction with the SCD/5-FC system.

3.4.2. Evaluation of Impairment of Hematopoietic Stem Cell Self-Renewal after Infection

After assessment of GFP$^+$ cells, the next step was to investigate the effect of OVs on the proliferative and differentiation capacity of HSCs.

For this purpose, a CFA was performed. This is a valuable tool to evaluate potential toxic effects of new therapeutics on the development of hematopoietic progenies *in vitro*. Hematopoietic progenitor cells were plated into semi-solid methylcellulose medium supplemented with cytokines and growth factors enabling the cells to proliferate and differentiate to produce phenotypically distinct colonies of maturing cells of the hematopoietic lineage. In this manner, myeloid multipotential progenitors and committed progenitors of the erythroid, monocyte and granulocyte lineages can be distinguished morphologically (Pereira et al., 2007; Frisch and Calvi, 2014). Thereby, a change in the frequency of colonies of specific differentiated hematopoietic cells and / or colony morphology and even individual cell morphology of compound-treated cultures compared to a control culture indicates toxicity (Clarke et al., 2007).

CD34$^+$ cells were subjected to the CFA assay at day 3 after infection (Figure 18A and Figure 18B). Following incubation for 11 days, colonies were identified and enumerated *in situ* by light microscopy. In each sample, all hematopoietic progeny of the myeloid and erythroid lineage covered by this tool were detected. Compared to mock-treated cells, no changes in total colony numbers and colony numbers of specific hematopoietic lineage as well as colony and single cell phenotype were found in any of the treatment groups. However, a slight decrease of the

total colony number of HSCs incubated with MV-NSe was found. This decrease was mainly attributed to a reduction of committed progenitor cells of both erythroid / macrophage lineages (BFU-E, CFU-G, CFU-M and CFU-GM). The difference in the proliferation and differentiation of cells derived from mock, cell lysate and virus-infected cells was not significant. However, we could not find any GFP^+ cell in the colonies. The results strongly indicate that the CD133-targeted viruses do not impair the hematopoietic capabilities of $CD34^+$ cells (Figure 19).

The data confirm that HSC properties of healthy stem cells are not impaired upon incubation with CD133-targeted viruses.

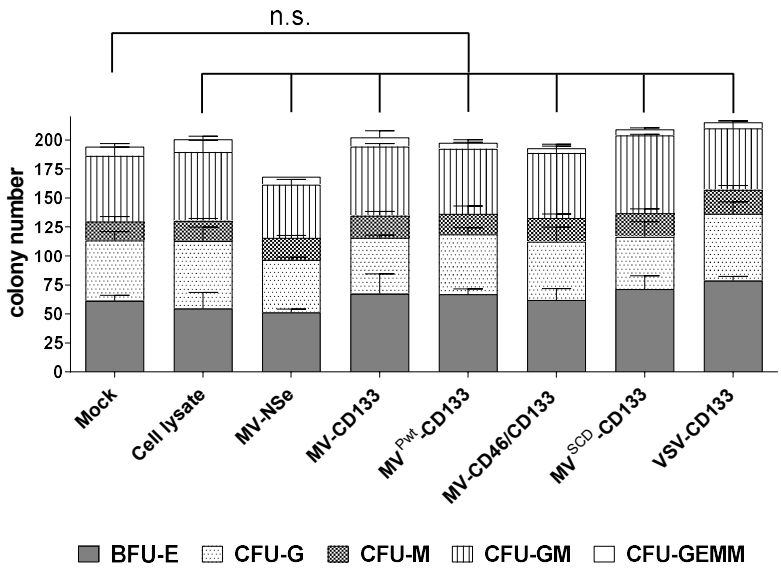

Figure 19. Hematopoietic stem cell properties are not impaired by infection
$CD34^+$ cells purified from granulocyte colony-stimulating factor (G-CSF) mobilized peripheral blood were incubated with the indicated viruses at a multiplicity of infection (MOI) of 1, mock or cell lysate from Vero-αHis cells, respectively. A colony-forming cell assay was performed by 11 days post infection to determine the number of colonies derived from erythroid and myeloid progenitors *in situ* by light microscopy. The proportion of the respective progenitors is shown in relation to the total colonies. Mean distribution ±SD of all colonies derived from three technical replicates are shown as a bar. The statistical analysis was carried out by a descriptive-explorative data analysis. Differences between treatment groups and mock control group were not significant according to 1-way ANOVA followed by Sidak's multiple comparison test: $P = 0.9993$ (cell lysate), $P = 0.4103$ (MV-NSe), $P > 0.9969$ (MV-CD133), $P > 0.9999$ (MV^{Pwt}-CD133), $P > 0.9999$ (MV-CD46/CD133), P =0.9036 (MV^{SCD}-CD133), $P= 0.6528$ (VSV-CD133). BFU-E, burst-forming unit erythroid; CFU-G, colony-forming unit-granulocyte; CFU-M, colony-forming unit-macrophage; CFU-GM, colony-forming unit-granulocyte, macrophage; CFU-GEMM, colony-forming unit-granulocyte, erythroid, macrophage, megakaryocyte; n.s., not significant. Adapted from (Kleinlützum et al., 2017).

3.5. Oncolytic Properties on Cultured Cells

Apart from the selective infection of target cells along with efficient replication in these cells, infection with the oncolytic agent pursues efficient demise of tumor cells. The various approaches to investigation aim to provide insights into the killing capabilities of the newly established OVs. In this context, the aim of these *in vitro* efficacy studies was the identification of the most efficiently performing virus for use it in further efficacy studies *in vitro* and *in vivo*.

3.5.1. Infection of Hepatocellular Carcinoma Cells

It was first assessed whether the OVs were able to infect cells that express high cell surface levels of CD133. For this purpose, the HCC cell line HuH7 was used because its cell surface expression levels are far over 90 % and infection and lysis by first generation CD133-targeted virus has already been proven *in vitro* and *in vivo* (Bach et al., 2013). Accordingly, we suspected that the newly generated CD133-targeted viruses could enhance oncolytic properties.

HuH7 cells were infected with MV-CD133 or VSV-CD133 at an MOI of 0.1, respectively. Every 4 hours, cells were microscopically checked for GFP expression. At 4 (corresponding to 20 hours after cell seed), 8, 24 and 32 hours after infection cells were stained with an APC-labeled antibody against CD133 (epitope AC133) or against IgG1 as isotype control to discern the positive signal from the background fluorescence. CD133 and GFP expression levels on uninfected (referred to as mock) and infected cells were analyzed by flow cytometry at the determined time points and compared to expression levels of uninfected cells.

As can be seen on the dot plots (Figure 20A), the CD133 cell surface expression levels were found to be stable (ranging between 74.13 and 86.22 %) on mock or MV-CD133 infected cells throughout the observation period of 32 hours after infection. Expression levels of cells infected with VSV-CD133 started to decrease 1 day after infection with 47.25 % by day 32 after infection. Over time, the mean fluorescence intensity (MFI) of mock and VSV-treated cells declined within 32 hours after infection (1358 and 555, respectively). However, in MV-CD133 treated cells, the MFI slightly increased by 24 hours after which it sharply decreased (Figure 20). At the last time point, cells infected with VSV-CD133 showed an MFI which was 50 % of that of MV-CD133.

While the loss of expression was negligible on MV-infected cells compared to mock treated cells, CD133 expression and MFI sharply dropped in VSV-infected cells between 24 and 32 hours after infection. Having analyzed the CD133 expression patterns in virus-infected cells *in vitro*, it will be important to examine the expression patterns in virus-treated HuH7 xenografts *in vivo*.

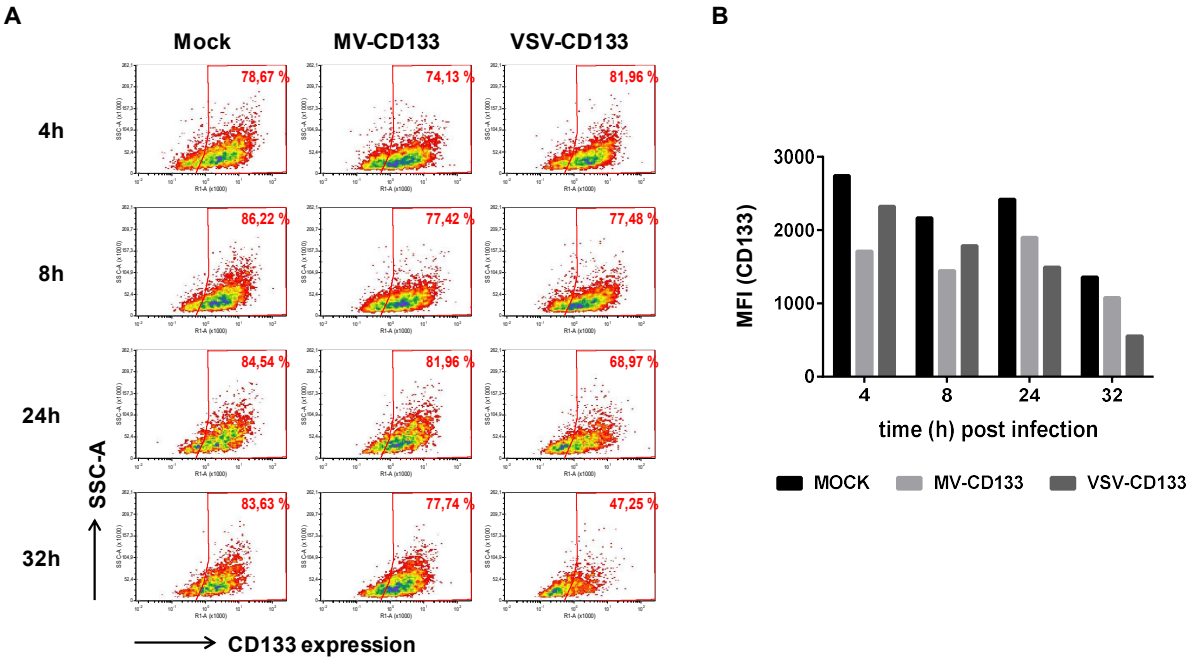

Figure 20. Cell surface expression levels of CD133 on infected HuH7 cells
HuH7 cells were infected with MV-CD133 or VSV-CD133 at a multiplicity of infection (MOI) of 0.1. Cell surface expression levels of CD133 were analyzed at 4, 8, 24 and 32 hours post infection by flow cytometry using APC-labeled antibodies directed against the epitope AC133. **(A)** Flow cytometry dot plots of uninfected cells (mock) and cells infected with MV-CD133 or VSV-CD133, respectively. The percentages of CD133 were assessed based on isotype control for threshold definition (red rectangle gates). **(B)** The bar graph shows the mean fluorescence intensities (MFI) as the median of the whole population of mock, MV-CD133 and VSV-CD133 infected cells, respectively, after subtraction of background fluorescence.

3.5.1.1. Oncolytic Performance on Hepatocellular Carcinoma Cells

Next, we studied the oncolytic activity of the recombinant viruses on HuH7 cells. Cells were infected at an MOI of 1 with MV-CD133, MV^{Pwt}-CD133, MV-CD46/CD133 and VSV-CD133. Cell viability was monitored in colorimetric cell proliferation assays over a time period of 120 hours post infection in comparison to mock infected cells. Cell viability was measured every 24 hours and each value was normalized to mock treated cells to obtain a kinetic curve of cell killing. Again, MV-CD133 was used representatively for studying solely the virus-mediated oncolysis of MV^{SCD}-CD133 (without addition of the prodrug 5-FC). As shown in Figure 21 all viruses except for MV-CD133 killed nearly 100 % of the cells within 72 hours post infection, while a comparable decimation of cells was not reached before 96 hours post infection in cells treated with MV-CD133. Moreover, cell viability was reduced to less than 50 % before 48 hours post infection in VSV-CD133 treated cells. VSV-CD133 thus succeeded in overtaking the oncolytic MVs by at least 11 hours on average when accounted for the time (hours) needed to kill 50 % of the cell population (for details see Table 4).

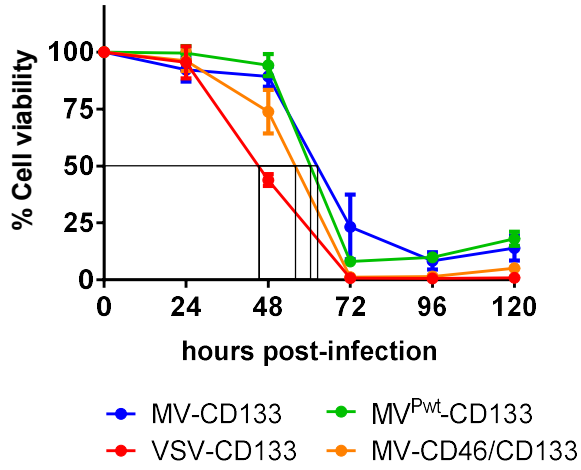

Figure 21. Killing kinetics of oncolytic viruses
HuH7 cells were infected with the indicated viruses at a multiplicity of infection (MOI) of 1. Cell viability was determined in 24 hourly steps up to 120 hours by WST-1 Cell Proliferation assays. Depicted is the percentage of viable cells relative to mock-treated cells, which was set to 100 %. The rectangle frames indicate the needed time (hours post infection) of each virus to reach reduction of cell viability to 50 %. Mean values ±SD of two biological and four technical replicates. Adapted from (Kleinlützum et al., 2017).

Table 4. Time-dependent killing capabilities of oncolytic viruses

Oncolytic Virus	Hours p.i. needed to reach cell killing of	
	50 %	90 %
MV-CD133	62	93
MVPwt-CD133	60	71
MV-CD46/CD133	56	69
VSV-CD133	45	67

p.i., post infection

After evaluating the killing properties during a specific period of time, we also wanted to elucidate a possible dose-dependent killing effect by applying a range of MOIs and analyze cytotoxicity at a defined time point. Cytotoxicity was assessed not later than 72 hours post infection, since, by then, cell killing by all examined viruses was advanced but not exhausted (Figure 21). Thus, the choice of this time-point to be investigated at a time-dependent manner would enable to capture subtle dose-dependent responses. Aside from comparing virus-related killing capabilities, we also wanted to investigate the synergistic effect of prodrug addition (0.1 mM 5-FC) to cells incubated with different MOIs of MV^{SCD}-CD133. 5-FC was added to cells 16 hours after infection with MV^{SCD}-CD133. To rather obtain a quantitative validity, we determined the effective concentration required to reduce cell viability to 50 % (EC_{50}) in relation to untreated cells.

As seen in Figure 22, all viruses killed HuH7 cells in a dose-dependent manner but at various extents. VSV-CD133 and MV^{SCD}-CD133 (in co-administration with 0.1 mM 5-FC) exhibited the most substantial cytotoxicity even at very low MOIs. Accordingly, in cells infected with VSV-CD133 and MV^{SCD}-CD133/5-FC [0.1 mM] up to 31-fold less infectious virus particles were needed to achieve EC^{50} values (Kleinlützum et al., 2017).

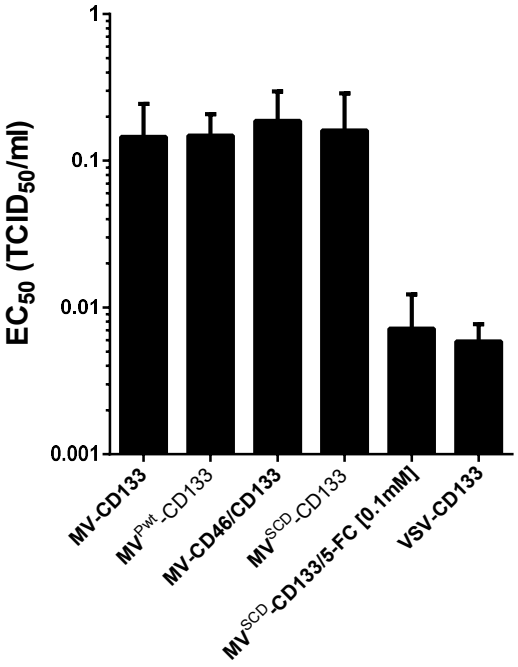

virus	EC_{50} value (mean)
MV-CD133	0,14589333
MV^{Pwt}-CD133	0,1481
MV-CD46/CD133	0,18707667
MV^{SCD}-CD133	0,16153
MV^{SCD}-CD133/5-FC [0,1mM]	0,00717867
VSV-CD133	0,00587167

Figure 22. Dose-dependent killing of HuH7 cells
HuH7 cells were infected with the indicated viruses at a broad range of multiplicity of infection (MOI). 16 hours post infection, the prodrug 5-fluorocytosine (5-FC) (0.1mM) was applied once only to cells infected with MV^{SCD}-CD133. Following incubation for 72 hours, cell viability related to mock-treated control cells was determined by WST assays. EC^{50} values were calculated from a standard curve. Mean values ±SD of three biological and four technical replicates. Adapted from (Kleinlützum et al., 2017).

3.5.2. Potentiated Oncolysis of MV^{SCD}-CD133 through Bystander-Mediated Killing of Target-Receptor Negative Cells

As we observed a major superiority of MV^{SCD}-CD133 / 5-FC to MV-CD133 in killing HuH7 cells, a HCC cell line with more than 90 % cell surface expression levels of CD133, we wanted to assess its oncolytic performance on cell cultures comprising CD133$^+$ and CD133$^-$ cells. For that purpose we used the fibrosarcoma cell line HT1080 that was used several times in our research group for selectivity experiments (Bach et al., 2013; Hanauer et al., 2018). In particular, we made use of the high selectivity of MV-CD133 (Figure 15) that would thus allow a reliable and specific target cell-restricted expression of the 5-FC converting enzyme SCD for achieving a localized chemotherapeutic effect also in non-infected cells (hereafter called “bystander effect”) combined with direct virus-mediated oncolysis. The aim of this arming approach was to potentiate oncolysis of CD133-targeted MV, by overcoming variability of CD133

expression on tumor cells that may potentially limit efficient cell-to-cell spread of MV and thus cell killing.

In order to directly quantify the bystander effect, we applied a FACS based assay allowing the discrimination of $CD133^+$ from $CD133^-$ cells. To do so, post-seed adhered co-cultures of parental HT1080 cells and CD133-transgenic HT1080 cells (hereafter-called HT1080-CD133) at a ratio of 1:1 were infected with MV-CD133 or MV^{SCD}-CD133, respectively. Thereby, the GFP reporter gene of MV-CD133 was used for unambiguous detection of infected cells, as MV^{SCD}-CD133 is not equipped with the reporter gene GFP. Uninfected control cells served as negative control. After 16 hours, cells were exposed to a broad range of 5-FC doses (from 0 mM up to 10 mM in steps of powers of 10). After 72 hours, cells were detached and cell suspensions were subjected to live/dead discrimination via covalently binding amine-reactive dyes following staining with APC-labeled anti-CD133/1 (epitope AC133). Thereafter, identical volumes of all individual samples were acquired by flow cytometry. Based on an absolute viable cell count, absolute numbers of viable red (APC^+; $CD133^+$) cells in a given volume were determined for each sample. Based thereon, the viable proportions of $CD133^-$ cells were calculated relatively to APC^+ cells (Figure 23A).

Both viruses killed approximately 25 % of HT1080/HT1080-CD133 mixed cultures by direct virus-mediated cytotoxicity (Figure 23B, upper left panel, 0 mM 5-FC). As seen in Figure 23B, bottom right panel, the reduction in the OS described above was apparently ascribed to the killing of $CD133^+$ cells, which was further enhanced when cells were infected with MV^{SCD}-CD133 and treated with 5-FC, thereby reaching dose-dependent cell killing of more than 90 % (Figure 23B, bottom left panel and Figure 23C). Unlike the $CD133^+$ cells, the killing of $CD133^-$ cells after addition of 5-FC was only mediated by MV^{SCD}-CD133 (bystander-mediated cytotoxicity) and even effective at the lowest prodrug concentration used (Figure 23B, bottom left panel, 0.001 mM 5-FC). Although 5-FC addition affected cell proliferation negatively (Figure 23B, Mock), cell survival was only reduced in cells previously infected with MV^{SCD}-CD133 and this reduction was significant. Treatment with 0.01 mM 5-FC resulted in 50 % reduction of viability in the $CD133^+$ proportion and in 75 % reduction of viability in the $CD133^+$ proportion within 72h after 5-FC treatment (Figure 23C).

3.6. Oncolytic Properties on Primary Tumor Cells

To further elucidate the therapeutic impact of CD133-targeted OVs we used another tumor entity whose aggressiveness in the patient strongly correlates with CD133 expression (Yan et al., 2011). Accordingly, we chose the primary sphere cell line NCH644 that was derived

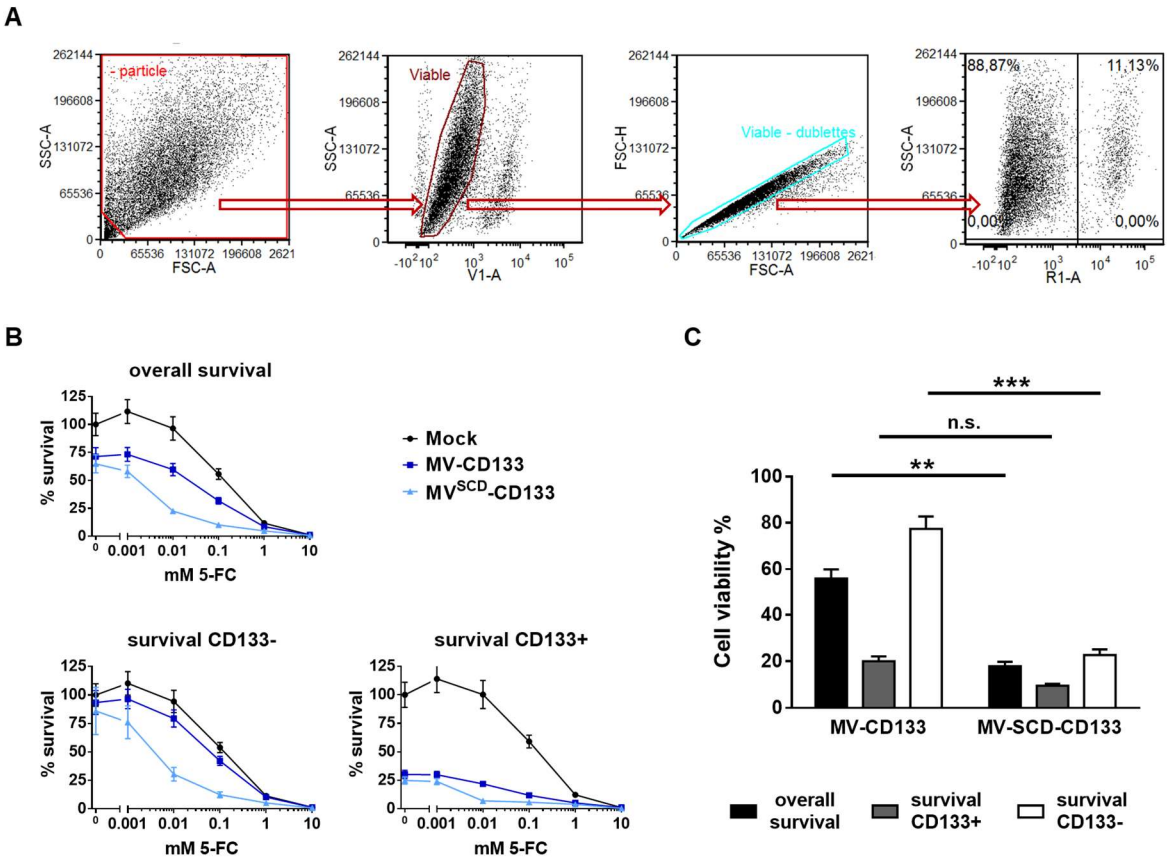

Figure 23. Enhanced cell killing by MV^{SCD}-CD133-mediated bystander killing
Co-Culture of HT1080 and HT1080-CD133 (1:1) infected with the indicated viruses at a multiplicity of infection (MOI) of 1. After 16 hours post infection, cells were exposed to a broad dose range of the prodrug 5-fluorocytosine (5-FC). 72 hours post 5-FC treatment, the proportions of the viable overall population and the viable subfractions of CD133-positive (survival CD133^{+}) and CD133-negative (survival CD133^{-}) cells were determined following discrimination via amine-reactive viability dyes and APC-labeled anti-CD133/1 antibodies (epitope AC133/1). **(A)** Gating strategy for flow cytometry analysis. As illustrated from left to right, the cell population is excluded from debris (SSC-A vs. FSC-A) and further analyzed for its uptake of viability dye to distinguish live versus dead cells (SSC-A vs. V1-A). The resulting viable gate is gated for singlets (FSC-H vs. FSC-A). Finally, single viable cells are gated for their CD133 expression (SSC-A vs. R1-A). In the SSC-A vs. V1-A density plot, shifted cells represent dead cells. In the SSC-A vs. R1-A plot shifted cells represent CD133-positive cells. Unstained cells and isotype control cells define the gate borders. **(B)** Dose-dependency curves. Values represent survival (%) compared to untreated PBS control (Mock). *n* = 3; mean±SD of three biological and four technical replicates. **(C)** The bar graph shows the mean distribution ±SD of the indicated cell fractions of virus-infected co-cultures treated with 0.01 mM 5-FC relative to untreated PBS control cells. The results are an average of three independent experiments each done in quadruplicates. One-way ANOVA with Sidak's multiple comparison test, ***P = 0.0002, **P = 0.0021.

from a human GBM specimen (Campos et al., 2014). NCH644 sphere cells are known to form spheres under serum-free conditions and to express over 90 % CD133 on their cell surface (Bach et al., 2013). Being kept that way, they recapitulate a subpopulation of glioma stem-like cells, capable of differentiating into the actively expanding tumor bulk specimen (Bach et al., 2013; Campos et al., 2014; Phillips et al., 2016). Using these cells allowed us to evaluate a potential anti-tumoral efficacy in a clinically more relevant setup.

3.6.1. Cell Surface Expression Levels of CD46 and CD133 on NCH644 Cells

Target cell surface expression is the major prerequisite for successful oncolysis. Thus, before killing properties on NCH644 sphere cells were analyzed, cell surface expression levels of CD133 using two different epitopes, CD133/1 (AC133) and CD133/1 (AC141.1) were analyzed via flow cytometry. Upon culturing NCH644 in serum-free medium supplemented with bovine insulin transferrin (BIT_{100}), human fibroblast growth factor (FGF)-basic) and human epidermal growth factor (EGF) at 20 ng/mL each, glioma stem-cell like behavior such as sphere formation with accompanied up-regulation of CD133 is known to be initiated (Bach et al., 2013). To confirm the expression level found in literature, NCH644 cells were cultured in aforementioned GSC medium for 14 days to obtain stem cell conditions and subsequently subjected to flow cytometry analysis. NCH644 spheres were separated to single cells using a 70 µm strainer. To avoid false positive antibody binding due to detection of CD133 on dying or dead cells, cells were stained with Live Dead Fixable Violet Dead Cell stain prior to incubation with PE-labeled antibodies against CD133 and FITC-labeled antibodies against CD46, respectively. Cells stained with isotype control (Mouse IgG1 for anti-CD133 antibodies and REA control (S) antibodies for CD46) served as negative controls.

As seen in Figure 24, the cell surface expression levels of human CD46 (99.79 %) differed slightly from the cell surface expression levels of human CD133/1 (AC133) (92.92 %) and human CD133/2 (AC141.1) (98.02 %), While MFI of both CD133 expression markers, were similar, MFI of CD46 expression was found to be 1-log level higher than of that of CD133-expression of both epitopes.

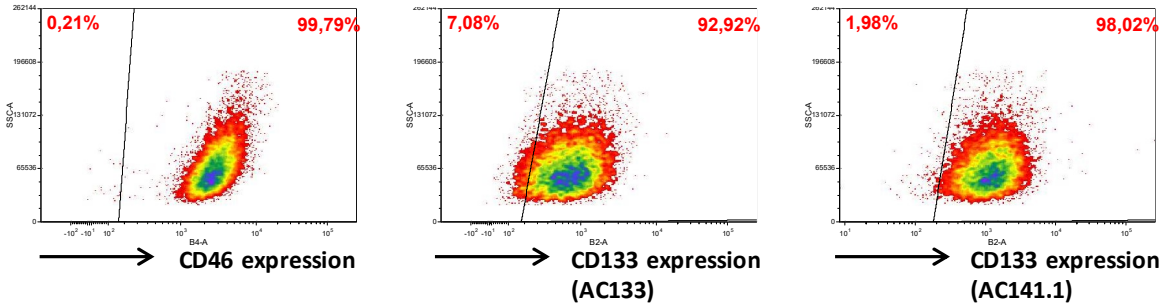

Figure 24. Cell surface expression levels of CD46 and CD133 on glioma sphere cells
Human glioma sphere cells were cultured under serum-free conditions for 14 days, followed by determination of cell surface expression levels of human CD46 and human CD133 (epitopes AC133 and AC141.1) by flow cytometry analysis using FITC- and PE-labeled antibodies, respectively. Live Dead Fixable Violet Dead Cell stain and FcR Blocking Reagent were used to avoid false positive antibody binding of dead or dying cells. Percent of cells for positive for CD46, CD133/1 (epitope AC133) and CD133/2 (epitope AC141.1) are the shifted cell population depicted in density dot plots, respectively. Adapted from (Kleinlützum et al., 2017).

The results demonstrated that the GSC line NCH644 is a suitable target. Testing the efficacy of viruses in an orthotopic environment will be rewarding for assessment of oncolytic performance. Thus, the following experiments for the characterization of the oncolytic performances of viruses on glioma will include *in vitro* cytotoxicity testing prior to *in vivo* experimentation.

3.6.2. Time and Dose Response Killing of Primary Glioma Sphere Cells

To investigate the susceptibility of NCH644 sphere cells to the CD133-targeted viruses, single cell suspensions were infected with MV-CD133, MV^{Pwt}-CD133, MV-CD46/CD133, VSV-MV or VSV-CD133 at an MOI of 1. Cells were observed by fluorescence microscopy every 6 hours until green fluorescent signals were detectable and afterwards every 24 hours.

At 24 hours post infection, green fluorescent cells became detectable (Figure 25). At that time point, all viruses had infected the cells. Strongest signals were seen in MV-CD133 and MV-CD46/CD133 infected cells with the latter exhibiting the most prominent CPE characterized by syncytia formation. While green fluorescent signals increased within 96 hours in cell cultures infected with MVs, signals became weaker in cell cultures infected with VSV-MV and VSV-CD133.

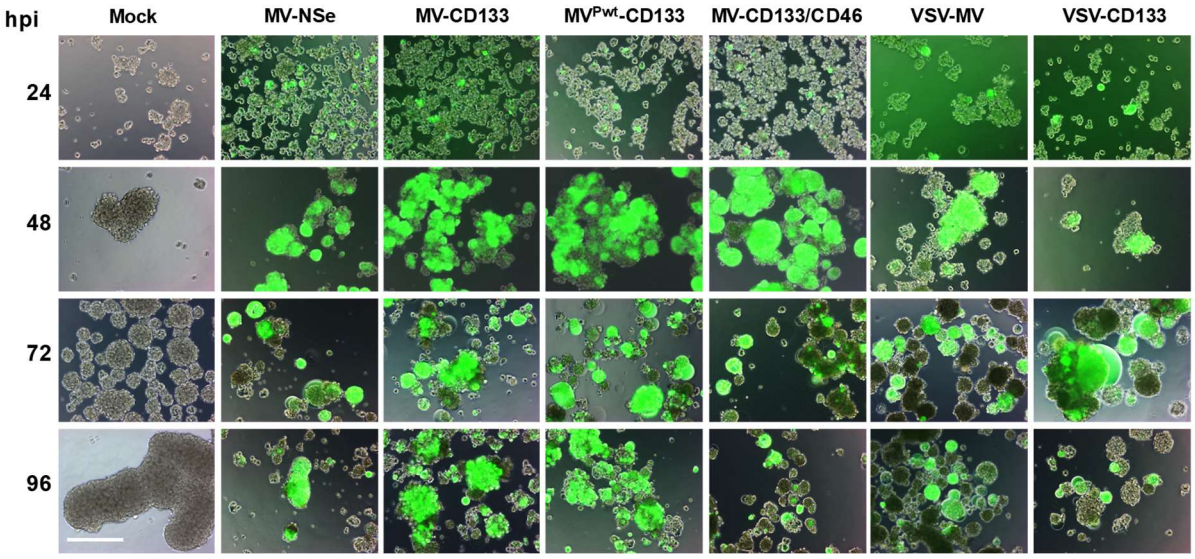

Figure 25. Infection and killing of primary glioma sphere cells
Single cells suspensions of NCH644 cells were infected with the indicated viruses at an MOI of 1. Cells were monitored microscopically for GFP expression up to 96 hours post infection. Scale bar, 500 µm. Adapted from (Kleinlützum et al., 2017).

To obtain more information about the oncolytic performance with regard to time and dose dependency we quantified cell killing over time while applying a range of MOIs. All viruses showed a dose-dependent cytotoxicity (Figure 26B). Regarding the time course of infection at an MOI of 1, initially, all viruses led to a steady decline in cell viability (Figure 26A). However,

48 hours after infection, cell killing with VSV-derived viruses had reached its maximum. In fact, these cells reversed to propagation while infection with MV-derived viruses led to further reduction of cell numbers. MV-CD46/CD133 and MV^{Pwt}-CD133 killed larger cell quantities of NCH644 cells than MV-CD133. Over the period of 72 hours, killing by MV-CD46/CD133 was superior over MV^{Pwt}-CD133: While MV^{Pwt}-CD133 reduced cell viability for 25 % more than MV-CD46/CD133 between 24 and 48 hours post infection, this head start was outpaced by MV-CD46/CD133 at 48 hours post infection. From that time point, killing superiority over MV^{Pwt}-CD133 occurred when using MOIs of 0.1 and above.

As MV^{SCD}-CD133 was not included in the *in vitro* cytotoxicity assays, next, it was tested in a comparable experimental setup, but with including different concentrations of 5-FC.

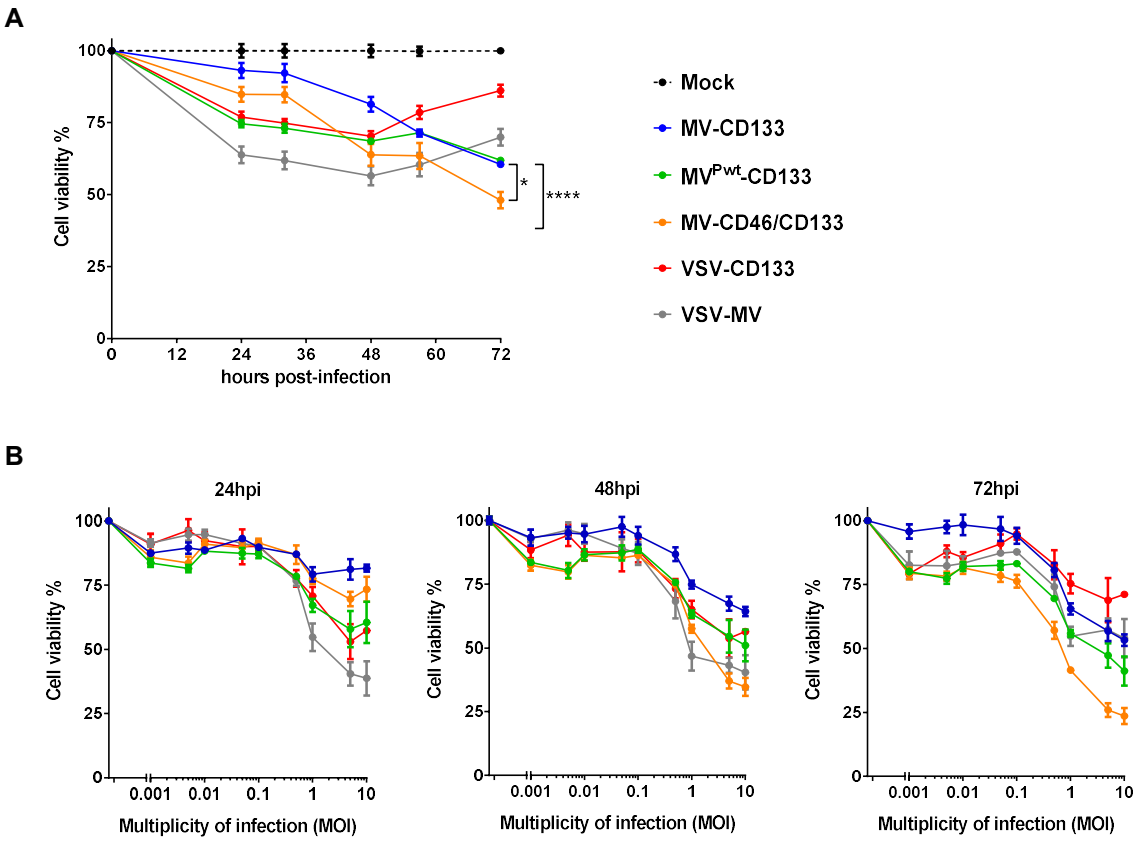

Figure 26. Differential killing kinetics of oncolytic viruses on glioma sphere cells
Single cell suspensions were infected with the indicated viruses at various MOIs ranging from 0.01 to 10. Cell viability of the glioma sphere cells was determined twice a day for 72 hours after virus addition using the RealTime-Glo MT Cell viability assay. **(A)** Time course of killing at an MOI of 1. Depicted is the percentage of viable cells relative to mock-treated cells, which was set to 100 %. Mean values ±SD of three biological and three technical replicates. One-way ANOVA with Dunnett's multiple comparison test, *$P < 0.05$; ****$P < 0.0001$. **(B)** Dose response curves of selected time points as indicated. Depicted is one representative biological experiment. Each value is the mean of three technical replicates. Adapted from (Kleinlützum et al., 2017).

3.6.3. Enhanced Killing of Primary Glioma Sphere Cells by MV^{SCD}-CD133

As the MV^{SCD}-CD133 / 5-FC system was able to potentiate oncolysis of HCC and fibrosarcoma cells as well as exerting bystander-mediated tumor cell killing, it was investigated whether oncolysis of NCH644 cells could also be further enhanced with MV^{SCD}-CD133 / 5-FC. In order to compare the oncolytic performance of MV^{SCD}-CD133 with oncolytic measles and vesicular stomatitis viruses the cytotoxicity assay was carried out in the same way as described in the previous section (chapter 3.6.2).

Again, single cell suspensions were infected with MV-CD133 or MV^{SCD}-CD133 at an MOI of 1. After 21 hours incubation, different concentrations of 5-FC were added to the cells. Using RealTime-Glo MT Cell Viability assays, cell viability was quantified in 12 hourly steps for up to 72 hours after infection.

As shown in Figure 27B, MV^{SCD}-CD133 (+ 5-FC) was superior to its counterpart MV-CD133 even at a prodrug concentration of 0.01 mM 5-FC and above. Bystander-mediated cytotoxicity was further enhanced with increasing prodrug concentrations reaching its maximum with a prodrug concentration of 1 mM 5-FC. At this concentration, viability of cells incubated with MV^{SCD}-CD133 was reduced by more than 19 % compared to MV-CD133. However, cytotoxicity was the same, when an MOI of 10 was used. The oncolytic potentiation of MV^{SCD}-CD133 / 5-FC became already apparent after 32 hours after infection (corresponding to 11 hours after

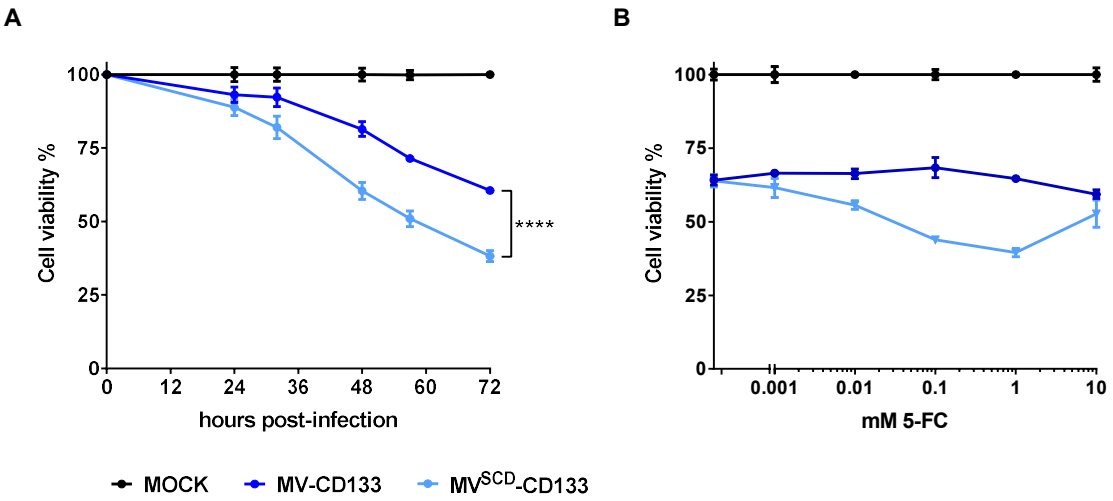

Figure 27. Time and dose dependency of 5-FC mediated cell killing of MV^{SCD}-CD133 on primary glioma sphere cells

Glioma sphere cells were dissociated to a single-cell suspension and infected with MV-CD133 or MV^{SCD}-CD133. 5-Fluorocytosine (5-FC) was added 21 hours after infection to a total concentration of 1 mM. Cell viability was quantified by RealTime-Glo MT Cell Viability assay twice a day for 72 hours after infection. **(A)** Time course of killing at an MOI of 1. Depicted is the percentage of viable cells relative to mock-treated cells, which was set to 100 %. Mean values ±SD of three biological and three technical replicates. One-way ANOVA with Dunnett's multiple comparison test, ****$P < 0.0001$. **(B)** Dose response curves at an MOI of 1 at 72 hpi. Depicted is one representative biological experiment. Each value is the mean ±SD of three technical replicates. Adapted from (Kleinlützum et al., 2017).

5-FC addition) using an MOI of 1 (Figure 27A). With the same kinetics, killing of cells incubated with MC^{SCD}-CD133 / 5-FC became significantly higher than cells incubated with MV-CD133 at 48 hours post infection.

As killing properties were confirmed *in vitro*, the next experiments aimed at oncolytic activity studies *in vivo.*

3.7. Efficacy *In Vivo*

Once we had characterized the CD133-targeted viruses *in vitro* with regard to activity, selectivity and safety, we wanted to address these points in the context of appropriate *in vivo* models. In particular, the following mice models were applied to elucidate whether the superior oncolytic effects of VSV-CD133, MV^{Pwt}-CD133, MV^{SCD}-CD133 and MV-CD46/CD133 demonstrated *in vitro* translate into prolonged survival in the respective mice models.

3.7.1. Activity of Intratumorally Applied CD133-Targeted Viruses in a Subcutaneous Xenograft Model of Hepatocellular Carcinoma

As shown in previous studies on a subcutaneous xenograft model of HCC, MV-CD133 was able to significantly reduce tumor burden in NOD/Scid mice compared to mock treated mice upon four intratumoral applications (Bach et al., 2013). However, total remission was reached in none of the animals. To compare treatment responses among the newly generated viruses, we used the same tumor model and treatment schedule as in the above mentioned study (Bach et al., 2013). Briefly, 5 x 10^6 HuH7 cells were inoculated subcutaneously on both flanks of NOD/Scid mice. Once tumors had reached a mean tumor volume of 100 mm^3, treatment was initiated consisting of four consecutive intratumoral applications of 1 x 10^6 $TCID_{50}$ of each virus, or virus-free Vero-αHis lysate in medium as control (mock). Tumor volumes were determined by digital caliper measurements twice a week. The study was performed in a blinded fashion, and treatment assignments were not uncovered until the end of the study.

Compared to mock-treated mice, all viruses were able to reduce tumor growth, with VSV-CD133 being by far superior over its MV counterparts (Figure 28A). The reduction in tumor burden was significant for VSV-CD133 as reflected by the AUC of tumor growth curves on day 40, by which all mice of the mock group had to be sacrificed due to exceeding tumor volumes (Figure 28B). As seen in Figure 28C, the positive treatment response was also affirmed by the Kaplan-Meier survival curves, which showed that treatment with VSV-CD133 resulted in the most pronounced survival benefit (mean survival 67 days). Growth behaviors of tumors infected with MV-CD46/CD133 were comparable with those of tumors infected with MV-CD133 or MV^{Pwt}-CD133, respectively. However, 2 out of 3 mice treated with MV-CD46/CD133 survived 11 days longer on average than the median survival of mice treated with MV-CD133

(46.5 days). Thus, the median survival of mice infected with MV-CD46/CD133 resulted in an intermediate value in between VSV-CD133 and its MV counterparts (54 days), and thus was the second most effective oncolytic agent in this model.

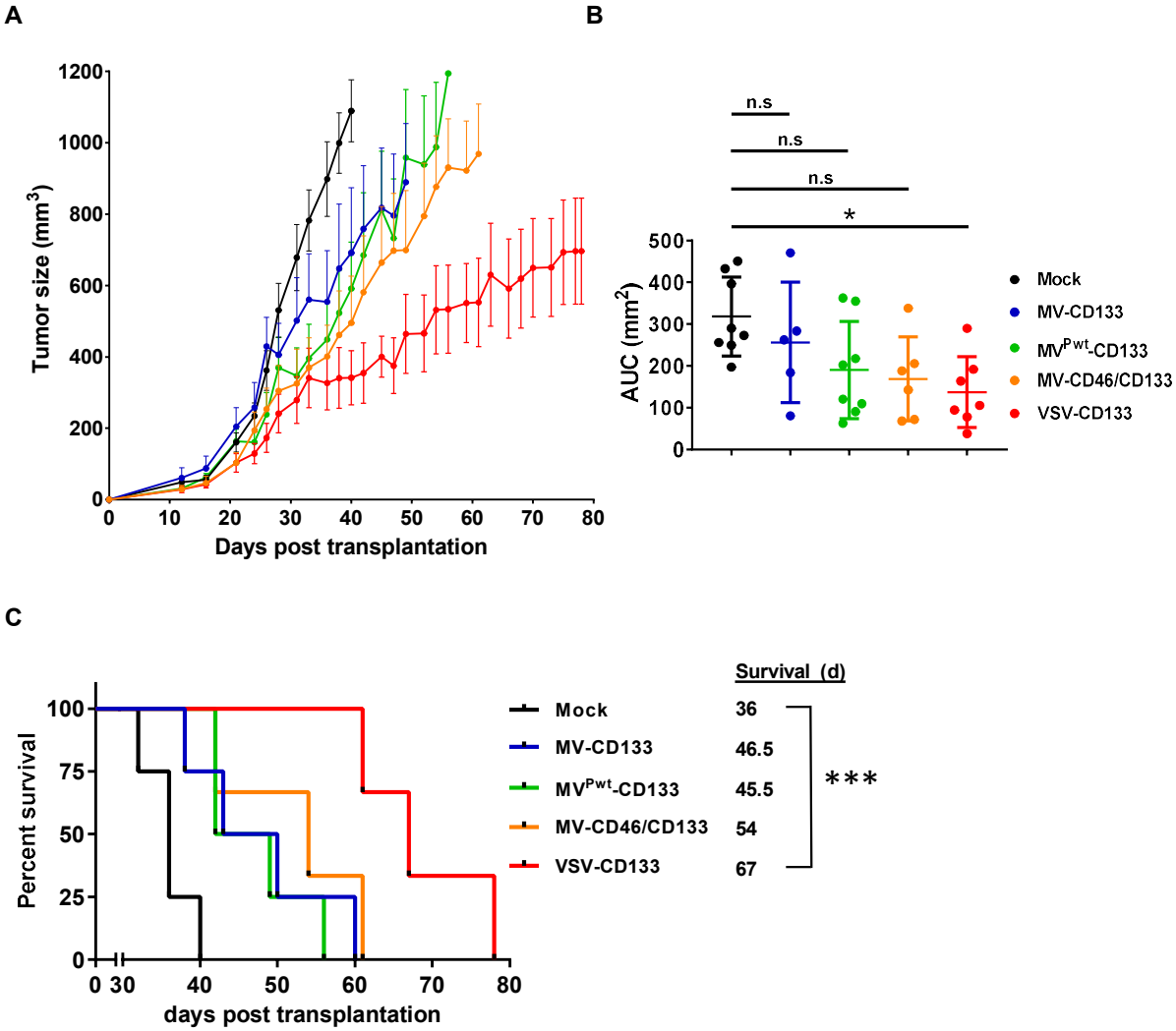

Figure 28. Oncolytic activities of intratumorally applied oncolytic viruses in a subcutaneous xenograft model of hepatocellular carcinoma

HuH7 cells were implanted subcutaneously into the flank of NOD/Scid mice. Tumor size was monitored using a caliper. Intratumoral treatment was initiated at a mean tumor volume of 100 mm^3 with four applications of 1 x 10^6 $TCID_{50}$ of each of the indicated viruses or Vero-αHis lysate in medium as control (mock) on four consecutive days. Treatment and tumor volume measurements were carried out in a blinded fashion over the whole course of the study until sacrifice. **(A)** Tumor dimensions of each individual animal were measured twice a week. The mean tumor volume (mm^3) of each treatment group was calculated and plotted against the course of the observation point. **(B)** Group comparisons were performed by determining the area under the curve (AUC) for each individual animal normalized against the value obtained from the last survivor of the mock group (40 days after treatment). The values were plotted as box and whiskers. One-way ANOVA with Dunnett's multiple comparison test, $*P < 0.05$. **(C)** Survival data were depicted as Kaplan-Meier survival curves. Comparison between the group with the lowest median survival (MV^{Pwt}-CD133) and the mock group was conducted by a log-rank test with Bonferroni adjustment for multiple comparisons. Mock, $n = 4$; measles virus (MV)-CD133, $n = 4$; MV^{Pwt}-CD133, $n = 4$; MV-CD46/CD133, $n = 3$; vesicular stomatitis virus (VSV)-CD133, $n = 3$. $**P < 0.01$. Adapted from (Kleinlützum et al., 2017).

Considering the outcome of oncolytic performance in this model, it was important to analyze tumors for replicating virus and their distribution patterns within tumors. Thus, tumor slices were made for immunofluorescence staining against GFP.

3.7.2. Characterization of Explanted Tumors Infected with MV-CD133 and VSV-CD133

As the oncolytic virotherapy did not result in total or at least partial remissions, after study termination, tumors treated with MV-CD133 and VSV-CD133, respectively, were analyzed for replicating virus and target receptor selectivity. To preserve tissue structure and GFP signals, mice were sacrificed by transcardial perfusion with PBS following perfusion with 4 % formaldehyde in PBS. After explantation, tumors were cut into 6 cross-sections (approximately 2-3 mm thick slices) as illustrated in (Figure 30A) and fixed in 4 % formaldehyde in PBS for 24 h following cryopreservation. Slices of 8 µm thickness were obtained with a cryostat (Leica CM1900). After permeabilization with 0.2 % Triton X100 in PBS, slices were subjected to different antibody staining procedures to detect virus and / or targeted cells.

3.7.2.1. Distribution of Virus within Tumor Tissue

Although viruses were highly selective for their target as shown by infection experiments with transgenic cell lines (Figure 15), it was analyzed if that also holds true for an *in vivo* situation. To assess selectivity *in vivo*, GFP signal distribution and localization within xenograft tumor tissue and across boundaries to adjacent mouse tissue were examined. An anti-GFP antibody was applied to amplify GFP-signals, which otherwise would be reduced by fixation or fade by lengthy light exposure of large resolution pictures. Slides were mounted with anti-fading mounting medium with DAPI allowing counter-stain of DNA and contributing to preservation.

For visualization of GFP-fluorescent areas within tumor cross-sections, the whole cross-view to be captured was split into tiles each of a 10 x magnification using the AxioVision MosaiX software. Using a fully automated Axio-Observer Z1 microscope a tile-by-tile acquisition of the GFP channel was performed. Depending on the size of the tumor, up to approximately 400 adjacent tiles were assembled and stitched to obtain an overview image.

As seen in a representative microphotograph of virus-infected tumor slices (Figure 29A), infection with VSV-CD133 resulted in multifocally to diffusely distributed infection centers which could be identified as multinucleated cells. Compared to VSV-CD133, infection with MV-CD133 resulted in few infection foci. As in VSV-CD133 infected slices, the infections centers comprised multiple fused cells (referred to as syncytia) as it is expected for MV-related CPEs.

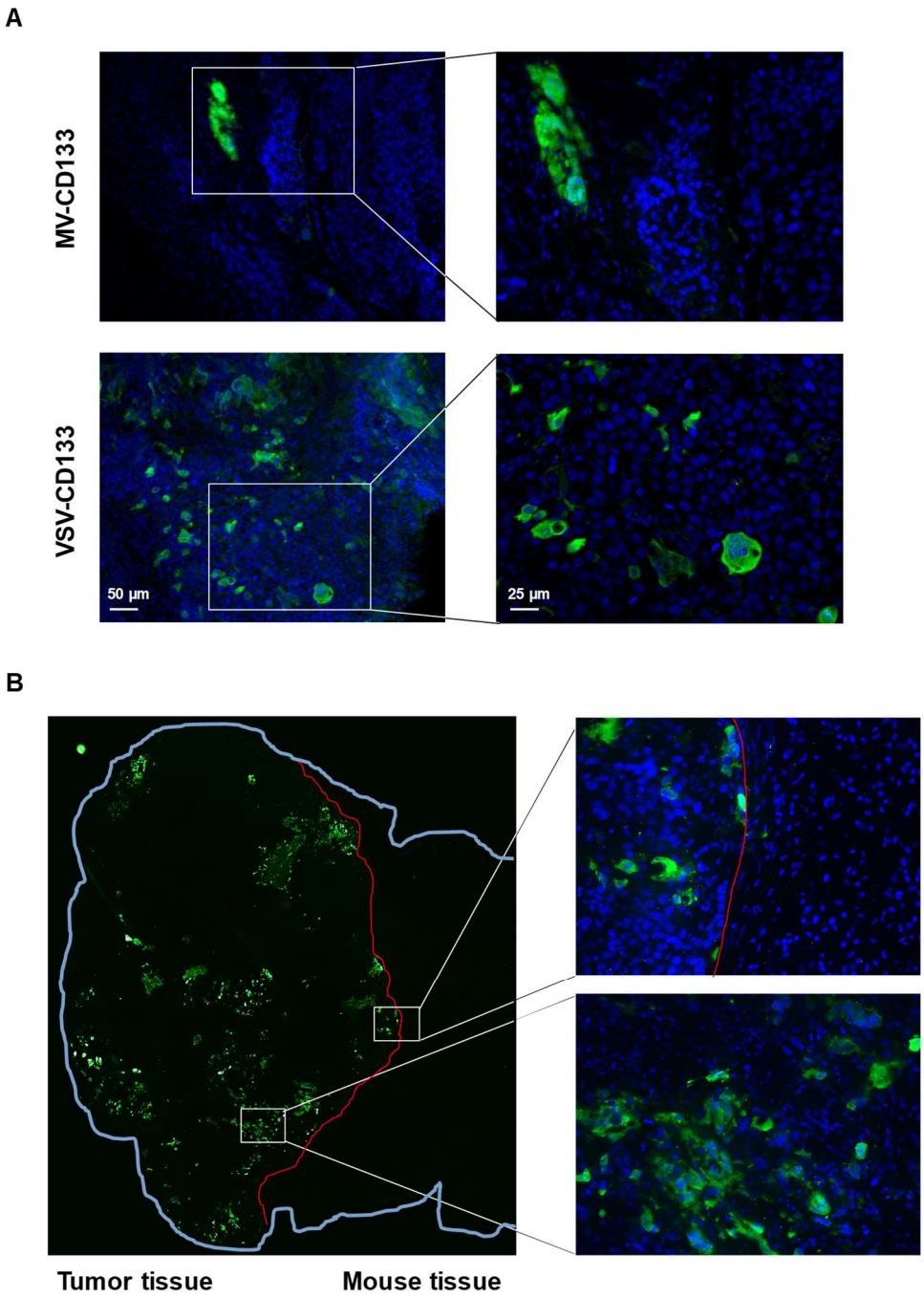

Figure 29. Virus distribution pattern in intratumorally infected tumors
Overview images of tumor sections from mice treated with MV-CD133 or VSV-CD133. Explanted tumors shown in Figure 28 were stained against green fluorescence protein (GFP, green) and counterstained with 4', 6-diamidino-2-phenylindole (DAPI, blue). **(A)** Representative overview image of MV-CD133 and VSV-CD133 infected tumors (left side) showing the distribution of virus (right top and bottom). The zoom-in images show infection centers of MV-CD133 (top right) and VSV-CD133 (bottom right), respectively. **(B)** Overview image of a VSV-CD133 treated tumor with adjacent mouse tissue (left side). The light blue line indicates the borders of the specimen. The red line indicates the human-to-mouse tissue border. The white squares display a zoom-in (bottom right) and the human-to-mouse tissue border (top right).

However, syncytia in MV-CD133 infected tumors were greater compared to VSV-CD133 infected tumors. Despite unrestricted distribution properties in the tumor, infection was restricted to tumor tissue as observed in VSV-CD133 infected tumors (Figure 29B). Here, the tumor area

was sharply demarked by a band of connective tissue and well recognizable due to a cell morphology characteristic of human cells (larger cell bodies and nuclei). Although GFP^+ spots were distributed diffusely throughout the tumor tissue of tumors infected with VSV-CD133, the spots were not found beyond human to murine tissue borders and within adjacent mouse tissue. Infection areas predominantly consisted of multinucleated giant cells.

The results indicated that VSV-CD133 selectively infected targeted tumor tissue while sparing mouse tissue. This implicates the feasibility for human application. In a next step, GFP^+ tumor-areas in specimens infected with MV-CD133 and VSV-CD133, respectively, were quantified.

3.7.2.2. Quantitative Analysis of Immunofluorescent Data

To obtain quantitative data of infected tumor area the above-mentioned acquisition method was applied for six different sites within two tumors of each virus treatment groups (MV-CD133 and VSV-CD133) and of the mock-treated group as control. Due to different tumor sizes, areas of cross-sections ranged from 326.1 to 1235.7 mm^3, thus up to 400 adjacent tiles per tumor were assembled at 10x magnification.

The analysis revealed that only half of the tumor slices from MV-CD133 treated tumors showed GFP^+ areas, whereas each tumor slice from VSV-CD133 treated mice contained GFP^+ spots. The latter exhibited multifocal GFP^+ spots that were in part widely fused together as opposed to GFP^+ tumor slices from MV-CD133 infected mice that showed only focal infection areas. VSV-CD133 infected 1×10^2 times larger area than MV-CD133 when analyzed tumor areas were normalized to a tumor area of 326.1 mm^3. By comparing the single slices of MV and VSV-infected tumors, it was noticed that VSV-CD133 was able to distribute throughout the whole tumor, because all six slices were GFP^+. As seen in Figure 30C (right) VSV-CD133 was able to reach areas containing up to 2×10^4 times more GFP^+ areas than the most abundant infection area from a MV-CD133 treated tumor (Figure 30C, left).

Having detected infected area in tumors, tumor slices were subsequently examined for co-expression of CD133 and GFP.

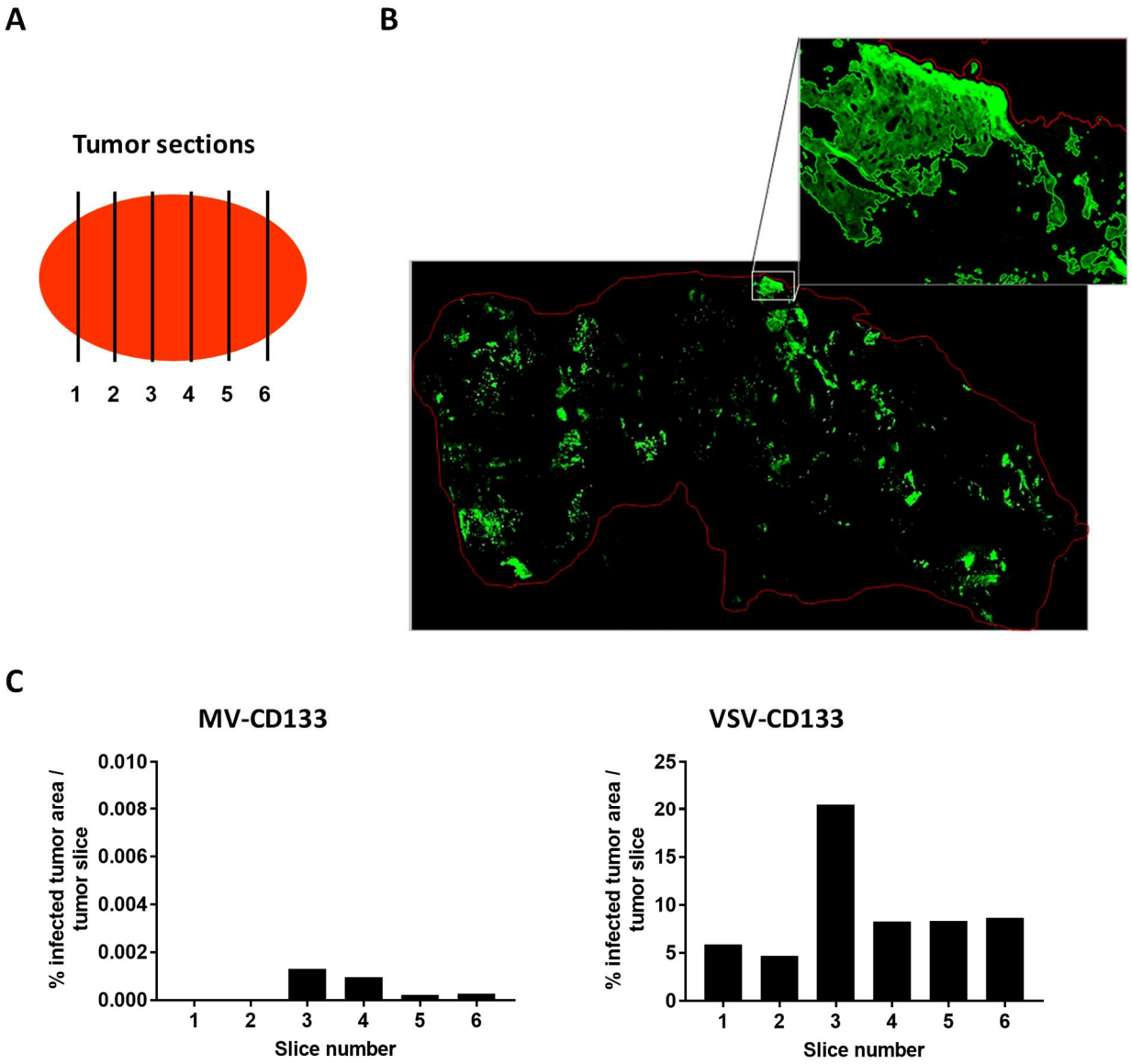

Figure 30. Quantification of infected areas in explanted tumors
Cryosections of explanted tumors from mice treated with VSV-CD133 or MV-CD133 shown in Figure 28 were immunostained against green fluorescence protein (GFP) to visualize virus infection centers. **(A)** Schematic illustration of the distribution of sections chosen to cover the complete tumor. **(B)** Representative overview image of a cross-section of a tumor from mice injected with VSV-CD133. Shown is a composite image that was generated by tile-by-tile acquisition using the AxioVision MosaiX software. The zoom-in represents the output image of one tile reconstructed by the CellProfiler software. The red line indicates the tumor border. **(C)** Bar graph showing the quantification of infected tumor area per slice of one tumor. The percentage of infected tumor area within the whole tumor area is plotted for each tumor site indicated in panel (A). Adapted from (Kleinlützum et al., 2017).

3.7.2.3. GFP Co-Staining with CD133$^+$ Tumor Cells

It has been shown by us (see Figure 20 and (Bach et al., 2013)) and others (Welstead et al., 2004; Doi et al., 2016; Lin and Richardson, 2016), that cell surface receptors are down-regulated upon infection with MV and other viruses. Thus, co-localization of GFP and CD133 cannot be used to prove cell type specificity. On the other hand, absence or low proportion of CD133 expression would prove success of oncolytic targeting. For that reason, we performed a multi-fluorescence staining utilizing a three-channel fluorescent system: DAPI for visualizing nuclei, Alexa Fluor 488 for antibody staining of GFP and Alexa Fluor 680 for antibody staining of the CD133 epitope AC133 (Figure 31).

Both viruses tested here were able to infect the tumor and replicate in tumor cells. While tumors infected with MV-CD133 exhibited only multifocal infection sites mostly comprising of single GFP$^+$ cells, tumors infected with VSV-CD133 showed diffusely distributed infection sites. Zoom-in revealed that infected single cells displayed a granular GFP$^+$ cytoplasm whereas larger infection sites mostly consisted of multinucleated cells displaying typical GFP$^+$ syncytia. In both patterns found, GFP$^+$ signals diffusely filled the whole cell body. In all specimens stained, CD133$^+$ cells were present. Identified cells showed no distinct difference in cell morphology compared to unstained cells bright field images. However, CD133 signals in both, MV- and VSV treated tumors, were characterized by a diffuse cytoplasmatic and spotty staining pattern. Unlike CD133$^+$ cells in virus-treated tumors, CD133 signals in mock-treated tumors were more often membranous than cytoplasmatic indicating a round and smooth cell phenotype. As expected, GFP signals rarely colocalized with CD133 staining. If they did, CD133 signals either irregularly lined the cell surface or displayed subcellular spots. Infection sites, in particular syncytia, were mostly devoid of CD133 signals as best illustrated by black and white images (Figure 31). These observations were especially made for VSV-CD133 infected tumors (Figure 31C) and were consistent with HuH7 cell cultures infected *in vitro* (Figure 20).

It was essential to know whether the tumors contained replicating virus. As distinct differences between MV and VSV infected slides were apparent, the slides were subjected to a quantitative analysis in the next steps.

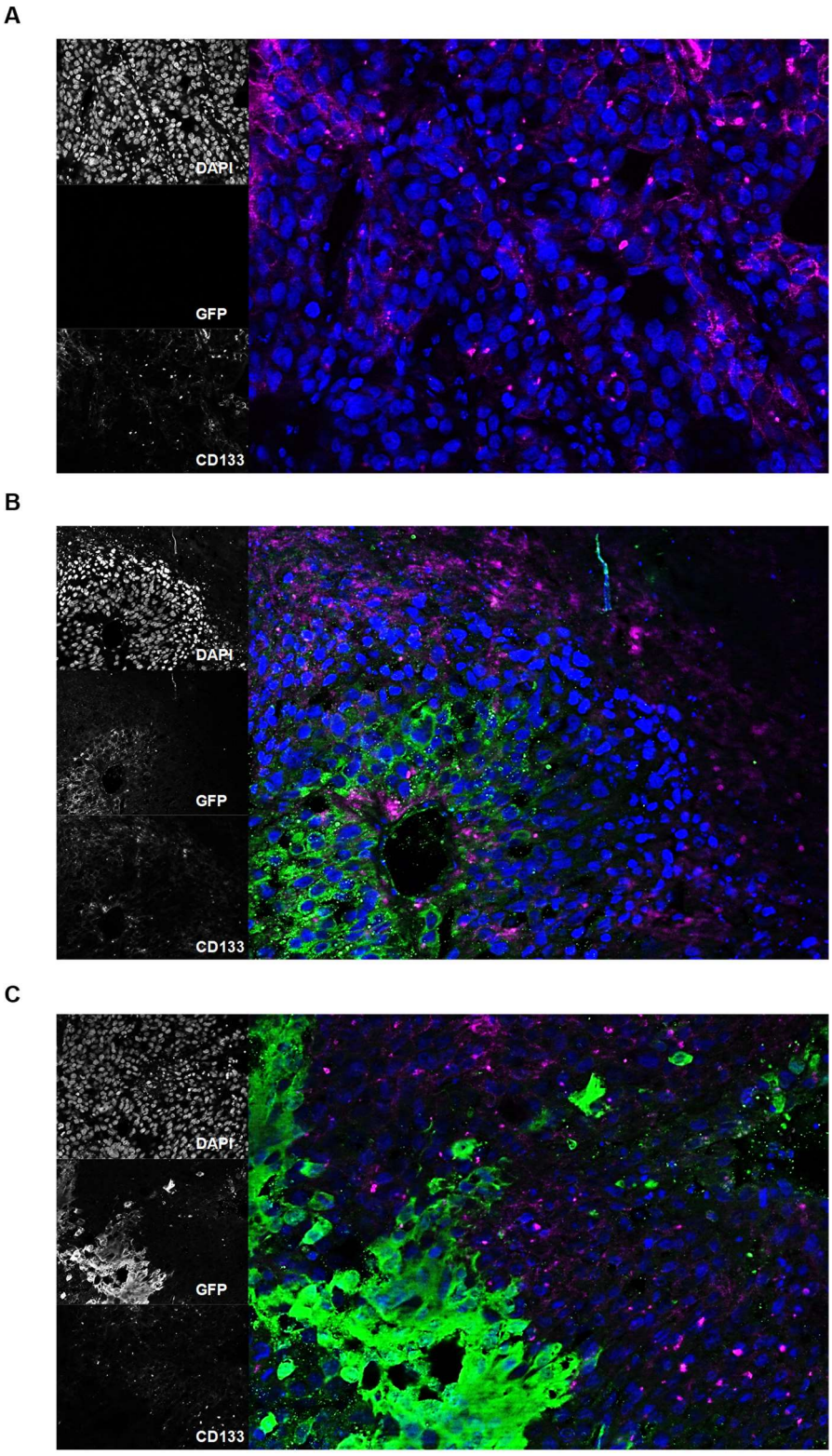

Figure 31. GFP-CD133 co-staining on subcutaneous hepatocellular carcinoma
Representative images of explanted subcutaneous HuH7 hepatocellular carcinoma tumors from **(A)** mock, **(B)** MV-CD133 or (**C)** VSV-CD133 treated mice shown in Figure 28. Images were acquired by fluorescence staining against CD133 (black-white, bottom left), GFP (black-white, middle left) and counterstain for nuclei using 4', 6-diamidino-2-phenylindole (DAPI, black-white, top left). Merged images of CD133 (pink), Green Fluorescent Protein (GFP, green) and DAPI (blue) are depicted on the right side.

3.7.3. Activity of Systemically Administered CD133-Targeted Viruses against a Subcutaneous Xenograft Model of Hepatocellular Carcinoma

As solitary and easily accessible tumors rarely occur in practients, we performed a clinically more relevant model: We injected viruses intravenously into NOD/Scid mice bearing subcutaneous HuH7 tumors. At a mean tumor volume of 100 mm^3, the multiple dosing schedule consisting of three applications of 1 x 10^6 $TCID_{50}$ of virus every second day was initiated. Control mice received virus-free Vero-αHis lysate in medium as control (mock). Tumor volumes were measured twice a week using a digital caliper.

Compared to control mice, tumor growth was delayed in all virus treatment groups. The quantification of tumor volumes by AUC determination was done at day 38 by which all mice of the control group had to be sacrificed due to outsized tumor volumes. On that day, tumor growth of all treated mice was reduced with smallest and most homogenous tumors being among VSV-CD133 treated mice. Tumor volumes of mice treated with MV-CD46/CD133 did not differ significantly from those of tumors of MV-CD133 treated mice until day 42 after transplantation. Accordingly, AUC values and survival data did not differ notably from other treatment groups. Mice treated with MV-CD46/CD133 surving longer than 42 days post transplantation showed a reduced tumor volume and survived until day 54 and day 70 after transplantation (Figure 32A and C). Compared to mock-treated mice, MV^{Pwt}-CD133 treated mice survived 1 day longer on average. Accordingly, AUC calculations showed that responsiveness to treatment was heterogeneous with a wide dispersion of AUC values ranging from 131 mm^3 to 564 mm^3 covering data points comparable to those of MV-CD46/CD133 and mock (Figure 32B). However, growth rate of tumors treated with VSV-CD133 was less than in tumors treated with any other virus. Growth of tumors treated with MV-CD46/CD133 stagnated by day 40 post transplantation. The therapeutic outcome also affected survival of virus treated mice positively: Compared to control mice, mice treated with MV-CD133 survived 6.5 days longer on average, while mice treated with VSV-CD133 survived 13.5 days longer on average.

After having analyzed oncolytic performance in HuH7 cells, in the next experiment an orthotopic tumor model was used. NCH644 was chosen for that purpose since this cell line was characterized *in vitro*. Moreover, there is a high medical need to find anti-glioma treatments.

3.7.4. Activity of CD133-Targeted Viruses in an Orthotopic Glioma Model

To provide a microenvironment for glioma cells that resembles the natural tumor niche for tumorigenesis, we pursued an orthotopic glioma xenograft model. In order to exclude possible detrimental effects of the carrier solution Vero-αHis lysate, we performed a preventive glioma model by injecting pre-infected cells. This allowed us to cautiously approach this setting to the therapy with hitherto untested viruses.

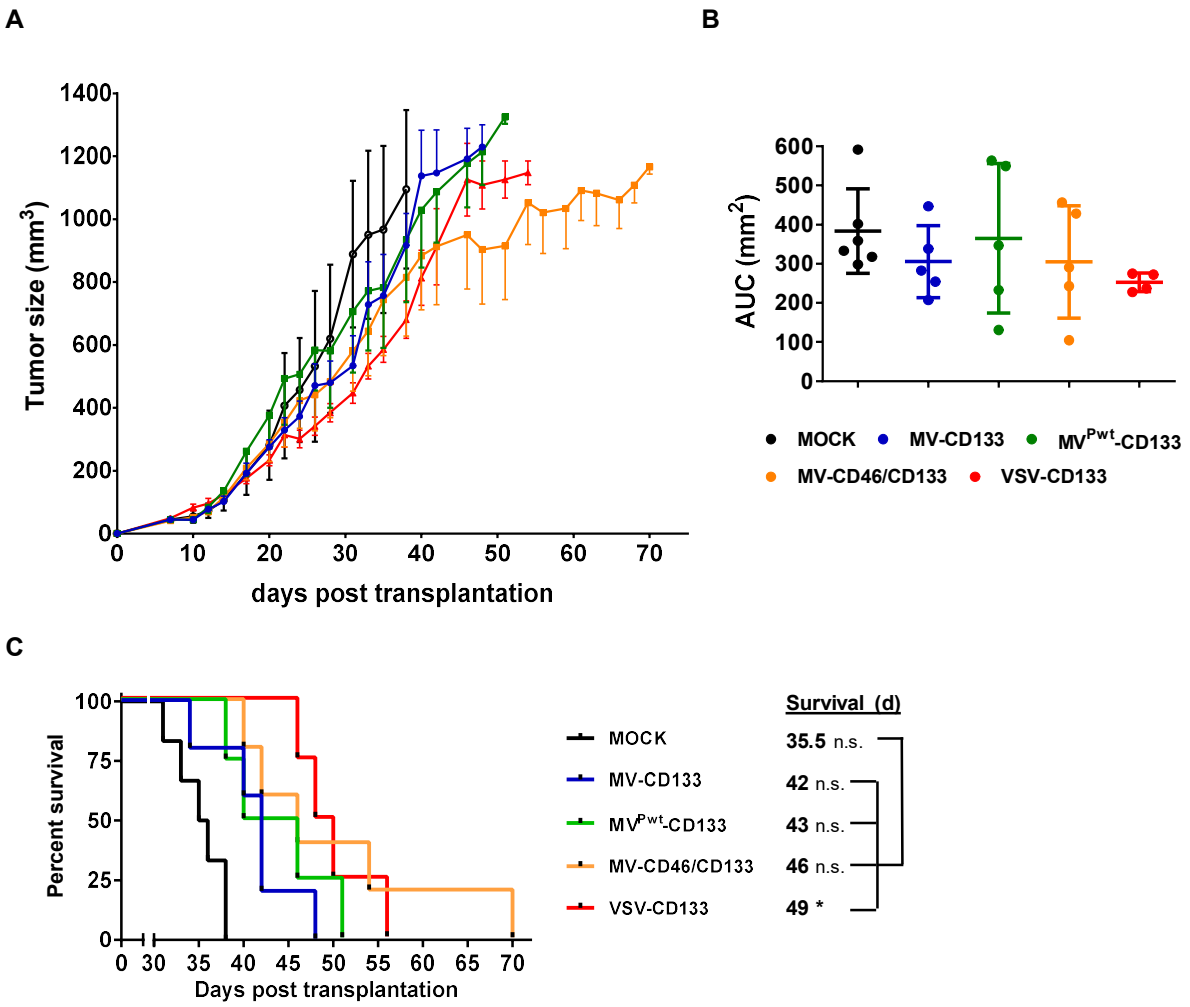

Figure 32. Oncolytic activity of intravenously administered viruses in a subcutaneous xenograft model of hepatocellular carcinoma

HuH7 cells were implanted subcutaneously into the right flank of NOD/Scid mice. Intravenous injection of 1 x 10^6 $TCID_{50}$ of the indicated viruses, or Vero-αHis lysate in medium as control (mock) was initiated at an approximate tumor volume of 100 mm^3 and performed three times every second day. **(A)** Tumor volume of each individual was determined twice a week. The mean tumor volume (mm^3) of each treatment group was calculated and plotted against the course of the observation point. **(B)** Comparisons between treatment groups were done by determining the Area Under The Curve (AUC) shown in (A) of each individual animal normalized against the value obtained from the last survivor of the mock group (38 days after treatment). Differences between treatment groups and mock control group were not significant according to one-way ANOVA with Dunnett's multiple comparison test. **(C)** Survival data were depicted as Kaplan-Meier survival curves. Comparisons of each treatment group with the mock group were conducted by a Bonferroni-adjusted log-rank test. *P < 0.05. Mock, n = 6; measles virus (MV)-CD133, n = 5; MV^{Pwt}-CD133, n = 5; MV-CD46/CD133, n = 5; vesicular stomatitis virus (VSV)-CD133, n = 4. Adapted from (Kleinlützum et al., 2017).

NCH644 cells cultured under serum-free conditions were infected with viruses at an MOI of 0.5. Following 16 hours of incubation, tumor sphere cells were dissociated and 1 x 10^5 in 5 µl stereotactically implanted into the corpus striatum of the right hemisphere (1.7 mm lateral, 0.5 mm rostral to bregma at 3 mm depth) of 6- to 8-week old NOD/Scid mice. Control mice received PBS (mock). Mice that reached onset of neurological symptoms and/or weight loss of more than 20 % were sacrificed by transcardial perfusion under Ketamin Xylazin anesthesia. Brains

were explanted and visually inspected. Some of the brains were fixed in 10 % formaldehyde in PBS for 72 hours and subjected to H.E. staining to determine their histopathological features. The other brains were analyzed for their residual capacity to self-renew and proliferate by culturing 2 x 10^5 single cells under serum-free conditions in T25 flasks until spheres had formed, and a cell density of about 1 x 10^6 was reached.

Except for VSV-CD133, all mice treated with OVs survived considerably longer than mock control mice (Figure 33A). Among the tested viruses, MV-CD46/CD133 was most effective in prolonging survival (median survival time = 89 days versus 67.5 days in MV-CD133 treated mice). In both treatment groups, there were individual mice surviving much longer than the average median survival of each other treatment cohort. The survival pattern of mice injected with MV^{SCD}-CD133 infected tumor sphere cells was heterogeneous, with 27 % of mice surviving considerably longer (108 days, 125 days and 186 days) than the average of MV-CD46/CD133 treated mice. The other 73 % of this group survived comparably long as mice treated with MV-CD133. For that reason the median survival of mice injected with MV^{SCD}-CD133 injected cells (median survival = 66 days) was below that of the MV-CD46/CD133. Unexpectedly, mice that received VSV-CD133 infected cells suffered from severe neurological symptoms, which were almost uniformly fatal at an average of 8 days. At termination, some individual mice treated with MV-derived viruses showed a tumor mass comparably large to tumors of mock treated mice. By contrast, other individual mice treated with MV-derived viruses had no macroscopically visible tumor mass at sacrifice (MV-CD133, 55 days after transplantation; MV^{Pwt}-CD133, 76, 78 and 94 days after transplantation; MV^{SCD}-CD133, 125 and 186 days after transplantation; MV-CD46/CD133, 84, 84 and 89 days after transplantation).

In *ex vivo* sphere formation assays, all samples derived from mock (n=4), MV-CD133 (n=2) and MV^{Pwt}-CD133 (n=4) treated mice were able to produce spheres reaching a total cell density of 1 x 10^6 (Figure 33B). These stemness properties were only featured in three out of four MV-CD46/CD133 treated tumors (n=4) and in half of the tumors treated with MV^{SCD}-CD133 (n=4). Those tumors that did not reach the stemness features set in this assay, either failed to grow straight after seed or died because they did not form spheres. In one of the samples derived from MV^{SCD}-CD133 infected tumors that did not show stemness features as described above, rather displayed a morphology characteristic of stroma cells. At date, these cells were not further analyzed with molecular means as they came across in low quantities. Lymphocytes or lymphocyte-like cells were often apparent in dissociated cultures but were not further analyzed for the above mentioned reasons. There were no signs for GFP expression in these cells that could point to a persistent infection with virus. In conclusion, there was a slight correlation between the time required for cell re-expansion to a defined cell number and OS time, suggesting that a higher proliferative activity is associated with shorter survival time.

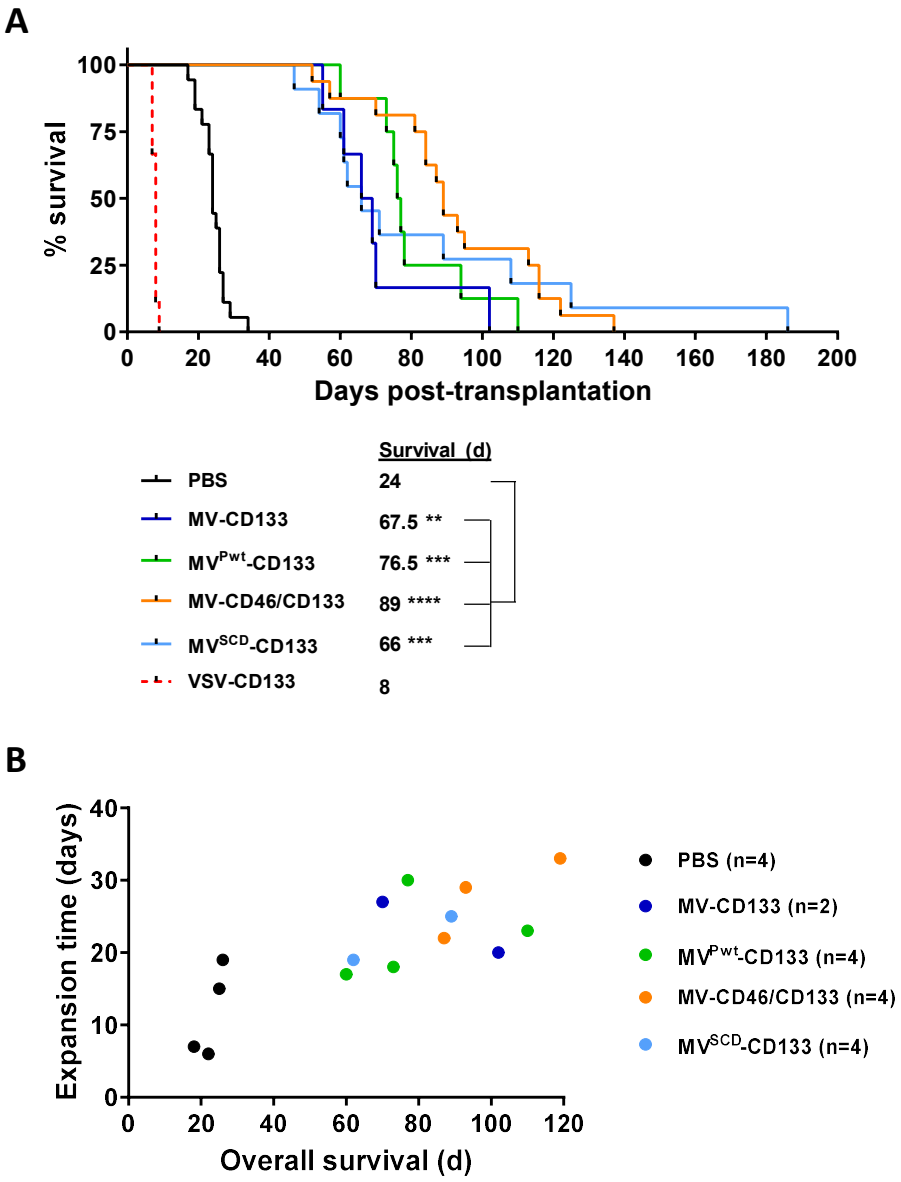

Figure 33. Intracranial implantation of preinfected glioma sphere cells
Primary glioma sphere cells were infected with the indicated viruses at an MOI of 0.5 following stereotact-assisted implantation into the corpus striatum of NOD/Scid mice 16 h later. Mice having received MV^{SCD}-CD133-infected cells received 5-fluorocytosine (5-FC, 200 mg/kg body weight) twice per day intraperitoneally initiated 3 d post implantation for 4 consecutive days. **(A)** Health status and body weight was monitored daily. Mice were sacrificed with onset of neurological symptoms and/or weight loss of more than 20 %. Based on the defined end points a Kaplan-Survival curve was generated. Comparison of the mean survival periods between the mock control and the treatment groups was conducted by a log-rank test followed by a Bonferroni correction for multiple comparisons. Log-rank test, ***, P<0.001; PBS, n = 18; MV-CD133, n = 6; MV^{Pwt}-CD133, n = 8; MV-CD46/CD133, n =16; MV^{SCD}-CD133, n = 11; VSV-CD133, n = 9. **(B)** At the experimental endpoint, tumors were explanted and identical numbers of cells cultivated. The time required to expand to a cell count of 1×10^6 was plotted against the median survival time of the respective animal. Adapted from (Kleinlützum et al., 2017).

In Figure 34, low magnification microphotographs show the morphological appearance of brains of mice bearing glioma from pre-infected cells. In both treatment cohorts, tumors could be discriminated from healthy brain parenchyma through their highly cellular tumor bulk of rather uniform atypical basophilic cell type loosely organized. Nuclei varied in size and shape. Characteristically, glioma cells preferentially grew alongside the injection site, with occasional distinct transition into the ventricles or even the left hemisphere. Clinically apparent mice presented with an enlarged (doming) cranium. Hemorrhages were apparent in mice of both treatment groups, especially in the early disease (Figure 34A and B). In mock-treated mice at later time point post transplantation (day 19 post transplantation and later), proliferations were replaced by acellular spongiosa-like matrix (Figure 34C). At that time points (around the median survival time of the mock cohort), tumors had already expanded throughout the right hemisphere while not transiting the boundaries between neoplastic and normal tissue. In direct comparison of tumors from both treatment cohorts at the same time post transplantation (Figure 34A versus Figure 34B), morphological appearance of tumors differed in their dimensions and growth behavior. While mock-treated mice generally beared larger more compact tumors, irrespective of the time post transplantation, tumors of VSV-CD133 treated mice were smaller. The latter were composed of nests of tumor cells growing irregularly alongside the injection site. Apoptotic cells (appearing as karyopyknotic and less basophilic cells) and mitoses occurred in mice of both treatment groups, albeit apoptosis was more frequent in VSV-CD133 infected tumors (Figure 34A).

In mock-treated mice lethal neurological symptoms seemed to be linked to an oversized intracranial tumor mass. However, in VSV-CD133 treated tumors no oversized tumor mass was visible. Further histological analysis such as the detection of virus and neuropathology associated markers is required to elicit causative mechanism of VSV-CD133 associated neurotoxicity. Intracranial injections of virus into naïve mice were next performed to investigate a causative relationship between the virus and the onset of neurotoxicity.

In the next step we performed a set-up that is much more authentic. We established glioma tumors as described above but with uninfected (naïve) cells. We allowed them to grow 5 days *in situ*, a treatment time point we determined prior to infection studies. After that incubation time, 2 x 10^5 $TCID_{50}$ of the OVs were stereotactically injected through the same surgical access hole as described above. Monitioring and termination were also done as described above.

Mice treated with MV-CD46/CD133 tended to survive longer (median survival = 28.5 days) than mock-treated mice. All mice treated with VSV-CD133 showed the onset of severe neurological symptoms within 15 days, and thus had to be sacrificed earlier than PBS-treated mice (Figure 35). In this model the time gap between the neurological onset in individuals of each treatment cohort was larger than in the pre-infected glioma model (Figure 33). Especially for

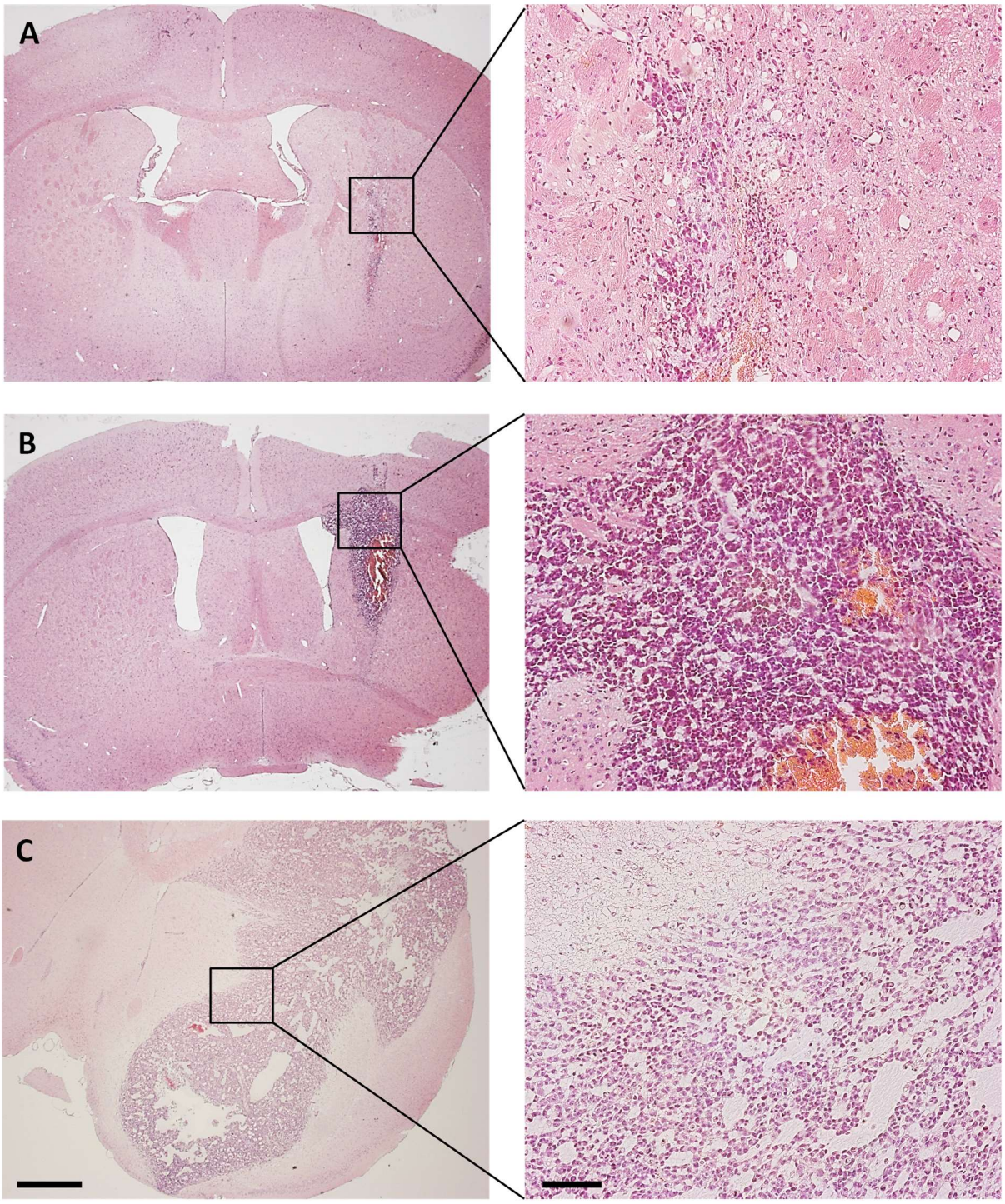

Figure 34. Histopathology of explanted brains of mice bearing pre-infected glioma
Representative images of coronar paraffin sections of brains from mice enrolled in the pre-infected glioma model (Figure 33). Brains were explanted after transcardial perfusion and subsequent fixation in 10 % formaldehyde solution for 72 hours, embedded in paraffin and sectioned at 4 µm thickness. **(A)** Representative overview image of a brain section from a mouse bearing VSV-CD133 infected glioma spheres after reaching termination criteria at day 7 post transplantation (left). Rectangle represents a zoom in (right) of an area showing single nests of tumor cells and hemorrhages. **(B)** Overview image of a control mouse (PBS) at 9 days post transplantation for the purpose of comparison with (A) (left). Rectangle represents a zoom in (right) of the tumor bulk constricting the lateral ventricle. Mouse did not reach termination criteria. **(C)** Representative overview image of a control mouse (PBS) after reaching termination criteria at day 19 post transplantation (left). Rectangle shows a zoom in the ventrally expanded tumor mass at the tumor-brain border (right). Hematoxylin and eosin stain; scale bar of overview section of magnification with x1.25 = 800 µm; scale bar of zoom in of magnification with x10 = 100 µm.

mice treated with VSV-CD133, survival was heterogeneous. Except for mice treated with MV-CD46/CD133, median survival times were comparable to those dates observed for the pre-established glioma model (Figure 33A). Thus, the subsequent study was intended to evaluate the toxicity of VSV-CD133 without the potential interaction between virus and tumor to elucidate causatives.

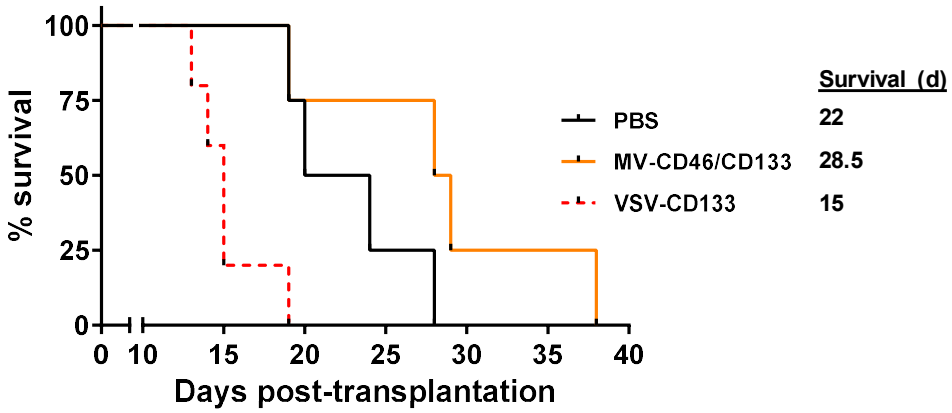

Figure 35. Intracranial injection of oncolytic viruses into pre-established glioma
$1x10^5$ primary glioma sphere cells were stereotactically implanted into the corpus striatum of NOD/Scid mice. After 5 days, $2×10^5$ $TCID_{50}$ of the indicated viruses in 5 µl PBS or vehicle (PBS) was stereotactically injected into the same coordinates. Health status and body weight were monitored daily. Mice were sacrificed with onset of neurological symptoms and/or loss of weight by more than 20 %. Based on the defined end points, Kaplan-Meier survival plots were generated. Comparison between the control and the MV-CD46/CD133 treated groups was conducted by a log-rank test followed by a Bonferroni correction for multiple comparisons. Log-rank test, *, P<0.05; PBS, n = 4; MV-CD46/CD133, n =4; VSV-CD133, n = 5. Adapted from (Kleinlützum et al., 2017).

3.7.5. Direct Intracranial Application of Oncolytic Viruses into Naïve mice

As we observed the severe neurological symptoms only in VSV-CD133 treated mice bearing glioma (Figure 33 and Figure 35) and no indication for causatives in histopathologic examination (Figure 34), we applied VSV-CD133 or UV-inactivated VSV-CD133, respectively, by direct intracranial injections by the same coordinates as used in tumor settings to exclude a possible influence by the tumor cells or the tumor-created environment. As control we applied VSV-MV as it does not use CD133 as entry receptor. While mice injected with irradiated VSV-CD133 survived up to study end without developing any symptoms, VSV-CD133 and VSV-MV injected mice developed neurological symptoms within 9 days on average. One individual of the VSV-MV injected mice were not sacrificed before day 22 after injection although single mice started to lose weight on day 15 after injection. The onset of adverse events in both VSV-related viruses must thus have been caused by combining the MV glycoproteins with VSV but not by display of CD133-specific scFvs.

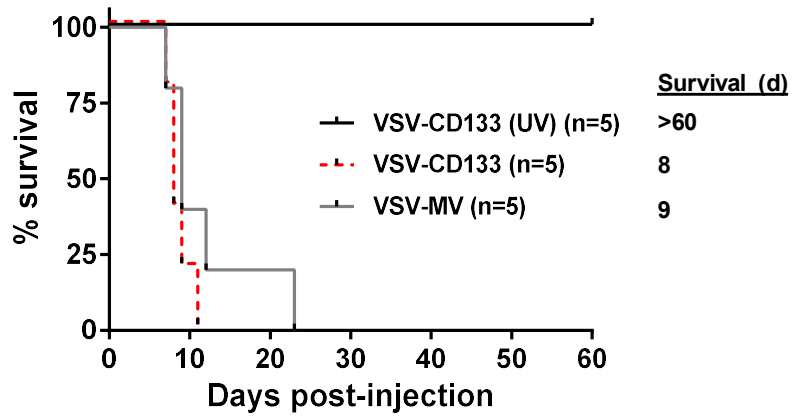

Figure 36. Intracranial injection of oncolytic viruses into naïve mice
2×10^5 $TCID_{50}$ of VSV-CD133, UV-inactivated (UV) VSV-CD133, or VSV-MV in 5 µl PBS, respectively, were stereotactically injected into the corpus striatum of NOD/Scid mice. Health status and body weight were monitored daily. Mice were sacrificed with onset of neurological symptoms and/or weight loss of more than 20 %. n = 5. Adapted from (Kleinlützum et al., 2017).

4. DISCUSSION

So far, the therapeutic benefit of most of the current options for cancer therapy has been limited and often failed in late phase clinical trials. Among other factors, therapeutic failure is ascribed to CSCs as the seed of tumor initiation, chemoresistance and, as a consequence, drivers of metastatic dissemination. Here, CD133-targeted virotherapeutic strategies exploiting the MV envelope retargeting system have shown promising preclinical results (Bach et al., 2013). CSCs are rare in tumor tissue and thus represent a major challenge for CD133-targeted viruses to be hit and infected. It can be challenging to improve MV-CD133 on the basis of the cell killing mechanisms of MV. Different strategies were explored to enhance virus-mediated cell killing of $CD133^+$ tumor cells towards a higher rate of killing of $CD133^-$ tumor cells. To do this we performed a comparative analysis of a panel of genetically engineered CD133-targeted MVs for their oncolytic activity. Our results from *in vitro* and *in vivo* studies open new concepts and implications for oncolytic virotherapy with recombinant MV, especially with regard to neurotropism of chimeric viruses.

4.1. CD133 as Target Receptor

Considering the tumorigenic capabilities of CD133-expressing cells, the CD133 antigen appears to be a good candidate for targeting cancer cells on various cancer types. As discussed in the Introduction (1.6), we hypothesized that CD133-targeted therapy might be an efficient strategy to eradicate tumors. Several immunotherapeutic strategies are currently under development to target $CD133^+$ tumor cells with the goal of translation into the clinic. These include, amongst others, CD133-specific antibodies conjugated to toxins, so called antibody-drug conjugates, CD133-specific bi-specific T cell engagers (BiTEs), or CD133-targeted chimeric antigen receptors (Waldron et al., 2011; Venugopal et al., 2015; Prasad et al., 2015; Zhu et al., 2015). Previously, we have shown that *in vivo* targeting of $CD133^+$ tumor cells can be achieved with MV-CD133 (Bach et al., 2013). Starting from these studies, this thesis describes further modified CD133-targeted OVs with the aim to improve the antitumoral efficacy of MV-CD133 by addressing critical barriers to efficient OV multiplication and spread. Specifically, these modifications were aimed to improve infection and eradication of malignant tissue, while avoiding the infection of healthy tissues. This was achieved through arming either with the suicide gene SCD or the P gene from wt MV, through extending receptor usage to CD46, and by transferring the CD133-targeting MV envelope to VSV (Kleinlützum et al., 2017).

Besides its expression on CSCs, CD133 is known to be expressed on normal hematopoietic, neuronal and endothelial progenitors (Yin et al., 1997). Human HSCs express high cell surface expression levels of human CD46 (99.10 %) and human CD133 (94.16 %). Importantly, these are considerably higher than CD133 expression levels in tumors of patients. Thus, potential

“on-target, off-target” infection of the bone marrow stem cell compartment might present an immediate concern for patients undergoing CD133-targeted therapies. Infection of these cells by CD133-targeted OVs could result in tremendous adverse reactions such as myelosuppression, e.g. aplastic anemia. Myelosuppression is an important dose-limiting side-effect of cancer therapeutics (Wang et al., 2006). For that reason, we performed a careful safety assessment for possible toxic effects on $CD34^+$ / $CD133^+$ human HSCs. This was conducted by assessing the potential impairment of human HSCs to produce clonal clusters of progenitor cells of the hematopoietic lineage after inoculation with the panel of viruses using a semisolid permissive culture system. While inoculation of the MV-derived viruses with the HSCs showed GFP^+ cells that increased over time, no single GFP^+ cell could be detected after infection with VSV-CD133 (Figure 18A and B). Provided that the GFP^+ events were not the result of a potential GFP transfer, the effect of the MV-derived viruses on HSCs appeared to be dependent on the receptor utilization: HSCs inoculated with MV-NSe showed more GFP^+ cells than cells inoculated with MV-CD46/CD133 (Figure 18). This was totally unexpected because MV-CD46/CD133 uses both, CD46 and CD133 as viral entry receptors. This observation suggests that receptor attachment is not the crucial step for oncolytic MV to infect HSCs. It is rather likely that the innate immune response of these cells controls infection. This notion is reaffirmed by the observation made with the inoculation of HSCs with MV^{Pwt}-CD133 which showed the most GFP^+ HSCs cells of all tested unispecific MV-derived OVs (Figure 18). MV^{Pwt}-CD133 is suspected to circumvent the antiviral IFN mediated immune response through the actions of the wt P/V/C gene products (Haralambieva et al., 2007).

In contrast, HSCs displayed a strong resistance to infection with VSV-CD133. This observation is in line with infection studies on healthy cells which strongly indicate that normal tissue e.g. glial cells and melanocytes are protected from VSV infection (Barber, 2004; Wollmann et al., 2007). The oncoselectivity of VSV is based on its sensitivity to IFN-mediated antiviral defenses that protects normal cells from infection (Bishnoi et al., 2018). However, the GFP^+ cells observed by MV-CD133, MV^{Pwt}-CD133 and MV-CD46/CD133 did not give rise to a functional impairment in proliferation and differentiation capacity. Instead, infection with MV-NSe resulted in a slight decrease in the total colony number (Figure 19). An alternative explanation is proposed by De Carvalho et al., who discovered extracellular vesicles (EVs) containing the HIV receptor that were able to attach to viral particles thereby decreasing the numbers of virions that would otherwise infect CD4+ T cells (Carvalho et al., 2014). Indeed, HSCs are known to release CD133 containing EVs (Bauer et al., 2011). EVs have also been proven by multiple research groups to facilitate viral infection and enhance cytotoxicity (Rozmyslowicz et al., 2003; Arenaccio et al., 2014; Wang et al., 2018; Garofalo et al., 2019). The safe use of the OVs tested in this setting is an important result with respect to the clinical translation of CD133-targeted viruses.

While all newly generated viruses were highly selective for CD133⁺ cells, MV-CD46/CD133 additionally infected CD46⁺ cells (Figure 15). For each tumor type, we identified different virus types as best treatment option. *In vitro,* VSV-CD133 was by far most efficient in infection and lysis of HuH7 cells compared to all other viruses (Figure 21 and Figure 22). *In vivo*, VSV-CD133 was also best suited for the treatment of HuH7 xenografts (Figure 28), where it reached basically all parts of the tumor tissue after intratumoral application thus covering an area more than 10^4 times larger than that reached by MV-CD133 during the same period (Figure 30). VSV-CD133 was also more efficacious when injected intravenously, which was reflected by significantly longer survival times (median survival = 49 days) (Figure 32). Among the MV-derived viruses, MV-CD46/CD133 was the most effective OV in slowing tumor growth and thus prolonging survival via the i.t. and also the i.v. application route (Figure 28 and Figure 32). Notably, two out of five mice treated with intravenous doses of MV-CD46/CD133 survived substantially longer than the average median survival of the VSV-CD133 group (54 days and 70 days). The other three mice of the MV-CD46/CD133 group survived comparably long as mice of the MV^{Pwt}-CD133 and MV-CD133 group, which translated in a lower median survival than that of the VSV-CD133 group (MV-CD46/CD133, median survival = 46 days) (Figure 32). The superior oncolytic performance of targeted VSV-MV compared to targeted MV is in line with previously published data on VSV-MV viruses targeted to Her2/neu or CD30 (Ayala Breton et al., 2015; Hanauer et al., 2018). The impressive capacity in spreading through tumor tissue that we quantified for VSV-CD133 compared to MV-CD133 can be regarded as an important property to reach and destroy CSCs in a clinical situation of HCC, where CD133⁺ CSCs represent a minor percentage of all cells in a tumor mass (Kleinlützum et al., 2017).

The results of the subcutaneous HuH7 xenograft model are in sharp contrast to the result obtained with primary glioma sphere cells. In cell killing assays, VSV-CD133 was able to reduce cell viability more effectively than its MV counterparts only within the first 48 h after infection (Figure 26). Interestingly, glioma sphere cells started to re-expand 2-3 days after infection. Even when VSV-CD133 was used at an MOI of 10 it was unable to kill more than 60 % of the cells, unlike the MV-derived viruses, which caused a continuous decrease in cell viability, most efficiently with MV-CD46/CD133 and MV^{SCD}-CD133 (Figure 26). The pronounced cell killing by both MV-derived viruses is most likely due to the killing of CD133⁻ tumor cells. The enhanced oncolysis of MV-CD46/CD133 might be explained by a greater supply of target cell receptors in close proximity that results in greater fusion capabilities and cell-to-cell spread. In contrast, destruction of CD133⁻ tumor tissue by MV^{SCD}-CD133 is mediated by the so-called bystander effect that depends on the transfer of the transgene SCD to CD133⁺ cells. Given the superior cell killing performance of MV^{SCD}-CD133 compared to each of the other MV-derived OVs (Figure 27) argues against a loss of CD133 expression as a possible explanation for the poor results of VSV-CD133 on glioma sphere cells. Furthermore, cells infected with VSV-MV, which

relies on CD46 receptor usage (Ayala-Breton et al., 2013), showed the same re-expansion as VSV-CD133 did (Figure 26). We therefore assumed that the cells became resistant through a postentry mechanism. The sustained viability of glioma spheres infected with VSV-CD133 and VSV-MV, respectively, could thus be related to an intact type-I IFN response in some of the cells that impeded virus replication. After clearing virus in the cell culture by apoptosis-induction, the cells might have recovered which is reflected by the re-expansion of cells.

Notably, IFN-α was absent in the supernatants of VSV-infected cells. Although we did not measure IFN-β, this made an influence of the IFN type I system rather unlikely. This is further supported by the poor oncolytic performance of MV^{Pwt}-CD133 that was similar to that of MV-CD133. These observations argue for an alternative mechanism which must be the subject of further studies. One alternative explanation was brought up by a study, in which several pancreatic ductal adenocarcinoma cell lines showed resistance to VSV but were shown to be defective in producing type I IFN (Murphy et al., 2013). Interestingly, in these cells, the expression levels of IFNAR were equal to those of IFN sensitive cells of the same tumor subtype. The authors found significantly higher expression levels of IFN stimulated genes (ISGs), MxA and OAS in these cells which were shown to mediate sensitivity to type I IFNs and thus resistance to VSV and other IFN sensitive OVs (Saloura et al., 2010; Paglino and van den Pol, 2011; Moerdyk-Schauwecker et al., 2013; Guo et al., 2017). Whether the resistance of glioma sphere cells infected with VSV-CD133 and VSV-MV was associated with the upregulation of such ISGs in the present study remains to be determined. The authors of these studies suggested to test both IFN sensitivity and type I IFN production to predict the responsiveness of the respective cell line to oncolytic therapy (Murphy et al., 2013; Matveeva and Chumakov, 2018).

The superiority of MV-CD46/CD133 over the other viruses in the killing of glioma sphere cells *in vitro* was also reflected *in vivo*. Here, MV-CD46/CD133 was able to significantly prolong survival in mice intracranially transplanted with pre-infected glioma sphere cells (median survival time = 89 days versus 67.5 days in MV-CD133 treated mice) (Figure 33). Notable, the survival period of mice treated with MV^{SCD}-CD133 was heterogeneous, with two thirds of the mice showing similarly long lifespans as mice treated with MV-CD133 (median survival = 67.5 days). The other third of the MV^{SCD}-CD133 group survived considerably longer than the average median survival times of each other treatment cohort. Overall, this conferred on the MV^{SCD}-CD133 group the lowest median survival among the MV-derived viruses (median survival = 66 days), although individual mice showed a relatively long-term survival (108 days, 125 days and 186 days) (Figure 33). At necropsy, some mice treated with the MV-derived viruses presented a tumor mass of a comparable size than that of mock treated mice presented at their termination date (median survival = 24 days). Individual mice of these groups, however, had no microscopically visible tumor mass although they showed neurological symptoms. Although one cannot draw precise conclusions from a macroscopical examination, the absence of a clinically

relevant tumor size indicates another cause behind (Chapter 4.2). In contrast, VSV-CD133 rapidly killed mice when applied intracranially via infected glioma sphere cells. Given the restrictions of NOD/Scid mice in IFN sensing and signaling, a resistance to VSV due to IFN sensitivity as assumed for the poor results seen *in vitro* is rather unlikely in the *in vivo* setting. Additionally, histological examination of coronar sections across the injection site revealed smaller tumors compared to those of mock-treated mice after the same period (Figure 34), which on the other hand is in line with the initial killing kinetic of VSV-CD133 *in vitro*.

Likewise in the HuH7 model, the oncolytic virotherapy of orthotopic glioma resulted in a reduced tumor growth, but it did not lead to a complete elimination of tumor cells by none of the viruses (Kleinlützum et al., 2017). Indeed, complete tumor remissions are in general rarely seen in preclinical models (Junttila and Sauvage, 2013). This applies in particular to immunodeficient mice, where an antitumoral immune response triggered by the virus infection cannot add to the oncolytic effect. Reasons for incomplete tumor destruction and recurrence in the present study can be, but are not limited to, an inaccessibility of the tumor cells, low virus dose or resistance against the virus in a small subset of tumor cells. While formally it cannot be excluded that *in vivo* all $CD133^+$ tumor cells have been eliminated by the virotherapy, another scenario would be that a subset of $CD133^-$ tumor-initiating cells (TICs) within the tumor gave rise to $CD133^+$ tumor cells that repopulated the tumor. Bi-directional transition between CSC and bulk cancer cells have also been described for breast cancer, colorectal cancer and melanoma (Gupta et al., 2011; Schwitalla et al., 2013; Roesch et al., 2010). Theoretically, the transitioned $CD133^+$ tumor cells should be hit and lysed by the virus progenies, but virus dissemination can be hindered spatially by non-tumorous tissue, a pitfall that is often described for OVs (Russell et al., 2012). Given the strong replicative capabilities of VSV-CD133, it was expected to rather show a diffuse than a multifocal distribution pattern in HuH7 tumors (Figure 29 and Figure 30). From the performed experiments, however, it is not conceivable why the virus was hindered to diffusely infect the tumor. Given this, it would be worth to test MV^{SCD}-CD133 or MV-CD46/CD133 in this setting to obtain debulking of non-infected tumor tissue and ease spreading beyond the interstitial tissue. Moreover, on the basis of the oncolytic performance of VSV-CD133, it would be worth to modify the virus with one of the above mentioned alterations. Results from lineage-tracing and cell-ablation studies increasingly indicate that cancer therapies can provoke non-TICs or quiescent TIC clones to regrow and drive tumor recurrence (Batlle and Clevers, 2017). By inducing plasticity, single cell clones can regain selective growth advantage over adjacent cells. This re-evolution of a tumor population can result in a heterogenous tumor that consists of cells with different clonality, and thereby complicating treatment. Transferred onto the present model, this would suggest that upon treatment the cell composition was altered towards additional CSC receptors, besides CD133. However, as long as these cells are $CD46^+$, they should be infectable by MV-CD46/CD133.

Therefore, in order to be effective, CSC targeted therapies will need to combine different CSC markers (e.g. CD44) or therapies active against both the CSCs and the bulk cancer cells to break the CSC plasticity. By taking our approach, OVs with extension of their receptor usage could address this challenge, but optimal dosing regimens and assurance of accessibility of tumor cells to virus are necessary to fully exploit the potential of oncolytic virotherapy. Moreover, their oncolytic activity needs to be assessed in immunocompetent mouse models to involve the immune system.

4.2. Neurotoxicity

An unexpected outcome in the orthotopic glioma model was the severe neurotoxicity exerted by VSV-CD133 (Kleinlützum et al., 2017). All mice intracranially transplanted with glioma sphere cells infected with VSV-CD133 had to be sacrificed due to the onset of severe neurological symptoms within 10 days after infection (Figure 33 and Figure 35). Indeed, one of the main concerns when using VSV as OV is its inherent neurovirulence, due to its broad tropism for different types of cells including neurons. Infection of neurons can result in fatal viral encephalitis that is ascribed to the functions of the G and partly to functions of the M protein (Bishnoi et al., 2018). In immunocompetent mice lethal encephalitis is typically occurring within ten days of infection with wt VSV (Muik et al., 2014). However, strategies have been developed to attenuate the virus' neuroselectivity to obtain safe oncolytic VSVs, e.g. VSV-IFNβ that is currently investigated in clinical studies (Felt and Grdzelishvili, 2017). In the present study, neuroattenuation was achieved by detargeting from neural cells at the entry level and pseudotyping with the MV envelope glycoproteins (Ayala-Breton et al., 2014). Using this approach, VSV-CD133 was generated by pseudotyping VSVΔG with the envelope glycoproteins of MV that were ablated for binding to CD46 and SLAM, but retargeted to CD133 using a scFv specific for CD133 (Kleinlützum et al., 2017). These modifications were expected to abrogate the major neuropathogenicity determinants of VSV and MV, respectively. Accordingly, VSV-CD133 specifically infected $CD133^+$ tumor cells, while it neither infected $CD46^+$ or $SLAM^+$ cells (Figure 15). By contrast, VSV-MV that displays non-mutant MV-F/H infected cells positive for the natural MV receptors CD46 and SLAM (Hanauer et al., 2018). As demonstrated by Ayala-Breton et al., VSV-MV caused neurotoxicity in CD46 transgenic and IFN receptor deficient mice after intravenous injection, while this was not the case for fully retargeted VSV displaying scFV with specificity to EGFR, PSMA, folate receptor or Her-2/neu receptor (Ayala-Breton et al., 2012; Ayala Breton et al., 2015). Likewise, no signs of neurotoxicity were observed after intravenous administration of VSV-CD133 in NOD/Scid and VSV-CD30 in NSG mice (Kleinlützum et al., 2017; Hanauer et al., 2018). In contrast, vaccine strain-derived oncolytic MVs are known to exhibit neurotoxicity only in CD46 transgenic and IFN receptor deficient mice after intracranial injection (Friedrich et al., 2013; Mrkic et al., 1998). These studies indicate that the susceptibility

of a mouse model depends on the virus type, the route of administration and on its degree of immune deficiency for which the type I IFN response is the major factor (van den Pol et al., 2017). As such, IFN-deficient mice seem to be most sensitive towards VSV, even more than NOD/Scid mice, which showed no adverse response after intracranial inoculation with a VSV-Lassa virus chimera (Wollmann et al., 2015). IFN-deficient mice are totally unresponsive to IFNs of any communicating cell and thus cannot mediate cellular downstream signaling to trigger the secretion of cytotoxic substances (Manchester and Rall, 2001). Moreover, IFNs are also known to tighten the blood-brain-barrier (BBB). As a consequence, in IFN-deficient mice, the virus is not recognized and cleared, and can enter the brain from blood and spread intracranially (van den Pol et al., 2017; Drokhlyansky et al., 2016; Finke et al., 1995). By contrast, mice with a scid mutation possess a functional innate immune response, but lack functional T- and B cells as the major source of IFN-γ (Finke et al., 1995; Weidinger et al., 2000). In these mice, the cross-linking of innate and adaptive immune responses via cytokines (e.g. type I IFNs) for efficient viral clearance does not exist due to deficiency in adaptive immune responses. However, some innate components such as resident microglia are partly functional and as such can become efficient antigen presenters upon uptake of proteins from apoptotic cells (Patterson et al., 2002). Although activated microglia may by this way contribute to virus control, as recently shown for neurotropic herpesvirus (Fekete et al., 2018), this cascade may be highly inefficient in NOD/Scid mice as the cells to be activated and recruited are not present. These factors, among others, render these mice strains highly susceptible to virus infections (Marty et al., 2015; Mura et al., 2018). They may explain the different susceptibility of NOD/Scid and IFN-deficient mice strains to neurotropic viruses and by different administration routes. In experimental models, VSV pseudotyped with the Nipah virus glycoproteins is currently considered the most neurotoxic chimeric variant as it was rapidly neurotoxic even when intracranially injected in adult immunocompetent mice (van den Pol et al., 2017).

In the present study, intracranial injection of VSV-CD133 infected glioma sphere cells caused neurotoxicity in NOD/Scid mice, which do not express human CD46 (Kleinlützum et al., 2017; Takaki et al., 2017). Microscopic examinations of H.E. stained paraffin sections revealed a highly loosely organized tumor bulk that appeared well-circumscribed and non-infiltrative in the corpus striatum of the right hemisphere. A zoom-in showed that the tumor is composed of atypical basophilic cells and apoptotic cells embedded in an edematous matrix. Neutrophils were shown to diffusely infiltrate the tumor being more frequent in mock-treated mice. Compared to mock-treated mice, the tumor dimensions in mice treated with VSV-CD133 were smaller, but comprised more apoptotic cells, which is a hallmark of VSV induced encephalitis. The center showed necrosis that was probably the result of extensive growth of tumor cells injected into an artificial cavity created by the needle tract (Figure 34). The neurotoxicity was also apparent upon intracranial injection of VSV-CD133 and VSV-MV in non-tumor bearing

mice (Figure 36), thus excluding virus burst from preinfected cells as potential trigger for neurotoxic infection. In this mouse model, VSV-MV could not infect murine brain tissue via the known receptors for MV. Moreover, the absence of the known MV receptors in the utilized mice model, and the onset of neurological signs through both viruses, VSV-CD133 and VSV-MV, preclude CD133 or rather CD46 as entry receptors to initiate a neurotoxic infection. Possible explanations for the neurotoxicicity include, but are not limited to, the engagement of another, yet unknown neuronal MV receptor interacting with H (Young and Rall, 2009), or a membrane fusion process that occurred independently from a contact with the H protein. In recent SSPE and MIBE cases, such a process has been suggested as partly causation of the strong cytopathology of the MV variants. The underlying hyperfusogenic F proteins possess substitutions at specific regions of the ectodomain of the F protein, which in turn decrease the conformational stability of the prefusion form of the F protein. This metastable F protein is triggered more easily to interact even with molecules beyond SLAM and nectin-4. Unlike wt MV strains, recombinant MVs (endowed with a mutant F protein) propagate faster in SLAM- and nectin-4 receptor positive and negative cells, and induce larger syncytia (Watanabe et al., 2013). In the setting of the present study, such hyperfusogenic F protein-like changes in the original F protein of VSV-MV are impossible to occur within the given duration. In fact, fusogenicity in this setting would have to be ascribed to other viral proteins of VSV-MV and VSV-CD133. Indeed, mutations of the MV-M protein are frequently found in SSPE and MIBE patients (Rima and Duprex, 2005). These mutations can either occur primarily or secondarily to mutations in the P gene as a result of an increase in the level of transcriptional P-M readthrough that translates into aberrant or absent M proteins (Ayata et al., 2002). Cathomen et al. demonstrated that MV variants devoid of M proteins (MVΔM) elicit extensive hyperfusogenicity. MVΔM with additional changes in the cytoplasmic tail of the F protein, another common characterstic feature of neuropathogenic variants of MV, exhibits increased cell-to-cell fusion activity but produces less virus particles compared to the original MV (Cathomen et al., 1998a; Cathomen et al., 1998b; Tahara et al., 2007). All mentioned changes may affect the overall fusogenicity of the F protein (Sato et al., 2018), but are unlikely to occur in the short duration of our studies.

As mentioned above, the neurotoxicity of VSV-CD133 and VSV-MV could also be explained by the existence of a so far unidentified neuronal receptor for MV. Unlike its fusogenic features *in vitro* on NCH644 and on Vero-αHis virus stock producer cells as well as *in vivo* on s.c. HuH7 xenografts, VSV-CD133 did not induce syncytia in the brain of inoculated mice as would be typical for a productive MV infection (Figure 34). Thus, we assumed that the lethal infection must have been promoted by other cytopathological mechanisms than formation of syncytia. In fact, one of the characteristic features of neuropathogenic paramyxoviruses including recombinant MVs based on wt MV is the lack of syncytia in the affected brains (Young and Rall, 2009; Watanabe et al., 2015). The same viruses can efficiently spread from initially infected

neurons along axons to connected neurons (Watanabe et al., 2015; Sato et al., 2018). As the spread of MV in these cases could be blocked by fusion inhibiting protein (FIP), the F protein was assumed to be actively involved in the cell-to-cell viral transmission (Sato et al., 2018). Studies with CDV indicated SLAM- and nectin-4-independent noncytolytic spread between astrocytes, which unlike previous studies with MV did not require hyperfusogenic F proteins (Alves et al., 2015). The authors of these studies uniformely proposed microfusion events at the synaptic membranes as a mechanism of MV trans-synaptic spread (Young and Rall, 2009).

Among the proposed explanations, from our point of view, the engagement of a yet unknown neuronal receptor by the VSV-MV chimeras is the most likely one. This assumption is supported by the fact that the neurotoxicity was apparent in mice that neither express CD46 nor any of the other known MV receptors in their brains. Furthermore, we observed the same extent of neurotoxicity with VSV-MV (Figure 36), which argues against an intratumoral virus amplification as potential root of the observed neurovirulence. Based on this premise, the interaction of MV H with the putative neuronal receptor may then activate MV F that might be hyperfusogenic through placement in the context of VSV. Accordingly, the faster replication cycle of VSV and the apoptosis-inducing M-protein would be causative for the neurovirulence observed with the VSV-MV chimeras. One could further speculate that a chimeric virus such as VSV-MV attaches to its target neuronal cells by interaction of the H protein with the putative neuronal receptor, which in turn triggers hyperfusogenic F proteins. In concordance with the present data and studies of others, it seems plausible that the virus RNP complex is transmitted trans-synaptically in a cell-to-cell manner due to the spatial expression of the putative receptor on synapses. From the present study, however, one cannot conclude whether the utilization of different proteins derived from MV vaccine strains and VSVΔG for generation of a chimeric virus would eventually affect the interactions of these proteins and result in hyperfusogenic virus competences of the VSV-MV chimeras. It is not inconceivable that the OVs MV-CD133, MV-CD46/CD133, MV^{Pwt}-CD133 or MV^{SCD}-CD133 would have caused the same neurovirulence, if their replication was as fast as those of VSV. Possibly, MV was eliminated by residual immune activity before the infection could spread and progress to lethal disease. Indeed, at necropsy, no tumor was detectable macroscopically in individual long-term survivors of groups treated with MV-CD46/CD133 and MV^{SCD}-CD133. This indicates that these mice must have been succumbed to another genesis than that of the tumor itself.

To test all the above mentioned hypotheses, we propose additional experiments tailored to identify the proposed neuronal receptor and the mechanisms of neurovirulence on the replicative background of VSV-MV. This could for example be done by analysing brain slices for GFP reactivity, but also by histological stainings for microglia and neutrophils which are the only present and functional immune cell populations in NOD/Scid mice. Possible examinations may include, amongst others, a staining of microglia and their toxic oxygen intermediate products.

The histological characterization of microglia can help to elucidate the state of immune activation and their role in virus control as well as their contributions to virus transmission in the brain. In this context, studies conducted in immunocompromized mice or human CD46-transgenic and IFNAR KO (IFNAR$^{-/-}$ CD46GE) mice have to be cautiously interpreted and cannot be easily transferred onto the human situation (Young and Rall, 2009). Therefore, VSV-MV chimeric viruses need also to be assessed in immunocompetent mice for the development of neurotoxicity. Notwithstanding, it still has to be elucidated whether orthologues of the human receptor molecule are used for MV propagation in animal brains.

4.3. Clinical Application of Receptor-Targeted Oncolytic Viruses

Receptor-targeted OVs have not yet progressed to clinical testing even though preclinical studies have proven their therapeutic feasibility for various tumor entities (Chaurasiya et al., 2018). Instead, current clinical development does rely on the inherent tumor selectivity of OVs and equips these viruses with immune-stimulatory transgenes such as GM-CSF (Granulocyte macrophage colony-stimulating factor). The latter transgene is encoded by the herpes virus based oncolytic agent ImylgicTM (Talimogene laherparepvec or T-vec), which has recently been granted marketing authorization for the treatment of advanced melanoma (Pol et al., 2016). However, several preclinical studies using receptor-targeted OVs are ongoing, and preliminary results are very promising. We and others have demonstrated an increase in the therapeutic index of receptor-targeted chimeric VSV-MV compared to non-targeted MVs. Indeed, the main rationale of receptor-targeting is an increase in safety through detargeting to the widespread native entry receptors of MV. On the other hand, the modification should not compromise on efficacy. Recently, oncolytic VSV strains with ablated VSV-G and tumor-selectivity have been generated. While tumor cells were selectively infected and lysed, healthy target receptor positive cells, e.g. human CD133^{+} hematopoietic stem cells (Kleinlützum et al., 2017), human CD30^{+} activated T lymphocytes (Hanauer et al., 2018) or human and rat primary neurons (Muik et al., 2011) were spared from infection. This observation seems to be independent from the non-malignant cell type, but rather be a result of the selective attenuation of VSV in IFN-responsive non-malignant cells (Hastie and Grdzelishvili, 2012). By contrast, in malignant tissues, VSV retains its capacity to replicate and lyse tumor cells with defective cellular innate immune responses.

In a subcutaneous tumor model of HCC, we identified VSV-CD133 as the most potent oncolytic agent by far exceeding the oncolytic potency of its MV counterparts. The impressive capacity of VSV-CD133 in spreading from an initial infection center set by intratumoral injections beyond neighboring cells through fusion can be regarded as important property to reach and destroy rare CSCs within a patients' tumor. It can be assumed that the fusogenic property of VSV-

CD133 minimizes the release of viral progeny into the surrounding tissue. In the preclinical tumor model we applied here, this might result in the multifocal replication pattern that translated into incomplete elimination of the tumor. In a clinical situation, where $CD133^+$ cells represent only a minor portion of the tumor cell population, it can be speculated that this fusogenic ability might reduce the risk of off-target effects and viremia. This could also explain why neurotoxic effects were not detected upon subcutaneous and intravenous virus application in the same mouse model (4.2). Given the safe use with regard to human HSCs and the absence of neurotoxicity upon intratumoral and intravenous application, VSV-CD133 exhibits a great therapeutic index for the therapy of this type of cancer. By contrast, VSV-CD133 is contraindicated for the therapy of intracranial malignancy as demonstrated by intracranial injections of VSV-MV chimeric viruses (4.2). These results underline that careful safety assessment is a mandatory requirement for any new type of chimeric virus and indication.

In general, safety issues may also arise when higher doses or more potent oncolytic viruses such as VSV are considered (Msaouel et al., 2018). Higher doses might be desirable in a systemic application not only to assess disseminated tumor sites but also to reach meaningful titers after dilution in the circulating blood volume (~ 5 l). Doses required for therapy via the intravenous route may have to be up to 1000-fold higher than for intratumoral administration, but can be associated with manufacturing challenges and adverse events such as hepatotoxicity, neurotoxicity, thrombocytopenia, lymphopenia and disseminated intravascular coagulation (Russell et al., 2012). Here, retargeted chimeric viruses can be advantageous. Substituting the surface glycoproteins of VSV with those of measles retargeted to a cell surface receptor of choice may not only increase oncoselectivity but also combine the advantages of each of the viruses. Oncolytic MVs based on the vaccine strain are known to be safe and its envelope glycoprotein complex is easily amenable for retargeting strategies (Msaouel et al., 2018). VSV is one the most potent OVs, which can be explained by its strong lytic capabilities, its high replication capacity and therewith can be produced to higher titers than MV (Bishnoi et al., 2018). The oncolytic potency of hybrid viruses of fusogenic and otherwise cytopathic viruses proved to be particularly effective compared to each of the parental viruses (Kleinlützum et al., 2017; Hanauer et al., 2018). Abdullahi et al. investigated the safety and efficacy of a chimeric VSV-NDV (Newcastle Disease Virus) vector compared to each monotypic virus and could show that off-target infection was reduced by the glycoprotein exchange, allowing substantially higher doses of virus to be applied without the onset of severe toxic effects. Moreover, VSV-NDV was also safe in avian hosts due to omission of a virulence factor of NDV known to antagonize antiviral immune responses (Abdullahi et al., 2018).

Another important factor that may compromise the therapeutic activity of MV based OVs are pre-dose anti-measles antibodies that might neutralize virus. In the well-documented case by

Russell et al. (Russell et al., 2014), the two well-responding patients were measles-seronegative and treated with the immunosuppressive drug cyclosphosphamide known to promote viral replication (Fulci et al., 2006). Numerous strategies to encounter anti-measles immunity are currently being investigated. One of them is the use of delivery vehicles such as mesenchymal stem cells that is already investigated in patients with refractory or progressive ovarian cancer (ClinicalTrials.gov Identifier: NCT02068794). Another strategy is the replacement of the MV glycoproteins with those of related but not immunologically cross-reactive morbilliviruses such as CDV. Miest et al. demonstrated that CDV-pseudotyped MV is able to escape antibody neutralization and exhibit potent oncolysis following intravenous administration in immunocompetent mice (Miest et al., 2011). By contrast, MV applied locoregionally may be better protected from pre-existing anti-measles immunity than intravenously delivered MV. Intercellular fusion of MV might also decrease exposure of virus particles to neutralizing antibodies (Sattentau, 2008). Moreover, multinucleated syncytia as a product of cell-to-cell fusion have been shown to serve as excellent antigen presenting cells (Bateman et al., 2002).

Due to the intratumoral heterogeneity in response to evolutionary factors such as any kind of therapy (Lottaz et al., 2010), tumors can loose their initial target receptor expression or (re-)aquire other receptor expression profiles. Here, multi-targeted OVs such as MV-CD46/CD133 that was tested in the present work, might still be able to infect these cells through switching usage of entry receptor. Tumor cells that express CD46 levels below threshold levels for virus infection and thus escape infection might be lysed by complement-mediated cascade and vice versa. The results from preclinical and clinical studies suggest that viral retargeting to other or additional surface receptors might be feasible to further optimize treatment efficacy in patients who express CD46 or nectin-4 below expression threshold levels (Anderson et al., 2004; Galanis et al., 2010).

In conclusion, MV vaccine strain-derived receptor retargeted OVs represent a promising approach for cancer treatment. Despite the engineering for tumor cell specificity, off-target effects are still a severe safety concern. With regard to VSV, neurotoxic adverse events must be taken into account. Thus, each genetic engineering strategy and combination treatment must be addressed prior to clinical testing. Besides receptor retargeting, oncoselectivity and safety of VSV-CD133 could further be improved by encoding a mutant M protein (e.g. VSV-MΔ51) or IFN-β known to restrict replication of VSV to IFN-sensitive cells (Fang et al., 2012; Patel et al., 2015). Ongoing clinical studies will reveal if oncolytic activity can be synergistically potentiated by combination treatments with immune checkpoint inhibitors (LaRocca and Warner, 2018) or chimeric antigen receptor (CAR) T cells (Guedan and Alemany, 2018).

REFERENCES

Abdullahi, S., Jäkel, M., Behrend, S. J., Steiger, K., Topping, G., Krabbe, T., Colombo, A., Sandig, V., Schiergens, T. S., Thasler, W. E., Werner, J., Lichtenthaler, S. F., Schmid, R. M., Ebert, O., and Altomonte, J.: A Novel Chimeric Oncolytic Virus Vector for Improved Safety and Efficacy as a Platform for the Treatment of Hepatocellular Carcinoma, Journal of virology, 92, doi:10.1128/JVI.01386-18, 2018.

Aguilar, H. C. and Lee, B.: Emerging paramyxoviruses: molecular mechanisms and antiviral strategies, Expert reviews in molecular medicine, 13, e6, doi:10.1017/S1462399410001754, 2011.

Aldape, K., Zadeh, G., Mansouri, S., Reifenberger, G., and Deimling, A. von: Glioblastoma: pathology, molecular mechanisms and markers, Acta neuropathologica, 129, 829–848, doi:10.1007/s00401-015-1432-1, 2015.

Al-Hajj, M., Wicha, M. S., Benito-Hernandez, A., Morrison, S. J., and Clarke, M. F.: Prospective identification of tumorigenic breast cancer cells, Proceedings of the National Academy of Sciences of the United States of America, 100, 3983–3988, doi:10.1073/pnas.0530291100, 2003.

Alves, L., Khosravi, M., Avila, M., Ader-Ebert, N., Bringolf, F., Zurbriggen, A., Vandevelde, M., and Plattet, P.: SLAM- and nectin-4-independent noncytolytic spread of canine distemper virus in astrocytes, Journal of virology, 89, 5724–5733, doi:10.1128/JVI.00004-15, 2015.

Amarasinghe, G. K., Bào, Y., Basler, C. F., Bavari, S., Beer, M., Bejerman, N., Blasdell, K. R., Bochnowski, A., Briese, T., Bukreyev, A., Calisher, C. H., Chandran, K., Collins, P. L., Dietzgen, R. G., Dolnik, O., Dürrwald, R., Dye, J. M., Easton, A. J., Ebihara, H., Fang, Q., Formenty, P., Fouchier, R. A. M., Ghedin, E., Harding, R. M., Hewson, R., Higgins, C. M., Hong, J., Horie, M., James, A. P., Jiāng, D., Kobinger, G. P., Kondo, H., Kurath, G., Lamb, R. A., Lee, B., Leroy, E. M., Li, M., Maisner, A., Mühlberger, E., Netesov, S. V., Nowotny, N., Patterson, J. L., Payne, S. L., Paweska, J. T., Pearson, M. N., Randall, R. E., Revill, P. A., Rima, B. K., Rota, P., Rubbenstroth, D., Schwemmle, M., Smither, S. J., Song, Q., Stone, D. M., Takada, A., Terregino, C., Tesh, R. B., Tomonaga, K., Tordo, N., Towner, J. S., Vasilakis, N., Volchkov, V. E., Wahl-Jensen, V., Walker, P. J., Wang, B., Wang, D., Wang, F., Wang, L.-F., Werren, J. H., Whitfield, A. E., Yan, Z., Ye, G., and Kuhn, J. H.: Taxonomy of the order Mononegavirales: update 2017, Archives of virology, 162, 2493–2504, doi:10.1007/s00705-017-3311-7, 2017.

Ammayappan, A., Nace, R., Peng, K.-W., and Russell, S. J.: Neuroattenuation of vesicular stomatitis virus through picornaviral internal ribosome entry sites, Journal of virology, 87, 3217–3228, doi:10.1128/JVI.02984-12, 2013.

Anderson, B. D., Nakamura, T., Russell, S. J., and Peng, K.-W.: High CD46 receptor density determines preferential killing of tumor cells by oncolytic measles virus, Cancer research, 64, 4919–4926, doi:10.1158/0008-5472.CAN-04-0884, 2004.

Anliker, B., Abel, T., Kneissl, S., Hlavaty, J., Caputi, A., Brynza, J., Schneider, I. C., Münch, R. C., Petznek, H., Kontermann, R. E., Koehl, U., Johnston, I. C. D., Keinänen, K., Müller, U. C., Hohenadl, C., Monyer, H., Cichutek, K., and Buchholz, C. J.: Specific gene transfer to neurons, endothelial cells and hematopoietic progenitors with lentiviral vectors, Nature methods, 7, 929–935, doi:10.1038/nmeth.1514, 2010.

Aref, S., Bailey, K., and Fielding, A.: Measles to the Rescue: A Review of Oncolytic Measles Virus, Viruses, 8, doi:10.3390/v8100294, 2016.

Arenaccio, C., Chiozzini, C., Columba-Cabezas, S., Manfredi, F., Affabris, E., Baur, A., and Federico, M.: Exosomes from human immunodeficiency virus type 1 (HIV-1)-infected cells license quiescent CD4+ T lymphocytes to replicate HIV-1 through a Nef- and ADAM17-dependent mechanism, Journal of virology, 88, 11529–11539, doi:10.1128/JVI.01712-14, 2014.

Ayala Breton, C., Wikan, N., Abbuhl, A., Smith, D. R., Russell, S. J., and Peng, K.-W.: Oncolytic potency of HER-2 retargeted VSV-FH hybrid viruses: the role of receptor ligand affinity, Molecular therapy oncolytics, 2, 15012-, doi:10.1038/mto.2015.12, 2015.

Ayala-Breton, C., Barber, G. N., Russell, S. J., and Peng, K.-W.: Retargeting vesicular stomatitis virus using measles virus envelope glycoproteins, Human gene therapy, 23, 484–491, doi:10.1089/hum.2011.146, 2012.

Ayala-Breton, C., Russell, L. O. J., Russell, S. J., and Peng, K.-W.: Faster Replication and Higher Expression Levels of Viral Glycoproteins Give the Vesicular Stomatitis Virus/Measles Virus Hybrid VSV-FH a Growth Advantage over Measles Virus, Journal of virology, 88, 8332–8339, doi:10.1128/JVI.03823-13, 2014.

Ayala-Breton, C., Suksanpaisan, L., Mader, E. K., Russell, S. J., and Peng, K.-W.: Amalgamating oncolytic viruses to enhance their safety, consolidate their killing mechanisms, and accelerate their spread, Molecular therapy the journal of the American Society of Gene Therapy, 21, 1930–1937, doi:10.1038/mt.2013.164, 2013.

Ayata, M., Komase, K., Shingai, M., Matsunaga, I., Katayama, Y., and Ogura, H.: Mutations affecting transcriptional termination in the p gene end of subacute sclerosing panencephalitis viruses, Journal of virology, 76, 13062–13068, 2002.

Bach, P., Abel, T., Hoffmann, C., Gal, Z., Braun, G., Voelker, I., Ball, C. R., Johnston, I. C. D., Lauer, U. M., Herold-Mende, C., Mühlebach, M. D., Glimm, H., and Buchholz, C. J.: Specific elimination of CD133+ tumor cells with targeted oncolytic measles virus, Cancer research, 73, 865–874, doi:10.1158/0008-5472.CAN-12-2221, 2013.

Barber, G. N.: Vesicular stomatitis virus as an oncolytic vector, Viral immunology, 17, 516–527, doi:10.1089/vim.2004.17.516, 2004.

Bateman, A. R., Harrington, K. J., Kottke, T., Ahmed, A., Melcher, A. A., Gough, M. J., Linardakis, E., Riddle, D., Dietz, A., Lohse, C. M., Strome, S., Peterson, T., Simari, R., and Vile, R. G.: Viral fusogenic membrane glycoproteins kill solid tumor cells by nonapoptotic mechanisms that promote cross presentation of tumor antigens by dendritic cells, Cancer research, 62, 6566–6578, 2002.

Batlle, E. and Clevers, H.: Cancer stem cells revisited, Nature medicine, 23, 1124–1134, doi:10.1038/nm.4409, 2017.

Bauer, N., Wilsch-Bräuninger, M., Karbanová, J., Fonseca, A.-V., Strauss, D., Freund, D., Thiele, C., Huttner, W. B., Bornhäuser, M., and Corbeil, D.: Haematopoietic stem cell differentiation promotes the release of prominin-1/CD133-containing membrane vesicles--a role of the endocytic-exocytic pathway, EMBO molecular medicine, 3, 398–409, doi:10.1002/emmm.201100147, 2011.

Beier, D., Hau, P., Proescholdt, M., Lohmeier, A., Wischhusen, J., Oefner, P. J., Aigner, L., Brawanski, A., Bogdahn, U., and Beier, C. P.: CD133(+) and CD133(-) glioblastoma-derived cancer stem cells show differential growth characteristics and molecular profiles, Cancer research, 67, 4010–4015, doi:10.1158/0008-5472.CAN-06-4180, 2007.

Bell, J. and McFadden, G.: Viruses for tumor therapy, Cell host & microbe, 15, 260–265, doi:10.1016/j.chom.2014.01.002, 2014.

Bhat, K. P. L., Balasubramaniyan, V., Vaillant, B., Ezhilarasan, R., Hummelink, K., Hollingsworth, F., Wani, K., Heathcock, L., James, J. D., Goodman, L. D., Conroy, S., Long, L., Lelic, N., Wang, S., Gumin, J., Raj, D., Kodama, Y., Raghunathan, A., Olar, A., Joshi, K., Pelloski, C. E., Heimberger, A., Kim, S. H., Cahill, D. P., Rao, G., Den Dunnen, W. F. A., Boddeke, H. W. G. M., Phillips, H. S., Nakano, I., Lang, F. F., Colman, H., Sulman, E. P., and Aldape, K.: Mesenchymal differentiation mediated by NF-κB promotes radiation resistance in glioblastoma, Cancer cell, 24, 331–346, doi:10.1016/j.ccr.2013.08.001, 2013.

Bhattacharjee, S. and Yadava, P. K.: Measles virus: Background and oncolytic virotherapy, Biochemistry and Biophysics Reports, 13, 58–62, doi:10.1016/j.bbrep.2017.12.004, 2018.

Bidlingmaier, S., Zhu, X., and Liu, B.: The utility and limitations of glycosylated human CD133 epitopes in defining cancer stem cells, Journal of molecular medicine (Berlin, Germany), 86, 1025–1032, doi:10.1007/s00109-008-0357-8, 2008.

Bishnoi, S., Tiwari, R., Gupta, S., Byrareddy, S. N., and Nayak, D.: Oncotargeting by Vesicular Stomatitis Virus (VSV): Advances in Cancer Therapy, Viruses, 10, doi:10.3390/v10020090, 2018.

Bluming, A. Z. and Ziegler, J. L.: Regression of Burkitt's lymphoma in association with measles infection, Lancet (London, England), 2, 105–106, 1971.

Bonnet, D. and Dick, J. E.: Human acute myeloid leukemia is organized as a hierarchy that originates from a primitive hematopoietic cell, Nature medicine, 3, 730–737, 1997.

Breitbach, C. J., Lichty, B. D., and Bell, J. C.: Oncolytic Viruses: Therapeutics With an Identity Crisis, EBioMedicine, 9, 31–36, doi:10.1016/j.ebiom.2016.06.046, 2016.

Brescia, P., Richichi, C., and Pelicci, G.: Current Strategies for Identification of Glioma Stem Cells: Adequate or Unsatisfactory?, Journal of Oncology, 2012, doi:10.1155/2012/376894, 2012.

Bruix, J., Reig, M., and Sherman, M.: Evidence-Based Diagnosis, Staging, and Treatment of Patients With Hepatocellular Carcinoma, Gastroenterology, 150, 835–853, doi:10.1053/j.gastro.2015.12.041, 2016.

Buchholz, C. J., Friedel, T., and Büning, H.: Surface-Engineered Viral Vectors for Selective and Cell Type-Specific Gene Delivery, Trends in biotechnology, 33, 777–790, doi:10.1016/j.tibtech.2015.09.008, 2015.

Buerki, R. A., Chheda, Z. S., and Okada, H.: Immunotherapy of Primary Brain Tumors: Facts and Hopes, Clinical cancer research an official journal of the American Association for Cancer Research, 24, 5198–5205, doi:10.1158/1078-0432.CCR-17-2769, 2018.

Calabrese, C., Poppleton, H., Kocak, M., Hogg, T. L., Fuller, C., Hamner, B., Oh, E. Y., Gaber, M. W., Finklestein, D., Allen, M., Frank, A., Bayazitov, I. T., Zakharenko, S. S., Gajjar, A., Davidoff, A., and Gilbertson, R. J.: A perivascular niche for brain tumor stem cells, Cancer cell, 11, 69–82, doi:10.1016/j.ccr.2006.11.020, 2007.

Campos, B., Gal, Z., Baader, A., Schneider, T., Sliwinski, C., Gassel, K., Bageritz, J., Grabe, N., Deimling, A. von, Beckhove, P., Mogler, C., Goidts, V., Unterberg, A., Eckstein, V., and Herold-Mende, C.: Aberrant self-renewal and quiescence contribute to the aggressiveness of glioblastoma, The Journal of pathology, 234, 23–33, doi:10.1002/path.4366, 2014.

Campos, B. and Herold-Mende, C. C.: Insight into the complex regulation of CD133 in glioma, International journal of cancer, 128, 501–510, doi:10.1002/ijc.25687, 2011.

Carr, B. I. (Ed.): Hepatocellular Carcinoma: Diagnosis and Treatment, Softcover reprint of the original 3rd edition 2016, Current Clinical Oncology, Springer International Publishing; Springer, Cham, XXI, 596 Seiten in 1 Teil, 2018.

Carvalho, J. V. de, Castro, R. O. de, da Silva, E. Z. M., Silveira, P. P., da Silva-Januário, M. E., Arruda, E., Jamur, M. C., Oliver, C., Aguiar, R. S., and daSilva, L. L. P.: Nef neutralizes the ability of exosomes from CD4+ T cells to act as decoys during HIV-1 infection, PLoS ONE, 9, e113691, doi:10.1371/journal.pone.0113691, 2014.

Cathomen, T., Mrkic, B., Spehner, D., Drillien, R., Naef, R., Pavlovic, J., Aguzzi, A., Billeter, M. A., and Cattaneo, R.: A matrix-less measles virus is infectious and elicits extensive cell fusion: consequences for propagation in the brain, The EMBO journal, 17, 3899–3908, doi:10.1093/emboj/17.14.3899, 1998a.

Cathomen, T., Naim, H. Y., and Cattaneo, R.: Measles viruses with altered envelope protein cytoplasmic tails gain cell fusion competence, Journal of virology, 72, 1224–1234, 1998b.

Chaurasiya, S., Chen, N. G., and Warner, S. G.: Oncolytic Virotherapy versus Cancer Stem Cells: A Review of Approaches and Mechanisms, Cancers, 10, doi:10.3390/cancers10040124, 2018.

Chen, R., Nishimura, M. C., Bumbaca, S. M., Kharbanda, S., Forrest, W. F., Kasman, I. M., Greve, J. M., Soriano, R. H., Gilmour, L. L., Rivers, C. S., Modrusan, Z., Nacu, S., Guerrero, S., Edgar, K. A., Wallin, J. J., Lamszus, K., Westphal, M., Heim, S., James, C. D.,

and VandenBerg, S. R.: A hierarchy of self-renewing tumor-initiating cell types in glioblastoma, Cancer cell, 17, 362–375, 2010.

Clarke, E., Pereira, C., Chaney, R., Woodside, S., Eaves, A. C., and Damen, J.: Toxicity testing using hematopoietic stem cell assays, Regenerative medicine, 2, 947–956, doi:10.2217/17460751.2.6.947, 2007.

Correnti, M. and Raggi, C.: Stem-like plasticity and heterogeneity of circulating tumor cells: current status and prospect challenges in liver cancer, Oncotarget, 8, 7094–7115, doi:10.18632/oncotarget.12569, 2017.

Doi, T., Kwon, H.-J., Honda, T., Sato, H., Yoneda, M., and Kai, C.: Measles virus induces persistent infection by autoregulation of viral replication, Scientific Reports, 6, 37163, doi:10.1038/srep37163, 2016.

Drokhlyansky, E., Göz Aytürk, D., Soh, T. K., Chrenek, R., O'Loughlin, E., Madore, C., Butovsky, O., and Cepko, C. L.: The brain parenchyma has a type I interferon response that can limit virus spread, Proceedings of the National Academy of Sciences of the United States of America, 114, E95-E104, doi:10.1073/pnas.1618157114, 2016.

Fang, X., Zhang, S., Sun, X., Li, J., and Sun, T.: Evaluation of attenuated VSVs with mutated M or/and G proteins as vaccine vectors, Vaccine, 30, 1313–1321, doi:10.1016/j.vaccine.2011.12.085, 2012.

Fargeas, C. A., Huttner, W. B., and Corbeil, D.: Nomenclature of prominin-1 (CD133) splice variants - an update, Tissue antigens, 69, 602–606, doi:10.1111/j.1399-0039.2007.00825.x, 2007.

Fekete, R., Cserép, C., Lénárt, N., Tóth, K., Orsolits, B., Martinecz, B., Méhes, E., Szabó, B., Németh, V., Gönci, B., Sperlágh, B., Boldogkői, Z., Kittel, Á., Baranyi, M., Ferenczi, S., Kovács, K., Szalay, G., Rózsa, B., Webb, C., Kovacs, G. G., Hortobágyi, T., West, B. L., Környei, Z., and Dénes, Á.: Microglia control the spread of neurotropic virus infection via P2Y12 signalling and recruit monocytes through P2Y12-independent mechanisms, Acta neuropathologica, 136, 461–482, doi:10.1007/s00401-018-1885-0, 2018.

Felt, S. A. and Grdzelishvili, V. Z.: Recent advances in vesicular stomatitis virus-based oncolytic virotherapy: a 5-year update, The Journal of general virology, doi:10.1099/jgv.0.000980, 2017.

Finke, D., Brinckmann, U. G., ter Meulen, V., and Liebert, U. G.: Gamma interferon is a major mediator of antiviral defense in experimental measles virus-induced encephalitis, Journal of virology, 69, 5469–5474, 1995.

Finkelmeier, F., Waidmann, O., and Trojan, J.: Nivolumab for the treatment of hepatocellular carcinoma, Expert review of anticancer therapy, 18, 1169–1175, doi:10.1080/14737140.2018.1535315, 2018.

Finkelshtein, D., Werman, A., Novick, D., Barak, S., and Rubinstein, M.: LDL receptor and its family members serve as the cellular receptors for vesicular stomatitis virus, Proceedings of the National Academy of Sciences of the United States of America, 110, 7306–7311, doi:10.1073/pnas.1214441110, 2013.

Fishelson, Z., Donin, N., Zell, S., Schultz, S., and Kirschfink, M.: Obstacles to cancer immunotherapy: expression of membrane complement regulatory proteins (mCRPs) in tumors, Molecular immunology, 40, 109–123, 2003.

Frank, A. M. and Buchholz, C. J.: Surface-Engineered Lentiviral Vectors for Selective Gene Transfer into Subtypes of Lymphocytes, Molecular therapy. Methods & clinical development, 12, 19–31, doi:10.1016/j.omtm.2018.10.006, 2019.

Friedrich, K., Hanauer, J. R., Prüfer, S., Münch, R. C., Völker, I., Filippis, C., Jost, C., Hanschmann, K.-M., Cattaneo, R., Peng, K.-W., Plückthun, A., Buchholz, C. J., Cichutek, K., and Mühlebach, M. D.: DARPin-targeting of measles virus: unique bispecificity, effective oncolysis, and enhanced safety, Molecular therapy the journal of the American Society of Gene Therapy, 21, 849–859, doi:10.1038/mt.2013.16, 2013.

Frisch, B. J. and Calvi, L. M.: Hematopoietic stem cell cultures and assays, Methods in molecular biology (Clifton, N.J.), 1130, 315–324, doi:10.1007/978-1-62703-989-5_24, 2014.

Fulci, G., Breymann, L., Gianni, D., Kurozomi, K., Rhee, S. S., Yu, J., Kaur, B., Louis, D. N., Weissleder, R., Caligiuri, M. A., and Chiocca, E. A.: Cyclophosphamide enhances glioma virotherapy by inhibiting innate immune responses, Proceedings of the National Academy of Sciences of the United States of America, 103, 12873–12878, doi:10.1073/pnas.0605496103, 2006.

Funke, S., Maisner, A., Mühlebach, M. D., Koehl, U., Grez, M., Cattaneo, R., Cichutek, K., and Buchholz, C. J.: Targeted cell entry of lentiviral vectors, Molecular therapy the journal of the American Society of Gene Therapy, 16, 1427–1436, doi:10.1038/mt.2008.128, 2008.

Galanis, E.: Therapeutic potential of oncolytic measles virus: promises and challenges, Clinical pharmacology and therapeutics, 88, 620–625, doi:10.1038/clpt.2010.211, 2010.

Galanis, E., Atherton, P. J., Maurer, M. J., Knutson, K. L., Dowdy, S. C., Cliby, W. A., Haluska, P., Long, H. J., Oberg, A., Aderca, I., Block, M. S., Bakkum-Gamez, J., Federspiel, M. J., Russell, S. J., Kalli, K. R., Keeney, G., Peng, K. W., and Hartmann, L. C.: Oncolytic measles virus expressing the sodium iodide symporter to treat drug-resistant ovarian cancer, Cancer research, 75, 22–30, doi:10.1158/0008-5472.CAN-14-2533, 2015.

Galanis, E., Hartmann, L. C., Cliby, W. A., Long, H. J., Peethambaram, P. P., Barrette, B. A., Kaur, J. S., Haluska, P. J., Aderca, I., Zollman, P. J., Sloan, J. A., Keeney, G., Atherton, P. J., Podratz, K. C., Dowdy, S. C., Stanhope, C. R., Wilson, T. O., Federspiel, M. J., Peng, K.-W., and Russell, S. J.: Phase I trial of intraperitoneal administration of an oncolytic measles virus strain engineered to express carcinoembryonic antigen for recurrent ovarian cancer, Cancer research, 70, 875–882, doi:10.1158/0008-5472.CAN-09-2762, 2010.

Garofalo, M., Villa, A., Rizzi, N., Kuryk, L., Rinner, B., Cerullo, V., Yliperttula, M., Mazzaferro, V., and Ciana, P.: Extracellular vesicles enhance the targeted delivery of immunogenic oncolytic adenovirus and paclitaxel in immunocompetent mice, Journal of controlled release official journal of the Controlled Release Society, 294, 165–175, doi:10.1016/j.jconrel.2018.12.022, 2019.

Ge, P., Tsao, J., Schein, S., Green, T. J., Luo, M., and Zhou, Z. H.: Cryo-EM model of the bullet-shaped vesicular stomatitis virus, Science (New York, N.Y.), 327, 689–693, doi:10.1126/science.1181766, 2010.

Glumac, P. M. and LeBeau, A. M.: The role of CD133 in cancer: a concise review, Clinical and translational medicine, 7, 18, doi:10.1186/s40169-018-0198-1, 2018.

Griffin, D. E.: Measles virus and the nervous system, Handbook of clinical neurology, 123, 577–590, doi:10.1016/B978-0-444-53488-0.00027-4, 2014.

Griffin, D. E., Lin, W.-H., and Pan, C.-H.: Measles virus, immune control, and persistence, FEMS microbiology reviews, 36, 649–662, doi:10.1111/j.1574-6976.2012.00330.x, 2012.

Griffin, D. E., Lin, W.-H. W., and Nelson, A. N.: Understanding the causes and consequences of measles virus persistence, F1000Research, 7, 237, doi:10.12688/f1000research.12094.1, 2018.

Grosse-Gehling, P., Fargeas, C. A., Dittfeld, C., Garbe, Y., Alison, M. R., Corbeil, D., and Kunz-Schughart, L. A.: CD133 as a biomarker for putative cancer stem cells in solid tumours: limitations, problems and challenges, The Journal of pathology, 229, 355–378, doi:10.1002/path.4086, 2013.

Guedan, S. and Alemany, R.: CAR-T Cells and Oncolytic Viruses: Joining Forces to Overcome the Solid Tumor Challenge, Frontiers in Immunology, 9, doi:10.3389/fimmu.2018.02460, 2018.

Guillerme, J.-B., Gregoire, M., Tangy, F., and Fonteneau, J.-F.: Antitumor Virotherapy by Attenuated Measles Virus (MV), Biology, 2, 587–602, doi:10.3390/biology2020587, 2013.

Guo, Z. S., Liu, Z., Kowalsky, S., Feist, M., Kalinski, P., Lu, B., Storkus, W. J., and Bartlett, D. L.: Oncolytic Immunotherapy: Conceptual Evolution, Current Strategies, and Future Perspectives, Frontiers in Immunology, 8, doi:10.3389/fimmu.2017.00555, 2017.

Gupta, P. B., Fillmore, C. M., Jiang, G., Shapira, S. D., Tao, K., Kuperwasser, C., and Lander, E. S.: Stochastic state transitions give rise to phenotypic equilibrium in populations of cancer cells, Cell, 146, 633–644, doi:10.1016/j.cell.2011.07.026, 2011.

Hanauer, J. D. S., Rengstl, B., Kleinlützum, D., Reul, J., Pfeiffer, A., Friedel, T., Schneider, I. C., Newrzela, S., Hansmann, M.-L., Buchholz, C. J., and Muik, A.: CD30-targeted oncolytic viruses as novel therapeutic approach against classical Hodgkin lymphoma, Oncotarget, 9, 12971–12981, doi:10.18632/oncotarget.24191, 2018.

Haralambieva, I., Iankov, I., Hasegawa, K., Harvey, M., Russell, S. J., and Peng, K.-W.: Engineering oncolytic measles virus to circumvent the intracellular innate immune response, Molecular therapy the journal of the American Society of Gene Therapy, 15, 588–597, doi:10.1038/sj.mt.6300076, 2007.

Hartkopf, A. D., Bossow, S., Lampe, J., Zimmermann, M., Taran, F.-A., Wallwiener, D., Fehm, T., Bitzer, M., and Lauer, U. M.: Enhanced killing of ovarian carcinoma using oncolytic measles vaccine virus armed with a yeast cytosine deaminase and uracil phosphoribosyltransferase, Gynecologic oncology, 130, 362–368, doi:10.1016/j.ygyno.2013.05.004, 2013.

Hastie, E., Cataldi, M., Marriott, I., and Grdzelishvili, V. Z.: Understanding and altering cell tropism of vesicular stomatitis virus, Virus research, 176, 16–32, doi:10.1016/j.virusres.2013.06.003, 2013.

Hastie, E. and Grdzelishvili, V. Z.: Vesicular stomatitis virus as a flexible platform for oncolytic virotherapy against cancer, The Journal of general virology, 93, 2529–2545, doi:10.1099/vir.0.046672-0, 2012.

Heinzerling, L., Künzi, V., Oberholzer, P. A., Kündig, T., Naim, H., and Dummer, R.: Oncolytic measles virus in cutaneous T-cell lymphomas mounts antitumor immune responses in vivo and targets interferon-resistant tumor cells, Blood, 106, 2287–2294, doi:10.1182/blood-2004-11-4558, 2005.

Holzmann, H., Hengel, H., Tenbusch, M., and Doerr, H. W.: Eradication of measles: remaining challenges, Medical microbiology and immunology, 205, 201–208, doi:10.1007/s00430-016-0451-4, 2016.

Irollo, E. and Pirozzi, G.: CD133: to be or not to be, is this the real question?, American Journal of Translational Research, 5, 563–581, 2013.

Jayakar, H. R., Murti, K. G., and Whitt, M. A.: Mutations in the PPPY motif of vesicular stomatitis virus matrix protein reduce virus budding by inhibiting a late step in virion release, Journal of virology, 74, 9818–9827, 2000.

Jeon, Y.-K., Kim, S.-H., Choi, S.-H., Kim, K.-H., Yoo, B.-C., Ku, J.-L., and Park, J.-G.: Promoter hypermethylation and loss of CD133 gene expression in colorectal cancers, World journal of gastroenterology, 16, 3153–3160, 2010.

Jiang, Y., Qin, Y., and Chen, M.: Host-Pathogen Interactions in Measles Virus Replication and Anti-Viral Immunity, Viruses, 8, doi:10.3390/v8110308, 2016.

Johnson, D. R., Brown, P. D., Galanis, E., and Hammack, J. E.: Pilocytic astrocytoma survival in adults: analysis of the Surveillance, Epidemiology, and End Results Program of the National Cancer Institute, Journal of neuro-oncology, 108, 187–193, doi:10.1007/s11060-012-0829-0, 2012.

Junttila, M. R. and Sauvage, F. J. de: Influence of tumour micro-environment heterogeneity on therapeutic response, Nature, 501, 346–354, doi:10.1038/nature12626, 2013.

Kane, J. R., Miska, J., Young, J. S., Kanojia, D., Kim, J. W., and Lesniak, M. S.: Sui generis: gene therapy and delivery systems for the treatment of glioblastoma, Neuro-oncology, 17 Suppl 2, ii24-ii36, doi:10.1093/neuonc/nou355, 2015.

Kelly, E. and Russell, S. J.: History of oncolytic viruses: genesis to genetic engineering, Molecular therapy the journal of the American Society of Gene Therapy, 15, 651–659, doi:10.1038/sj.mt.6300108, 2007.

Kemper, K., Grandela, C., and Medema, J. P.: Molecular identification and targeting of colorectal cancer stem cells, Oncotarget, 1, 387–395, 2010a.

Kemper, K., Sprick, M. R., Bree, M. de, Scopelliti, A., Vermeulen, L., Hoek, M., Zeilstra, J., Pals, S. T., Mehmet, H., Stassi, G., and Medema, J. P.: The AC133 epitope, but not the CD133 protein, is lost upon cancer stem cell differentiation, Cancer research, 70, 719–729, doi:10.1158/0008-5472.CAN-09-1820, 2010b.

Kleinlützum, D., Hanauer, J. D. S., Muik, A., Hanschmann, K.-M., Kays, S.-K., Ayala-Breton, C., Peng, K.-W., Mühlebach, M. D., Abel, T., and Buchholz, C. J.: Enhancing the Oncolytic Activity of CD133-Targeted Measles Virus: Receptor Extension or Chimerism with Vesicular Stomatitis Virus Are Most Effective, Frontiers in oncology, 7, 127, doi:10.3389/fonc.2017.00127, 2017.

Kleinlützum, D., Weaver, G., and Schley, D.: Within-group contact of cattle in dairy barns and the implications for disease transmission, Research in veterinary science, 95, 425–429, doi:10.1016/j.rvsc.2013.06.006, 2013.

Krause, M., Dubrovska, A., Linge, A., and Baumann, M.: Cancer stem cells: Radioresistance, prediction of radiotherapy outcome and specific targets for combined treatments, Advanced drug delivery reviews, 109, 63–73, doi:10.1016/j.addr.2016.02.002, 2017.

Kreso, A. and Dick, J. E.: Evolution of the cancer stem cell model, Cell stem cell, 14, 275–291, doi:10.1016/j.stem.2014.02.006, 2014.

Kuhlmann, J. D., Hein, L., Kurth, I., Wimberger, P., and Dubrovska, A.: Targeting Cancer Stem Cells: Promises and Challenges, Anti-cancer agents in medicinal chemistry, 16, 38–58, 2016.

Kumar, B., Manuja, A., Gulati, B. R., Virmani, N., and Tripathi, B. N.: Zoonotic Viral Diseases of Equines and Their Impact on Human and Animal Health, The open virology journal, 12, 80–98, doi:10.2174/1874357901812010080, 2018.

Lafaro, K. J., Demirjian, A. N., and Pawlik, T. M.: Epidemiology of hepatocellular carcinoma, Surgical oncology clinics of North America, 24, 1–17, doi:10.1016/j.soc.2014.09.001, 2015.

Laksono, B. M., Vries, R. D. de, McQuaid, S., Duprex, W. P., and Swart, R. L. de: Measles Virus Host Invasion and Pathogenesis, Viruses, 8, doi:10.3390/v8080210, 2016.

Lampe, J., Bossow, S., Weiland, T., Smirnow, I., Lehmann, R., Neubert, W., Bitzer, M., and Lauer, U. M.: An armed oncolytic measles vaccine virus eliminates human hepatoma cells independently of apoptosis, Gene therapy, 20, 1033–1041, doi:10.1038/gt.2013.28, 2013.

Lange, S., Lampe, J., Bossow, S., Zimmermann, M., Neubert, W., Bitzer, M., and Lauer, U. M.: A novel armed oncolytic measles vaccine virus for the treatment of cholangiocarcinoma, Human gene therapy, 24, 554–564, doi:10.1089/hum.2012.136, 2013.

LaRocca, C. J. and Warner, S. G.: Oncolytic viruses and checkpoint inhibitors: combination therapy in clinical trials, Clinical and translational medicine, 7, doi:10.1186/s40169-018-0214-5, 2018.

Lathia, J. D., Mack, S. C., Mulkearns-Hubert, E. E., Valentim, C. L. L., and Rich, J. N.: Cancer stem cells in glioblastoma, Genes & development, 29, 1203–1217, doi:10.1101/gad.261982.115, 2015.

Li, B., McCrudden, C. M., Yuen, H. F., Xi, X., Lyu, P., Chan, K. W., Zhang, S. D., and Kwok, H. F.: CD133 in brain tumor: the prognostic factor, Oncotarget, 8, 11144–11159, doi:10.18632/oncotarget.14406, 2017.

Li, Z.: CD133: a stem cell biomarker and beyond, Experimental Hematology & Oncology, 2, 17, doi:10.1186/2162-3619-2-17, 2013.

Lichty, B. D., Power, A. T., Stojdl, D. F., and Bell, J. C.: Vesicular stomatitis virus: re-inventing the bullet, Trends in molecular medicine, 10, 210–216, doi:10.1016/j.molmed.2004.03.003, 2004.

Lin, L.-T. and Richardson, C. D.: The Host Cell Receptors for Measles Virus and Their Interaction with the Viral Hemagglutinin (H) Protein, Viruses, 8, doi:10.3390/v8090250, 2016.

Llovet, J. M., Villanueva, A., Lachenmayer, A., and Finn, R. S.: Advances in targeted therapies for hepatocellular carcinoma in the genomic era, Nature reviews. Clinical oncology, 12, 408–424, doi:10.1038/nrclinonc.2015.103, 2015.

Lottaz, C., Beier, D., Meyer, K., Kumar, P., Hermann, A., Schwarz, J., Junker, M., Oefner, P. J., Bogdahn, U., Wischhusen, J., Spang, R., Storch, A., and Beier, C. P.: Transcriptional profiles of CD133+ and CD133- glioblastoma-derived cancer stem cell lines suggest different cells of origin, Cancer research, 70, 2030–2040, doi:10.1158/0008-5472.CAN-09-1707, 2010.

Louis, D. N., Perry, A., Reifenberger, G., Deimling, A. von, Figarella-Branger, D., Cavenee, W. K., Ohgaki, H., Wiestler, O. D., Kleihues, P., and Ellison, D. W.: The 2016 World Health Organization Classification of Tumors of the Central Nervous System: a summary, Acta neuropathologica, 131, 803–820, doi:10.1007/s00401-016-1545-1, 2016.

Ludlow, M., McQuaid, S., Milner, D., Swart, R. L. de, and Duprex, W. P.: Pathological consequences of systemic measles virus infection, The Journal of pathology, 235, 253–265, doi:10.1002/path.4457, 2015.

Magee, J. A., Piskounova, E., and Morrison, S. J.: Cancer stem cells: impact, heterogeneity, and uncertainty, Cancer cell, 21, 283–296, doi:10.1016/j.ccr.2012.03.003, 2012.

Manchester, M. and Rall, G. F.: Model Systems: transgenic mouse models for measles pathogenesis, Trends in microbiology, 9, 19–23, 2001.

Marrero, J. A., Fontana, R. J., Barrat, A., Askari, F., Conjeevaram, H. S., Su, G. L., and Lok, A. S.: Prognosis of hepatocellular carcinoma: comparison of 7 staging systems in an American cohort, Hepatology (Baltimore, Md.), 41, 707–716, doi:10.1002/hep.20636, 2005.

Marty, R. R., Knuchel, M. C., Morin, T. N. A., and Naim, H. Y.: An immune competent mouse model for the characterization of recombinant measles vaccines, Human Vaccines & Immunotherapeutics, 11, 83–90, doi:10.4161/hv.34358, 2015.

Matsuda, S., Yan, T., Mizutani, A., Sota, T., Hiramoto, Y., Prieto-Vila, M., Chen, L., Satoh, A., Kudoh, T., Kasai, T., Murakami, H., Fu, L., Salomon, D. S., and Seno, M.: Cancer stem cells maintain a hierarchy of differentiation by creating their niche, International journal of cancer, 135, 27–36, doi:10.1002/ijc.28648, 2014.

Matveeva, O. V. and Chumakov, P. M.: Defects in interferon pathways as potential biomarkers of sensitivity to oncolytic viruses, Reviews in medical virology, 28, e2008, doi:10.1002/rmv.2008, 2018.

McCormick, F.: Cancer gene therapy: fringe or cutting edge?, Nature reviews. Cancer, 1, 130–141, doi:10.1038/35101008, 2001.

Melzer, M. K., Lopez-Martinez, A., and Altomonte, J.: Oncolytic Vesicular Stomatitis Virus as a Viro-Immunotherapy: Defeating Cancer with a “Hammer” and “Anvil”, Biomedicines, 5, doi:10.3390/biomedicines5010008, 2017.

Miest, T. S., Yaiw, K.-C., Frenzke, M., Lampe, J., Hudacek, A. W., Springfeld, C., Messling, V. von, Ungerechts, G., and Cattaneo, R.: Envelope-chimeric entry-targeted measles virus escapes neutralization and achieves oncolysis, Molecular therapy the journal of the American Society of Gene Therapy, 19, 1813–1820, doi:10.1038/mt.2011.92, 2011.

Moerdyk-Schauwecker, M., Shah, N. R., Murphy, A. M., Hastie, E., Mukherjee, P., and Grdzelishvili, V. Z.: Resistance of pancreatic cancer cells to oncolytic vesicular stomatitis virus: role of type I interferon signaling, Virology, 436, 221–234, doi:10.1016/j.virol.2012.11.014, 2013.

Mota, H. C.: Infantile Hodgkin's disease: remission after measles, British medical journal, 2, 421, 1973.

Mrkic, B., Pavlovic, J., Rülicke, T., Volpe, P., Buchholz, C. J., Hourcade, D., Atkinson, J. P., Aguzzi, A., and Cattaneo, R.: Measles virus spread and pathogenesis in genetically modified mice, Journal of virology, 72, 7420–7427, 1998.

Msaouel, P., Opyrchal, M., Dispenzieri, A., Peng, K. W., Federspiel, M. J., Russell, S. J., and Galanis, E.: Clinical Trials with Oncolytic Measles Virus: Current Status and Future Prospects, Current cancer drug targets, 18, 177–187, doi:10.2174/1568009617666170222125035, 2018.

Mühlebach, M. D., Mateo, M., Sinn, P. L., Prüfer, S., Uhlig, K. M., Leonard, V. H. J., Navaratnarajah, C. K., Frenzke, M., Wong, X. X., Sawatsky, B., Ramachandran, S., McCray, P. B., Cichutek, K., Messling, V. von, Lopez, M., and Cattaneo, R.: Adherens junction protein nectin-4 is the epithelial receptor for measles virus, Nature, 480, 530–533, doi:10.1038/nature10639, 2011.

Muik, A., Dold, C., Geiß, Y., Volk, A., Werbizki, M., Dietrich, U., and Laer, D. von: Semireplication-competent vesicular stomatitis virus as a novel platform for oncolytic virotherapy, Journal of molecular medicine (Berlin, Germany), 90, 959–970, doi:10.1007/s00109-012-0863-6, 2012.

Muik, A., Kneiske, I., Werbizki, M., Wilflingseder, D., Giroglou, T., Ebert, O., Kraft, A., Dietrich, U., Zimmer, G., Momma, S., and Laer, D. von: Pseudotyping vesicular stomatitis virus with lymphocytic choriomeningitis virus glycoproteins enhances infectivity for glioma cells and minimizes neurotropism, Journal of virology, 85, 5679–5684, doi:10.1128/JVI.02511-10, 2011.

Muik, A., Stubbert, L. J., Jahedi, R. Z., Geiβ, Y., Kimpel, J., Dold, C., Tober, R., Volk, A., Klein, S., Dietrich, U., Yadollahi, B., Falls, T., Miletic, H., Stojdl, D., Bell, J. C., and Laer, D. von: Re-engineering vesicular stomatitis virus to abrogate neurotoxicity, circumvent humoral immunity, and enhance oncolytic potency, Cancer research, 74, 3567–3578, doi:10.1158/0008-5472.CAN-13-3306, 2014.

Mura, M., Ruffié, C., Billon-Denis, E., Combredet, C., Tournier, J. N., and Tangy, F.: hCD46 receptor is not required for measles vaccine Schwarz strain replication in vivo: Type-I IFN is the species barrier in mice, Virology, 524, 151–159, doi:10.1016/j.virol.2018.08.014, 2018.

Murphy, A. M., Besmer, D. M., Moerdyk-Schauwecker, M., Moestl, N., Ornelles, D. A., Mukherjee, P., and Grdzelishvili, V. Z.: Vesicular Stomatitis Virus as an Oncolytic Agent against Pancreatic Ductal Adenocarcinoma, Journal of virology, 87, 1923, doi:10.1128/JVI.02979-12, 2013.

Naim, H. Y.: Measles virus: A pathogen, vaccine, and a vector, Human Vaccines & Immunotherapeutics, 11, 21–26, doi:10.4161/hv.34298, 2014.

Nakamura, T., Peng, K.-W., Harvey, M., Greiner, S., Lorimer, I. A. J., James, C. D., and Russell, S. J.: Rescue and propagation of fully retargeted oncolytic measles viruses, Nature biotechnology, 23, 209–214, doi:10.1038/nbt1060, 2005.

Noyce, R. S. and Richardson, C. D.: Nectin 4 is the epithelial cell receptor for measles virus, Trends in microbiology, 20, 429–439, doi:10.1016/j.tim.2012.05.006, 2012.

Ostrom, Q. T., Bauchet, L., Davis, F. G., Deltour, I., Fisher, J. L., Langer, C. E., Pekmezci, M., Schwartzbaum, J. A., Turner, M. C., Walsh, K. M., Wrensch, M. R., and Barnholtz-Sloan, J. S.: The epidemiology of glioma in adults: a "state of the science" review, Neuro-oncology, 16, 896–913, doi:10.1093/neuonc/nou087, 2014.

Ostrom, Q. T., Gittleman, H., Liao, P., Vecchione-Koval, T., Wolinsky, Y., Kruchko, C., and Barnholtz-Sloan, J. S.: CBTRUS Statistical Report: Primary brain and other central nervous system tumors diagnosed in the United States in 2010-2014, Neuro-oncology, 19, v1-v88, doi:10.1093/neuonc/nox158, 2017.

Paglino, J. C. and van den Pol, A. N.: Vesicular stomatitis virus has extensive oncolytic activity against human sarcomas: rare resistance is overcome by blocking interferon pathways, Journal of virology, 85, 9346–9358, doi:10.1128/JVI.00723-11, 2011.

Pallini, R., Ricci-Vitiani, L., Banna, G. L., Signore, M., Lombardi, D., Todaro, M., Stassi, G., Martini, M., Maira, G., Larocca, L. M., and Maria, R. de: Cancer stem cell analysis and clinical outcome in patients with glioblastoma multiforme, Clinical cancer research an official journal of the American Association for Cancer Research, 14, 8205–8212, doi:10.1158/1078-0432.CCR-08-0644, 2008.

Patel, M. R., Jacobson, B. A., Ji, Y., Drees, J., Tang, S., Xiong, K., Wang, H., Prigge, J. E., Dash, A. S., Kratzke, A. K., Mesev, E., Etchison, R., Federspiel, M. J., Russell, S. J., and Kratzke, R. A.: Vesicular stomatitis virus expressing interferon-β is oncolytic and promotes antitumor immune responses in a syngeneic murine model of non-small cell lung cancer, Oncotarget, 6, 33165–33177, doi:10.18632/oncotarget.5320, 2015.

Pattabiraman, D. R. and Weinberg, R. A.: Tackling the cancer stem cells - what challenges do they pose?, Nature reviews. Drug discovery, 13, 497–512, doi:10.1038/nrd4253, 2014.

Patterson, C. E., Lawrence, D. M. P., Echols, L. A., and Rall, G. F.: Immune-mediated protection from measles virus-induced central nervous system disease is noncytolytic and gamma interferon dependent, Journal of virology, 76, 4497–4506, 2002.

Penheiter, A. R., Russell, S. J., and Carlson, S. K.: The sodium iodide symporter (NIS) as an imaging reporter for gene, viral, and cell-based therapies, Current gene therapy, 12, 33–47, 2012.

Pereira, C., Clarke, E., and Damen, J.: Hematopoietic colony-forming cell assays, Methods in molecular biology (Clifton, N.J.), 407, 177–208, doi:10.1007/978-1-59745-536-7_14, 2007.

Perry, A. and Wesseling, P.: Histologic classification of gliomas, Handbook of clinical neurology, 134, 71–95, doi:10.1016/B978-0-12-802997-8.00005-0, 2016.

Pfeffermann, K., Dörr, M., Zirkel, F., and Messling, V. von: Morbillivirus Pathogenesis and Virus-Host Interactions, Advances in virus research, 100, 75–98, doi:10.1016/bs.aivir.2017.12.003, 2018.

Phillips, E., Lang, V., Bohlen, J., Bethke, F., Puccio, L., Tichy, D., Herold-Mende, C., Hielscher, T., Lichter, P., and Goidts, V.: Targeting atypical protein kinase C iota reduces viability in glioblastoma stem-like cells via a notch signaling mechanism, International journal of cancer, 139, 1776–1787, doi:10.1002/ijc.30234, 2016.

Plaks, V., Kong, N., and Werb, Z.: The cancer stem cell niche: how essential is the niche in regulating stemness of tumor cells?, Cell stem cell, 16, 225–238, doi:10.1016/j.stem.2015.02.015, 2015.

Plemper, R. K.: Cell entry of enveloped viruses, Current opinion in virology, 1, 92–100, doi:10.1016/j.coviro.2011.06.002, 2011.

Pol, J., Kroemer, G., and Galluzzi, L.: First oncolytic virus approved for melanoma immunotherapy, Oncoimmunology, 5, e1115641, doi:10.1080/2162402X.2015.1115641, 2016.

Prasad, S., Gaedicke, S., Machein, M., Mittler, G., Braun, F., Hettich, M., Firat, E., Klingner, K., Schüler, J., Wider, D., Wäsch, R. M., Herold-Mende, C., Elsässer-Beile, U., and Niedermann, G.: Effective Eradication of Glioblastoma Stem Cells by Local Application of an AC133/CD133-Specific T-cell-Engaging Antibody and CD8 T Cells, Cancer research, 75, 2166–2176, doi:10.1158/0008-5472.CAN-14-2415, 2015.

Qiu, L., Li, H., Fu, S., Chen, X., and Lu, L.: Surface markers of liver cancer stem cells and innovative targeted-therapy strategies for HCC, Oncology Letters, 15, 2039–2048, doi:10.3892/ol.2017.7568, 2018.

Quail, D. F. and Joyce, J. A.: The microenvironmental landscape of brain tumors, Cancer cell, 31, 326–341, doi:10.1016/j.ccell.2017.02.009, 2017.

Radecke, F., Spielhofer, P., Schneider, H., Kaelin, K., Huber, M., Dötsch, C., Christiansen, G., and Billeter, M. A.: Rescue of measles viruses from cloned DNA, The EMBO journal, 14, 5773–5784, 1995.

Ramakrishnan, M. A.: Determination of 50% endpoint titer using a simple formula, World journal of virology, 5, 85–86, doi:10.5501/wjv.v5.i2.85, 2016.

Reardon, D. A., Wen, P. Y., Wucherpfennig, K. W., and Sampson, J. H.: Immunomodulation for glioblastoma, Current opinion in neurology, 30, 361–369, doi:10.1097/WCO.0000000000000451, 2017.

Redondo, N., Madan, V., Alvarez, E., and Carrasco, L.: Impact of Vesicular Stomatitis Virus M Proteins on Different Cellular Functions, PLoS ONE, 10, doi:10.1371/journal.pone.0131137, 2015.

Reifenberger, G., Wirsching, H.-G., Knobbe-Thomsen, C. B., and Weller, M.: Advances in the molecular genetics of gliomas - implications for classification and therapy, Nature reviews. Clinical oncology, 14, 434–452, doi:10.1038/nrclinonc.2016.204, 2017.

Rima, B. K. and Duprex, W. P.: Molecular mechanisms of measles virus persistence, Virus research, 111, 132–147, doi:10.1016/j.virusres.2005.04.005, 2005.

Robinson, S. and Galanis, E.: Potential and clinical translation of oncolytic measles viruses, Expert opinion on biological therapy, 17, 353–363, doi:10.1080/14712598.2017.1288713, 2017.

Roesch, A., Fukunaga-Kalabis, M., Schmidt, E. C., Zabierowski, S. E., Brafford, P. A., Vultur, A., Basu, D., Gimotty, P., Vogt, T., and Herlyn, M.: A temporarily distinct subpopulation of slow-cycling melanoma cells is required for continuous tumor growth, Cell, 141, 583–594, doi:10.1016/j.cell.2010.04.020, 2010.

Rozmyslowicz, T., Majka, M., Kijowski, J., Murphy, S. L., Conover, D. O., Poncz, M., Ratajczak, J., Gaulton, G. N., and Ratajczak, M. Z.: Platelet- and megakaryocyte-derived microparticles transfer CXCR4 receptor to CXCR4-null cells and make them susceptible to infection by X4-HIV, AIDS (London, England), 17, 33–42, doi:10.1097/01.aids.0000042948.95433.3d, 2003.

Russell, S. J., Federspiel, M. J., Peng, K.-W., Tong, C., Dingli, D., Morice, W. G., Lowe, V., O'Connor, M. K., Kyle, R. A., Leung, N., Buadi, F. K., Rajkumar, S. V., Gertz, M. A., Lacy, M. Q., and Dispenzieri, A.: Remission of disseminated cancer after systemic oncolytic virotherapy, Mayo Clinic proceedings, 89, 926–933, doi:10.1016/j.mayocp.2014.04.003, 2014.

Russell, S. J., Peng, K.-W., and Bell, J. C.: Oncolytic virotherapy, Nature biotechnology, 30, 658–670, doi:10.1038/nbt.2287, 2012.

Saloura, V., Wang, L.-C. S., Fridlender, Z. G., Sun, J., Cheng, G., Kapoor, V., Sterman, D. H., Harty, R. N., Okumura, A., Barber, G. N., Vile, R. G., Federspiel, M. J., Russell, S. J., Litzky, L., and Albelda, S. M.: Evaluation of an attenuated vesicular stomatitis virus vector expressing interferon-beta for use in malignant pleural mesothelioma: heterogeneity in interferon responsiveness defines potential efficacy, Human gene therapy, 21, 51–64, doi:10.1089/hum.2009.088, 2010.

Sato, Y., Watanabe, S., Fukuda, Y., Hashiguchi, T., Yanagi, Y., and Ohno, S.: Cell-to-Cell Measles Virus Spread between Human Neurons Is Dependent on Hemagglutinin and Hyperfusogenic Fusion Protein, Journal of virology, 92, doi:10.1128/JVI.02166-17, 2018.

Sattentau, Q.: Avoiding the void: cell-to-cell spread of human viruses, Nature reviews. Microbiology, 6, 815–826, doi:10.1038/nrmicro1972, 2008.

Schmohl, J. U. and Vallera, D. A.: CD133, Selectively Targeting the Root of Cancer, Toxins, 8, doi:10.3390/toxins8060165, 2016.

Schwitalla, S., Fingerle, A. A., Cammareri, P., Nebelsiek, T., Göktuna, S. I., Ziegler, P. K., Canli, O., Heijmans, J., Huels, D. J., Moreaux, G., Rupec, R. A., Gerhard, M., Schmid, R., Barker, N., Clevers, H., Lang, R., Neumann, J., Kirchner, T., Taketo, M. M., van den Brink, G. R., Sansom, O. J., Arkan, M. C., and Greten, F. R.: Intestinal tumorigenesis initiated by dedifferentiation and acquisition of stem-cell-like properties, Cell, 152, 25–38, doi:10.1016/j.cell.2012.12.012, 2013.

Singh, S. K., Clarke, I. D., Terasaki, M., Bonn, V. E., Hawkins, C., Squire, J., and Dirks, P. B.: Identification of a cancer stem cell in human brain tumors, Cancer research, 63, 5821–5828, 2003.

Singh, S. K., Hawkins, C., Clarke, I. D., Squire, J. A., Bayani, J., Hide, T., Henkelman, R. M., Cusimano, M. D., and Dirks, P. B.: Identification of human brain tumour initiating cells, Nature, 432, 396–401, doi:10.1038/nature03128, 2004.

Song, W., Li, H., Tao, K., Li, R., Song, Z., Zhao, Q., Zhang, F., and Dou, K.: Expression and clinical significance of the stem cell marker CD133 in hepatocellular carcinoma, International journal of clinical practice, 62, 1212–1218, doi:10.1111/j.1742-1241.2008.01777.x, 2008.

Springfeld, C., Messling, V. von, Frenzke, M., Ungerechts, G., Buchholz, C. J., and Cattaneo, R.: Oncolytic efficacy and enhanced safety of measles virus activated by tumor-secreted matrix metalloproteinases, Cancer research, 66, 7694–7700, doi:10.1158/0008-5472.CAN-06-0538, 2006.

Stojdl, D. F., Lichty, B. D., tenOever, B. R., Paterson, J. M., Power, A. T., Knowles, S., Marius, R., Reynard, J., Poliquin, L., Atkins, H., Brown, E. G., Durbin, R. K., Durbin, J. E., Hiscott, J., and Bell, J. C.: VSV strains with defects in their ability to shutdown innate immunity are potent systemic anti-cancer agents, Cancer cell, 4, 263–275, 2003.

Stupp, R., Brada, M., van den Bent, M. J., Tonn, J.-C., and Pentheroudakis, G.: High-grade glioma: ESMO Clinical Practice Guidelines for diagnosis, treatment and follow-up, Annals of oncology official journal of the European Society for Medical Oncology, 25 Suppl 3, iii93-101, doi:10.1093/annonc/mdu050, 2014.

Sun, J.-H., Luo, Q., Liu, L.-L., and Song, G.-B.: Liver cancer stem cell markers: Progression and therapeutic implications, World journal of gastroenterology, 22, 3547–3557, doi:10.3748/wjg.v22.i13.3547, 2016.

Tahara, M., Takeda, M., and Yanagi, Y.: Altered interaction of the matrix protein with the cytoplasmic tail of hemagglutinin modulates measles virus growth by affecting virus assembly and cell-cell fusion, Journal of virology, 81, 6827–6836, doi:10.1128/JVI.00248-07, 2007.

Takaki, H., Oshiumi, H., Shingai, M., Matsumoto, M., and Seya, T.: Development of mouse models for analysis of human virus infections, Microbiology and immunology, 61, 107–113, doi:10.1111/1348-0421.12477, 2017.

Tatsuo, H., Ono, N., Tanaka, K., and Yanagi, Y.: SLAM (CDw150) is a cellular receptor for measles virus, Nature, 406, 893–897, doi:10.1038/35022579, 2000.

Tong, Y. and Qian, W.: Targeting cancer stem cells with oncolytic virus, Stem cell investigation, 1, 20, doi:10.3978/j.issn.2306-9759.2014.11.01, 2014.

van den Pol, A. N. and Davis, J. N.: Highly attenuated recombinant vesicular stomatitis virus VSV-12'GFP displays immunogenic and oncolytic activity, Journal of virology, 87, 1019–1034, doi:10.1128/JVI.01106-12, 2013.

van den Pol, A. N., Mao, G., Chattopadhyay, A., Rose, J. K., and Davis, J. N.: Chikungunya, Influenza, Nipah, and Semliki Forest Chimeric Viruses with Vesicular Stomatitis Virus: Actions in the Brain, Journal of virology, 91, doi:10.1128/JVI.02154-16, 2017.

Venugopal, C., Hallett, R., Vora, P., Manoranjan, B., Mahendram, S., Qazi, M. A., McFarlane, N., Subapanditha, M., Nolte, S. M., Singh, M., Bakhshinyan, D., Garg, N., Vijayakumar, T., Lach, B., Provias, J. P., Reddy, K., Murty, N. K., Doble, B. W., Bhatia, M., Hassell, J. A., and Singh, S. K.: Pyrvinium Targets CD133 in Human Glioblastoma Brain Tumor-Initiating Cells, Clinical cancer research an official journal of the American Association for Cancer Research, 21, 5324–5337, doi:10.1158/1078-0432.CCR-14-3147, 2015.

Visvader, J. E. and Lindeman, G. J.: Cancer stem cells in solid tumours: accumulating evidence and unresolved questions, Nature reviews. Cancer, 8, 755–768, doi:10.1038/nrc2499, 2008.

Völker, I., Bach, P., Coulibaly, C., Plesker, R., Abel, T., Seifried, J., Heidmeier, S., Mühlebach, M. D., Lauer, U. M., and Buchholz, C. J.: Intrahepatic application of suicide gene-armed measles virotherapeutics: a safety study in transgenic mice and rhesus macaques, Human gene therapy. Clinical development, 24, 11–22, doi:10.1089/humc.2012.242, 2013.

Vries, R. D. de, Duprex, W. P., and Swart, R. L. de: Morbillivirus infections: an introduction, Viruses, 7, 699–706, doi:10.3390/v7020699, 2015.

Waldron, N. N., Kaufman, D. S., Oh, S., Inde, Z., Hexum, M. K., Ohlfest, J. R., and Vallera, D. A.: Targeting tumor-initiating cancer cells with dCD133KDEL shows impressive tumor reductions in a xenotransplant model of human head and neck cancer, Molecular cancer therapeutics, 10, 1829–1838, doi:10.1158/1535-7163.MCT-11-0206, 2011.

Walker, P. J., Blasdell, K. R., Calisher, C. H., Dietzgen, R. G., Kondo, H., Kurath, G., Longdon, B., Stone, D. M., Tesh, R. B., Tordo, N., Vasilakis, N., Whitfield, A. E., and Ictv, R. C.: ICTV Virus Taxonomy Profile: Rhabdoviridae, The Journal of general virology, 99, 447–448, doi:10.1099/jgv.0.001020, 2018.

Wang, T., Fang, L., Zhao, F., Wang, D., and Xiao, S.: Exosomes Mediate Intercellular Transmission of Porcine Reproductive and Respiratory Syndrome Virus, Journal of virology, 92, doi:10.1128/JVI.01734-17, 2018.

Wang, Y., Probin, V., and Zhou, D.: Cancer therapy-induced residual bone marrow injury-Mechanisms of induction and implication for therapy, Current cancer therapy reviews, 2, 271–279, 2006.

Watanabe, S., Ohno, S., Shirogane, Y., Suzuki, S. O., Koga, R., and Yanagi, Y.: Measles virus mutants possessing the fusion protein with enhanced fusion activity spread effectively in neuronal cells, but not in other cells, without causing strong cytopathology, Journal of virology, 89, 2710–2717, doi:10.1128/JVI.03346-14, 2015.

Watanabe, S., Shirogane, Y., Suzuki, S. O., Ikegame, S., Koga, R., and Yanagi, Y.: Mutant fusion proteins with enhanced fusion activity promote measles virus spread in human neuronal cells and brains of suckling hamsters, Journal of virology, 87, 2648–2659, doi:10.1128/JVI.02632-12, 2013.

Weidinger, G., Czub, S., Neumeister, C., Harriott, P., ter Meulen, V., and Niewiesk, S.: Role of CD4(+) and CD8(+) T cells in the prevention of measles virus-induced encephalitis in mice, The Journal of general virology, 81, 2707–2713, doi:10.1099/0022-1317-81-11-2707, 2000.

Welstead, G. G., Hsu, E. C., Iorio, C., Bolotin, S., and Richardson, C. D.: Mechanism of CD150 (SLAM) down regulation from the host cell surface by measles virus hemagglutinin protein, Journal of virology, 78, 9666–9674, doi:10.1128/JVI.78.18.9666-9674.2004, 2004.

Wesseling, P. and Capper, D.: WHO 2016 Classification of gliomas, Neuropathology and applied neurobiology, 44, 139–150, doi:10.1111/nan.12432, 2018.

Wojton, J. and Kaur, B.: Impact of tumor microenvironment on oncolytic viral therapy, Cytokine & growth factor reviews, 21, 127–134, doi:10.1016/j.cytogfr.2010.02.014, 2010.

Wollmann, G., Drokhlyansky, E., Davis, J. N., Cepko, C., and van den Pol, A. N.: Lassa-vesicular stomatitis chimeric virus safely destroys brain tumors, Journal of virology, 89, 6711–6724, doi:10.1128/JVI.00709-15, 2015.

Wollmann, G., Robek, M. D., and van den Pol, A. N.: Variable deficiencies in the interferon response enhance susceptibility to vesicular stomatitis virus oncolytic actions in glioblastoma cells but not in normal human glial cells, Journal of virology, 81, 1479–1491, doi:10.1128/JVI.01861-06, 2007.

World Scientific (Firm): Biology and pathogenesis of rhabdo- and filoviruses, World Scientific Pub. Co, Singapore, Hackensack, N.J, 627 pp., 2015.

Wörns, M.-A. and Galle, P. R.: HCC therapies--lessons learned, Nature reviews. Gastroenterology & hepatology, 11, 447–452, doi:10.1038/nrgastro.2014.10, 2014.

Wu, B., Sun, C., Feng, F., Ge, M., and Xia, L.: Do relevant markers of cancer stem cells CD133 and Nestin indicate a poor prognosis in glioma patients? A systematic review and meta-analysis, Journal of Experimental & Clinical Cancer Research CR, 34, doi:10.1186/s13046-015-0163-4, 2015.

Xiang, Y., Yang, T., Pang, B.-Y., Zhu, Y., and Liu, Y.-N.: The Progress and Prospects of Putative Biomarkers for Liver Cancer Stem Cells in Hepatocellular Carcinoma, Stem cells international, 2016, 7614971, doi:10.1155/2016/7614971, 2016.

Xie, Q., Mittal, S., and Berens, M. E.: Targeting adaptive glioblastoma: an overview of proliferation and invasion, Neuro-oncology, 16, 1575–1584, doi:10.1093/neuonc/nou147, 2014.

Yan, X., Ma, L., Yi, D., Yoon, J.-g., Diercks, A., Foltz, G., Price, N. D., Hood, L. E., and Tian, Q.: A CD133-related gene expression signature identifies an aggressive glioblastoma subtype with excessive mutations, Proceedings of the National Academy of Sciences of the United States of America, 108, 1591–1596, doi:10.1073/pnas.1018696108, 2011.

Yin, A. H., Miraglia, S., Zanjani, E. D., Almeida-Porada, G., Ogawa, M., Leary, A. G., Olweus, J., Kearney, J., and Buck, D. W.: AC133, a novel marker for human hematopoietic stem and progenitor cells, Blood, 90, 5002–5012, 1997.

Yin, S., Li, J., Hu, C., Chen, X., Yao, M., Yan, M., Jiang, G., Ge, C., Xie, H., Wan, D., Yang, S., Zheng, S., and Gu, J.: CD133 positive hepatocellular carcinoma cells possess high capacity for tumorigenicity, International journal of cancer, 120, 1444–1450, doi:10.1002/ijc.22476, 2007.

Young, V. A. and Rall, G. F.: Making it to the synapse: measles virus spread in and among neurons, Current topics in microbiology and immunology, 330, 3–30, 2009.

Zeppernick, F., Ahmadi, R., Campos, B., Dictus, C., Helmke, B. M., Becker, N., Lichter, P., Unterberg, A., Radlwimmer, B., and Herold-Mende, C. C.: Stem cell marker CD133 affects clinical outcome in glioma patients, Clinical cancer research an official journal of the American Association for Cancer Research, 14, 123–129, doi:10.1158/1078-0432.CCR-07-0932, 2008.

Zhang, L., Steele, M. B., Jenks, N., Grell, J., Suksanpaisan, L., Naik, S., Federspiel, M. J., Lacy, M. Q., Russell, S. J., and Peng, K.-W.: Safety Studies in Tumor and Non-Tumor-Bearing Mice in Support of Clinical Trials Using Oncolytic VSV-IFNβ-NIS, Human gene therapy. Clinical development, 27, 111–122, doi:10.1089/humc.2016.061, 2016.

Zhong, C., Wu, J.-D., Fang, M.-M., and Pu, L.-Y.: Clinicopathological significance and prognostic value of the expression of the cancer stem cell marker CD133 in hepatocellular carcinoma: a meta-analysis, Tumour biology the journal of the International Society for Oncodevelopmental Biology and Medicine, 36, 7623–7630, doi:10.1007/s13277-015-3487-y, 2015.

Zhu, X., Prasad, S., Gaedicke, S., Hettich, M., Firat, E., and Niedermann, G.: Patient-derived glioblastoma stem cells are killed by CD133-specific CAR T cells but induce the T cell aging marker CD57, Oncotarget, 6, 171–184, doi:10.18632/oncotarget.2767, 2015.

Zucman-Rossi, J., Villanueva, A., Nault, J.-C., and Llovet, J. M.: Genetic Landscape and Biomarkers of Hepatocellular Carcinoma, Gastroenterology, 149, 1226-1239.e4, doi:10.1053/j.gastro.2015.05.061, 2015.

LIST OF PUBLICATIONS

Parts of this thesis have been published

Enhancing the Oncolytic Activity of CD133-Targeted Measles Virus: Receptor Extension or Chimerism With Vesicular Stomatitis Virus Are Most Effective
Kleinlützum D, Hanauer JDS, Muik A, Hanschmann KM, Kays SK, Ayala-Breton C, Peng KW, Mühlebach M, Abel T and Buchholz CJ
Frontiers in Oncology, 2017, 7, 127

CD30-Targeted Oncolytic Viruses As Novel Therapeutic Approach Against Classical Hodgkin Lymphoma
Hanauer JDS, Rengstl B, Kleinlützum D, Reul J, Pfeiffer A, Friedel T, Schneider IC, Newrzela S, Hansmann ML, Buchholz CJ Muik A
Oncotarget, 2018, 9 (16), 12971-12981

Other publications

Endothelial Transcription Factor KLF2 Negatively Regulates Liver Regeneration Via Induction Of Activin A
Manavski Y, Abel, T, Hu J, Kleinlützum D, Buchholz CJ; Belz C, Augustin HG; Boon RA, Dimmeler S
PNAS, 2017, 114 (15), 3993-3998

A Case Of Gallstones In An African Green Monkey (*Chlorocebus aethiops*)
Kleinlützum D, Plesker R
Primate Biology, 2017, 4, 33-37

Within-Group Contact Of Cattle In Dairy Barns And The Implications For Disease Transmission
Kleinlützum D, Weaver G, Schley D
Research in Veterinary Science, 2013, 95 (2), 425-429

Parts of this thesis have been orally presented at scientific conferences

Oncolytic Viruses Retargeted To The Tumor Stem Cell Marker CD133
Kleinlützum D, Muik A, Hanauer JDS, Kays SK, Ayala-Breton C, Peng KW, Buchholz CJ
27. Annual Meeting of the Society for Virology (GfV), Marburg, 2017 Mar

Oncolytic Vesicular Stomatitis Virus Retargeted to The Tumor Stem Cell Marker CD133
Kleinlützum D, Muik A, Kays SK, Ayala-Breton C, Peng KW, Buchholz CJ
60. Jahrestagung und 22. Schnittseminar der Fachgruppe Pathologie der Detuschen Veterinärmedizinischen Gesellschaft, Fulda, 2017 Mar

Oncolytic Vesicular Stomatitis Virus Retargeted to The Tumor Stem Cell Marker CD133
Kleinlützum D, Muik A, Hanauer JDS, Kays SK, Ayala-Breton C, Peng KW, Buchholz CJ
Annual PEI Retreat, Ronneburg, 2017 Jan

Oncolytic Vesicular Stomatits Virus Retargeted To The Tumor Stem Cell Marker CD133
Kleinlützum D, Muik A, Hanauer JDS, Kays SK, Ayala-Breton C, Peng KW, Buchholz CJ
22nd Annual Meeting of the German Society for Gene Therapy (DGGT), Heidelberg, 2016 Sept

Oncolytic Vesicular Stomatits Virus Retargeted To Tumor Stem Cells
Kleinlützum D, Muik A, Kays SK, Bönig H, Buchholz CJ
Summer School of the LOEWE Cell and Gene Therapy (CGT), Langen, 2015 Oct

Parts of this thesis have been presented on posters at scientific conferences

Oncolytic Vesicular Stomatits Virus Retargeted To The Tumor Stem Cell Marker CD133
Kleinlützum D, Muik A, Hanauer JDS, Kays SK, Ayala-Breton C, Peng KW, Buchholz CJ
American Society of Gene & Cell Therapy Meeting, Washington DC, 2016 Mar

Oncolytic Vesicular Stomatitis Virus Retargeted to The Tumor Stem Cell Marker CD133
Kleinlützum D, Muik A, Hanauer JDS, Kays SK, Ayala-Breton C, Peng KW, Buchholz CJ
7. UCT Science Day, Frankfurt a.M., 2016 Oct

Oncolytic Vesicular Stomatits Virus Retargeted To The Tumor Stem Cell Marker CD133
Kleinlützum D, Muik A, Kays SK, Bönig H, Buchholz CJ
Annual PEI Retreat, Ronneburg, 2016 Jan

Transgene-Armed Measles Virotherapeutics Targeted Against Cancer Stem Cells
Kleinlützum D, Muik A, Kays SK, Buchholz CJ
Annual PEI Retreat, Heidelberg, 2015 Jan

Stem Cell Targeted And Transgene Armed Measles Virotherapeutics
Kleinlützum D, Muik A, Kays SK, Bönig H, Buchholz CJ
Summer School of the LOEWE Cell and Gene Therapy (CGT), Bad Nauheim, 2014 Oct

Cancer Stem Cell Targeted And Trangene-Armed Measles Virotherapeutics
Kleinlützum D, Muik A, Buchholz CJ
Annual PEI Retreat, Heidelberg, 2014 Jan

DANKSAGUNG

Mein besonderer Dank gilt Prof. Dr. Christian J. Buchholz für die Möglichkeit, meine Doktorarbeit in seiner Arbeitsgruppe durchführen zu können. Die stetigen konstruktiven wissenschaftlichen Diskussionen - verbunden mit der guten Betreuung in dem wissenschaftlichen Umfeld seiner Gruppe - haben maßgeblich zu der Entstehung dieser Arbeit beigetragen.

Ich bedanke mich ebenso bei Prof. Dr. Heinz-Jürgen Thiel für die freundliche und unkomplizierte Betreuung seitens der Universität Gießen. Er gehörte zusammen mit Prof. Dr. Christian J. Buchholz, Dr. Alexander Muik und Prof. Dr. Dr. Ute Modlich dem Thesis Committee an, in dessen meetings ich wertvolles Input für meine Arbeit erhalten habe. Vielen Dank dafür!

Zudem möchte ich mich bei Dr. Roland Plesker für die lehrreichen Pathologie-Fortbildungsstunden, bei Dr. Michael Mühlebach und Dr. Edgar Holznagel für fachliche Tipps und bei Kay-Martin Hanschmann für den statistischen Support bedanken. Ich bedanke mich bei Alex für die wissenschaftliche Begleitung und bei Tobi für das technisch-wissenschaftliche Input.

Allen meinen Kollegen aus der AG „Molekulare Biotechnologie und Gentherapie“ möchte ich mich für die schöne Zeit bedanken. Die großartige hochmotivierende Arbeitsatmosphäre, die große Hilfsbereitschaft und fachliche Tipps haben den Weg zu meiner Arbeit gepflastert. Ich blicke zurück auf eine tolle Zeit mit euch als Kollegen! Insbesondere bedanke ich mich bei Alex, Tobi, Julia, Tatjana, Sarah, Jessi, Frederic, Thorsten, Anett, Johanna, Anke, Gundi, Manu, Ruth, Laura, Annika, Irene und Ruben. Ihr habt mir ein Lächeln ins Gesicht gezaubert, wenn ich es gebraucht habe. Ich spiele damit u.A. auf den „Mouse-Mover“ an, der maßgeblich zum Gelingen der Fluoreszenzaufnahmen beigetragen hat! Ich möchte nicht meine aktuellen Kollegschaft unerwähnt lassen, die während dieser Zeit viel Verständnis für mich hatten und mir Rede und Antwort standen, z.B. bei Fragen wie: “Wie war das den bei euch…?”.

Ein besonderer Dank geht an die Tierpfleger, die sich täglich um das Wohl der Mäuse gekümmert haben. Ohne euer Engagement wären die betreuungsintensiven Tumor-Modelle nicht möglich gewesen. In dem Zusammenhang bedanke ich mich bei der Tierhausleitung, sowie bei Marion Weidinger, die mit großer Gewissenhaftigkeit die Gehirne bearbeitet hat.

Bei meinen Freunden möchte ich mich für all die schönen Stunden abseits der Diss und ihr Verständnis für meine Priorität auf meine Doktorarbeit bedanken. Das gilt in besondere für meine Freundin Micha, die mir während dieser Zeit sehr ans Herz gewachsen ist.

Mein größter Dank gilt meinen Eltern für die Ermöglichung meiner gesamten Ausbildung und die bedingungslose und uneingeschränkte Unterstützung während dieser Zeit. Ohne euch hätte ich diesen Weg nicht gehen können. Zu guter Letzt bedanke ich mich bei meinem Mann Sebastian für seine unglaubliche Geduld, sein Verständnis und seinen großartigen Humor. Sebastian, es ist so schön, dich an meiner Seite zu haben!

EHRENWÖRTLICHE ERKLÄRUNG

Ich habe die vorgelegte Dissertation ohne unerlaubte fremde Hilfe und nur mit den Hilfen angefertigt, die ich in der Dissertation angegeben habe. Alle Textstellen, die wörtlich oder sinngemäß aus veröffentlichten oder nicht veröffentlichten Schriften entnommen sind und alle Angaben, die auf mündlichen Auskünften beruhen, sind als solche kenntlich gemacht. Bei den von mir durchgeführten und in der Dissertation erwähnten Untersuchungen habe ich die Grundsätze guter wissenschaftlicher Praxis, wie sie in der “Satzung der Justus-Liebig-Universität Gießen zur Sicherung guter wissenschaftlicher Praxis” niedergelegt sind, eingehalten.

Gießen, den _____

.....

Dina Schadel

ISBN: 978-3-86345-534-7

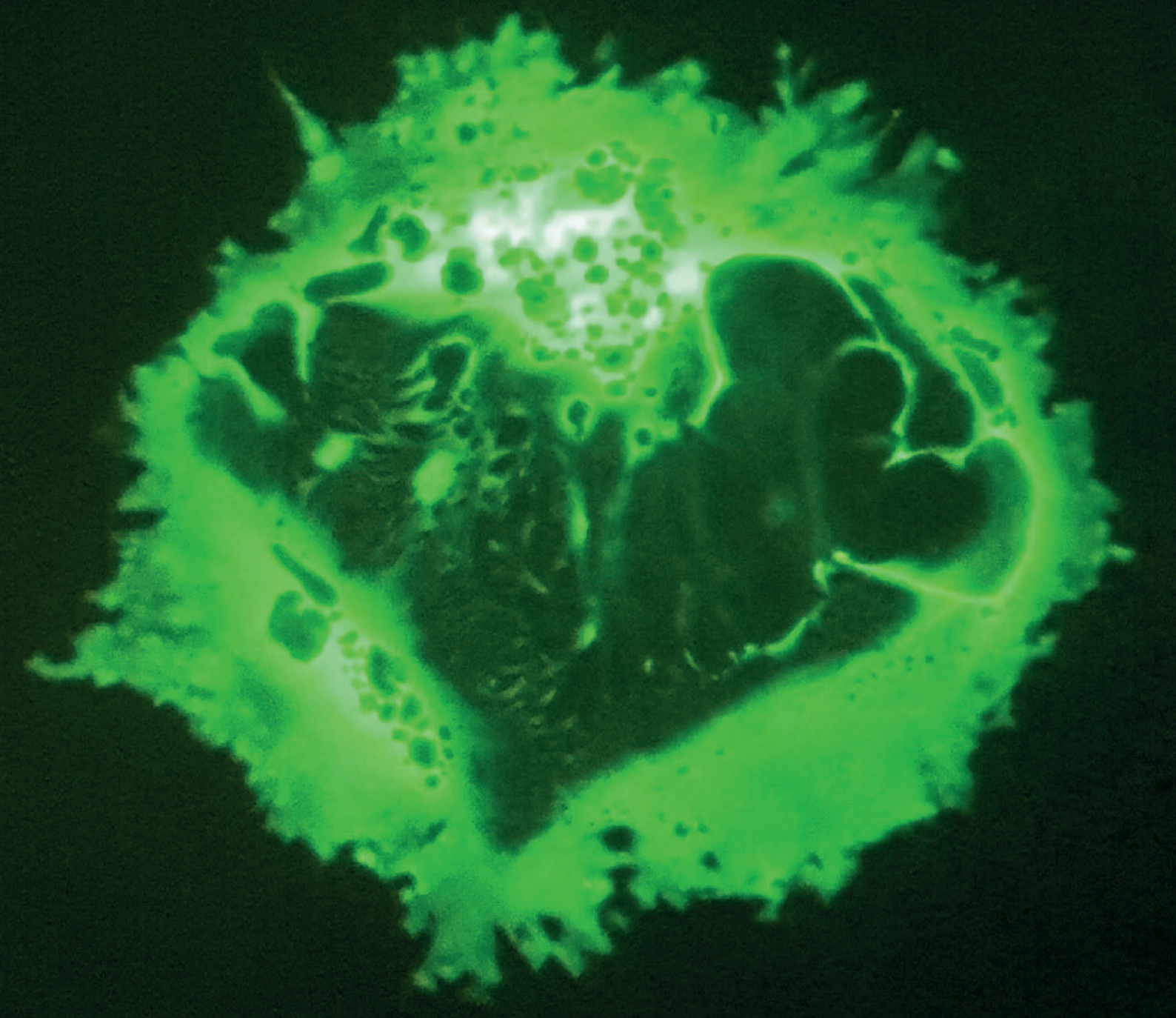

Verlag der DVG Service GmbH
Friedrichstraße 17 • 35392 Gießen
Tel.: 0641 / 24466 • Fax: 0641 / 25375
E-Mail: info@dvg.de • Web: www.dvg.de